1-1-2015

Ef-G:trna Dynamics During the Elongation Cycle of Protein Synthesis

Rong Shen
University of Pennsylvania, shenrong@sas.upenn.edu

Ef-G:trna Dynamics During the Elongation Cycle of Protein Synthesis

Abstract
During polypeptide elongation cycle, prokaryotic elongation factor G (EF-G) catalyzes the coupled translocations on the ribosome of mRNA and A- and P-site bound tRNAs. Continued progress has been achieved in understanding this key process, including results of structural, ensemble kinetic and single-molecule studies. However, most of work has been focused on the pre-equilibrium states of this fast process, leaving the real time dynamics, especially how EF-G interacts with the A-site tRNA in the pretranslocation complex, not fully elucidated.

In this thesis, the kinetics of EF-G catalyzed translocation is investigated by both ensemble and single molecule fluorescence resonance energy transfer studies to further explore the underlying mechanism. In the ensemble work, EF-G mutants were designed and expressed successfully. The labeled EF-G mutants show good translocation activity in two different assays. In the smFRET work, by attachment of a fluorescent probe at position 693 on EF-G permits monitoring of FRET efficiencies to sites in both ribosomal protein L11 and A-site tRNA. The EF-G:L11 FRET efficiency is constant during the entire EF-G occupancy on the ribosome, while the EF-G:tRNA FRET proceeds from high to intermediate to low FRET values. Transition from intermediate to low is the rate-limiting step with a small FRET change, whereas transition from high to intermediate is fast, showing a large FRET change. In total, we capture a ~12 Ã? relative movement of A-site tRNA away from EF-G during translocation. This indicates that EF-G:A-site tRNA distance increases progressively during translocation, with our results providing the first good estimates of the timing of such changes. This EF-G:tRNA smFRET measurement was applied to bifunctional rhodamine labeled EF-G derivatives (BR-EF-G) and comparable kinetic results were obtained. FRET changes of BR-EF-G:Cy5-tRNA pair are larger if the BR group is located closer to the EF-G hinge region, suggesting that parts of domain IV of EF-G, which penetrate to the decoding region of the ribosome, move together with the A-site tRNA during translocation.

Degree Type
Dissertation

Degree Name
Doctor of Philosophy (PhD)

Graduate Group
Chemistry

First Advisor
Barry S. Cooperman

Keywords
EF-G, SmFRET, tRNA, ribosome, kinetics

EF-G:tRNA DYNAMICS DURING THE ELONGATION CYCLE OF PROTEIN SYNTHESIS

Rong Shen

A DISSERTATION

in

Chemistry

Presented to the Faculties of the University of Pennsylvania

in

Partial Fulfillment of the Requirements for the

Degree of Doctor of Philosophy

2015

Supervisor of Dissertation

_____

Dr. Barry S. Cooperman, Professor of Chemistry

Graduate Group Chairperson

_____

Dr. Gary A. Molander, Hirschmann-Makineni Professor of Chemistry

Dissertation Committee:

Dr. Ivan J. Dmochowski, Associate Professor of Chemistry

Dr. Yale E. Goldman, Professor of Physiology

Dr. E. James Petersson, Assistant Professor of Chemistry

Dedicated to my father Changming Shen and my mother Yan Shen

ACKNOWLEDGEMENT

A PhD journey is never easy. It is a pleasure and an honor to thank many people who made this thesis possible. First and foremost, this thesis would never have happened without the encouragement, guidance and support from my research advisor Dr. Barry S. Cooperman. It is my highest honor to be one of his students. From him, I have learned how to think critically which would greatly benefit my future career. His enthusiasm toward science and immense knowledge not only inspire me but also make the learning process a great fun for me. After five years research work in Dr. Cooperman's lab, I find where my interest is and how I should pursue my future career.

I would like to show my greatest gratitude towards our major collaborator with this project. Dr. Yale Goldman is not only a committee member, but also a very close collaborator with our group. In the text you will notice that a large portion of my work is smFRET study which was carried out in Dr. Yale Goldman's lab. I attended his journal club and enjoy discussing my data with him. His inspiring insights into my work have proved to be priceless.

I am indebted to my dissertation committee members, Prof. Ivan Dmochowski and Prof. Petersson for their constructive suggestions to my work and support to my study at Penn. I learned how to think about my research from other perspectives and without their help, it would have been impossible for me to accomplish my thesis.

It is a great pleasure for me to thank all my current and past group members. When I first joined in the lab, Dr. Haibo Zhang taught me how to purify protein and helped

me with my everyday work. Dr. Hanqing Liu helped me with the quench flow experiment. I learned how to do kinetic experiments and analyze the complicated data with the help of Dr. Wei Liu, who also shared a lot of invaluable experience with me about data interpretation. Dr. Ian Farrell and Dr. Jaskiran Kaur helped me with tRNA preparation. Dr. Chunlai Chen and Dr. Darius Kavaliauskas helped me with the smFRET experiment and spent a lot of time on discussing smFRET data with me. Dr. Amy Weil, Dr. Dulce Alonso, Dr. Gabi Rosenblum, Mr. Yuanwei Chen, Mr. Martin Ng and Ms. Adrienne Pesce have been incredible to work with and learn from.

I would like to thank my roommates Na Zhang and Dr. Zhaoxia Qian, my dear friends Dr. Han Wei, Dr. Jiadi Zhang and Yanran Ai, with whom I came to Penn six years ago and Jie Qing, Fang Liu, Minyan Li, with whom I shared laughter and interesting conversations.

I own my deepest gratitude to my family. I would like to thank my parents for their love, support and encouragement during these years and I will never know how far I could have made it without their support. I also want to thank my dog, lele, who is one of my dear family members and brought a lot of laughter to me.

ABSTRACT

EF-G:tRNA DYNAMICS DURING THE ELONGATION CYCLE OF PROTEIN SYNTHESIS

Rong Shen

Barry S. Cooperman

During polypeptide elongation cycle, prokaryotic elongation factor G (EF-G) catalyzes the coupled translocations on the ribosome of mRNA and A- and P-site bound tRNAs. Continued progress has been achieved in understanding this key process, including results of structural, ensemble kinetic and single-molecule studies. However, most of work has been focused on the pre-equilibrium states of this fast process, leaving the real time dynamics, especially how EF-G interacts with the A-site tRNA in the pretranslocation complex, not fully elucidated.

In this thesis, the kinetics of EF-G catalyzed translocation is investigated by both ensemble and single molecule fluorescence resonance energy transfer studies to further explore the underlying mechanism. In the ensemble work, EF-G mutants were designed and expressed successfully. The labeled EF-G mutants show good translocation activity in two different assays. In the smFRET work, by attachment of a fluorescent probe at position 693 on EF-G permits monitoring of FRET efficiencies to sites in both ribosomal protein L11 and A-site tRNA. The EF-G:L11 FRET efficiency is constant

during the entire EF-G occupancy on the ribosome, while the EF-G:tRNA FRET proceeds from high to intermediate to low FRET values. Transition from intermediate to low is the rate-limiting step with a small FRET change, whereas transition from high to intermediate is fast, showing a large FRET change. In total, we capture a ~12 Å relative movement of A-site tRNA away from EF-G during translocation. This indicates that EF-G:A-site tRNA distance increases progressively during translocation, with our results providing the first good estimates of the timing of such changes. This EF-G:tRNA smFRET measurement was applied to bifunctional rhodamine labeled EF-G derivatives (BR-EF-G) and comparable kinetic results were obtained. FRET changes of BR-EF-G:Cy5-tRNA pair are larger if the BR group is located closer to the EF-G hinge region, suggesting that parts of domain IV of EF-G, which penetrate to the decoding region of the ribosome, move together with the A-site tRNA during translocation.

TABLE OF CONTENTS

LIST OF TABLES

LIST OF ILLUSTRATIONS

CHAPTER I INTRODUCTION

1.1 The central dogma and ribosome-catalyzed translation

Nucleotides are ubiquitous molecules with high structural diversity. Their polymeric forms, deoxyribonucleic acids (DNAs) and ribonucleic acids (RNA) are important in storage and expression of genetic information. As determined by James Watson and Francis Crick in 1953, the double helix structure of DNA is well known now. DNA in a parent cell is replicated through its double helix, propagating genetic information to the daughter cells (Watson *et al*., 1953a; Watson *et al*., 1953b). A great variety of enzymes are involved in DNA replication. Single-stranded parental DNA is used as the template to synthesize the complementary strand for both leading and lagging strands, with high fidelity. As DNA strand can only be extended from 5' to 3', for the lagging strand, semi-discontinuous replication is performed and the DNA fragments are later joined together by DNA ligase. DNA polymerases (Pol) catalyze DNA strand extension (Caruthers *et al*., 2002). In *E. coli*, Pol I and Pol III have both polymerase and exonulcease activities, and the latter functions as a proofreading mechanism which contributes to the high fidelity of DNA replication, with only one mismatching occurring per 10^8 base pair replication (Rothwell *et al*., 2005).

RNAs are classified according to their functions, including decoding RNA which is messenger RNA (mRNA) and non-decoding RNA. mRNA serves as the template for protein synthesis on the ribosome. Non-decoding RNA includes transfer RNA (tRNA), ribosomal RNA (rRNA), small interfering RNA (siRNA), micro RNA (miRNA), small nuclear RNA (snRNA), etc. tRNAs recognize the complementary triplet sequences of mRNA through codon-anticodon interactions and deliver specific amino acids that incorporate into nascent protein chains. tRNA has an L-shaped structure and is about 60

Å in length from its elbow region to the anticodon region (Fig 1.1). The amino acid is covalently attached to the CCA- end of tRNA, in a reaction catalyzed by an aminoacyl-tRNA synthetase. There are two classes of aminoacyl-tRNA synthetases, denoted Class I and Class II, with both a catalytic and an editing site to ensure the accuracy of this process (Nureki *et al*., 1998). Another non-decoding RNA, denoted rRNAs account for ~ 60% of the ribosome by weight.

According to the central dogma (Fig 1.2), the base sequences of DNA are copied into mRNA during the transcription process (Crick *et al*., 1970). mRNA then directs protein synthesis by having the ribosome translate its nucleotide sequence into an amino acid sequence. The transcription of DNA is carried out by RNA polymerases using nucleotides including adenine (A), cytosine (C), guanine (G) and uridine (U) (Cramer *et al*., 2002). Unlike DNA replication, RNA synthesis is initiated at a specific site called the promoter region and the single strand of mRNA is extended from 5' to 3'. Posttranscriptional processing alters certain features of the primary transcript and the transcripts are subjected to several modifications, for instance, 5' capping, poly (A) tail addition and splicing for eukaryotic mRNA transcripts (Black. *et al*., 2003; Nishikura *et al*., 2006; Wahl *et al*., 2009). The transcription process is rapid, with the *in vivo* rate of 20 to 50 nucleotides per second at 37 °C. However, the accuracy of transcription is one out of 10^4 mis-transcribed, which is much lower than replication. Three consecutive mRNA nucleotides code for a particular amino acid. Protein synthesis is carried out on the ribosome, which we will discuss in detail in **Section 1.3.**

1.2 Ribosome components

The ribosome is a ribonucleoprotein particle which is composed of a large and a

small subunit. The ribosome is built of two-thirds rRNA and one third ribosomal proteins (Table 1.). The *E. coli* ribosome, which has been extensively investigated, is a 2.5 MDa ribonucleoprotein assembly with a diameter of ~ 250 Å and a sedimentation coefficient of 70S, where S stands for the Svedberg unit of sedimentation velocity. The complete 70S ribosome is formed from 50S and 30S subunits (Kaltschmidt *et al*., 1970). The 30S subunit consists of 16S rRNA (about 1500 nucleotides) together with 21 proteins. The 50S contains 23S rRNA (about 3000 nucleotides), 5S rRNA and 34 proteins. Their eukaryotic counterparts are termed 60S and 40S, which together form an 80S ribosome.

1.3 The prokaryotic translation cycle

In bacteria, protein synthesis can be divided into three major stages including initiation, elongation and termination, which requires correlated movements among ribosomal proteins, rRNA, protein factors and tRNAs (Fig 1.3).

1.3.1 Initiation of protein synthesis

The initiation step requires mRNA, the initiator tRNA fMet-tRNA^{fMet} and initiation factors 1-3 (IF 1-3). In the initiation step, mRNA binds to the 30S subunit on the ribosome at the anti Shine-Dalgarno (SD) sequence of 16S rRNA that is complementary to an SD sequence in the mRNA. The initiator tRNA fMet-tRNA^{fMet}, positioned in a P-like site of the 30S subunit, forms codon-anticodon interactions with the start codon. The binding site of IF-1 partially overlaps with the decoding center, suggesting that IF-1 does not only assist IF-3 binding but also prevents the aminoacyl tRNA binding at this premature stage (Moazed *et al*., 1995). IF2 is a GTPase and it binds with GTP and fMet-tRNA^{fMet} to form a ternary complex (Boelens *et al*., 2002; Tsai *et al*., 2012). IF3 helps to dissociate vacant 70S ribosomes resulting from protein synthesis termination and

prevents the premature docking of 50S subunit onto the 30S subunit. During the initiation process, IF3 first binds to the 30S subunit, followed by the association of mRNA, IF1, IF2, and initiator tRNA to form the 30S initiation complex (30SIC). The release of IF1 and IF3 promotes the 30SIC and 50S subunit joining to form the 70S initiation complex (70SIC), followed by IF2 catalyzed GTP hydrolysis, Pi release, and IF2·GDP dissociation. This results in the initiator tRNA fMet-tRNA^{fMet} moving to the P-site of the 70S ribosome, ready for the next stage of the elongation reaction.

1.3.2 Peptide elongation

The elongation cycle can be divided into three stages, including decoding, peptide bond formation and translocation (Schmeing *et al*., 2009a). At the beginning of this cycle, the ribosome contains a peptidyl-tRNA in the P-site, with an empty A-site. EF-Tu delivers the cognate aminoacyl tRNA to the mRNA codon in the A-site of the ribosome in the form of ternary complex (TC: aa-tRNA·EF-Tu·GTP) (Pape *et al*., 1998; Rodnina *et al*., 1994). The TC complex first binds to the L7/L12 stalk and the anticodon of tRNA penetrates into the decoding center on the 30S subunit with the acceptor arm and EF-Tu interacting with the GTPase activation center on the 50S subunit (Schmeing *et al*., 2009b). As a result, tRNA is said to be in the A/T state, in which it displays a distorted conformation relative to the structure of tRNA bound within either a TC or free in solution. The cognate codon-anticodon interaction at the decoding center triggers conformational changes in both tRNA and the ribosome complex which are later transmitted to the interface of EF-Tu and tRNA (Voorhees *et al*., 2010). After fast GTP hydrolysis and Pi release, EF-Tu·GDP dissociates from the ribosome and the A/T tRNA is accommodated into the A/A site. Decoding is followed by fast peptide bond formation,

leaving deacylated-tRNA in the P site. Both structural work (Agirrezabala *et al*., 2008; Fu *et al*., 2011) and kinetic studies, including ensemble measurements (Dorner *et al*., 2006) and single molecule experiments (Blanchard *et al*., 2004b; Blanchard *et al*., 2004a; Chen *et al*., 2011a; Fei *et al*., 2008) show that classic (A/A, P/P) and hybrid (A/P, P/E) tRNA binding states interconvert reversibly prior to EF-G·GTP binding. EF-G binds to the L7/L12 stalk on the ribosome, sharing the same binding site as EF-Tu (Gao *et al*., 2009; Schmeing *et al*., 2009b). Upon EF-G·GTP binding, rapid GTP hydrolysis is triggered, followed by Pi release. The energy generated from this process promotes unidirectional movement of tRNAs, together with mRNA, from the A-, P- sites to the P-, E-sites, in a process that proceeds via at least two intermediates (Pan *et al*., 2007). This leaves an empty A-site, which is ready for the next cycle of elongation.

1.3.3 Termination of protein synthesis

The elongation cycle continues until a stop codon (UAA, UAG or UGA) moves into the A-site, signaling translation termination. RF1 (Class 1 release factor, recognizing UAA, UAG) or RF2 (Class 1 release factor, recognizing UAA, UGA) reads the stop codon, resulting in conformational changes of conserved bases (G530, A1492 and A1493) in the decoding center (Korostelev *et al*., 2008; Laurberg *et al*., 2008; Weixlbaumer *et al*., 2008). The conserved GGQ motif on RFs is positioned in the PTC and promotes the hydrolysis of peptidyl tRNA in the P-site, followed by peptide chain release from the ribosome (Laurberg et al., 2008; Weixlbaumer et al., 2008). RF3, a Class II RF binds to the ribosome in the GTP form and, accompanied by GTP hydrolysis (Zavialov *et al*., 2002), destabilizes RF 1/2 binding, accelerating their dissociation from the ribosome. Then RF3 dissociates, leaving inactive mRNA and deacylated tRNA bound to the

ribosome. This inactive complex is recycled into 30S and 50S subunits, free mRNA and tRNA, assisted by ribosome recycling factor (RRF) and EF-G (Franckenberg *et al*., 2012; Hirashima *et al*., 1973). Then IF3 binds to the ribosome to the 30S subunit (Hirokawa *et al*., 2008; Karimi *et al*., 1999), ready for the next round of translation.

1.4 Ribosome structure

Elucidation of ribosome structure is a daunting task due to its size and lack of symmetry. The ribosome structure initially began to emerge via electron microcopy but with a low resolution (Hall *et al*., 1959). An early view of single particle reconstruction using cryo-EM came in 1986 (Frank *et al*., 1986) and structures with better resolution (below 10 Å) were reported by Valle et al. in 2003. With advanced experimental techniques and data refining methods, high resolution structure of 30S and 50S structures at atomic resolution, determined by X-ray crystallography study (~ 3 Å), were first reported in 2000 as the efforts from several groups (Ban *et al*., 2000; Carter *et al*., 2000; Harms *et al*., 2001; Schluenzen *et al*., 2000; Wimberly *et al*., 2000). In 2001, Noller group reported the first low resolution (5.5 Å) 70S ribosome structure from *Thermus thermophilus* containing mRNA, A-, P- and E-site tRNAs (Yusupov *et al*., 2001), showing that the core of the interface between 30S and 50S is mainly made up of RNA with protein located at the periphery.

The 5'and 3' domains of the 16S RNA are located in the body and head of the 30S subunit, respectively, with the central domain located in the platform region (Fig 1.4). There are three long helices in 30S subunits, h44, h16/17, and h7, with most of the small ribosomal protein located on the exterior side. The primary role of 30S is to bind mRNA and tRNA, providing the location for the decoding process, which occurs at the upper

part of 30S body and lower part of the head (Ban *et al*., 2000; Schluenzen *et al*., 2000; Wimberly *et al*., 2000) with nucleotides 1492 to 1498 and 1302 to 1408 of h44 forming parts of the A- and P- tRNA sites. 50S has a stable core structure with a strong mobility of the protuberances, for instance, the L7/L12 stalk and the L1 stalk (Fig 1.5, Fig 1.6). The six domains of 23S RNA are interwoven and the 5S RNA is located in the center of the protuberance (Harms *et al*., 2001). There are three tRNA binding sites on the ribosome: the A site for the incoming aminoacyl-tRNA, the P site for peptidyl-tRNA and the E site for the deacylated tRNA to exit from the ribosome after the elongation cycle (Schmeing *et al*., 2009a; Yonath *et al*., 2010). The tRNA binds at the 30S:50S interface, forming interactions with the decoding center of 30S and the peptidyl transferase center (PTC) on the 50S subunit, and moves through a tunnel from the A site located close to the L7/L12 stalk to the E site located close to L1 stalk in a stepwise manner during translocation (Fig 1.6). mRNA binds to the small unit between the platform and the head region with 5' end of mRNA, forming contacts with the back of the platform, and wraps around the neck of 30S to place the nucleotides into A, P and E sites (Yusupov *et al*., 2001).

High resolution (~ 3 Å) structures of 70S ribosome were obtained successfully by both Cate *et al*. and Ramakrishnan *et al*. in 2005 and 2006, separately (Schuwirth *et al*., 2005; Selmer *et al*., 2006). Cate et al. reported two ribosome structures with a detailed view of the interface of 50S and 30S as well as the conformation of the PTC. By defining one structure as the standard, the comparison between the two structures indicated two types of motions of the 30S subunit, including swivelling of the head of 30S ribosome ~ 6° and the rotation movement of 30S relative to 50S subunit (Fig 1.7). The 2006 paper

provided a detailed study of the ribosome interactions with mRNA, cognate A-, P- site tRNAs and non-cognate E-site tRNA, suggesting that a metal ion stabilized kink structure of mRNA is potentially important to prevent mRNA slippage. Since then, several high resolution X-ray and cryo-EM structures have been reported, focusing on revealing different aspects of translation, including mRNA decoding (Demeshkina *et al*., 2012; Jenner *et al*., 2010), translocation (Agirrezabala *et al*., 2008; Connell *et al*., 2008; Frank *et al*., 2007; Frank *et al*., 2000; Julián *et al*., 2008; Ratje *et al*., 2010) and termination (Korostelev *et al*., 2008; Laurberg *et al*., 2008).

For mRNA decoding, by comparing the crystal structures of the ribosome with uncharged cognate tRNA, or with a near-cognate tRNA, or without the A-site tRNA, Yusupova and coworkers proposed a proofreading mechanism, suggesting that this process begins with monitoring the tRNA anticodon loop, followed by the elbow region of tRNA being examined by rRNA and ribosomal protein on the 50S subunit to decide if the acceptor end of tRNA is to be accommodated or not.

During translocation, the ribosome undergoes a large scale conformational rearrangement. Frank *et al*. (2000) reported a cryo-EM structure of 70S ribosome from *E. coli*, showing that EF-G binding and GTP hydrolysis promote a ratchet-like rotation of 30S relative to 50S (Frank *et al*., 2000; Zhang *et al*., 2009). This movement of the ribosome is believed to couple with the formation of hybrid state tRNAs but can be decoupled with the addition of antibiotics, e.g., viomycin. The L1 stalk undergoes a closure movement to form interactions with the deacylated P-site tRNA and such interaction persists throughout translocation (Fei *et al*., 2008). A spontaneous ribosome ratcheting movement (~ 8 to 10 degree) was observed with tRNAs in A/P, P/E hybrid

states by Julian *et al*. (2008) and Agirrezabala *et al*. (2008), separately. Ratje *et al*. (2010) presented two cryo-EM structures of EF-G-ribosomes complex from *Thermus thermophilus* and one of the characterized structures containing a partly translocated tRNA. A swivelling movement of 30S head stabilized by Domain IV of EF-G, was described and this movement was believed to be coupled with translocation and unratcheting of the 30S body(Ratje *et al*., 2010). This result provides a new insight into the structure of translocation intermediates.

Concerning the termination process, Laurberg *et al*. reported a structure of 70S ribosome from *Thermus thermophilus* with release factor 1(RF1), P-, E- site tRNAs and mRNA containing stop codon UAA at 3.2 Å resolution, suggesting that RF1 interaction with the PTC is stabilized by the A-site of 30S, and repositioning of GGQ motif promotes hydrolysis of peptidyl-tRNA (Laurberg *et al*., 2008). Noller and coworkers (2008) obtained 70S ribosome with release factor 2 (RF2), P-, E- site tRNAs and mRNA containing a UAA stop codon. This high resolution structure (3 Å) supports the idea that the conformational changes transmitted from the decoding center to the PTC as the result of recognition of the stop codon promote the docking of GGQ motif into the PTC to catalyze peptidyl-tRNA hydrolysis (Korostelev *et al*., 2008).

1.5 Prior results of special pertinence to work presented in this thesis

Previous research has been heavily focused on the pre-equilibrium states of EF-G catalyzed translocation, leaving the real time dynamics, especially how EF-G first interacts with the A-site tRNA or with ribosomal protein in the GTPase associated center (GAC) within the pretranslocation complex, not fully elucidated. In my work, we want to

show how EF-G correlates its movements with tRNAs, and with ribosomal protein to promote different sub-steps of translocation.

1.5.1 EF-G structures in solution or bound to the ribosome

Of particular interest is the structure of EF-G under different conditions, including the structures of EF-G in solution (AEvarsson *et al*., 1994; al-Karadaghi *et al*., 1996; Czworkowski *et al*., 1994; Hansson *et al*., 2005), EF-G bound to the ribosome (Brilot *et al*., 2013; Chen *et al*., 2013b; Gao *et al*., 2009; Pulk *et al*., 2013; Ramrath *et al*., 2013; Tourigny *et al*., 2013; Zhou *et al*., 2013; Zhou *et al*., 2014) and of EF-G-2, a homolog of EF-G bound to the ribosome (Connell *et al*., 2008). In 1994, two crystal structures of EF-G from *Thermus thermophilus*, either lacking any guanine nucleotide (AEvarsson *et al*., 1994) or with GDP (Czworkowski *et al*., 1994) were reported separately. These two papers provided the fundamental information of EF-G structure. EF-G has overall dimensions of 50 × 60 × 118 Å and five domains. Its GTP binding domain has a core structure which is similar to those of other GTPases. EF-G has a unique inserted domain about 90 residues in length. The overall EF-G·GDP structure resembles the structure of the ternary complex, with Domains I, II resembling EF-Tu in the GTP form and Domains III, IV and V resembling tRNA. Al-karadaghi *et al*. reported another EF-G·GDP structure and compared this structure with nucleotide-free EF-G structure. The results imply that upon GDP release, the phosphate binding loop (P-loop) in the G domain of EF-G undergoes a conformational change which can be transmitted to other parts of EF-G and prepares EF-G for next round of GTP binding. Hansson *et al*., 2005 solved the structure of the T84A EF-G mutant, which is located in the G domain, bound with non-hydrolysable GTP analogue GDPNP, providing the first structure of EF-G conformation

in the GTP form. With the improved experimental techniques, some well-ordered ribosome crystal structures were obtained and brought new insights into the structure of ribosome-bound EF-G. EF-G binds to the ribosome subunit interface: Domain I binds to the sarcin-ricin loop; Domains II and III bind to h15 of 16S rRNA and S12 of 30S; Domain IV binds to h23 of 16S rRNA and the mRNA; Domain V binds to L11 stalk of 50S. Gao *et al*. (2009) presented a crystal structure of ribosome bound EF-G with the antibiotic fusidic acid (FA) in the posttranslocation state at 3.6 Å resolution. In this work, EF-G was trapped in an intermediate conformation between guanosine triphosphate and guanosine diphosphate states with loops I and II on G domain in a conformation similar to the GDP and GTP forms, respectively. In 2013, three ribosome-bound EF-G structures were published in Science. Cate and coworkers reported an EF-G-ribosome complex with non-hydrolyzable GTP analogue GDPCP at 3 Å. Binding of EF-G in the GDPCP state orders the switch regions in the GTPase associated center (GAC) compared to GDP state. Also, Domain II of EF-G moves about 7 Å toward Domain III and Domain IV is positioned into the A-site decoding center but without contacts with the 30S head, such that the presence of EF-G most likely precludes tRNA occupancy. EF-G-ribosome structure with a non-hydrolyzable GTP analog GDPCP and P/E tRNA was obtained at 2.9 Å (Tourigny *et al*., 2013). Domain IV of EF-G was observed to be in an intermediate conformation which was between ribosome free EF-G and EF-G-ribosome in the post state. As was found by Pulk *et al*., an ordered structure stabilized by the sarcin-ricin RNA loop of 50S in the GAC was obtained and the conformation of conserved residues in the GTPase active site was different from both the ribosome-free and other ribosome-bound structures. Fusidic acid bound to EF-G in a position that overlapped with switch loop I of

G domain on EF-G in the GTP form and stabilized contacts between Domains I and II (Zhou *et al*., 2013). Although all these high resolution structures provide a detailed view of the ribosome bound EF-G structure, especially Domain I which catalyzes GTP hydrolysis and Domain IV which extends to the decoding center, all of them lack the A-site tRNA and are from either the posttranslocation state or an intermediate state, leaving the pretranslocation state not fully elucidated. Since 2013, two papers have been published with EF-G-ribosome in a PRE-like state. Cryo-EM reconstruction of the pretranslocation complex was obtained with viomycin (VIO) and FA to increase the binding stability of the A-site tRNA. Although this structure is not of high resolution (7.6 Å), a distinct EF-G conformation which is different from all previously characterized EF-G structures was observed, suggesting that EF-G undergoes a structural rearrangement during translocation. Domain IV of EF-G is outside the A-site of 30S and the tip of Domain IV makes an extensive contact with the anti-codon loop of the A-site tRNA. Compared with EF-G-ribosome complex in the posttranslocation state (Gao *et al*., 2009), the tip of Domain IV in this work is 20 Å farther from the A site, and a rotation about 20° around the sarcin-ricin loop was observed to avoid a steric clash of Domain IV with the A-site tRNA. A more recent published result (Zhou *et al*., 2014) improved the resolution of the EF-G-ribosome structure in a PRE-like state to 3.8 Å, but in the presence of antibiotics, with the deacylated P-site tRNA partly moving to a pe/E site and the A-site peptidyl tRNA to an ap/ap state, revealing how the rearrangement of rRNA promotes tRNA movements during translocation.

1.5.2 Structural analogs of the active EF-G-ribosome structure

As Domain IV of EF-G has a steric clash with the A-site tRNA, the stable structure

of EF-G-ribosome in a pretranslocation state in the absence of antibiotics is not fully characterized. Such a structure would be useful in choosing sites of fluorescent probe introduction into EF-G for FRET studies. Here, we will briefly discuss EF-Tu-ribosome and EF4-ribosome structures which can be considered as analogs of ribosome bound EF-G.

1.5.2.1 EF-Tu-ribosome structure

EF-Tu is elongation factor Tu which delivers aminoacyl tRNA to the ribosome. EF-Tu has three domains. Domain I contains a nucleotide binding site and catalyzes GTP hydrolysis. Domains II and III regulate the interaction of Tu with antibiotics and with EF-Ts which catalyzes the exchange between GDP and GTP on EF-Tu. Aminoacyl tRNA binds to the interface of Domain I and II of EF-Tu, with the acceptor stem-loop contacting Domains I and II and the T-stem contacting Domain III (Nissen *et al*., 1995). In 2009, a high resolution (3.6 Å) EF-Tu-ribosome structure with kirromycin and paramomycin was reported (Schmeing *et al*., 2009b). This structure shows a detailed picture of the distortion of tRNA, which allows the tRNA to interact with both the decoding center at the 30S subunit and the binding site on EF-Tu. Another high resolution EF-Tu-ribosome structure (3.2 Å) was reported in 2010 with paramomycin and GDPNP (Voorhees *et al*., 2010). EF-Tu is in an active conformation with the switch loop I showing an ordered structure and the catalytic histidine positioned to attack the γ-phosphate, which provides a mechanism for GTPase activation on the ribosome.

1.5.2.2 EF4-ribosome structure

EF4 (Lep A) is a highly-conserved GTPase which competes with EF-G for binding to the PRE complex and leads to a transient inhibition of elongation (Liu *et al*., 2011; Liu

et al., 2010; Qin *et al*., 2006). *E. coli* EF4 protein is made up of 599 amino acid residues with a weight of 67 kDa. EF4 exhibits a strong similarity with EF-G in structure, and the protein domains of EF4 are homologies of domains I, II, III, and V of EF-G, but neither G' or Domain IV is found in EF4. EF4 has a unique C-terminus which contains two β-strands and two helices. The lack of Domain IV makes the stable structure of the A site tRNA and EF4 on the ribosome possible. In 2008, Spahn *et al*. and Steitz *et al*. reported EF4 structure free of the ribosome (Evans *et al*., 2008) or bound to the ribosome (Connell *et al*., 2008), separately. The direct comparison between EF-G and EF4 structure indicates that the orientations of Domains III and V in EF4 are different from EF-G (~ 10° rotation relative to structure of H573A EF-G mutant), suggesting that the hinge region of Domains III, IV, and V on EF-G undergoes a large movement during translocation (Evans *et al*., 2008; Laurberg *et al*., 2000). With EF4, a tRNA state which has not been characterized before was obtained and denoted A/L tRNA. The anticodon loop of the A/L tRNA extends to the decoding center in a similar position as A/A tRNA. However, it deviates from the A/A tRNA conformation, pivoting around the anticodon loop with the largest distance displacement about 14 Å in T-loop and 13 Å in 5'-end (Connell *et al*., 2008).

1.5.3 Ensemble kinetic studies of EF-G catalysis of translocation

Ensemble kinetic studies of the ribosome primarily rely on site-specific labeling of different translation components. As translocation is of great importance to my work, here we will focus on discussing the ensemble kinetic studies of the EF-G catalyzed translocation process (Fig 1.8). The commonly used methods including introduction of fluorescently labeled ribosome components, GTP hydrolysis assays, peptide formation

assays and puromycin reactivity assays (Pan *et al*., 2007; Rodnina *et al*., 1997; Savelsbergh *et al*., 2003). EF-G·GTP binds to L7/L12 stalk on the ribosome (Diaconu el al., 2005), followed by a rapid GTP hydrolysis with a rate constant ~ 150 s^{-1}. Addition of the antibiotic viomycin, which inhibits translocation, does not slow down GTP hydrolysis, suggesting that GTP hydrolysis precedes translocation. A slower step with a rate constant of 25 s^{-1} measured by the fluorescence change of proflavin (prf) labeled A-site tRNA which is attributed to ribosome conformational changes termed the unlocking process (Savelsbergh *et al*., 2003) limits rates of mRNA-tRNA movement on the ribosome as well as Pi release. The substitution of GTP with its non-hydrolysable analog (i.e., GDPNP) largely reduces the rate constant of this process (50 fold slower, Rodnina *et al*., 1997; 6 fold slower, Zavialov *et al*., 2003; 5 fold slower, Pan *et al*, 2007). The intact structure and flexibility of Domain IV is of crucial importance as EF-G variants with Domain IV truncated, or with a Domain I-V cross-linked EF-G which limits the motions of Domain IV, induce only slow translocation and catalyze only single turnover (Savelsbergh *et al*., 2000). Although both mRNA-tRNA movement and Pi release are limited by unlocking, these two processes are independent of each other. This is confirmed by antibiotic studies, such as those showing that viomycin inhibits mRNA-tRNA movement, but allows Pi release (Peske *et al*., 2000; Savelsbergh *et al*., 2003). Both mRNA-tRNA movement and Pi release have to occur to allow subsequent steps, including relocking of the ribosome before EF-G·GDP dissociation. The dissociation process is important for multiple rounds of translocation. Substitution of GTP with GDPNP only allows single round translocation by preventing EF-G dissociation.

1.5.4 Single molecule FRET studies of elongation cycle

Protein synthesis is a highly dynamic process that involves multi-components. Although as we discussed above, the ensemble measurement provides great insights concerning the mechanism of translation, it is limited by ensemble averaging in bulk solution which may make it difficult to detect important intermediates or conformational changes of ribosome components. Measurement at the single molecule level provides a powerful tool as it can reveal the population distribution for heterogeneous species without averaging over all populations. As my work is based on single molecule fluorescence studies, we will focus on discussing single molecule fluorescence or fluorescence resonance energy transfer (FRET) results applied to the ribosome complexes during translation. Single molecule fluorescence experiments can reveal the movements of ribosome components or protein factors based on the fluorescence intensity differences in different local environments. As well, changes in FRET efficiency between two fluorophores attached to two ribosomal complex components can be used to monitor relative movement between the two components.

In 2004, two papers were reported by Puglisi and coworkers, focusing on tRNA dynamics on the ribosome. By using Cy3 labeled P-site fMet-tRNA^{fMet} and Cy5 labeled A-site Phe-tRNA^{Phe}, direct tRNA - tRNA FRET was observed, showing three FRET states, which are assigned to the codon recognition, GTPase-activated and accommodated states. Comparisons of FRET values reveal differences in intermediate state sampling upon cognate or near-cognate tRNA binding (Blanchard *et al.*, 2004a). The same fluorescent labels were introduced to elucidate tRNA dynamics. The A-site tRNA was observed to fluctuate between the classic and hybrid states. Peptide bond formation

modulates the fluctuation of tRNA between these two states, favoring the hybrid state (Blanchard *et al*., 2004b). The effects of different experimental conditions (e.g., Mg^{2+} concentration, acylation or not of aminoacyl-tRNA in the A-site tRNA) on tRNA equilibrium between classic and hybrid states were characterized, showing that when A-site tRNA is not acetylated, Mg^{2+} concentration does not shift the equilibrium, while if it is acetylated, the classic state is stabilized by a high Mg^{2+} concentration (Kim *et al*., 2007). A new hybrid intermediate state was identified by Blanchard and coworkers with A/A, P/E site tRNAs and expanded previous reported tRNA states (Munro *et al*., 2007). FRET studies of ribosome dynamics and correlating ribosome tRNA movements have been carefully investigated since 2007. By engineering extended rRNA hairpins, which allows site-specific hybridization of fluorescently labeled oligonuleotides, 30S and 50S were labeled to monitor ribosome intersubunit rotations (Chen *et al*., 2013b; Marshall *et al*., 2008b; Marshall *et al*., 2008a). L1 stalk motions during translocation were later characterized. Interestingly, L1 stalk shows equilibrium between open and closed conformations, and only interacts with the P/E site tRNA in the closed conformation. EF-G binds to the hybrid state and shifts L1 equilibrium to favor the closed form, collaborating allosterically with L1 to direct tRNA movements along the translocation trajectories (Fei *et al*., 2009; Fei *et al*., 2008). In contrast to Fei's results that EF-G only binds to tRNAs in the hybrid state, Chen from our group monitored tRNA-tRNA and tRNA-L11 FRET, and these FRET results suggest that EF-G binds to both hybrid and classic tRNAs, which is later confirmed by work from Puglisi group in 2013. Chen *et al*. (2011) also observed that translocation starting with classic tRNAs proceeds via a transient intermediate hybrid state (lifetime~ 80 ms), in agreement with the ensemble

results of *Pan et al*. (2007).

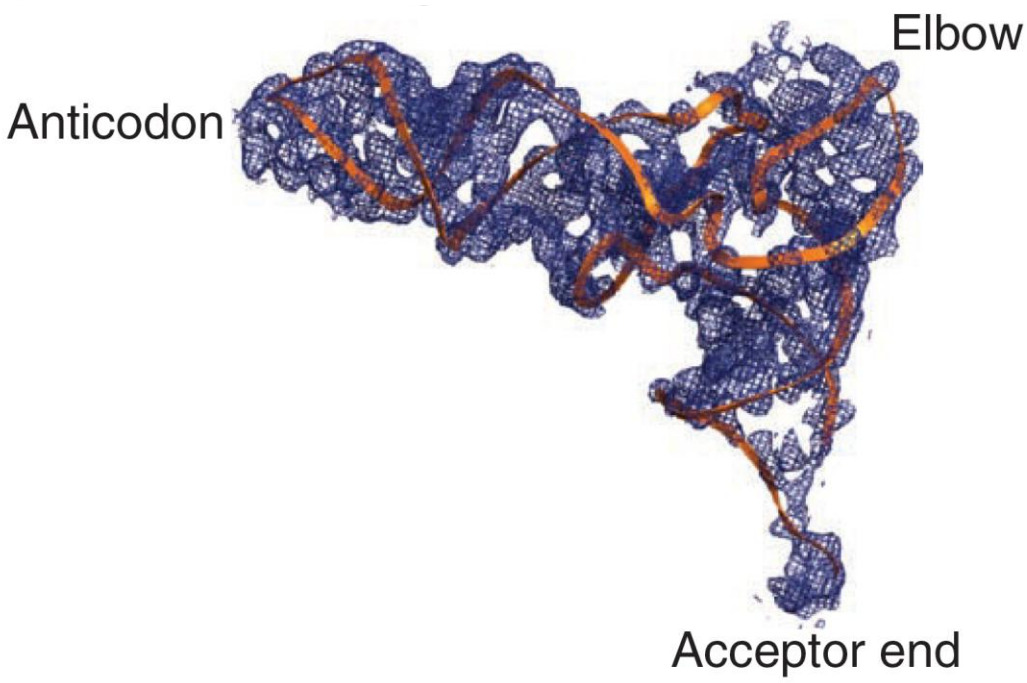

Figure 1.1 Overview of tRNA tertiary structure. (Adapted from Jenner et al., 2010)

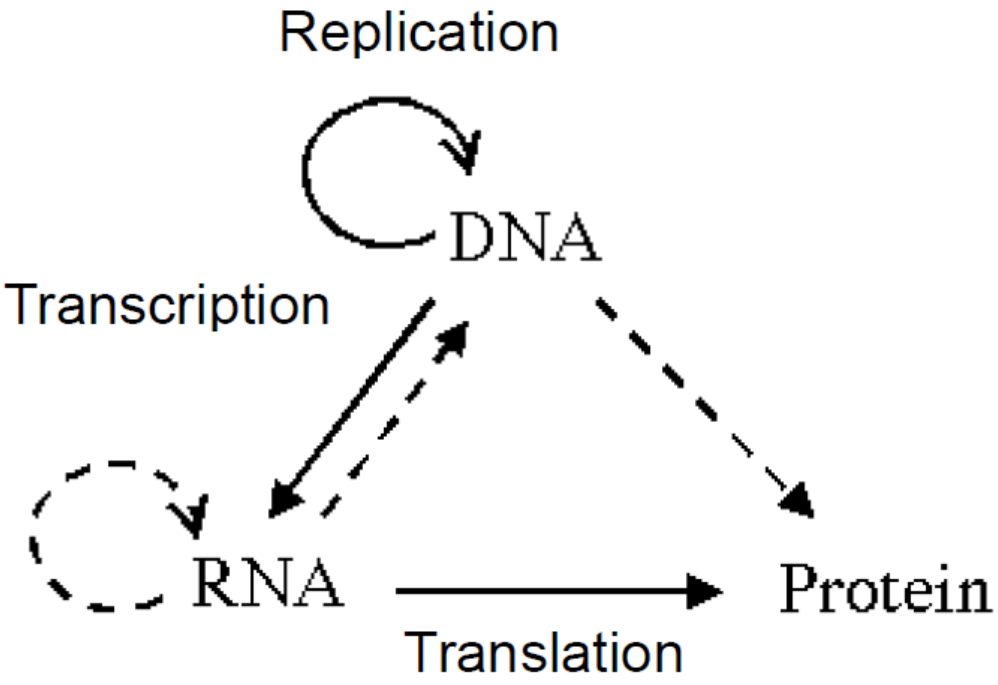

Figure 1.2 Central dogma of molecular biology. (Adapted from Crick et al., 1970).

Ribosome/subunit	70S	50S	30S
Molecular weight (kD)	2520	1590	930
rRNA components	23S, 16S 5S	23S and 5S	16S
Number of nucleotides in rRNA	4566	23S, 2904 nts 5S, 120 nts	16S, 1542 nts
rRNA molecular weight (kD)	1664	1104	560
Number of ribosomal proteins	55	34	21
Protein molecular weight (kD)	857	487	370

Table 1.1 Components of *E. coli* ribosomes. This table is adapted from Voet et al., 2006

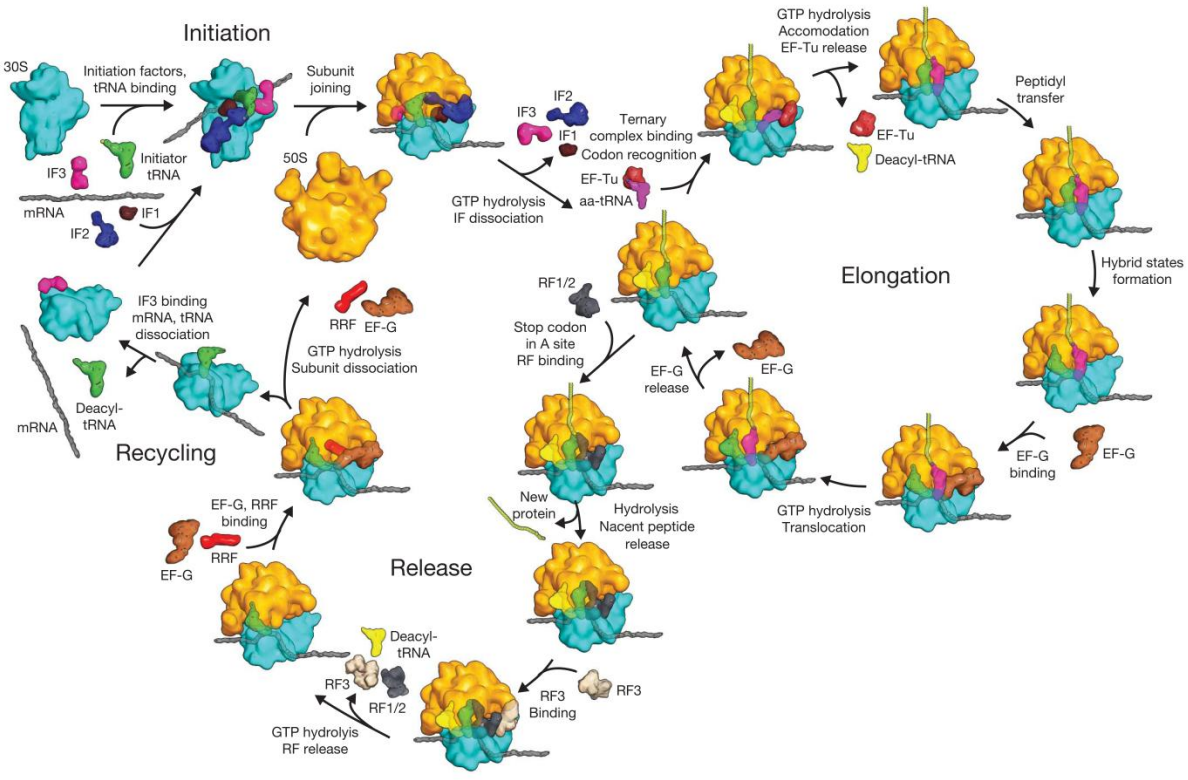

Figure 1. 3 Overview of bacterial translation. (Adapted from Schmeing et al., 2009).

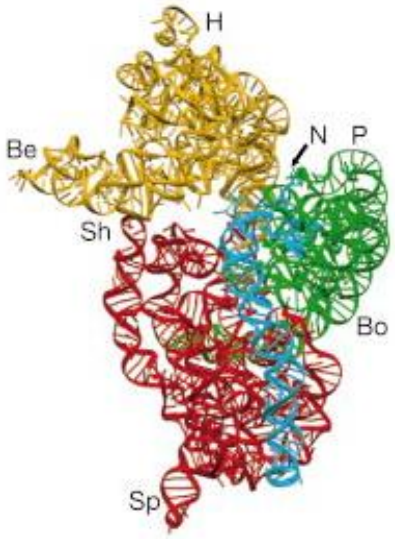

Figure 1.4 Stereo view of the tertiary structure of 16S RNA. H, head; Be, beak; N, neck; P, platform; Sh, shoulder; Sp, spur; Bo, body. 3' and 5' domain are colored yellow and red, respectively. (This figure is taken from Wimberly et al, 2000)

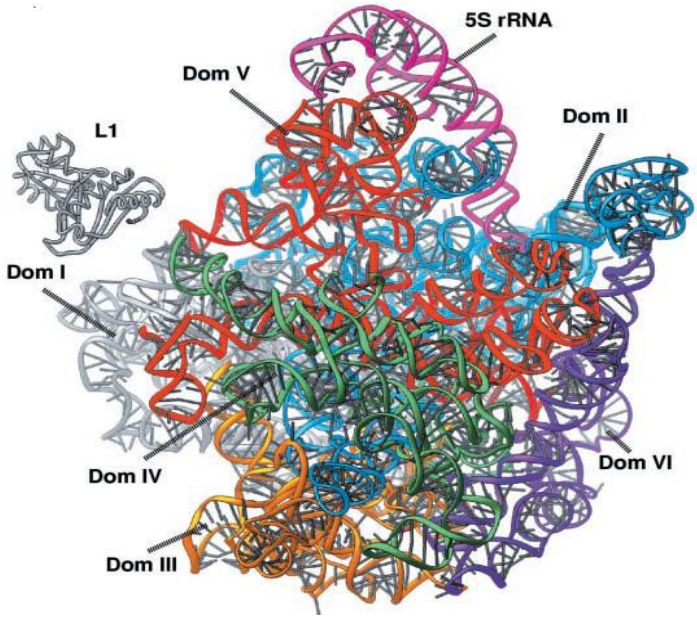

Figure 1.5 The tertiary structure of rRNA on the large ribosomal subunit. The subunit particle is in its crown view. (This figure is taken from Ban et al, 2000)

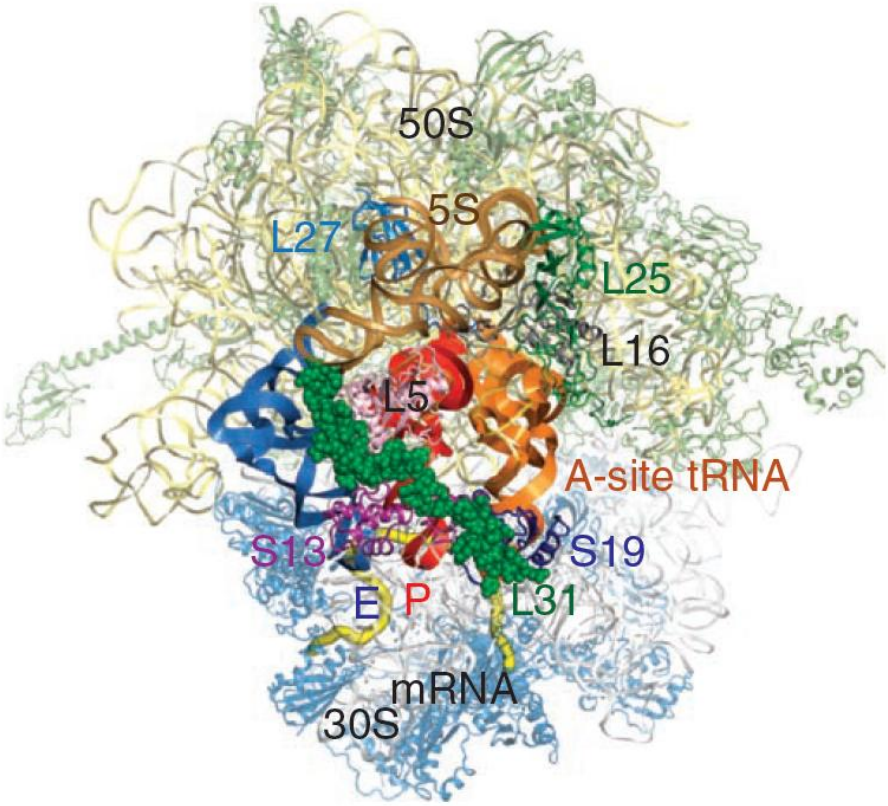

Figure 1.6 Overview of the ribosome structure. Ribosomal proteins and RNA of the small subunit (blue and gray) and large (green and yellow) subunits are showed in transparency. Three tRNAs (A-, P- E- site tRNAs) are colored in orange, red and blue. (Adapted from Jenner et al., 2010)

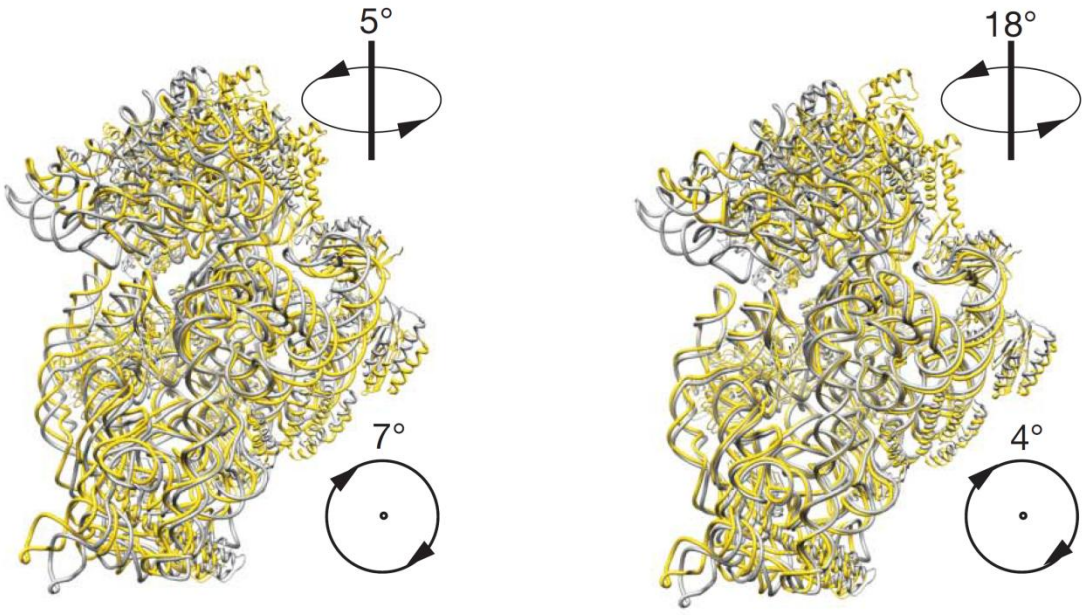

Figure 1.7 Overview of swiveling and ratcheting movements of 30S subunit. Two intermediate states I (left) and II (right) of 70S-EF-G-GDP-FAcomplex. The 30S subunit of intermediate states I and II (yellow) is compared with the 30S subunit of the POST (gray, Gao, et al., 2009) by aligning the respective 50S subunits. Arrows with numbers indicate the direction and magnitude of the head-swivel and inter-subunit rotation from the non-rotated state to the intermediate states I and II. (Adapted from Ratje, et al., 2010)

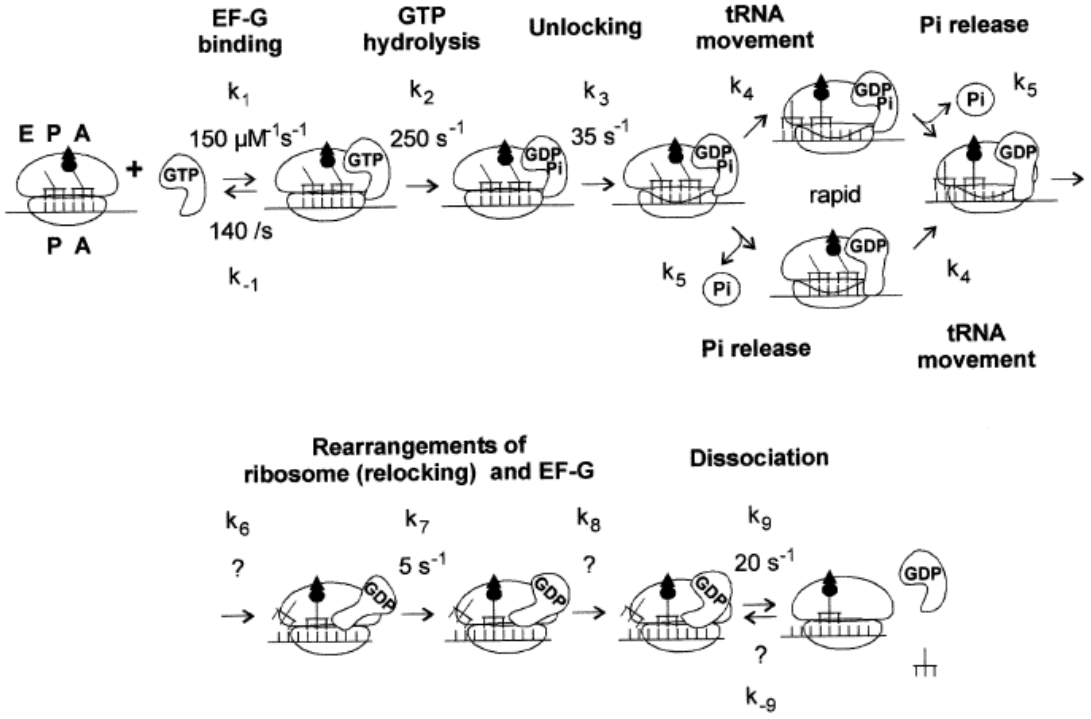

Figure 1.8 Kinetic model of EF-G catalyzed translocation. This figure is taken from Savelsbergh et al., 2003.

CHAPTER II MATERIALS AND METHODS

2.1 Materials

2.1.1 Buffers

All of the following buffers were prepared and the pH was adjusted at 25°C. Unless otherwise specified, experiments in Chapters 3-5 were performed in Buffers A (WB buffer) and TAM^{15}, respectively.

Buffer A (WB): 50 mM Tris-HCl pH 7.5, 70 mM NH_4Cl, 30 mM KCl, 7 mM $MgCl_2$ and 1 mM DTT.

TAM^{15} buffer: 50 mM Tris-HCl pH 7.5, 70 mM NH_4Cl, 30 mM KCl, 15 mM $MgCl_2$ and 1 mM DTT.

Polyamine buffer: 50 mM Tris-HCl pH 7.5, 70 mM NH_4Cl, 30 mM KCl, 15 mM $MgCl_2$ 5 mM putrescine 1 mM spermidine and 1 mM DTT.

Buffer B: 50 mM Tris-HCl pH 7.5, 70 mM NH_4Cl, 30 mM KCl, 7 mM $MgCl_2$ and 1 mM DTT, 100 μM GTP, 2 mM phosphoenolpyruvate, 100 μg/mL pyruvate kinase.

Buffer C: 20 mM Tris-HCl pH 7.6, 200 mM NH_4Cl, 10 mM $MgAc_2$.

IF3 lysis buffer: 50 mM Tris-HCl pH 8.0, 1 mM EDTA, 10 mM 2-mercaptoethanol, 0.2 mM PMSF.

IF3 purification buffer A: 10 mM Tris-HCl pH 8.0, 200 mM NaCl, 5% glycerol, 1 mM 2-mercaptoethanol.

IF3 purification buffer B: 10 mM Tris-HCl pH 8.0, 500 mM NaCl, 5% glycerol, 1 mM 2-mercaptoethanol.

L11 dialysis buffer A: 20 mM Hepes-HCl pH 7.0, 0.5 mM EDTA, 6 M urea, 6 mM 2-mercaptoethanol, 10 mM NaCl.

L11 lysis buffer: 50 mM NaH_2PO_4 pH 8.0, 300 mM NaCl, 0.5 mM Imidazole, 0.5 mM 2-mercaptoethanol

L11 purification buffer A: 20 mM Hepes-HCl pH 7.0, 0.5 mM EDTA, 6 M urea, 6 mM 2-mercaptoethanol, 10 mM NaCl, 10 mM $MgCl_2$.

L11 purification buffer B: 20 mM Hepes-HCl pH 7.0, 0.5 mM EDTA, 6 M urea, 6 mM 2-mercaptoethanol, 400 mM NaCl, 10 mM MgCl2.

L11 labeling buffer: 25 mM Tris-HCl pH 7.0, 100 mM NaCl, 2 mM EDTA.

EF-G washing buffer: 50 mM Tris-HCl pH 8.0, 300 mM NaCl.

EF-G washing buffer A: 50 mM Tris-HCl pH 8.0, 300 mM NaCl, 5 mM Imidazole.

EF-G washing buffer B: 50 mM Tris-HCl pH 8.0, 300 mM NaCl, 125 mM Imidazole.

EF-G elution buffer: 50 mM Tris-HCl pH 8.0, 300 mM NaCl, 300 mM Imidazole.

EF-G labeling buffer (M-labeling buffer): 25 mM Tris-HCl pH 7.0, 100 mM NaCl, 2 mM EDTA.

EF-G purification buffer A: 50 mM Tris-HCl pH 7.5, 10 mM $MgCl_2$, 50 mM KCl, 0.5 mM EDTA.

EF-G purification buffer B: 50 mM Tris-HCl pH 7.5, 10 mM $MgCl_2$, 1M KCl, 0.5 mM EDTA.

EF-G storage buffer: 50 mM Tris-HCl pH 7.5, 70 mM NH_4Cl, 30 mM KCl, 7 mM $MgCl_2$.

TBE buffer: 45 mM Tris-HCl pH=8.0, 45 mM H_3BO_3, 1 mM EDTA pH=8.0.

Hybridization buffer: 100 mM Tris-HCl pH 7.5, 1 M NaCl, 10 mM EDTA.

Aminoacylation buffer A: 100 mM Tris-HCl pH 8.0, 4 mM ATP, 20 mM $MgCl_2$, 1 mM EDTA (pH 8.0), 7 mM 2-mercaptoethanol, 10 mM KCl, 0.01 unit/μL thermostable inorganic pyrophosphatase, 720 μM formyl donor (see section 2.2.2.1), 67 μM [^{35}S]-fMet stock, 0.75 mg/mL *E. coli* aminoacyl- tRNA synthetases.

Aminoacylation buffer B: 100 mM Tris-HCl pH 8.0, 10 mM ATP, 50 mM $MgCl_2$, 2.5 mM EDTA (pH 8.0), 3 mM 2-mercaptoethanol, 200 μM [^{3}H]-Phe, 3 mg/mL yeast aminoacyl-tRNA synthetases.

Aminoacylation buffer C: 100 mM Tris-HCl pH 8.0, 4 mM ATP, 5 mM MgAc2, 250 μM EDTA (pH 8.0), 7 mM 2-mercaptoethanol, 150 μM [^{3}H]-Phe, 1 μM *E. coli* Phe-tRNA synthetase.

Aminoacylation buffer D: 100 mM Tris-HCl pH 8.0, 4 mM ATP, 20 mM $MgCl_2$, 1 mM EDTA (pH 8.0), 7 mM 2-mercaptoethanol, 0.005 unit/μL inorganic pyrophosphatase, 100 μM [^{3}H]Val or 67 μM [^{3}H]-Arg or 100 μM [^{3}H]-Lys, 3 mg/mL *E. coli* aminoacyl-tRNA synthetase.

Aminoacylation buffer E: 30 mM Hepes-HCl pH 7.0, 30 mM KCl, 15 mM MgCl2, 5 mM DTT, 4 mM ATP, 100 μM [^{3}H]-Val, 0.01 unit/μL thermostable inorganic pyrophosphatase, 3 mg/mL of *E. coli* aminoacyl-tRNA synthetase.

tRNA Phe purification buffer HPLC A: 20 mM NH_4Ac (pH 5.0), 10 mM $MgAc_2$ and 400

mM NaCl.

tRNA Phe purification buffer HPLC B: 20 mM NH_4Ac (pH 5.0), 10 mM $MgAc_2$, 400 mM NaCl, 30% EtOH.

2.1.2 Reagents

All the aqueous solutions and buffers were prepared using either double-deionized water (DDI) from Milli-A Water System (Millipore) and treated with a BioPak filter (Millipore) to remove the DNase, RNase and protease or diethyl pyrocarbonate DEPC-treated water (Fisher BioReagents^{TM}). Unless otherwise specified, all the concentrations mentioned are the final concentrations.

The following materials were purchased from the indicated suppliers: *E. coli* $tRNA^{fMet}$, *E. coli* $tRNA^{Phe}$, *E. coli* $tRNA^{Val}$, *E. coli* $tRNA^{Arg}$, *E. coli* $tRNA^{Lys}$, and yeast $tRNA^{Phe}$ (Chemical Block). Cy3/Cy5 maleimide dye and Cy3/Cy5 hydrazide dye (GE Healthcare Amersham^{TM}); S. O. C. medium and Top 10 competent cells (Invitrogen); Fusidic acid, IPTG, GTP, GDPNP, streptomycin, puromycin, glucose, phenyl-methanesulfonylfluoride (PMSF), tris(2-carboxyethyl)phosphine hydrochloride (TCEP), N-hydroxysuccinimide ester, folinic acid, glutathione and proflavin salt (Sigma Aldrich); Talon Superflow Metal Affinity Resin, NAP-5 column and pETZ24a plasmid (GE Healthcare); phosphoenolpyruvate (PEP), pyruvate kinase (PK), RNase T1, catalase and bulk tRNA from *E. coli.* MRE600 cells (Roche); Phusion DNA polymerase and DpnI (New England Biolabs); DNA purification kit and Ni-NTA Superflow resin (QIAGEN); BL21(DE3) competent cells and QuickChange site-directed Mutagenesis Kit (Stratagene); ampicillin and trichloroacetic acid (TCA) (Fischer Scientific); AG 50W-X8 cation exchange resin(Bio-Rad); thermostable inorganic pyrophosphatase (New England

BioLabs); PEG-succinimidyl valerate (Laysan Bio); Amicon Ultra ultrafiltration units, Ultrafree centrifugal filter unit, and nitrocellulose filters (Millipore).

2.2 Methods of preparation

2.2.1 Proteins

The cloned *E. coli* His-tagged proteins IF3 (N-terminal His-tagged), EF-G (C-terminal His-tagged), EF-Tu (C-terminal His-tagged), and ribosomal protein L11 (N-terminal His-tagged) were prepared, purified and labeled as previously reported (Pan *et al*., 2007; Seo *et al*., 2006).

2.2.1.1 Purification of IF3

All steps below were performed at 4 °C. 10 g of frozen BL21(DE3) IF3 cells were kept on ice for 10 min, and then resuspended in 30 mL of IF3 lysis buffer followed by French Press (12,000-14,000 psi) twice. The mixture was subject to centrifugation (10 K rpm, 30 min and SS-34 rotor) to pellet the cell debris. The supernatant was loaded onto a 10 mL Ni-NTA column (18 mm in diameter, 15cm in height) which was pre-washed with 60 mL of water and pre-equilibrated with 60 mL of IF3 lysis buffer.

The column was then washed by 60 mL of IF3 purification buffer A followed by 30 mL of IF3 purification buffer B. IF3 protein was eluted by using a hyperbolic imidazole gradient in IF3 purification buffer B (5 mM imidazole, 40 mL; 10 mM imidazole, 20 mL; 20 mM imidazole, 10 mL; 300 mM imidazole, 50 mL) and collected in fractions. Fractions with large amounts of IF3 were identified by 15% SDS-PAGE gel and pooled for dialysis against buffer A (Fig 2.1). IF3 was concentrated by an Amicon Ultra ultrafiltration units [molecular weight cutoff (MWCO): 10,000] and the concentration was determined by Bradford assay (Bradford *et al*., 1976).

2.2.1.2 Purification and labeling of WT-L11 and L11 (C38S/S87C)

L11 protein was grown and purified as previously reported (Seo *et al*., 2006). Wild-type and (C38S/S87C) double mutant N-terminal *E. coli* His-tagged L11 cells were grown in LB medium in the presence of 100 µg ampicillin/mL at 37 °C. 1mM final concentration of IPTG was added to the medium and the cells were grown for another 4 hours. The cell pellet was harvested by (10 K rpm, SS-34 rotor) centrifugation at 4 °C for 20 minutes each cycle, then fast frozen and stored in a -80 °C refrigerator. 14 g of pellet was dissolved in 20 mL of L11 lysis buffer with 3 µL of DNase I (2000 U/mg) for an hour. Cells were broken by French press (12,000 - 16,000 psi) twice and centrifuged at 15 K rpm, SS-34 rotor at 4 °C for 30 min twice. 12 mL of Ni-NTA Superflow resin (Qiagen) were placed into a plastic flex column **(**18 mm in diameter, 15cm in height**).** After the resin settled, the column was washed with water twice and pre-equilibrated with lysis buffer. The supernatant was loaded onto prepared Ni-NTA column and washed with 50 mL each of L11 elution buffers A and B. Then L11 was eluted with 50 mL of elution buffer C and the product was collected. These procedures were repeated once. Elution product by buffer C was analyzed by 5-14% SDS-PAGE gel (Fig 2.2, Lane 5). The product was dialyzed against L11 dialysis buffer at 4 °C overnight and purification buffer A at 4°C for 3 hours. After concentration (1 mL) using Amicon Ultra ultrafiltration units (MWCO Molecular weight cut-off: 10,000), crude L11 product was purified by a MonoS™ (5/50 GL) FPLC column and pure L11 was eluted using a linear gradient from L11 purification buffer A to L11 purification buffer B (Fig 2.2, Lanes 1 and 2). Then an Amicon Ultra ultrafiltration unit (MWCO: 10,000) was used to remove the urea and replace the buffer with L11 storage buffer to allow the proper folding of L11 protein. The final concentration of L11 was determined by Bradford assay (Bradford *et al*., 1976) and

adjusted by multiplying by 0.6 as the conversion factor (Congdon *et al*., 1993).

L11 labeling with either Cy3 or Cy5 was purified as reported (Chen *et al*., 2011a). Nap-5 column (bed volume 500 μL) was used to exchange buffer from L11 storage buffer to L11 labeling buffer. Nap-5 column was pre-washed by DDI water 6 times, then by L11 labeling buffer 6 times. 500 μL of L11 protein was loaded to the column and eluted by 1 mL of L11 labeling buffer. 100 μM L11 in 1 mL of labeling buffer was incubated with 300 μM fresh prepared TCEP for 40 min to free disulfide bonds formed by two cysteines, followed by addition of 500 μM Cy3 or Cy5 maleimide and incubated at room temperature in dark for 3 hours. The reaction was quenched with 3 μL of 14.3 βMe and the mixture was loaded onto MonoS™ (5/50 GL, bed volume 500 μL, diameter 5 mm) FPLC column for further dye protein separation and purification. Labeled L11 was eluted by using a linear gradient from L11 purification buffer A to L11 purification buffer B. Pure dye came out in the first 2 - 4 tubes and labeled product was washed out in later fractions. Different FPLC fractions were pooled and determined by 5-14% SDS-PAGE gel (Fig 2.3). Fractions 19 - 20 were collected and combined. An Amicon Ultra ultrafiltration unit (MWCO: 10,000) was used to further concentrate the products. L11 concentration was determined by Bradford assay as described above and corrected by multiplying a factor of 0.6. Dye concentration was determined by A_{550} for Cy3 and A_{650} for Cy5 (Extinction coefficients: 150,000 and 250,000 M^{-1} cm^{-1} for Cy3 and Cy5, respectively). Typical dye/L11 ratio was 0.8 - 0.9.

2.2.1.3 Purification and labeling of EF-G and the derivatives

2.2.1.3.1 Purification of EF-G

EF-G protein and its variants were grown and purified as previously reported in

published paper (Seo *et al*., 2006) and optimized conditions were explored. Expression vectors for C-terminal His-tagged *E. coli* EF-G were based on the pET-21a vector. EF-G plasmid (3 μL, 50-80 ng) was transformed into BL21 (DE3) competent cells (50 μL) and incubated on ice for 30 min. The cells were then incubated at 42 °C for 30 s, 250 μL of pre-warmed Super Optimal Broth (S.O.C.) medium were added, and the resulting mixture was maintained at 37 °C for one hour. The cell cultures were plated onto LB-Agar plate supplemented with 50 μg/mL of kanamycin and grown overnight at 37 °C. A single colony on the plate was picked and transferred to 5 mL LB medium containing 50 μg/mL kanamycin and incubated overnight at 37 °C. The cell culture was transferred to 100 mL of LB medium, then to 1L of LB medium at 37 °C in the presence of 50 μg/mL kanamycin (final concentration). Incubation was maintained until A_{600} was 0.4 larger than the initial value (generally A_{600} is ~0.4 - 0.6), followed by addition of 1 mM IPTG to induce over-expression of EF-G protein, and the incubation was continued for another 3 hours. The cell pellet was harvested by centrifugation at 4 °C for 20 min (7 K rpm, GS3 rotor). Cell pellets were fast frozen and stored at -80°C. 8 g of cell pellet was dissolved in 15 mL of EF-G elution buffer with 3 μL of lysozyme (50 units/mL) for an hour at 4 °C. Cells were broken by two cycles of French press (12,000 - 16,000 psi) and centrifuged at 15 K rpm with SS34 rotor at 4 °C for 30 min twice.

The supernatant was loaded onto a prepared Ni-NTA column (18 mm in diameter and 15 cm in height) and washed by 50 mL of EF-G elution buffers A and B. The EF-G protein fractions eluted by 50 mL of elution buffer C were collected and this purification procedure was repeated once. Sample was collected to run 5-14% SDS-PAGE gel (Fig 2.4, Lane 9) to confirm the presence of EF-G. The solution was dialyzed against EF-G

purification buffer A without $MgCl_2$ at 4 °C overnight and buffer A with $MgCl_2$ at 4 °C for four hours (MWCO Molecular weight cut-off dialysis membrane: 15,000). After concentration using Amicon Ultra ultrafiltration units (MWCO Molecular weight cut-off: 30,000), EF-G was further purified by self packed Q-Sepharose FPLC column (bed volume 1 mL). Purified EF-G protein was eluted using a linear gradient from EF-G purification buffer A to purification buffer B (Fig 2.5). Fractions with EF-G band, as determined by 5-14% SDS-PAGE (Fig 2.4, lanes 2 - 8), were pooled and dialyzed against WB buffer overnight at 4 °C. After concentrating by Amicon Ultra ultrafiltration units (MWCO Molecular weight cut-off: 30,000), EF-G concentration was measured by Bradford assay without correction factor applied.

2.2.1.3.2 Labeling of EF-G

EF-G was labeled with Cy3 or Cy5 maleimide. Nap-5 column (bed volume 500 μL) was used to exchange buffer from WB to EF-G labeling buffer and remove βMe which reacted with maleimide dye. Nap-5 column was pre-washed with DDI water and with EF-G labeling buffer 6 times separately. 500 μL of EF-G protein (334 μM) was loaded to the column and eluted by 1 mL of labeling buffer. The protein concentration after buffer exchange was measured by Bradford assay and diluted to 100 μM in 1 mL volume as the final concentration, which was incubated with a 5-fold molar excess of Cy3 or Cy5 maleimide dye for 3 hours at 37 °C in dark and then quenched by 3 μL of 14.3 M βMe. The mixture was further purified by self packed Q-Sepharose FPLC column as previously described. Fractions were collected and examined by 5-14% SDS-PAGE (Fig 2.6). Fractions containing EF-G were pooled and dialyzed against 1L of WB buffer overnight at 4 °C (MWCO membrane: 15,000). Amicon Ultra ultrafiltration units (MWCO: 30,000)

were used to concentrate the EF-G protein and the final concentration was determined by Bradford assay without any conversion factor applied. Dye concentration was determined by A_{550} for Cy3 and A_{650} for Cy5 (Extinction coefficients: 150,000 and 250,000 M^{-1} cm^{-1} for Cy3 and Cy5, respectively). Typical dye/EF-G ratio was 0.5 - 0.9, depending on which EF-G mutant was labeled.

2.2.1.3.3 Mutants of EF-G

2.2.1.3.3.1 PCR primer design

The Stratagene QuikChange site-directed mutagenesis kit was used to construct EF-G variants. The primers were designed according to the following principles (adapted from Stratagene QuikChange site-directed mutagenesis kit Manual):

1) Both of the mutagenic primers must contain the desired mutation and anneal to the same sequence on opposite strands of the plasmid.

2) Primers should be between 25 and 45 bases in length, with a melting temperature (*T*m) of ≥78°C. Primers longer than 45 bases may be used, but using longer primers increases the likelihood of secondary structure formation, which may affect the efficiency of the mutagenesis reaction. The following formula is commonly used for estimating the *T*m of primers:

$$T\text{m}=81.5 + 0.41(\%\ \text{GC}) - 675/N - \%\ \text{mismatch}$$

For calculating *T*m:

• *N* is the primer length in bases

• Values for % GC and % mismatch are whole numbers

For calculating *T*m for primers intended to introduce insertions or deletions, use this modified version of the above formula:

*T*m=81.5 + 0.41(% GC) - 675/*N*

where N does not include the bases which are being inserted or deleted.

The designed primer sequences can be found in Fig 2.7 with the mutant sites colored in red.

2.2.1.3.3.2 EF-G DNA purification

Wild type EF-G cell pellet was harvested as described above. Plasmid DNA was purified by using the QIAprep Spin Miniprep Kit (QIAGEN). (Procedures were adapted from QIAprep Miniprep Handbook)

1) Resuspend pellet bacterial cells in 250 μL Buffer P1 and transfer to a microcentrifuge tube.

2) Add 250 μL Buffer P2 and mix thoroughly by inverting the tube 4 - 6 times.

3) Add 350 μL Buffer N3 and mix immediately and thoroughly by inverting the tube 4 - 6 times.

4) Centrifuge for 10 min at 13,000 rpm (~17,900 x *g*) in a table-top microcentrifuge.

5) Apply the supernatants from step 4 to the QIAprep spin column by decanting or pipetting.

6) Centrifuge for 30 - 60 s. Discard the flow-through.

7) Recommended: Wash the QIAprep spin column by adding 0.5 mL Buffer PB and

centrifuging for 30 - 60 s. Discard the flow-through.

8) Wash spin column by adding 0.75 mL Buffer PE and centrifuging for 30 - 60 s.

9) Discard the flow-through, and centrifuge at full speed for an additional 1 min to remove residual wash buffer.

10) Place the QIAprep column in a clean 1.5 mL microcentrifuge tube. To elute DNA, add 50 μL Buffer EB (10 mM Tris-Cl, pH 8.5) or water to the center of each QIAprep spin column, let stand for 1 min, and centrifuge for 1 min. The concentration of purified DNA is measured by $\boldsymbol{A}_{260}$ (1 $\boldsymbol{A}_{260}$=50 ng/ μL) and about 50 -80 ng/ μL was obtained.

2.2.1.3.3.3 PCR amplification

Mutant strand synthesis reactions were performed by Thermal Cycler using the Stratagene QuikChange site-directed mutagenesis kit. 5 μL of 10× reaction buffer, 5 ng, 10 ng, 20 ng, 50 ng of wild type EF-G plasmid, 125 ng of primer 1, 125 ng of primer 2 (Fig 2.8), 1 μL of dNTP were mixed and double-distilled water (DDI H_2O) was added to a final volume 50 μL, followed by addition of 1 μL of 2.5 U/μL *PfuTurbo* DNA polymerase. The PCR machine was programmed for two segments: 1) one cycle at 95 °C for 30 sec; 2) eighteen cycles at 95 °C for 30 sec, at 55°C (or 60 °C, or 62 °C, 65 °C) for 1 min (annealing), and at 68 °C for 5.5 min (1min/kb of plasmid length). After the final cycle, the reaction was stopped and kept at 4 °C overnight. DpnI was added to digest the amplification products. 1 μL of 10 U/μL DpnI restriction enzyme, 4.5 μL of reaction buffer 4 and 40 μL of PCR amplification product were gently mixed at 37 °C for 1 hour to digest the parental supercoiled dsDNA. Nucleotides of dsDNA in EF-G were expected to be 5.2 Kb in length and final products were confirmed by 1% DNA Agarose gel in

TBE buffer, showing expected brand located between 5 Kb and 6 Kb (Fig 2.8). The desired PCR products were sequenced. The DNA plasmids confirmed by sequencing results were transformed and then purified as described in section **2.2.1.3.3.2**.

2.2.1.4 Purification of EF-Tu

EF-Tu protein was expressed and purified as previous reported (Liu *et al.*, 2014). Expression vectors for C-terminal His-tagged *E. coli* EF-Tu variants were based on the pET15b vector. EF-Tu plasmids (50 - 80 ng) were transformed into BL21(DE3) competent cells, and the strains was grown in Super Optimal Broth (S.O.C.) medium at 37 °C for one hour. The cell cultures were plated onto LB-Agar plate with 100 μg/mL of ampicillin and grown overnight at 37 °C. Single colony on the plate was inoculated into 6 mL of LB medium containing 100 μg/mL of ampicillin for overnight growth at 37 °C. The cell culture was transferred into 1 L of LB medium with 100 μg/mL of ampicillin for growth until A_{600} reached ~0.6 - 0.8. Protein expression was induced by addition of 1 mM IPTG and continued for another 3 hours at 37 °C. The cell pellet was harvested by centrifugation at 4 °C for 20 min each cycle (7 K rpm, GS3 rotor). The pellets were resuspended in 25 mL of EF-Tu purification buffer A and the mixture was magnetically stirred for 30 min at 4 °C. A second incubation at room temperature for 20 min was performed after addition of 3 μL of lysozyme (50 units/mL). Cell was broken by French press twice (12,000 - 14,000 psi) and centrifuged (4 °C, 20K rpm with SS34 rotor, 20 min) to remove the cell debris. The supernatant was mixed with Co(II)-Sepharose (Talon) resin (bed volume 3 mL), pre-washed twice with 30 mL of EF-Tu purification buffer A, and shaken at 4 °C for 1 hour. Resin bound with EF-Tu was collected by centrifugation (4 °C, 5K rpm with SS34 rotor, 5 min), washed twice by 30 mL of EF-Tu purification buffer A,

and transferred to a small gravity column (18 mm in diameter, 4 cm in height). The column was washed with 10 mL of EF-Tu purification buffer A, 10 mL of EF-Tu purification buffer B and 10 mL of EF-Tu purification buffer C, respectively. EF-Tu was eluted by EF-Tu elution buffer and the collected fraction was examined by 5-14% SDS-PAGE gel (Fig 2.9). Amicon Ultra ultrafiltration units (MWCO: 10,000) were used to concentrate the samples and replace the elution buffer with EF-Tu storage buffer. EF-Tu concentration was determined by Bradford assay without any conversion factor applied for correction.

2.2.2 tRNAs

2.2.2.1 Preparation of formyl donor

Formyl donor was prepared as described (Dubnoff *et al*., 1971). 25 mg of folinic acid was dissolved in 2.0 mL of 50 mM 2-mercaptoethanol, followed by addition of 1.0 M HCl 0.22 mL, and the mixture was reacted for 3 hours at room temperature. Some precipitation can occur during the reaction, which could be re-dissolved on gentle heating in a water bath set at 37 °C. Formyl donor concentration was determined by A_{355} (at 355 nm, 1 μmol/mL = 25 A_{355}). The product was then aliquoted for storage at -80 °C. Before being used for $tRNA^{fMet}$ aminoacylation, the pH of formyl donor was activated by adjusting to its neutral pH with 1/4 volume of 1 M Tris-HCl, pH 8.0 and incubating at room temperature for 15 min.

2.2.2.2 Formylaminoacylation of $tRNA^{fMet}$

Wild type commercial *E. coli* $tRNA^{fMet}$ was formylated by formyl donor and charged by bulk *E. coli* tRNA synthetase, synthetase S-100 (Kirillov *et al*., 1981). 7 μL of [^{35}S]-Met was mixed with 21 μL of 670 μM non-isotopic labeled Met and DDI water to form

Met stock in a total volume of 210 μL. 36 nmol of $tRNA^{fMet}$ was incubated in 2 mL of aminoacylation buffer A (which contains formyl donor) at 37 °C for 45 min. The reaction was quenched by 200 μL, 20% (w/w) KAc (pH=5.0), aliquoted in four tubes. The reaction mixture was extracted with 1:1 (v/v) phenol (Tris-saturated, pH 4.3, Fisher) once and 1:1 (v/v) chloroform once. Each time, the reaction mixture was centrifuged at 8 K rpm for 5 min (Table centrifuge, Thermo Scientific Micro 17, 24×15/2.0 mL rotor) and the upper aqueous layer was taken for EtOH precipitation. After addition of 50 μL of 20% KAc (pH=5.0), 1400 mL of 99% ethanol was added to the reaction mixture, then stored at -80 °C for 40 min and centrifuged at 13 K rpm for 25 min (Table centrifuge, Thermo Scientific Micro 17, 24×15/2.0 mL rotor).

The formylaminoacylated tRNA pellet was suspended in 1 mL of tRNA FPLC buffer A and further purified by FPLC using a self-packed column (bed volume, 1 mL) with Q-Sepharose resin. The final product was eluted by a gradient from tRNA FPLC buffer A (30 mL) to tRNA FPLC buffer B (30 mL) and the product was collected as determined by both UV peak position and radioactivity. The pooled fMet-$tRNA^{fMet}$ fractions were aliquoted in 500 μL, and 20% KAc pH 5.0 (50 μL) was added, followed by 1400 μL of ethanol. The reaction mixture was stored at -80 °C for 40 min and centrifuged at 13 K rpm for 25 min (Table centrifuge, Thermo Scientific Micro 17, 24×15/2.0 mL rotor). The resulting precipitate was collected and dissolved in 60 μL DEPC-treated water. The concentration of tRNA and charging efficiency was determined by A_{260} (1 unit A_{260} =1.8 μM) and radioactivity. Typical aminoacylation stoichiometry was 1100 - 1300 pmol/*A*260.

2.2.2.3 Aminoacylation of $tRNA^{Phe}$

Commercial $tRNA^{Phe}$ from yeast and *E. coli* was aminoacylated in the similar

procedures as in the preparation of fMet-tRNA^{fMet}, except that for yeast tRNA^{Phe} and *E. coli* tRNA^{Phe}, aminoacylation buffer A was replaced by aminoacylation buffers B and C, respectively. Typical aminoacylation stoichiometries were 550 - 700 pmol/*A*260, for both yeast and *E. coli* Phe-tRNA^{Phe}.

2.2.2.4 Aminoacylation of E. coli tRNA^{Arg}, tRNA^{Val}

Commercial tRNA^{Arg} and tRNA^{Val} from *E. coli* was aminoacylated in the similar procedures as above. Similar aminoacylation steps were applied expect that: 1) *E. coli* tRNA^{Arg}, 2 mL of reaction mix was in aminoacylation buffer D and the typical aminoacylation stoichiometry was 500 - 650 pmol/*A*260; 2) *E. coli* tRNA^{Val}, 2 mL of reaction mix was in aminoacylation buffer E and the typical aminoacylation stoichiometry was 1000 - 1200 pmol/*A*260.

2.2.2.5 Proflavin labeling fMet-tRNA^{fMet}

E. coli fMet-tRNA^{fMet} was fluorescently labeled by proflavin followed the protocol reported by Pan *et al*., 2007. The dihydrouridine residues on the D-loop of tRNA were reduced by $NaBH_4$ in 0.01 M KOH and replaced by proflavin. 32 nmol of uncharged tRNA were incubated in 40 mM Tris-HCl pH 7.5 and rapidly mixed with 35.8 μL of 100 mg/mL $NaBH_4$ (final concentration, 10 mg/mL). The reaction mixture was maintained on ice for 1 hour, with H_2 released every 10 min. The reduction reaction was quenched by adding 60 μL of 6 M HAc dropwise and three EtOH precipitations were performed to purify the tRNA pellet. After proper dilution, tRNA concentration was measured by A_{260} and stored at -80 °C. Formylmethionylation and purification were performed as described above. Product pellet was resuspended in 100 μL of H_2O and mixed with 1 mL of 0.52 mg/mL proflavin in 0.1 M HCOONa (pH 3.7) at 37°C for 45 min. After incubation, the

solution was adjusted to pH 7.5 by addition of 1/10 volume of 1 M Tris, and extracted twice with 1:1(v/v) phenol (Tris-saturated, pH 6.5). Labeled tRNA was EtOH precipitated twice after addition of 1/10 volume of 20% KAc (pH 6.5). Charging and labeling efficiencies were generally obtained as follows: 700 - 900 pmol/*A*260 and 0.9 - 1.1 prf/tRNA for $tRNA^{fMet}$.

2.2.2.6 $tRNA^{Phe}$ labeling with Cy3 or Cy5

Yeast $tRNA^{Phe}$ was labeled with Cy3 (Pan *et al*., 2008; Pan *et al*., 2009) or Cy5 (Kaur *et al*., 2011) as reported. $tRNA^{Phe}$ was reduced and aminoacylated as described above. Pellet from last EtOH precipitation was resuspended in 800 μL of HPLC buffer A and purified by phenyl RP-HPLC (RP-C18 column, 4.6 × 250 mm, Alltech) with a gradient of 0% to 30% ethanol in 20 mM NH_4Ac (pH 5.0), 10 mM $Mg(Ac)_2$ and 400 mM NaCl. Pooled fractions were combined and EtOH precipitated with 20% KAc (pH 5.0). The dried pellet was resuspended in 16 μL of 0.1 M HCOONa (pH 3.7) with 4.3 μL of 300 mM fluorescence dye in DMSO to make the final concentration of dye 60 mM which was tested to be the best labeling condition. The reaction mixture was incubated at 37 °C for 2 hours, followed by lyophilizing the samples. The resulting solid was dissolved in 100 μL of DEPC-treated water, and then 10 μL of 20% KAc (pH 6.5) was added followed by ethanol precipitation. The solution-precipitation step was repeated a total of three times. Phe-$tRNA^{Phe}$ (Cy3 or Cy5) was obtained with an aminoacylation efficiency of ~900 pmol/A_{260} and ~0.5 Cy3 or Cy5/tRNA.

2.2.3 mRNA 022

mRNA 022 was purified as reported (Pan *et al*., 2007). 100 μL of mRNA 022 plasmid (2.9 μg/μL) from Wei Liu was linearized by incubating with Hind III enzyme

(30 μL, 100,000 units/mL), a type II restriction enzyme, 10 fold buffer 2, and DEPC water, all from Hind III-HF kit (New England BioLabs), at 37 °C overnight. Linearized mRNA plasmid was extracted once with 1:1 (v/v) phenol/chloroform and once with chloroform, followed by EtOH precipitation with 1/10 volume of 20% KAc (pH 5.0). The pellet was dried and dissolved by 100 μL of DEPC-treated water. Dilutions were performed to allow concentration of mRNA to be determined by A_{260} (0.1 - 1.0). Plasmid (9 μL, 150 ng/μL) was mixed with the following materials from the EPICENTRE AmpliscribeT7-Flash Transcription Kit: 36 μL of NTPs (100 mM, initial concentration, for each of ATP, CTP, GTP and UTP), 40 μL of DTT (100 mM, initial concentration), 40 μL of T7 enzyme (10,000 units/mL) and 127 μL RNase-free water in a total volume 400 μL. Following incubation of the mixture at 42 °C for 2 hours, 40 μL of DNase I (1 MBU/μL) was added and incubation was continued at 37 °C for 15 min. The reaction mixture was extracted by 400 μL of 1:1(v/v) phenol/ chloroform once and 400 μL of chloroform once. 400 μL of chilled 5 M LiCl was added to the upper aqueous layer and left on ice for 1hour, followed by centrifugation at 15 K for 20 min (Thermo Scientific Micro 17, 24×15/2.0 mL rotor in cold room). The mRNA pellet was resuspended in 200 μL of DEPC water and further purified by EtOH precipitation (99-100% ethanol). The pellet was washed by 400 μL of 70% ethanol and subjected to centrifugation at 15 K rpm for 5 min (Thermo Scientific Micro 17, 24×15/2.0 mL rotor in cold room). The purified pellet was dried and resuspended by 200 μL of DEPC water, followed by another EtOH precipitation and the final product was resuspended in 200 μL of DEPC water. The concentration and purity of mRNA was determined by A_{260}, assuming 0.04 mg/A_{260} and electrophoretic analysis on 2% Agarose gel, respectively (Fig 2.10).

2.2.4 70S ribosomal complexes

The mutant 70S ribosomes lacking L11 from *E. coli* AM77 cells and tight coupled wild-type 70S ribosomes from *E. coli* MRE600 cells were prepared and purified as previously reported (Liu *et al*., 2010; Pan *et al*., 2007).

2.2.4.1 Preparation of Cy3 or Cy5 labeled 70S ribosome

The reconstitution of 70S ribosomes containing $L11^{Cy3}$ or $L11^{Cy5}$ were performed as described (Chen *et al*., 2011a). A two-fold molar excess of C38-$L11^{Cy5}$ or C38S/S87C-$L11^{Cy5}$ was incubated with *E. coli* AM77 ribosome. 53 μL of 46 μM Cy5 labeled L11 (2400 pmol) and 64 μL of 19 μM AM77 70S (1200 pmol) were incubated separately at 37 °C for 5 min in WB buffer. Then the two solutions were mixed and continued incubating at 37 °C for 15 min. $MgCl_2$ was added to the mixture to increase the final Mg^{2+} concentration to 20 mM, and the mixture was subject to centrifugation through a sucrose cushion in WB buffer with 1.1 M sucrose, 1 mM DTT and 20 mM Mg^{2+} (SORVALL S120-AT2 rotor, 110K rpm, 40 min, 4 °C) to pull down the labeled 70S ribosome. The pellet was resuspended in 100 μL of WB buffer. 70S concentration was determined by A_{260} and dye concentration was determined by A_{550} for Cy3 or A_{650} for Cy5, respectively. A typical labeling efficiency is 0.8 - 1.0 dye per 70S ribosome.

2.2.4.2 Preparation of initiation complex

For ensemble experiments, 70S initiation complex was formed by incubating 2 μM WT or labeled ribosomes with 8 μM mRNA, 3 μM IF1, 3 μM IF2, 3 μM IF3, 1 mM GTP and 3 μM [^{35}S]-fMet-$tRNA^{fMet}$ or 3 μM [^{35}S]-fMet-$tRNA^{fMet}$ (prf 20) for 25 min at 37°C in WB buffer. The mixture was centrifuged through a sucrose cushion in WB buffer with 1.1 M sucrose and 1 mM DTT (SORVALL S120-AT2 rotor, 110K rpm, 40 min, and 4 °C)

to pull down 70S initiation complex and get rid of all unbound protein factors. Initiation complex concentration was determined by ribosome-bound [^{35}S]-fMet-tRNA^{fMet}. The stoichiometry per ribosome of tRNA bound [^{35}S]-fMet was typically ranged from 0.4-0.8, depending on ribosome preparation.

For single molecule experiments, two unlabeled initiation complexes and two labeled initiation complexes were prepared by mixing 1 μM WT or labeled ribosome with 4 μM mRNA, 1.5 μM each of IF1, IF2, IF3, 1 mM GTP and 1.5 μM [^{35}S]-fMet-tRNA^{fMet} for 25 min at 37 °C in a total volume of 40 μL. IC-1 contains mRNA MVF and WT ribosomes; IC-2 contains mRNA MFK and WT ribosomes; IC-3 contains mRNA MFK and C38L11^{Cy5}-ribosomes; IC-4 contains mRNA MFK and C38S/C87L11^{Cy5}-ribosomes. The initiation complex was subjected to centrifuge through a sucrose cushion in WB with 1.1 M sucrose and 1 mM DTT (SORVALL S120-AT2 rotor, 110K rpm, 40 min at 4 °C).

2.2.4.3 Preparation of ternary complex

Ternary complex was formed by incubating EF-Tu (4.5 - 6 μM) with 1 mM GTP, 1.5 mM phosphoenolpyruvate (Roche Diagnostics), 0.005 mg/mL pyruvate kinase (Roche Diagnostics) in WB buffer for 5 min to activate EF-Tu. Then unlabeled or labeled Phe-tRNA^{Phe} (3 μM), or unlabeled or labeled Val-tRNA^{Val}, or unlabeled Arg-tRNA^{Arg}, or unlabeled Lys-tRNA^{Lys} (3 μM) was added and incubated for another 5 min at 37 °C in WB buffer.

2.2.4.4 Preparation of PRE complex

PRE complex was formed as published preparation (Pan *et al*., 2007). Initiation complex (1 μM, final concentration) and ternary complex (2 μM, final concentration) were incubated at 37 ºC for 45 sec. The product was purified by ultracentrifugation

through a 1.1 M sucrose cushion in WB buffer with 20 mM Mg^{2+}(SORVALL S120-AT2 rotor, 110K rpm, 40 min, 4 °C). PRE complex concentration was determined from ribosome-bound fMet-[^{3}H]-Phe-tRNA^{Phe}, which typically varied from 0.6 - 0.8/ribosome. The stoichiometry per ribosome of tRNA bound [^{3}H]-Phe was typically 0.6 - 0.7. In single molecule experiments of the A-site tRNA and EF-G interaction, two PRE complexes were used. PRE-I was formed by incubating IC-1 (0.4 - 1 pmol) with Cy5 labeled Val-tRNA^{Val} ternary complex (0.8 - 2 pmol) on ice for 1 min. PRE-II was prepared similarly by incubating IC-2 with Cy5 labeled Phe-tRNA^{Phe} ternary complex. For single molecule experiments measuring L11^{Cy5} and EF-G^{Cy3} interaction, PRE-II$^{38\text{-}Cy5}$ was formed by incubating C38L11^{Cy5}-IC-3 with wild type Phe-tRNA^{Phe} ternary complex and labeled PRE-II$^{87\text{-}Cy5}$ was formed by incubating Cy5 C38S/C87L11 labeled IC-4 with wild type Phe-tRNA^{Phe} ternary complex on ice for 1 min.

2.2.4.5 Preparation of POST complex

POST complex was prepared by incubation of initiation complex (1 μM) and ternary complex (2 μM) at 37 ºC for 45 sec, followed by addition of 5 μM EF-G and 1 mM GTP at 37 ºC for 10 min, and ultracentrifugation through a 1.1 M sucrose cushion (SORVALL S120-AT2 rotor, 110K rpm, 40 min, 4 °C) in WB buffer. POST complex concentration was calculated from the amount of ribosome-bound fMet-[^{3}H]-Phe-tRNA^{Phe}. The stoichiometry per ribosome of tRNA bound [^{3}H]-Phe was typically 0.6-0.7

2.2.5 Ensemble fluorescence measurements

All the ensemble experiments were measurements and associated incubation steps were performed at 25.0 °C.

2.2.5.1 Static fluorescence experiments

Steady-state fluorescence was measured on a photon-counting instrument (Fluorolog-3 spectrofluorometer, Horiba Jobin Yvon). The Cy5 fluorophore was excited at 600 nm wavelength and the emission spectrum from 610 - 740 nm wavelength was recorded. The Cy3 fluorophore was excited at 514 nm wavelength and the emission spectrum from 530 - 750 nm wavelength was recorded.

Solutions containing Cy3 labeled EF-G and wild type 70S or PRE complexes were excited at 514 nm and the emission was monitored from 530 to 750 nm wavelength. Solutions containing Cy3 labeled EF-G and $L11^{Cy5}$-70S or $L11^{Cy5}$-PRE complex were excited at 514 nm and the emission was monitored from 530 to 750 nm wavelength. Solutions containing wild type EF-G and $L11^{Cy5}$-70S or $L11^{Cy5}$-PRE complex were excited at 600 nm and the emission was monitored from 610 - 740 nm wavelength. The same wavelengths were utilized for experiments performed with fusidic acid. The four samples in each case differ only in the presence or absence of the donor (Cy3) or acceptor (Cy5) dyes, and they are designated D*A (donor-containing), D*A* (donor- and acceptor-containing), DA* (acceptor-containing), and DA (a blank sample without donor or acceptor dyes). Signal of DA was subtracted from those of D*A*, D*A and DA* to correct the light scattering and background fluorescence. Fluorescence of $D^*A \frac{\text{peak value of } D^*A^*}{\text{peak value of } D^*A}$ was subtracted from D*A* signal as a correction for donor leakage in the acceptor channel. Then DA* signal upon 514 nm excitation was subtracted from the corrected value of D*A* signal, yielding the extracted D*A (Cy5) fluorescence from energy transfer (Seo *et al*., 2006).

2.2.5.2 Kinetic experiments

2.2.5.2.1 Stopped-flow fluorescence experiments

Experiments were performed in an SX.18MV stopped-flow spectrofluorometer (Applied Photophysics) with excitation ranging from 500 to 600 nm. The dead time is 1 - 2 ms, giving sufficient time resolution for most of the fluorescence or FRET changes monitored. For the fluorescence experiments, Cy3 dye was excited at 530 nm and monitored with a 570 ± 10 nm band pass filter. Proflavin was excited at 462 nm and monitored with a 515 ± 15 nm band pass filter. For FRET experiments, Cy3 dye was excited at 530 nm and monitored with 670 ± 10 nm band pass filter for Cy5 signal. Slit widths were 2 nm for the excitation. For every independent experiment, signals from the initial 2 to 3 shots were not collected to make sure the two chambers were filled with reaction mixtures. Collected fluorescence signals were averaged from at least 5 traces to make sure the abnormal traces were not counted and each experiment was repeated at least twice to make sure the results were reproducible. Apparent rate constants (k_{apps}) were obtained by either single $\boldsymbol{y} = y_0 + \mathrm{A}_1 \times \mathrm{e}^{-\frac{\mathrm{x}-\mathrm{x}_0}{\mathrm{t}1}}$ or double exponential fitting $\boldsymbol{y} = y_0 + \mathrm{A}_1 \times \mathrm{e}^{-\frac{\mathrm{x}-\mathrm{x}_0}{\mathrm{t}1}} + \mathrm{A}_2 \times \mathrm{e}^{-\frac{\mathrm{x}-\mathrm{x}_0}{\mathrm{t}2}}$ of each independent experiment using Origin 9.0 (OriginLab).

2.2.5.2.2 Puromycin assay

Puromycin (puro) experiments were designed as reported in Pan *et al*, 2007 and optimized experimental condition was tested. Puromycin is an analog of 3’ end tyrosyl-tRNA which has a 3000 fold greater reactivity with the P-site peptidyl tRNA than the A-site peptidyl tRNA. All experiments were performed at 37 °C in WB buffer. For the control group, 20 μL of PRE complex was incubated with 20 μL of puro for 10 sec and

then quenched with 150 μL of 0.3 M NaAc (pH=5.2). In the real experiment, 20 μL of PRE complex was incubated with 2 μM wild type EF-G or Cy3 labeled EF-G derivatives for 20 s, followed by addition of 20 μL puro for 10 sec and quenched with 150 μL of 0.3 M NaAc (pH=5.2). The quenched products were extracted by 600 μL of ethyl acetate and counted the radioactivity of [^{35}S]-fMet-tRNA^{fMet}.

2.2.6 Single molecule FRET experiments

2.2.6.1 Temperature

Single molecule experiments were performed at 21 °C.

2.2.6.2 Microscope

Microscope was set up as described in (Chen *et al*., 2011a). A custom-built objective-type total internal reflection fluorescence (TIRF) microscope was based on a commercial inverted microscope (Eclipse Ti, Nikon) with a 1.49 N.A. 100×oil immersion objective (Apo TIRF; Nikon, Tokyo, Japan). A Dual View splitter (Photometrics, Tucson, AZ) was used to separate fluorescence intensities of Cy3 channel (550-620 nm) from Cy5 channel (660-720 nm). Cy3 fluorophore was excited by a 532 nm laser (CrystaLaser, Inc.) and Cy5 fluorophore was excited by a 640 nm laser (Coherent, Inc.). The FRET signal between Cy3 and Cy5 was measured by the corrected emission of Cy5 fluorophore. Fluorescence signals were recorded with an electron multiplying charge-coupled device (EM-CCD) camera (Cascade II, Photometrics) at either an 11 ms or a 35 ms integration time, the 11 ms integration time was achieved by cutting the exposure area down to 128 pixels × 512 pixels without further binning and the 35 ms integration time was recorded by using the whole area (512 pixels × 512 pixels).

Fluorescence data was collected and analyzed as described below (adapted from

Chen *et al*., 2011). Collected movies were analyzed by a custom-made software program developed as an Image J Plugin. Fluorescence spots were fitted by a two-dimensional Gaussian function within 9 pixels × 9 pixels area, matching the donor and acceptor spots using a variant of the Hough transform (Illingworth *et al*., 1988). The background subtracted central intensity of the two-dimensional Gaussian peak was used as raw fluorescence intensity *I*. Actual FRET efficiency was calculated by

$$E = \left(1 + \frac{I_D}{I_A - \chi I_D}\gamma\right)^{-1} \quad \text{(Equation 2.1)}$$

where I_D is raw fluorescence intensity of donor, I_A is raw fluorescence intensity of acceptor, and χ is the cross-talk of the donor emission into the acceptor channel. γ accounts for the differences in quantum yield and detection efficiency between the donor and the acceptor and is calculated as the ratio of change in the acceptor intensity (ΔI_A) to change in the donor intensity (ΔI_D) upon acceptor photobleaching and transition between different FRET states ($\gamma = \Delta I_A / \Delta I_D$).

2.2.6.3. Preparation of PEG-coated slides

PEG-coated slides were prepared as described in Chen et al, 2011. Glass slides and coverslips (Fisher Scientific) were sonicated in acetone for 10 min at 40 °C, then washed with water 3 times and the entire procedure was repeated once. The slides and coverslips were sonicated in 200 mM KOH for 20 min at 40 °C and dried at room temperature. Slides and coverslips were aminosilanized by 1% (v/v) 3-aminopropyltriethoxysilane (United Chemical Technologies, Inc.) and 5% (v/v) acetic acid in methanol, and then the containers were sealed in dark overnight under room temperature. The slides and coverslips were washed by DDI water and EtOH five time each, followed by incubation

with a polyethylene glycol mixture, which is 20% (w/v) 5000 MW PEG-succinimidyl valerate (Laysan Bio) and 0.25% (w/v) 5000 MW biotin-PEG-succinimidyl valerate (Laysan Bio) in 100 mM $NaHCO_3$ solution for 3 hours in dark (Roy *et al*., 2008). The prepared sides and coverslips were dried, sealed and stored in a -20 °C refrigerator.

2.2.6.4 Immobilizing the ribosome complex onto the slides

All the smFRET studies were carried out at 21 °C in TAM^{15} buffer unless otherwise specified. 30 μL of 0.5 mg/mL streptavidin was added to the slides and the excess material was washed away by TAM^{15} buffer. Initiation complexes (0.4 - 1 pmol) containing a 5'-biotinylated mRNA (Dharmacon RNAi Tech) were mixed in a 1:2 ratio with ternary complexes (0.8 - 2 pmol) in 30 μL of reaction buffer for 1 min on ice to form PRE complexes, which were later immobilized onto a biotin/PEG-streptavidin coated glass surface and washed with buffer to remove unbound complexes. The washing buffer was composed of an enzymatic deoxygenation system of 3 mg/mL glucose, 100 μg/mL glucose oxidase, 40 μg/mL catalase, 1.5 mM 6-hydroxy-2,5,7,8-tetramethyl-chromane-2-carboxylic acid (Trolox, Sigma-Aldrich) and 1 mM GTP to diminish fluorophore photobleaching and blinking. After quick injection of 5 to 10 nM Cy3 labeled EF-G derivatives, real-time Cy3 and Cy5 fluorescence signals were collected for 1 min, then the microscope was moved to another area of the slide for data collection.

2.2.6.5 Data analysis of single molecule experiments

2.2.6.5.1 FRET efficiency distribution

FRET efficiency distribution was plotted in the range of -0.2 to 1.2 by collecting all the FRET traces and using 0.02 as the bin size. The FRET peaks were fitted by the Gaussian function.

$$\boldsymbol{y}=y_0 + \left(\frac{A}{\sigma\sqrt{2\pi}} e^{-\frac{(x-xc)^2}{2\sigma^2}}\right) \quad \text{(Equation 2.2)}$$

2.2.6.5.2 Dwell time distribution

Dwell time distribution was plotted in a range of 0 to 220 frames (35 ms per frame) by collecting all the FRET traces and using 1 or 2 frames as the bin size, depending on the number of traces collected. The dwell time distribution was fitted by either single (Equation 2.3) or double exponential decay (Equation 2.4). The fitting result is mostly contributed from the fast components of the FRET recordings as the best fit is obtained in this region, whereas the slow component is not that well fitted. However, this fitting strategy is reasonable, for the slow component is likely to be inactive ribosome complexes, for instance, complexes with unchanged tRNA in the P-site or less active PRE complexes. To simplify the term, we denote our fitting result as dwell time, but precisely, it is the result of fitting the fast components of the FRET traces.

$$\boldsymbol{y} = y_0 + A_1 \times e^{-\frac{x-x_0}{t1}} \quad \text{(Equation 2.3)}$$

$$\boldsymbol{y} = y_0 + A_1 \times e^{-\frac{x-x_0}{t1}} + A_2 \times e^{-\frac{x-x_0}{t2}} \quad \text{(Equation 2.4)}$$

2.2.6.5.3 ΔFRET, Initial and Final FRET distributions

FRET events which lasted longer than 6 frames were selected. The initial and final FRET was calculated as the averaged results of the first and last three frames, respectively. The global fitting results suggested that for some experiments, fast FRET change occurred soon after EF-G binding. For these events, only 4 frames were examined, with the first frame value defined as initial FRET and the last three averaged as the final FRET to avoid an averaging protocol that would miss the fast FRET change occurring

early in the event. Results were plotted as a two-dimensional transition density contour map. Similar selection criteria were applied and the transition density map was plotted by mapping the initial FRET value along the x axis and final FRET value along the y axis directly. In this way, the number of events with specific initial and final FRET values could be counted from the map. The FRET difference distribution, which was calculated by final FRET value minus initial FRET value, was plotted in the range of -0.8 to 0.8 using 0.02 as the bin size. The initial FRET and final FRET distributions were plotted in the same way.

2.2.6.5.4 Postsynchronized analysis

Postsynchronized analysis was performed as reported in previous two papers (Chen *et al*., 2012; Chen *et al*., 2011a) in order to reduce the noise of the data collected. All FRET events were lined up at an identifiable trigger transition and averaged. To get equal durations, all individual traces were extended at the prior and subsequent segment ends. FRET traces were aligned at the beginning (pre-synchronization) or end (post-synchronization). The averaged results revealed the dynamics of the molecules leading up to and following the transition and provided information which was previously hidden due to the noise of the collected data (Fig 2.11). The lifetime of any given state is equal to the reciprocal of transition rate of the given state and the apparent overall translocation rate is the reciprocal of the summed lifetimes of all states in translocation. Two kinetic models were built to study the transition rates by fitting the FRET efficiency. All the results were fitted by Scientist 3.0 (MicroMath) and the detail programs are as follows:

Three-state model 1: Fitted by FRET

Define:

T, time;

Y1, FRET efficiency of pre-synchronization trace;

Y2, FRET efficiency of post-synchronization trace;

k1, k2, k3: transition rates;

F1, F2, F3: FRET efficiencies of different complexes;

A, B, C: concentrations of different complexes in pre-synchronization analysis;

D, E, F: concentrations of different complexes in post-synchronization analysis.

```
// Simulations
IndVars: T
DepVars: Y1, Y2
Params: k1, k2, k3, F1, F2, F3
Y1=F1*A+F2*B+F3*C
A'=-k1*A
B'=k1*A-k2*B
C'=k2*B

Y2=F3*D+F2*E+F1*F
D'=-k3*D
E'=k3*D-k2*E
F'=k2*E
// Parameter values and constrains
//Initial conditions
T=0
A=1
B=0
C=0
D=1
E=0
F=0
```

>

Two-state model: Fitted by FRET

Define:

T, time;

Y1, FRET efficiency of pre-synchronization trace;

Y2, FRET efficiency of post-synchronization trace;

k1, k2: transition rates;

F1, F2: FRET efficiencies of different complexes;

A, B: concentrations of different complexes in pre-synchronization analysis;

D, E: concentrations of different complexes in post-synchronization analysis.

// Simulations

IndVars: T

DepVars: Y1, Y2

Params: k1, k2, F1, F2

Y1=F1*A+F2*B

A'=-k1*A

B'=k1*A

Y2=F2*D+F1*E

D'=-k2*D

E'=k2*D

// Parameter values and constrains

//Initial conditions

T=0

A=1

B=0

D

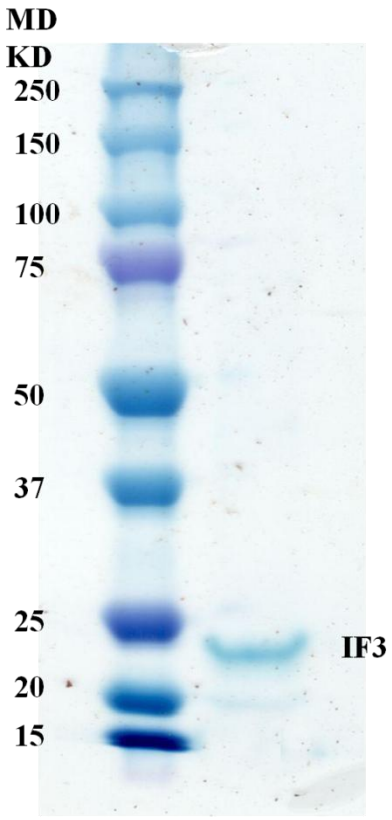

Figure 2.1 Electrophoretic analysis of IF3 by 15% SDS-PAGE gel. Protein concentration measured by Bradford is 180 µM, IF3 (21 KD).

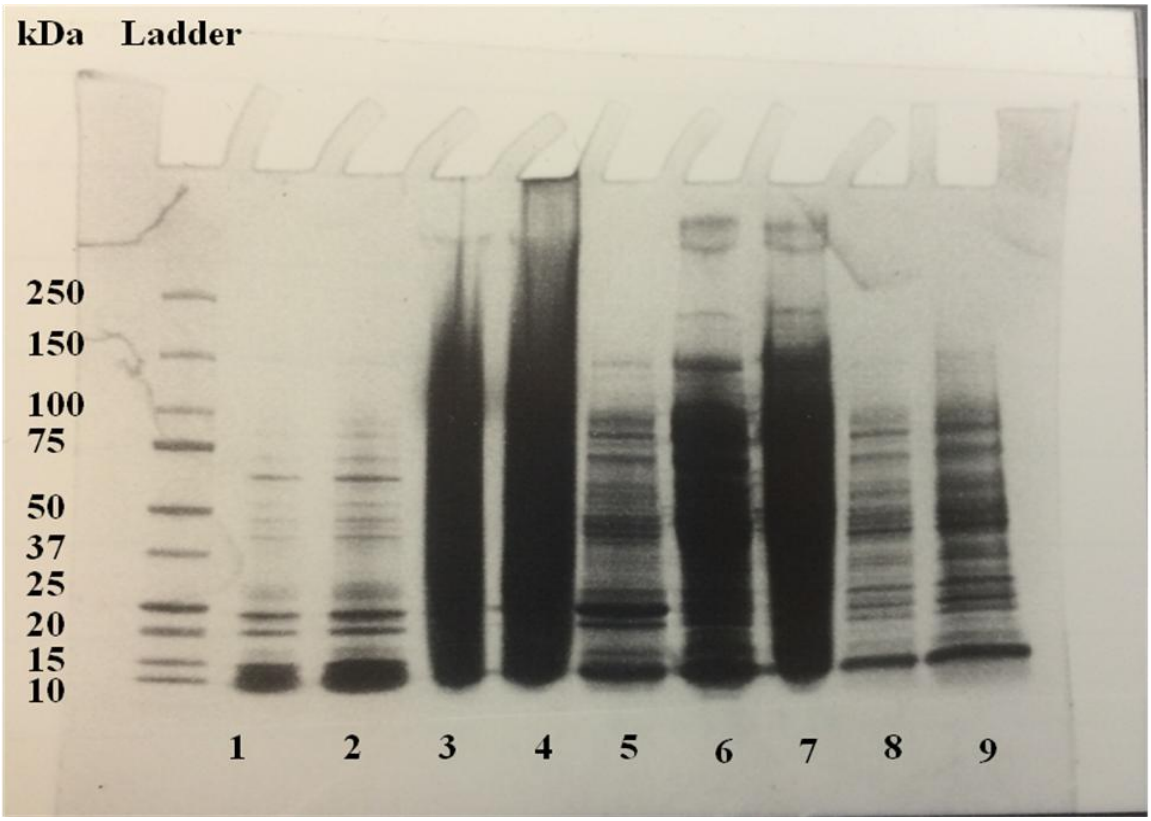

Figure 2.2 Electrophoretic analysis of His-tagged L11 fractions. Lane 1, L11 (14.5 kDa) after FPLC, 3µL; Lane 2, L11 after FPLC, 9µL; Lanes 3 and 4, L11 pellet debris after centrifugation and before Ni-NTA column purification; Lane 5, 2nd flow through of L11 elution buffer C of Ni-NTA column purification; Lane 6, 1st flow through of L11 elution buffer A of Ni-NTA column purification; Lane 7, 2nd flow through of L11 elution buffer A of Ni-NTA column purification; Lane 8, 1st flow through of L11 elution buffer B; Lane 9, 2nd flow through of L11 elution buffer B of Ni-NTA column purification.

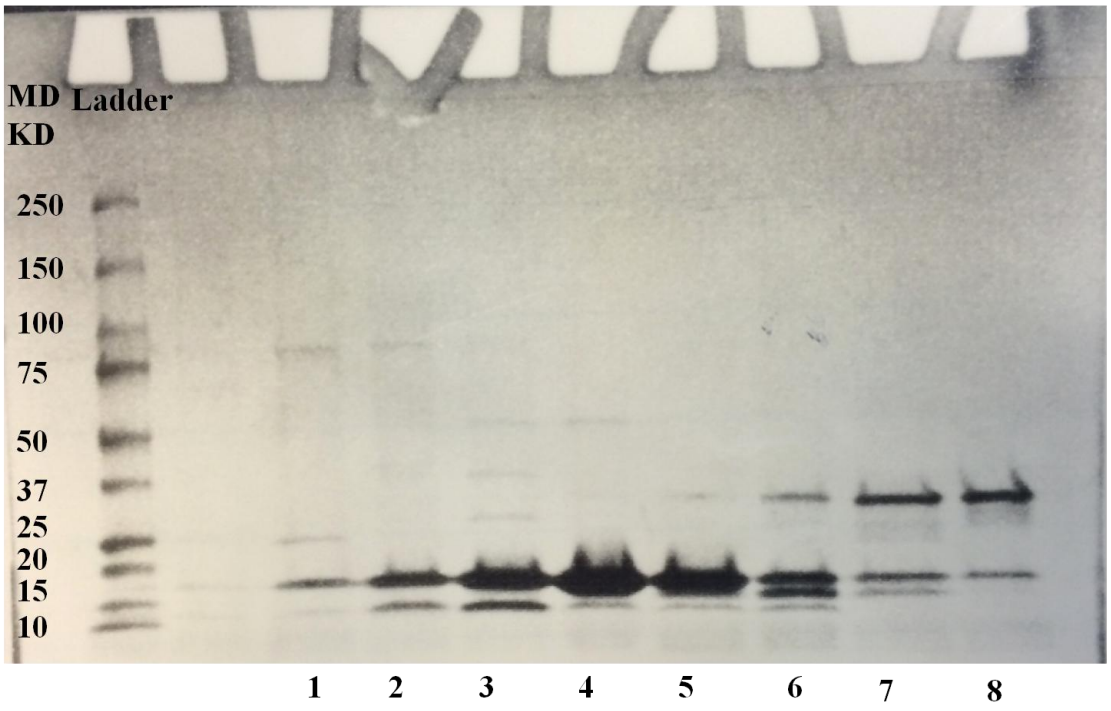

Figure 2.3 Electrophoretic analysis of labeled L11 fractions after FPLC. Lanes 1 - 8 corresponded to FPLC fractions 16 - 23. Fractions 19 - 20 (lanes 4 and 5) were collected and combined.

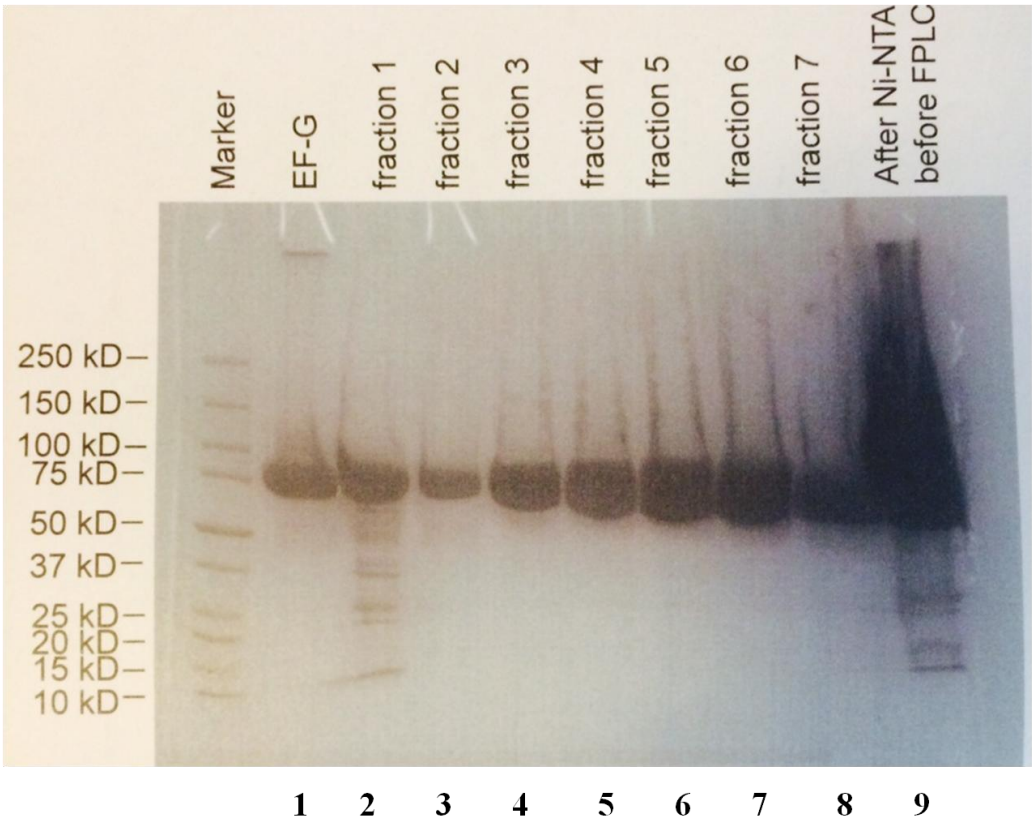

Figure 2.4 Electrophoretic analysis of EF-G fractions of FPLC. Lane 1, EF-G (74 kDa) after final concentration by Amicon Ultra ultrafiltration units (after FPLC); Lanes 2 - 8, different FPLC fractions of EF-G; Lane 9, EF-G protein eluted by EF-G elution buffer C after Ni-NTA column and before FPLC purification.

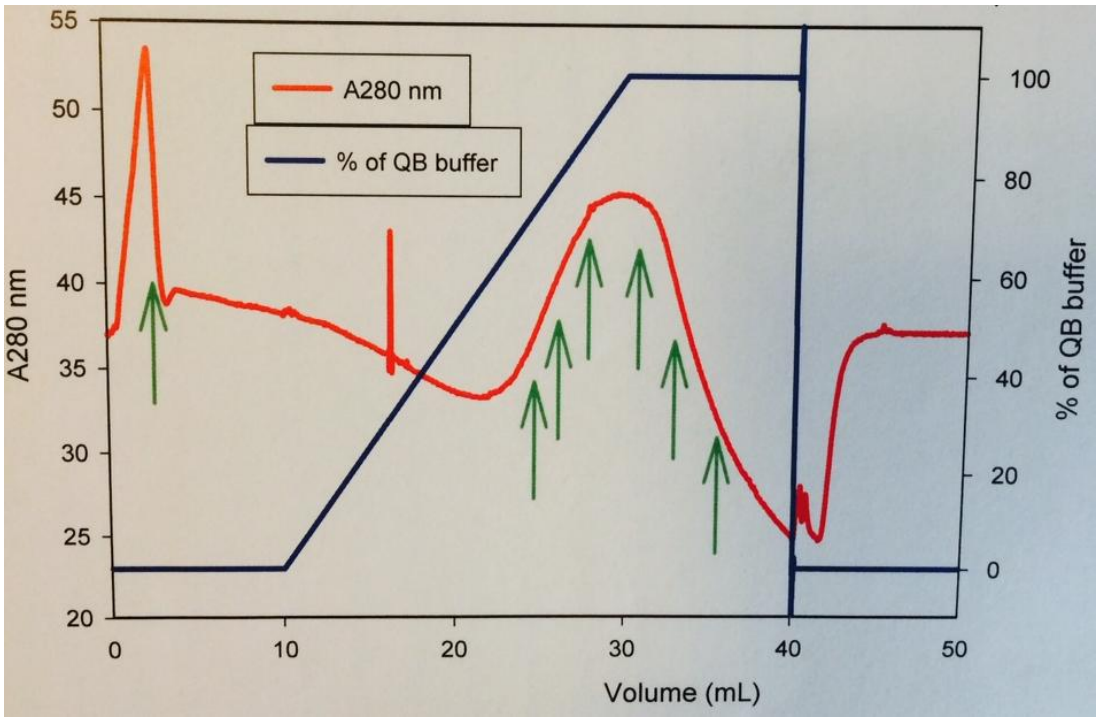

Figure 2.5 FPLC buffer gradient of EF-G purification. The second red peak (24 - 37 mL) indicated the elution fraction of EF-G protein.

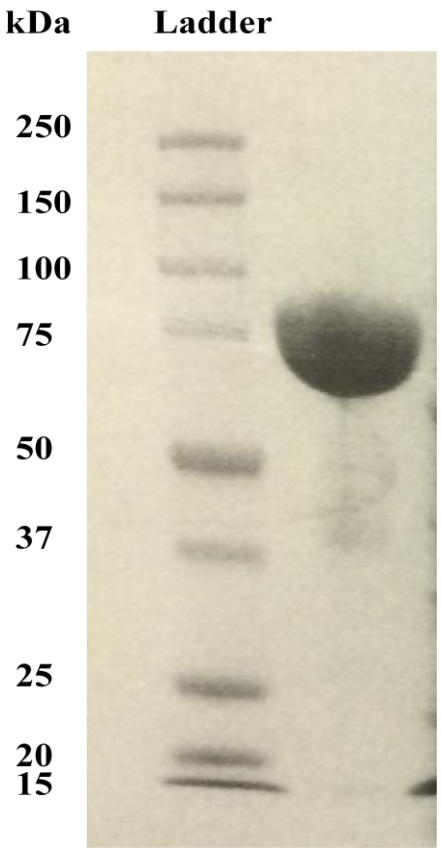

Figure 2.6 Electrophoretic analysis of labeled EF-G. The labeled product was purified product after FPLC.

Figure 2.7 Designed EF-G primers
(The mutant sites were marked red).

Primer 1 S453C (32- number of nucleotides)
GG ACT GAC GAA GAA **TGC** AAC CAG ACC ATC ATC
GAT GAT GGT CTG GTT **GCA** TTC TTC GTC AGT CC

Primer 2 N454C (32)
CT GAC GAA GAA TCT **TGC** CAG ACC ATC ATC GCG
CGC GAT GAT GGT CTG **GCA** AGA TTC TTC GTC AG

Primer 3 Q455C (32)
GAC GAA GAA TCT AAC **TGC** ACC ATC ATC GCG GG
CC CGC GAT GAT GGT **GCA** GTT AGA TTC TTC GTC

Primer 4 T456C (33)
GAA GAA TCT AAC CAG **TGC** ATC ATC GCG GGT ATG
CAT ACC CGC GAT GAT **GCA** CTG GTT AGA TTC TTC

Primer 5 G484C (36)
GTT GAA GCG AAC GTA **TGC** AAA CCGCAG GTT GCT TAC
GTA AGC AAC CTG CGG TTT **GCA** TAC GTT CGC TTC AAC

Primer 6 K485C (33)
GAA GCG AAC GTA GGT **TGC** CCGCAG GTT GCT TAC
GTA AGC AAC CTG CGG **GCA** ACC TAC GTT CGC TTC

Primer Q487C (33)
CG AAC GTA GGT AAA CCG **TGC** GTT GCT TAC CGT G
C ACG GTA AGC AAC **GCA** CGG TTT ACC TAC GTT CG

Primer V488C (32)
GTA GGT AAA CCG CAG **TGC** GCT TAC CGT GAA AC
GT TTC ACG GTA AGC **GCA** CTG CGG TTT ACC TAC

Primer A489C (33)
GGT AAA CCG CAG GTT **TGC** TAC CGT GAA ACT ATC
GAT AGT TTC ACG GTA **GCA** AAC CTG CGG TTT ACC

Primer A690C (32)
CTG AAG TAT GAT GAA **TGC** CCG AGT AAC GTT GC
GC AAC GTT ACT CGG **GCA** TTC ATC ATA CTT CAG

Primer S692C (34)
G TAT GAT GAA GCG CCG **TGC** AAC GTT GCT CAG GCC
GGC CTG AGC AAC GTT **GCA** CGG CGC TTC ATC ATA C

Primer N693C (31)
GAT GAA GCG CCG AGT **TGC** GTT GCT CAG GCC G
C GGC CTG AGC AAC **GCA** ACT CGG CGC TTC ATC

For 231 C-E (36)
GCA GCT GAA GCT TCT GAA **GAG** CTG ATG GAA AAA TAC
GTA TTT TTC CAT CAG **CTC** TTC AGA AGC TTC AGC TGC

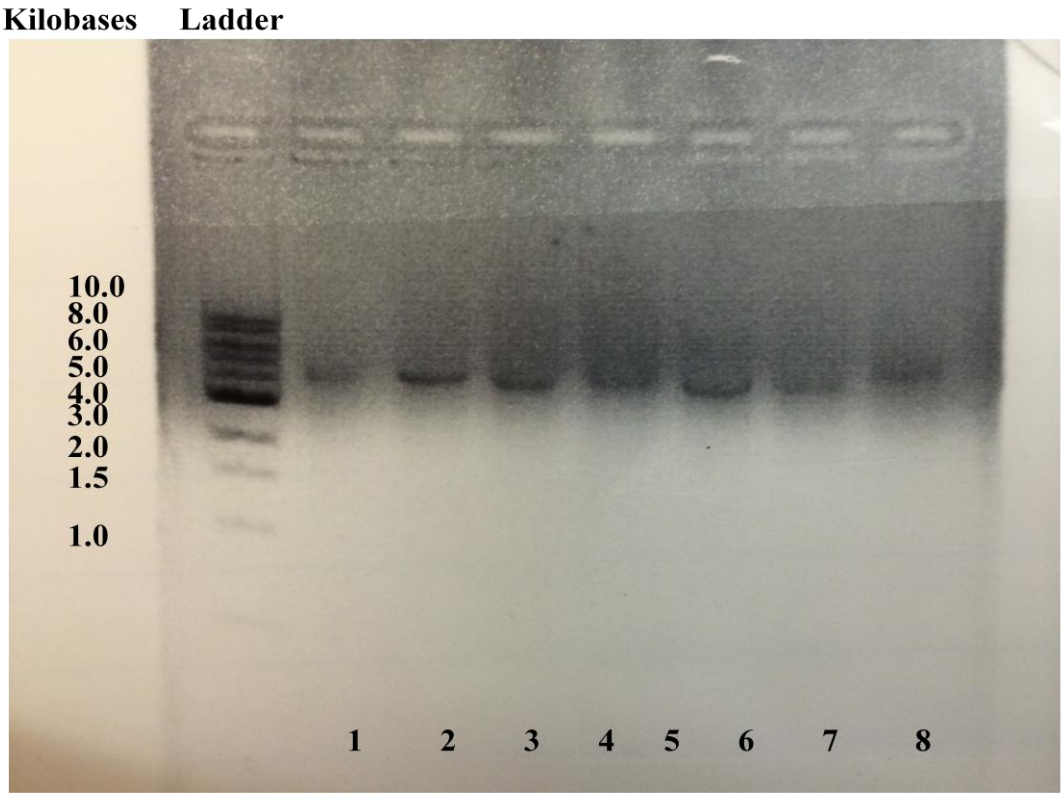

Figure 2.8 Electrophoretic analysis of PCR product of EF-G derivatives. This gel contains 1% agarose. Lanes 1, 4 and 8, A690C-EF-G DNA with annealing temperatures of 65 °C, 62 °C and 60 °C, respectively; Lanes 2 and 6, S692C-EF-G DNA with annealing temperatures of 65 °C and 62 °C respectively; Lanes 3 and 7, N693C-EF-G DNA with annealing temperatures of 65 °C and 62 °C respectively. Our experimental results confirmed the presence of dsDNA encoding EF-G protein, as it is expected to be 5.2 kilobases in length.

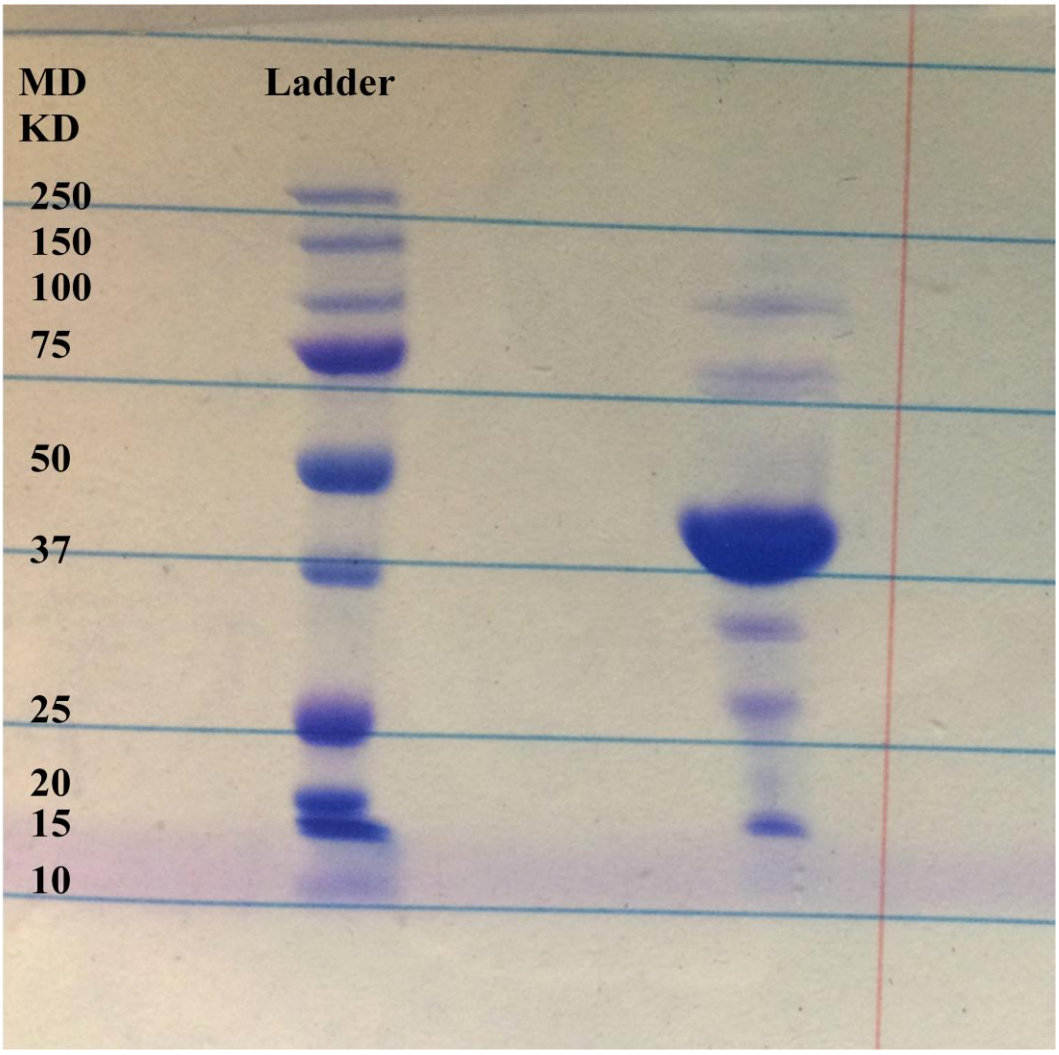

Figure 2.9 Electrophoretic analysis of wild type EF-Tu. Product was purified by Co(II)-Sepharose resin and the presence of EF-Tu (43.2 kDa) is confirmed by 4-15% SDS-PAGE gel.

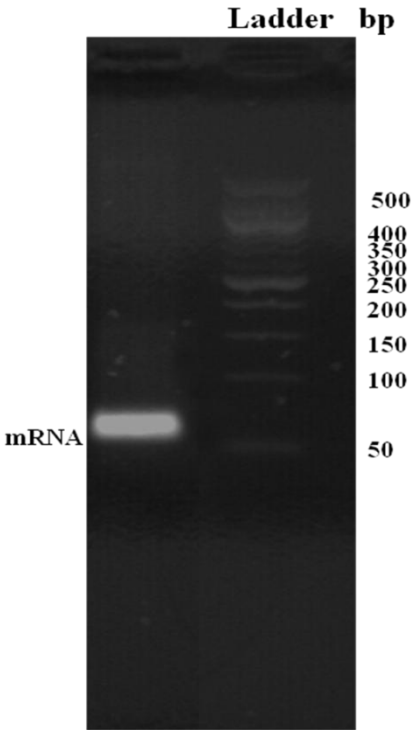

Figure 2.10 Electrophoretic analysis of mRNA. mRNA 022 (63 nucleotides) is labeled.

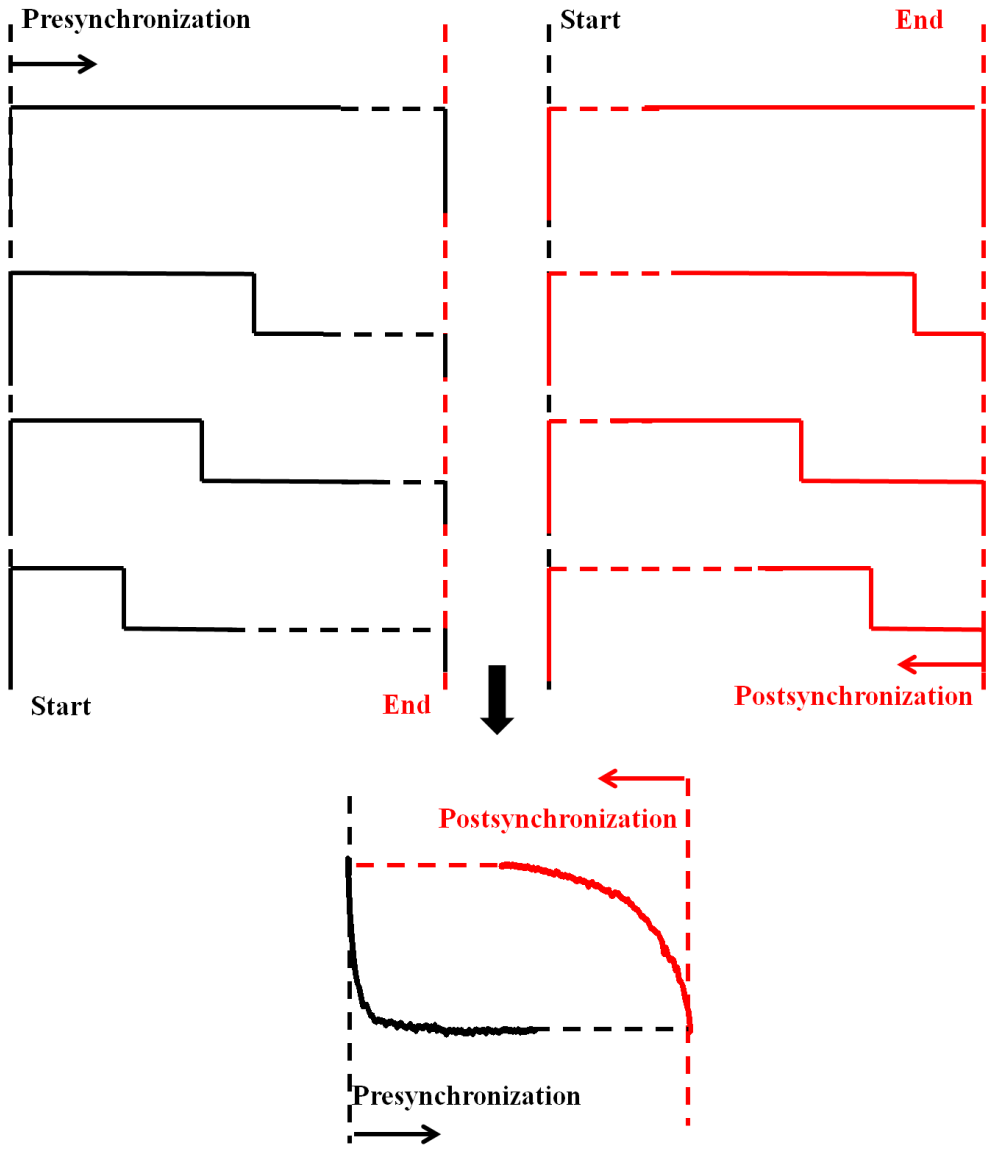

Figure 2.11 Scheme of postsynchronized analysis. All FRET events are lined up at an identifiable trigger transition and averaged. To get equal durations, all individual traces are extended at the prior and subsequent segment ends. FRET traces are aligned at the beginning (pre-synchronization, black) or at the end (post-synchronization, red).

CHAPTER III EF-G MUTANT SCREENING AND ENSEMBLE FLUORESCENCE STUDIES OF TRANSLOCATION

Abstract

Ribosomes are large ribonucleic particles with three tRNA binding sites. The main function of ribosomes is to carry out protein synthesis which can be divided into three basic processes: initiation, elongation and termination. EF-G, one of the two conserved translation elongation factors, catalyzes translocation of the A, P site tRNAs to the P, E sites. In this work, 15 different EF-G mutants in which a Cys residue replaced a wild type residue were designed with the help of two structural models, including EF-G bound to the ribosome in the presence of fusidic acid (FA) (Gao *et al*., 2009) and EF4 bound to the ribosome (Connell *et al*., 2008). Of these 15 EF-G derivatives, 7 were expressed successfully and were labeled at the introduced Cys residue with 40 - 90 % labeling efficiency (Fig 3.1). Each of these EF-G derivatives showed translocation activity in two different assays, with apparent rate constants ranging from 1.4 - 2.5 s^{-1}. In static experiments, all Cy3-EF-G derivatives showed FRET with large ribosomal protein L11 (L11) in the presence of either FA and GTP or GDPNP, although the FRET efficiency was different under these two experimental conditions. Different L11:EF-G FRET efficiencies were also obtained in comparing vacant 70S ribosomes and pretranslocation (PRE) complexes, suggesting the importance of the A-site tRNA in studies of EF-G function in translocation. None of the Cy3-labeled EF-G variants studied showed significant FRET changes in ensemble kinetic experiments in which EF-G was rapidly mixed with PRE complex. However, in the presence of FA, sizable EF-G:$L11^{38\text{-}Cy5}$ FRET changes were observed for $EF\text{-}G^{453\text{-}Cy3}$, $EF\text{-}G^{655\text{-}Cy3}$, and $EF\text{-}G^{693\text{-}Cy3}$, with apparent rate constants of 0.14 - 0.29 s^{-1}, suggesting that FA traps EF-G on the ribosome in a state that follows translocation. Preliminary single molecule fluorescence resonance energy transfer (smFRET) studies were carried out on these three mutants. FRET with both the A-site

tRNA and L11 was only observed for the EF-$G^{693\text{-}Cy3}$ mutant, so this mutant was picked to carry out the detailed smFRET studies described in Chapter 4.

3.1 Introduction

The detailed mechanism of EF-G catalyzed translocation during the elongation cycle is still unclear. A well accepted model is that after the peptide bond formation, the A-site tRNA oscillates between the classic (A/A) and hybrid states (A/P), and the 30S subunit is rotated counterclockwise about 6° relative to the 50S subunit as the ratcheted movement (Schuwirth *et al*., 2005; Zhang *et al*., 2009). EF-G·GTP first binds to the GTPase associated center (GAC) and the mobile C terminal domain (CTD) of L7/12 reaches into solution to promote this binding process. Compared to the isolated ribosome stalk, the CTD of L7/12 is close to N-terminal domain (NTD) of L11 and bridges the interaction of EF-G with L11 (Gao *et al*., 2009). EF-G hydrolyzes GTP immediately after binding to the ribosome, the rate of which is at least 5 fold faster than the translocation rate (Rodnina *et al*., 1997). By using a non-hydrolyzable GTP analogue GDPNP, a single round of translocation is promoted with a slower rate (Pan *et al*., 2007; Rodnina *et al*., 1997; Zavialov *et al*., 2003). The relative movements between Domains I, II and Domains III, IV, V are of crucial importance as Domains I and V cross-linked EF-G was inactive in both translocation and turnover on the ribosome (Peske *et al*., 2000). Domain IV contains two loops at its tip region, loop I (496 - 509) and loop II (567 - 579) with two conserved glycines (502 and 503) located on loop I to facilitate a tight turn which allows loop I to be inserted into the minor groove (Gao *et al*., 2009). The Domain IV truncated EF-G protein retained GTPase activity but only promotes single round of translocation (Savelsbergh *et al*., 2000). Because of this great functional importance of Domain IV in

translocation, when we selected potential sites on EF-G for fluorescent label introduction, many positions within Domain IV were not considered, to avoid potential effects on EF-G catalytic activity.

3.2 Results

3.2.1 Nomenclature

Cy3-labeled EF-G mutants H655C, Q669C, S453C, Q455C, Q487C, S692C, and N693C are denoted EF-G$^{655\text{-Cy3}}$, EF-G$^{669\text{-Cy3}}$, EF-G$^{453\text{-Cy3}}$, EF-G$^{455\text{-Cy3}}$, EF-G$^{487\text{-Cy3}}$, EF-G$^{692\text{-Cy3}}$, and EF-G$^{693\text{-Cy3}}$, respectively. 70S ribosomes and pretranslocation complexes containing Cy5 labeled L11 at position 38 are denoted 70S$^{38\text{-Cy5}}$ or PRE-II$^{38\text{-Cy5}}$, respectively. PRE complexes containing Cy5 labeled A-site fMet-Phe-tRNA^{Phe}(Cy5) are denoted PRE-II$^{tRNA\text{-Cy5}}$.

3.2.2 EF-G mutant screening

Potential mutant sites on EF-G for introduction of a fluorescent label should meet the following criteria: 1) L11 or the A site tRNA are within FRET (R_o) range of a Cy3/Cy5 pair (about 50 Å); 2) the labeling site should be exposed to the solvent instead of buried inside the structure; 3) the amino acid should not be conserved, and less likely to have functional importance. As we have material stocks and developed matured labeling strategies for position 38 on large ribosomal protein L11 and labeled tRNAs at the elbow region, the site of EF-G labeling was selected based on its distance to these two sites (Kaur *et al*., 2011; Seo *et al*., 2006). As there was no accessible structure of EF-G bound to the ribosome with A site tRNA in presence when we started the mutant selection, two structures were used to find proper mutant sites, including structure of EF-G bound ribosome complex containing P/P and E/E site tRNAs in the presence of FA (Gao *et al*.,

2009) and EF4 (Lep A) bound ribosome structure containing A/L, P/P, E/E site tRNAs, and GDPNP (Connell *et al*., 2008). FA prevents EF-G release from the ribosome after GTP hydrolysis. FA traps EF-G in a stable intermediate conformation as it locks switch II of G domain in a conformation similar to the GTP form even after GTP hydrolysis. This prevents the transmission of conformational changes to Domains III and IV while switch I is in a conformation similar to the GDP form (Gao *et al*., 2009). EF4 competes with EF-G for binding to the PRE complex and leads to a transient inhibition of elongation (Liu *et al*., 2011; Liu *et al*., 2010; Qin *et al*., 2006). The protein domains of EF4 are homologous of Domains I, II, III, and V of EF-G but with a unique C terminus (Fig 3.2). The lack of Domain IV in EF4 allows formation of a stable complex in which the A-site tRNA and EF4 are bound to the ribosome simultaneously (Fig 3.3). 3 mutant sites were picked based on the first structure and another 12 mutants were selected based on the latter one. Of these 15 EF-G derivatives, 7 were expressed successfully and with 60 - 90 % labeling efficiency, except for Q669C-EF-G which showed a labeling efficiency of 40 % (Table 3.1).

3.2.3 EF-G activity tests

3.2.3.1 Puromycin activity

Puromycin (Puro) is an analog of 3' end tyrosyl-tRNA which has a 3000-fold greater reactivity as a peptidyl acceptor when peptidyl-tRNA is bound in the P-site than when it is bound in the A-site (Dorner *et al*., 2006; Pan *et al*., 2007; Semenkov *et al*., 1992; Sharma *et al*., 2004). Therefore, formation of peptidyl-puromycin provides a quick way to determine if the mutant is active or not for translocation, as posttranslocation (POST) complexes have a much higher reactivity toward compared to PRE complexes. 70S

initiation complex (70SIC), in which fMet-tRNA^{fMet} is bound in the P-site while the A-site is empty, also shows a high activity toward transferring fMet to puro. PRE complex in which peptidyl-tRNA occupies the A-site has a very low reactivity toward puro. Reaction products on incubating PRE complex with wild type EF-G or Cy3-EF-Gs should show comparable puro reactivity if the Cy3 labeled EF-G derivatives are fully functional. As the labeling efficiencies of EF-Gs are 40 - 90 % and the reaction takes about 30s, it is hard to determine if the reactivity toward puro reflects the real activity of labeled EF-Gs or unlabeled species. However, all these mutants are confirmed to be active. Experiments were performed as described in Chapter 2 and the same amount of wild type EF-G was studied together with all the labeled EF-G mutants as the positive control. In this assay puro reactivities of IC and of POST complex formed from PRE complex by addition of WT-EF-G were approximately equal and ~3 to 4 fold greater than PRE complex (Fig 3.4). POST complexes formed with each of seven labeled EF-Gs showed equivalent reactivities to that seen with WT-EF-G. To simplify our descriptions of experimental conditions, all concentrations mentioned for both static and kinetic experiments are based on final concentrations after mixing.

3.2.3.2 Translocation rate constant

The previous assay only measured the stoichiometry of EF-G-induced translocation. A more stringent test of EF-G derivative activity comes from measuring the rate of EF-G catalyzed translocation. The kinetic activities of labeled EF-G were measured by a translocation assay, monitored by using proflavin (prf) labeled tRNA programmed at the ribosomal A site. Prf can be used to label dihydrouridines within the elbow region (D-loop) of tRNA. As reported by Pan *et al*., 2007, the prf fluorophore is sensitive to the

local environment. Yeast fMet-Phe-tRNA^{Phe}(prf), labeled at positions 16/17 shows an increase in fluorescence intensity on translocation from the A- to the P-site and can be used to monitor the kinetics of translocation (Fig 3.5). Upon rapid mixing of prf labeled PRE complex with EF-Gs, all seven labeled EF-G mutants catalyzed translocation with a rate constant 40 - 70 % of that of wild type EF-G catalyzed translocation. The concentration of EF-G utilized (2 μM) is close to its K_m value for translocation (Pan *et al*., 2007; Savelsbergh *et al*., 2003), so that for the highly labeled EF-G variants (S453C, Q455C, Q487C, S692C, N693C - see Table 3.1), the minor amounts of unlabeled EF-G in the reaction mixtures would not have been sufficient to account for the rates observed. However, the translocation rate constants for H655C-EF-G and Q669C-EF-G are somewhat ambiguous. For these mutants, the labeling efficiencies were only 60 % and 40 %, respectively, so that the measured rates could reflect, at least in major part, the activities of the unlabeled EF-G mutants.

3.2.4 Static FRET measurements

3.2.4.1 Static measurement of EF-G:L11 FRET

EF-G binds and dissociates from the ribosome dynamically even in the absence of the A-site bound tRNA. To monitor FRET between EF-G and L11 at equilibrium, either the antibiotic fusidic acid (FA) or GDPNP was added in order to trap Cy3-labeled EF-G on the ribosome.

FA interacts with switch II of Domains I, II, III of EF-G and traps EF-G on the ribosome by preventing EF-G release after GTP hydrolysis. Previous study indicated that FA does not affect single-turnover GTPase but instead inhibits single-turnover Pi release (Bodley *et al*., 1970). In contrast, Seo *et al*. (2006) showed that FA inhibits translocation

moderately by a gradually halting translocation after a number of GTPase turnovers, with higher concentrations of FA showing more marked effects. As we want to trap EF-G on the ribosome to produce FRET with L11, we utilized a high concentration of FA (1 mM).

GDPNP is a non-hydrolyzable GTP analogue, which catalyzes translocation at lower rate (50 fold slower, Katunin *et al.*; 6 fold slower, Zavialov *et al*., 2003; 5 fold slower, Pan *et al*., 2007) compared to GTP but without Pi release. In the presence of GDPNP, only single round translocation was promoted and there was, of course, no P_i release.

FA and GTP or GDPNP were added to study the interaction between Cy3-EF-Gs and Cy5-L11 and determine if the Cy3-EF-G:Cy5-L11 pair was within the FRET distance. As EF-G binds to the ribosome even in the absence of the A-site tRNA, both $70S^{38\text{-Cy5}}$ and $PRE\text{-}II^{38\text{-Cy5}}$ complexes were used to measure FRET with EF-G. To get an accurate measurement of the FRET efficiency, four differently labeled samples were employed for each EF-G mutant. They are designated D*A (donor-containing), D*A* (donor- and acceptor-containing), DA* (acceptor-containing), and DA (a blank sample without donor or acceptor dyes) and FRET efficiencies were calculated as described (Seo *et al*., 2006), with corrections for the labeling efficiencies of both EF-G and L11. Briefly, signal of DA was subtracted from those of D*A*, D*A and DA* to correct the light scattering and background fluorescence. Fluorescence of $D^*A \frac{\text{peak value of } D^*A^*}{\text{peak value of } D^*A}$ was subtracted from D*A* signal as a correction for donor leakage in the acceptor channel. Then DA* signal upon 514 nm excitation was subtracted from the corrected value of D*A* signal, yielding the extracted D*A (Cy5) fluorescence from energy transfer.

FRET efficiencies for EF-G interactions with vacant ribosomes (Fig 3.6) are listed in

Table 3.2. As the labeling efficiency of Q669C-EF-G was low, the mutant was not included in our study. All Cy3-EF-G derivatives showed FRET with $70S^{38\text{-Cy5}}$ in the presence of FA/GTP or GDPNP. For S453C-EF-G and N693C-EF-G, only minor FRET efficiency differences were obtained for FA/GTP vs. GDPNP. In contrast, significant decreases were seen for FA/GTP vs. GDPNP for $EF\text{-}G^{655\text{-Cy3}}$ and $EF\text{-}G^{692\text{-Cy3}}$ while $EF\text{-}G^{487\text{-Cy3}}$ showed a significant increase.

The A-site tRNA has a steric clash with the tip region of Domain IV on EF-G, making it hard to obtain a stable structure with A-site tRNA and EF-G bound simultaneously. In previous publications, EF-G bound to the A-site unoccupied ribosome was studied a lot to decipher the information of EF-G interaction with PRE complexes (Gao *et al*., 2009; Zhou *et al*., 2013). However, it turned out that the presence of the A-site tRNA may be of great importance for EF-G and ribosome conformations. To further understand the effect of the A-site tRNA on Cy3-EF-G:Cy5-L11 FRET pair, the static FRET of six Cy3-EF-Gs:$PRE\text{-}II^{38\text{-Cy5}}$ pairs was studied in the similar way as described above in the presence of either FA/GTP or GDPNP (Figure 3.7 and Table 3.3). Large FRET differences between FA and GDPNP stabilized complexes were observed for $EF\text{-}G^{655\text{-Cy3}}$, $EF\text{-}G^{455\text{-Cy3}}$and $EF\text{-}G^{692\text{-Cy3}}$, with other EF-G derivatives showing no significant FRET efficiency differences. With or without the A-site tRNA do bring a conformational difference between the labeling sites on EF-G and L11. However, the effect was complicated as it is not in one direction and both decreased (FRET efficiencies for $EF\text{-}G^{487\text{-Cy3}}$ with 70S or PRE in the presence of GDPNP are 0.25 and 0.17, respectively) and increased FRET (FRET efficiencies for $EF\text{-}G^{455\text{-Cy3}}$with 70S or PRE in the presence of FA/GTP are 0.13 and 0.33, respectively) were obtained.

For S692C and N693C on Domain V, the presence of the A-site tRNA increased the FRET between Cy3-EF-G:Cy5-L11. For instance, FRET efficiencies in the presence of FA/GTP for 70S or PRE are 0.4 and 0.25 respectively, and FRET efficiencies in the presence of GDPNP for 70S or PRE are 0.22 and 0.07 for EF-G$^{692\text{-Cy3}}$. Similar results were obtained for EF-G$^{693\text{-Cy3}}$, which seemed to contradict to our prediction as the presence of the A-site tRNA should constrain EF-G movement toward the A-site and push EF-G toward L11. The possible explanation would be that with the A-site tRNA, EF-G had some inter-domain reorientation which resulted in a decreased FRET efficiency of Cy3-EF-G:L11$^{38\text{-Cy5}}$. To sum up, FA stabilizes EF-G on the ribosome in a different confirmation compared to GDPNP. The occupancy of the A-site tRNA has an effect on the relative distances between ribosome protein L11 and EF-G, which could be due to the EF-G domain reorientation in the presence of the A-site tRNA.

3.2.4.2 Static measurement of EF-G:tRNA FRET

To monitor FRET between EF-G and tRNA at equilibrium, antibiotics FA and viomycin (VIO) were added to trap both Cy3 labeled EF-G and Cy5 labeled A-site tRNA on the ribosome. VIO is a cyclic peptide antibiotic that binds at the 16S and 23S ribosomal RNA interface and inhibits translocation by stabilizing tRNAs in the A and P sites (Modolell *et al*., 1977), although it does allow both EF-G binding and fast GTP hydrolysis (Ermolenko *et al*., 2007; Stanley *et al*., 2010).

We confirmed that simultaneous addition of FA and VIO does not impair EF-G binding, by measuring static FRET between EF-G$^{693\text{-Cy3}}$ and 70S$^{38\text{-Cy5}}$ (Fig 3.8), a result that is in accord with recent published results of Salsi *et al*. (2014), which showed that EF-G bound to PRE complexes in the presence of both FA and VIO by observing FRET

between EF-G and protein S12 (Salsi *et al*., 2014).

Accordingly, we carried out static FRET experiments in which Cy3-labeled EF-Gs were added to PRE-II$^{tRNA\text{-}Cy5}$ in the presence of FA/GTP or of FA/GTP plus VIO (Fig 3.9), in the expectation that a higher FRET signal would be seen in the presence of VIO than in its absence. However, none of the experiments gave an observable FRET signal. When a higher Mg^{2+} concentration (15 mM) was employed so as to increase the fraction of PRE complex in the classic state (Chen *et al*., 2011a) which should decrease EF-G:tRNA distance, still no FRET signal was obtained.

Our failure to detect FRET could result from neither of the two structures used for mutant selection being good models for EF-G interaction with the A-site tRNA in PRE state. As a result, the distances of labeled positions on A-site tRNA and EF-G would not be in the FRET range. However, the most recently published high resolution structure by Zhou *et al*. (2014) indicate that our selections are within FRET range to L11 and the A-site tRNA (Table 3.4). We think it more likely that the failure stems from slow translocation occurring even in the presence of FA and VIO which we employ in our experiments, although we cannot exclude the possibility that the presence of both FA and VIO used in the work changes the confirmations of EF-G and/or ribosome and increases the relative distances of Cy3-EF-G:Cy5-tRNA FRET pair.

3.2.5.1 Fast kinetic measurements of EF-G:L11 FRET

3.2.5.1.1 Experiments with vacant ribosomes and PRE complexes with EF-G·GTP in the presence or absence of FA

As described above, in the static measurement, we observed FRET between Cy3-EF-G:Cy5-L11 in the presence of either FA/GTP or GDPNP. The next step was to study the

real time interaction between Cy3-EF-G:Cy5-L11 measured by stopped flow for six EF-G derivatives. If position 38 of L11 is close enough to the labeled sites on EF-G used in this work, when EF-G binds to the ribosome, a FRET signal should be observed. As reported by Seo *et al*. (2006), the increase in FRET efficiency observed on addition of a Cy3-EF-G labeled at position 216 in domain G', quite far from the positions labeled in this work, to vacant ribosomes containing Cy5-L11 was biphasic, with rate constants equal to 20 ± 3 s^{-1} and 0.23 ± 0.02 s^{-1} and with the larger FRET change observed in the fast phase. In the work by Seo, addition of FA/GTP did not change either the fast or slow rate constants, but the overall magnitude of FRET change contributed from the slow phase was enhanced.

We used the same PRE and EF-G concentration as reported by Seo, so if FRET changes occurred they should have been observable within 0.5 s (fast phase) and/or 12 s (slow phase). However, we observed little if any FRET change in this study over these time scales when the Cy3-labeled EF-Gs were rapidly mixed with either $70S^{38\text{-Cy5}}$ (data not shown) or PRE-$II^{38\text{-Cy5}}$ (Fig 3.10).

In the presence of FA, anti-correlated fluorescence changes were observed when three of Cy3-labeled EF-Gs, EF-$G^{644\text{-Cy3}}$, EF-$G^{453\text{-Cy3}}$, and EF-$G^{693\text{-Cy3}}$ were rapidly mixed with either $70S^{38\text{-Cy5}}$ (Fig 3.11) or PRE-$II^{38\text{-Cy5}}$ (Fig 3.12) over 20 s time scale, however, when we zoomed in the initial 0.5 s time scale, no FRET change was observed. The FRET change occurred during 20 s time scale with apparent rate constants that varied from 0.15 - 0.30 s^{-1} which are much lower than the apparent translocation rate constants of 1.4 - 2.5 s^{-1} (Table 3.1). It is therefore likely that these FRET changes arise from slow, FA-induced conformational rearrangements of EF-G that follow translocation, rather than

from translocation itself.

3.2.5.1.2 Experiments with PRE complexes with GDPNP replacing GTP

Seo *et al*. (2006) found that on substitution of GDPNP for GTP, the increase in FRET efficiency observed on addition of a Cy3-EF-G labeled at position 216 in domain G', to vacant ribosomes containing Cy5-L11, but that the rate constants of both the fast and slow phases were reduced by about 100-fold and 30-fold to 0.20 ± 0.01 s^{-1} and 0.007 ± 0.001 s^{-1}, respectively. However, when GDPNP was substituted for GTP we found no evidence for FRET change out to 100 s on rapid mixing of each of the six Cy3-EF-G labeled mutants with PRE-$II^{38\text{-}Cy5}$ (data not shown).

The possible explanations for not observing FRET change in the real-time kinetic measurement would be as follows: 1) FA traps EF-G on the ribosome in a state which is not an intermediate of EF-G catalyzed translocation. Therefore, even FRET was obtained in the static measurement, no FRET was observed in real time kinetic measurement, and no FRET change could be observed accordingly; 2) As FRET events happened at different times, at a single time point, only a small portion of EF-G bound to the ribosome and contributed FRET signal. The scarcity of EF-G binding and the averaged results in bulk solution covered the real FRET change signal. On the other hand, FA enhanced binding of Cy3-EF-Gs to the ribosome and FRET change was observed only with FA.

3.2.5.2 Fast kinetic measurements of EF-G:tRNA FRET

Although no FRET was observed between Cy3-EF-Gs and PRE-$II^{tRNA\text{-}Cy5}$ in the static experiments in the presence of FA ± VIO (Figure 3.9), fast kinetic measurement by stopped flow were carried out to determine if an intermediate could be detected upon

rapid mixing of Cy3-EF-Gs and PRE-II$^{tRNA\text{-}Cy5}$ in the absence of any antibiotics. 2 μM Cy3-EF-G was rapidly mixed with 0.1 μM PRE-II$^{tRNA\text{-}Cy5}$ in TAM^{15} buffer and data was collected over a 1 s time scale, as the translocation rate constant ranged from 1.43 ± 0.01 to 3.54 ± 0.02 s^{-1} as measured by prf labeled A site tRNA (Table 3.1). However, no FRET change was obtained on this time scale. In addition, in an effort to decrease background fluorescence which could make FRET detection difficult, the standard 2 μM Cy3-EF-G was lowered to 0.4 μM and data was collected over a 5 s time scale instead of the 1 s time scale used at 2 μM Cy3-EF-G. However, neither of these changes resulted in detectable FRET changes.

3.3 Discussion

FA traps EF-G on the ribosome by preventing its dissociation and halts translocation after a number of GTPase turnovers (Seo *et al*., 2006). GDPNP functions similarly, but the effect is more stringent as only single turnover of translocation was allowed (Rodnina *et al*., 1997). The equilibrium FRET results displayed in Table 3.2 show a clear between the FA stabilized EF-G-70S structure and the GDPNP stabilized EF-G-70S structure, which suggests that EF-G-ribosome complexes stabilized by FA or GDPNP are in two different states. As the structure of the A-site tRNA bound to an EF-ribosome complex is not stable, a lot of efforts have been made to characterize EF-G-ribosome structure with an empty A-site to elucidate structural insights of the pretranslocation complex (Chen *et al*., 2013b; Pulk *et al*., 2013; Ramrath *et al*., 2013). However, by comparing FRET results in Tables 3.2 and 3.3, it is clear that the presence of the A-site tRNA does have effects on EF-G and/or ribosome structures. Interestingly, for both EF-G^{692} and EF-G^{693} mutants, decreased FRET between EF-G and L11 was observed for PRE vs. 70S. As the

presence of the A-site tRNA restricts the spatial movements of EF-G, FRET between EF-G and L11 protein is expected to increase. The decreased FRET efficiency between EF-G and L11 for PRE vs. 70S observed in our experiment suggests that reorientation of EF-G occurred when the A-site tRNA bound.

The results obtained in the ensemble rapid kinetic experiments are summarized in Table 3.5. FRET change was only observed under the experimental conditions of mixing Cy3-EF-Gs with $70S^{Cy5}$ or PRE-II^{Cy5} and 1mM FA/GTP, but with a rate constant much slower (0.15 - 0.30 s^{-1}) than the translocation rate constant (3.5 s^{-1}). A possible explanation for not observing FRET change in the real-time kinetic measurement in the absence of FA would be that during EF-G occupancy on the ribosome, EF-G has constant FRET with L11 and tRNA. However, the single molecule FRET (smFRET) experiments reported in Chapter 4 demonstrate changes in EF-G:tRNA FRET efficiency during translocation. A more likely explanation, consistent with the smFRET results, is that at any single time point, only a small portion of ribosomes contained bound EF-G capable of producing a FRET change, which would be difficult to detect in an ensemble experiment. The slow ensemble FRET change seen in the presence of FA is evidence that FA traps EF-G on the ribosome in a state which is not an intermediate of EF-G catalyzed translocation.

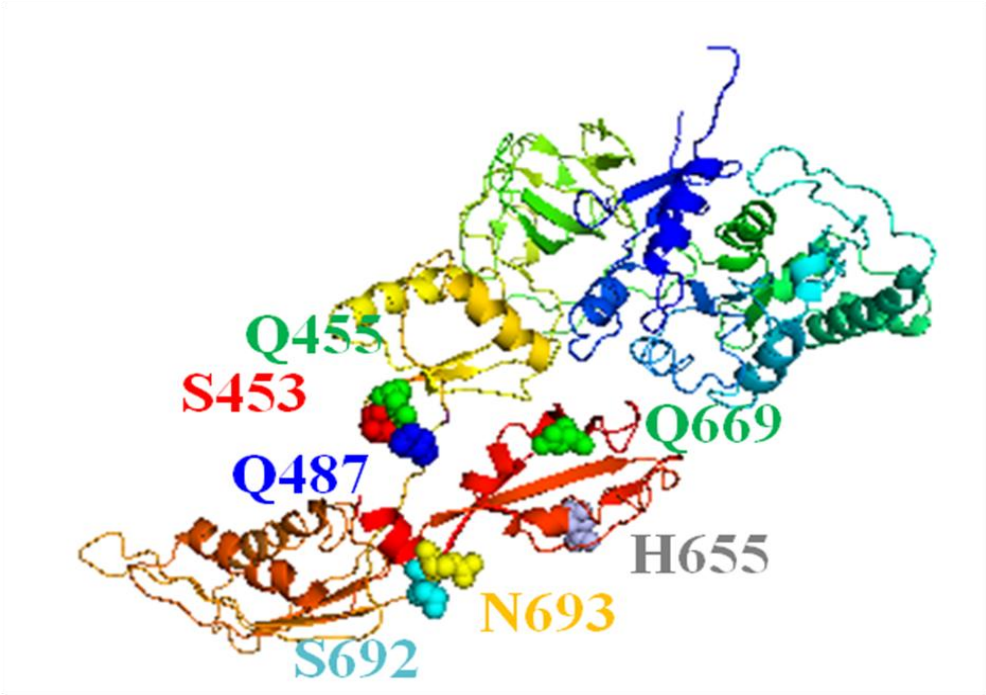

Figure 3.1 EF-G structure with mutant sites labeled. EF-G structure is adapted from 2WRI (PDB) (*Thermus thermophilus*) and the potential mutants are showed as sphere. The number of the mutant sites is base on the sequence of EF-G protein in *E. coli*.

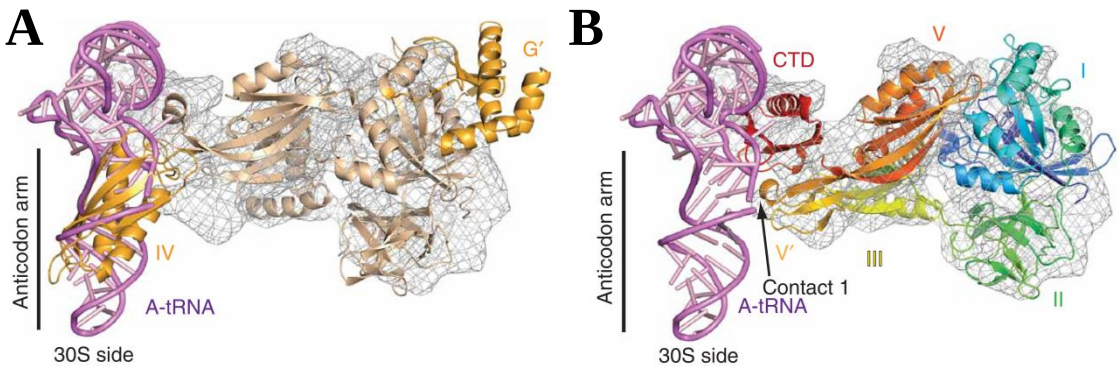

Figure 3.2 Comparison of EF-G and EF4 structures. A. Structure of EF-G (colored orange) bound with A-site tRNA (colored purple) and the structure of EF-G was superimposed on the cryo-EM density of EF4 (gray mesh); **B.** EF4 structure with the individual domains colored blue (I), green (II), yellow (III), orange (V) and red (CTD).

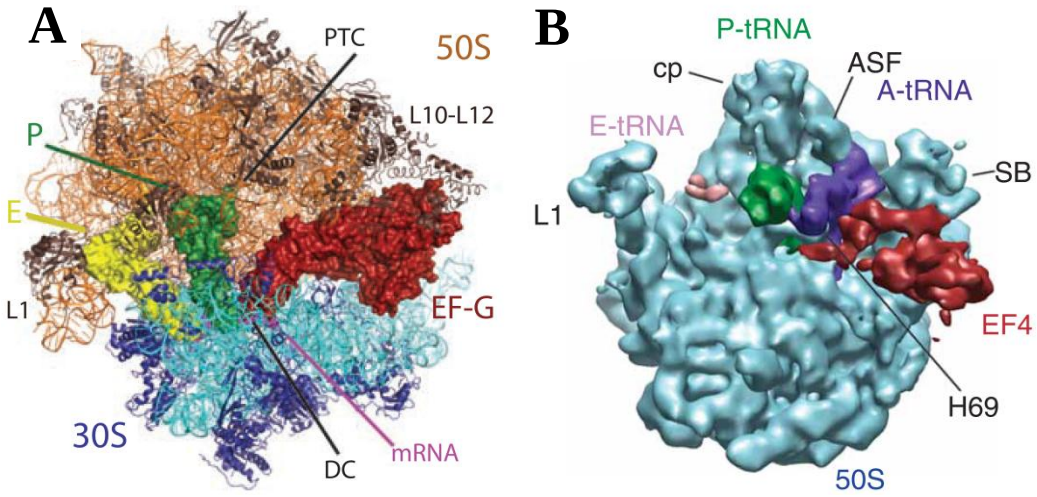

Figure 3.3 EF-G-ribosome and EF4-ribomse complexes. **A.** EF-G bound to the ribosome with P/P E/E site tRNAs, mRNA, GTP and FA (Gao et al, 2009); **B.** EF4 bound ribosome complex, containing A/L, P/P, E/E site tRNAs, mRNA and GDPNP (Connell *et al*., 2008).

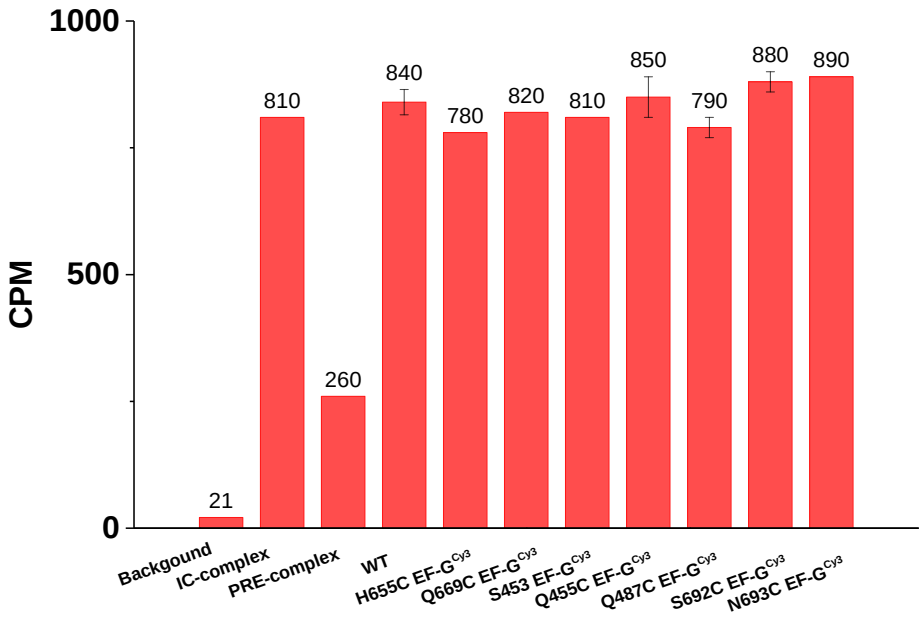

Figure 3.4 Puromycin reactivity tests of Cy3-EF-Gs. All concentrations mentioned are based on final concentrations after mixing. Background, no reactants was added; IC-complex, 10 µL of 0.3 µM IC was mixed with 10 µL WB buffer and incubated with 5mM puro at 37 °C for 20 sec and then quenched with 150 µL of 0.3 M NaAc (pH=5.2). PRE-complex, 20 µL of 0.3 µM PRE was incubated with 5mM puro at 37°C for 20 sec and then quenched with 150 µL of 0.3 M NaAc (pH=5.2). WT or EF-G^{Cy3}, 20 µL of 0.3 µM PRE was incubated with 2 µM wild type EF-G or Cy3-EF-Gs with 1 mM GTP for 1 min, followed by incubation with 5mM puro for 20 sec and then quenched with 150 µL of 0.3 M NaAc (pH=5.2). All the quenched products were extracted by 600 µL ethyl acetate and counted the radioactivity of [^{35}S]-fMet-tRNA^{fMet}. A second measurement was carried for some mutants and the error bar is within 5% which confirms the reliability of our measurement.

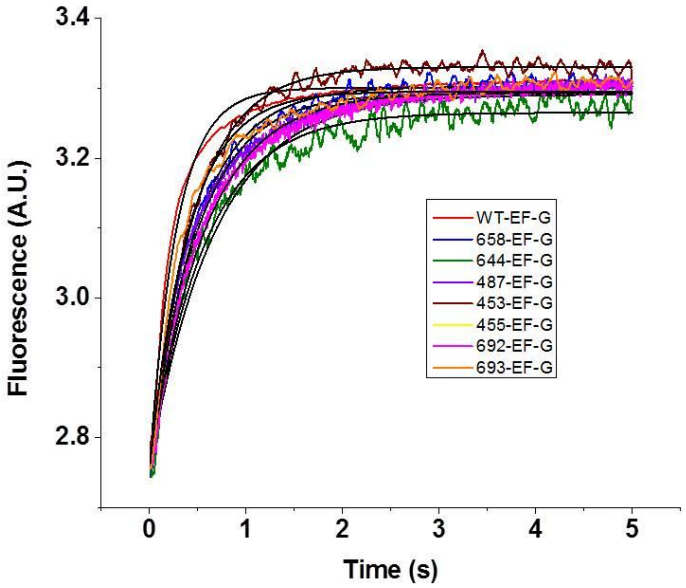

Figure 3.5 EF-G derivatives catalyzed fast translocation as measured by stopped flow fluorescence change. All the results were obtained by mixing 400 µL of 0.1 µM prf-tRNA-PRE with 400 µL of 2 µM EF-G and 1mM GTP in WB buffer at 37 °C. The latter concentration is close to the K_m value for EF-G (Pan *et al*., 2007; Savelsbergh *et al*., 2003). Both raw traces and fitted results of each trace are plotted.

EF-G derivatives (Domain)	Puromycin activity (CPM)	Prf-tRNA translocation activity (s^{-1})	Labeling efficiency
WT	840 ± 25	3.5 ± 0.8	
H655C(V)	780	1.7 ± 0.4	0.60
Q669C(V)	820	2.1 ± 0.4	0.40
S453C(III)	810	2.2 ± 0.7	0.92
Q455C(III)	850 ± 40	1.4 ± 0.3	0.93
Q487C (III)	790 ± 20	2.0 ± 0.7	0.77
S692C (CTD)	880 ± 20	1.8 ± 0.5	0.82
N693C (CTD)	890	2.5 ± 0.6	0.90

Table 3.1 Test of Cy3 labeled EF-G derivatives catalyzed fast translocation by stopped flow. 400 µL of 0.1 µM prf-tRNA-PRE was rapidly mixed with 2 µM EF-G and 1mM GTP in the same volume in WB buffer at 37 °C. Two independent determinations were performed to some mutants with the error listed.

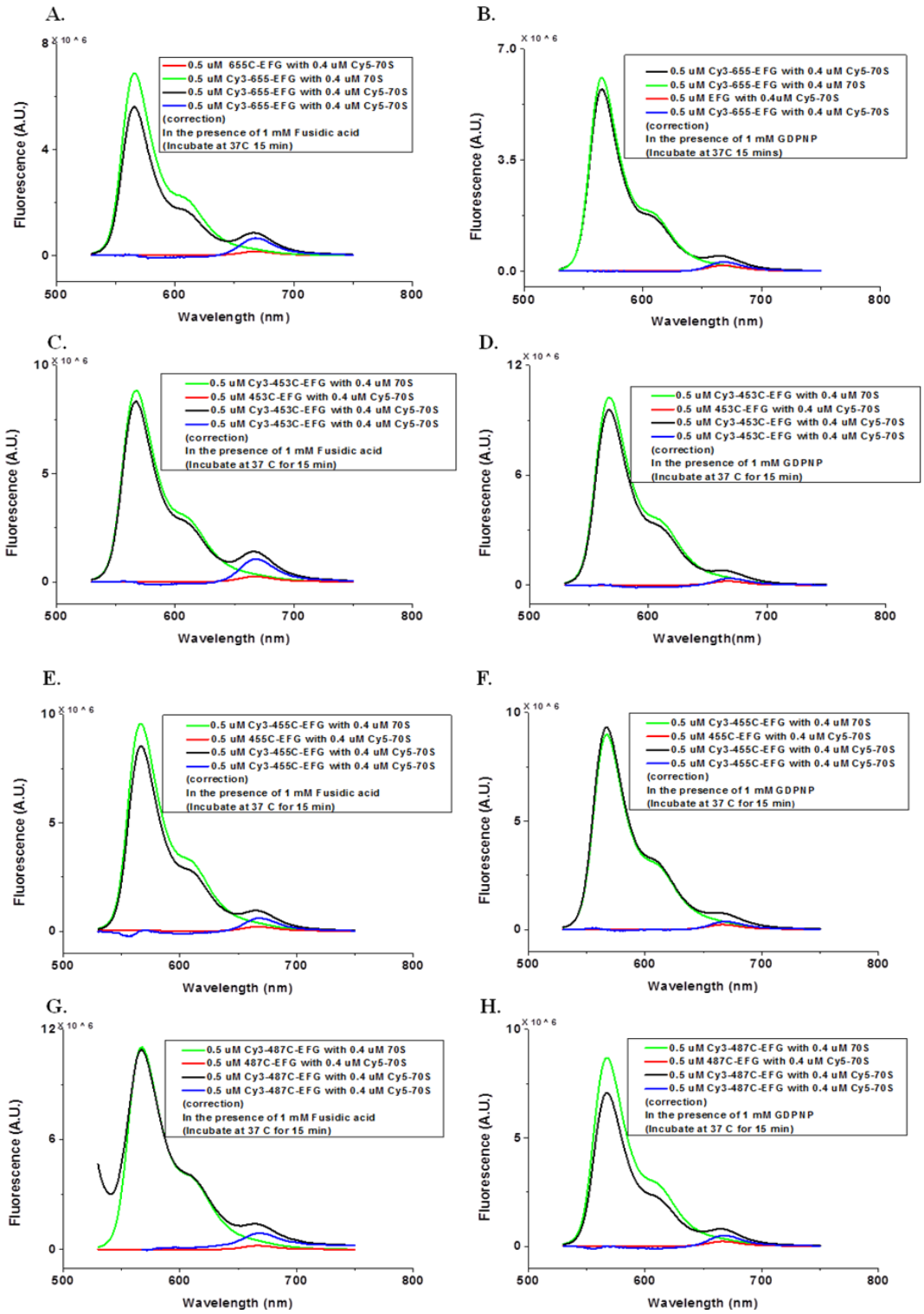
A.
X 10 ^ 6
Fluorescence (A.U.)
Wavelength (nm)
0.5 uM 655C-EFG with 0.4 uM Cy5-70S
0.5 uM Cy3-655-EFG with 0.4 uM 70S
0.5 uM Cy3-655-EFG with 0.4 uM Cy5-70S
0.5 uM Cy3-655-EFG with 0.4 uM Cy5-70S
(correction)
In the presence of 1 mM Fusidic acid
(Incubate at 37C 15 min)
B.
X 10 ^ 6
Fluorescence (A.U.)
Wavelength (nm)
0.5 uM Cy3-655-EFG with 0.4 uM Cy5-70S
0.5 uM Cy3-655-EFG with 0.4 uM 70S
0.5 uM EFG with 0.4uM Cy5-70S
0.5 uM Cy3-655-EFG with 0.4 uM Cy5-70S
(correction)
In the presence of 1 mM GDPNP
(Incubate at 37C 15 mins)
C.
X 10 ^ 6
Fluorescence (A.U.)
Wavelength (nm)
0.5 uM Cy3-453C-EFG with 0.4 uM 70S
0.5 uM 453C-EFG with 0.4 uM Cy5-70S
0.5 uM Cy3-453C-EFG with 0.4 uM Cy5-70S
0.5 uM Cy3-453C-EFG with 0.4 uM Cy5-70S
(correction)
In the presence of 1 mM Fusidic acid
(Incubate at 37 C for 15 min)
D.
X 10 ^ 6
Fluorescence (A.U.)
Wavelength(nm)
0.5 uM Cy3-453C-EFG with 0.4 uM 70S
0.5 uM 453C-EFG with 0.4 uM Cy5-70S
0.5 uM Cy3-453C-EFG with 0.4 uM Cy5-70S
0.5 uM Cy3-453C-EFG with 0.4 uM Cy5-70S
(correction)
In the presence of 1 mM GDPNP
(Incubate at 37 C for 15 min)
E.
X 10 ^ 6
Fluorescence (A.U.)
Wavelength (nm)
0.5 uM Cy3-455C-EFG with 0.4 uM 70S
0.5 uM 455C-EFG with 0.4 uM Cy5-70S
0.5 uM Cy3-455C-EFG with 0.4 uM Cy5-70S
0.5 uM Cy3-455C-EFG with 0.4 uM Cy5-70S
(correction)
In the presence of 1 mM Fusidic acid
(Incubate at 37 C for 15 min)
F.
X 10 ^ 6
Fluorescence (A.U.)
Wavelength (nm)
0.5 uM Cy3-455C-EFG with 0.4 uM 70S
0.5 uM 455C-EFG with 0.4 uM Cy5-70S
0.5 uM Cy3-455C-EFG with 0.4 uM Cy5-70S
0.5 uM Cy3-455C-EFG with 0.4 uM Cy5-70S
(correction)
In the presence of 1 mM GDPNP
(Incubate at 37 C for 15 min)
G.
X 10 ^ 6
Fluorescence (A.U.)
Wavelength (nm)
0.5 uM Cy3-487C-EFG with 0.4 uM 70S
0.5 uM 487C-EFG with 0.4 uM Cy5-70S
0.5 uM Cy3-487C-EFG with 0.4 uM Cy5-70S
0.5 uM Cy3-487C-EFG with 0.4 uM Cy5-70S
(correction)
In the presence of 1 mM Fusidic acid
(Incubate at 37 C for 15 min)
H.
X 10 ^ 6
Fluorescence (A.U.)
Wavelength (nm)
0.5 uM Cy3-487C-EFG with 0.4 uM 70S
0.5 uM 487C-EFG with 0.4 uM Cy5-70S
0.5 uM Cy3-487C-EFG with 0.4 uM Cy5-70S
0.5 uM Cy3-487C-EFG with 0.4 uM Cy5-70S
(correction)
In the presence of 1 mM GDPNP
(Incubate at 37 C for 15 min)

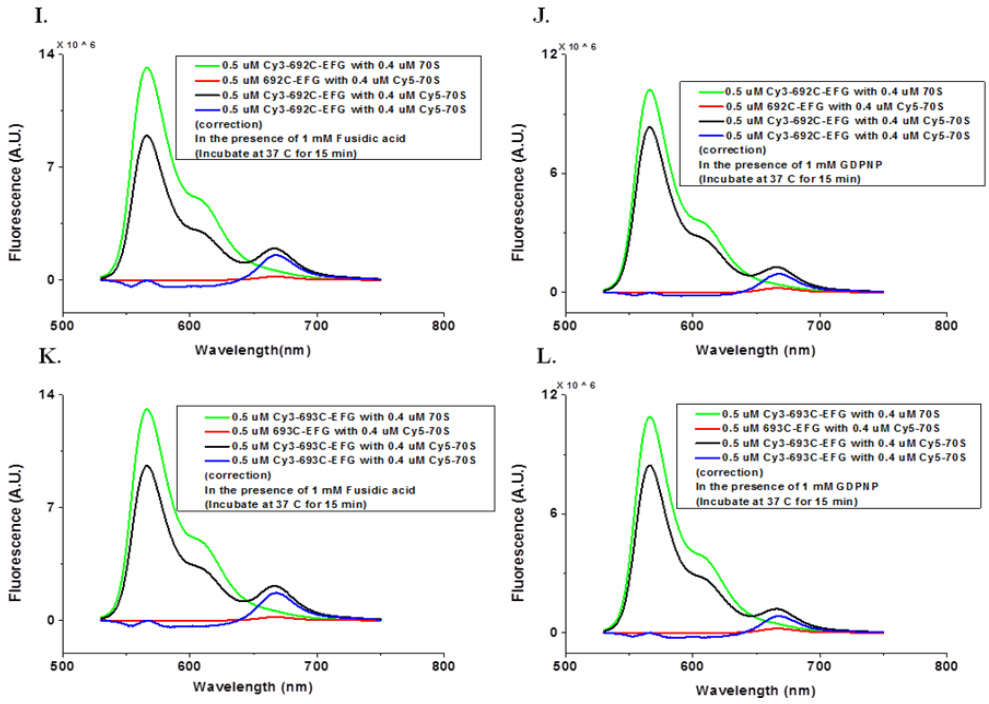

Figure 3.6 Static FRET of EF-G^{Cy3}:70S$^{38\text{-}Cy5}$. Samples were prepared at 25 °C in WB buffer, containing 70S (0.4 µM), EF-G (0.5 µM) and either 1 mM FA/GTP (left) or 1mM of GDPNP (right) for all EF-G derivatives.

EF-G derivatives (Domain)	Experimental conditions	Labeling efficiency	EF-G:L11 FRET efficiency E_{corr}
H655C(V)	70S, FA	0.60	0.30
	70S, GDPNP	0.60	0.10
S453C(III)	70S, FA	0.92	0.062
	70S, GDPNP	0.92	0.077
Q455C(III)	70S, FA	0.93	0.13
	70S, GDPNP	0.93	0.049
Q487C (III)	70S, FA	0.77	0.024
	70S, GDPNP	0.77	0.25
S692C (CTD)	70S, FA	0.82	0.40
	70S, GDPNP	0.82	0.22
N693C (CTD)	70S, FA	0.90	0.30
	70S, GDPNP	0.90	0.25

Table 3.2 Summary of static FRET of EF-G^{Cy3}:70S$^{38\text{-}Cy5}$ pair. All static FRET measurements were performed in WB at 25 °C. Samples were prepared containing 70S (0.4 µM) with EF-G (0.5 µM) and either 1mM FA and GTP or 1mM of GDPNP. FRET efficiencies are calculated as described in Seo *et al*., 2006.

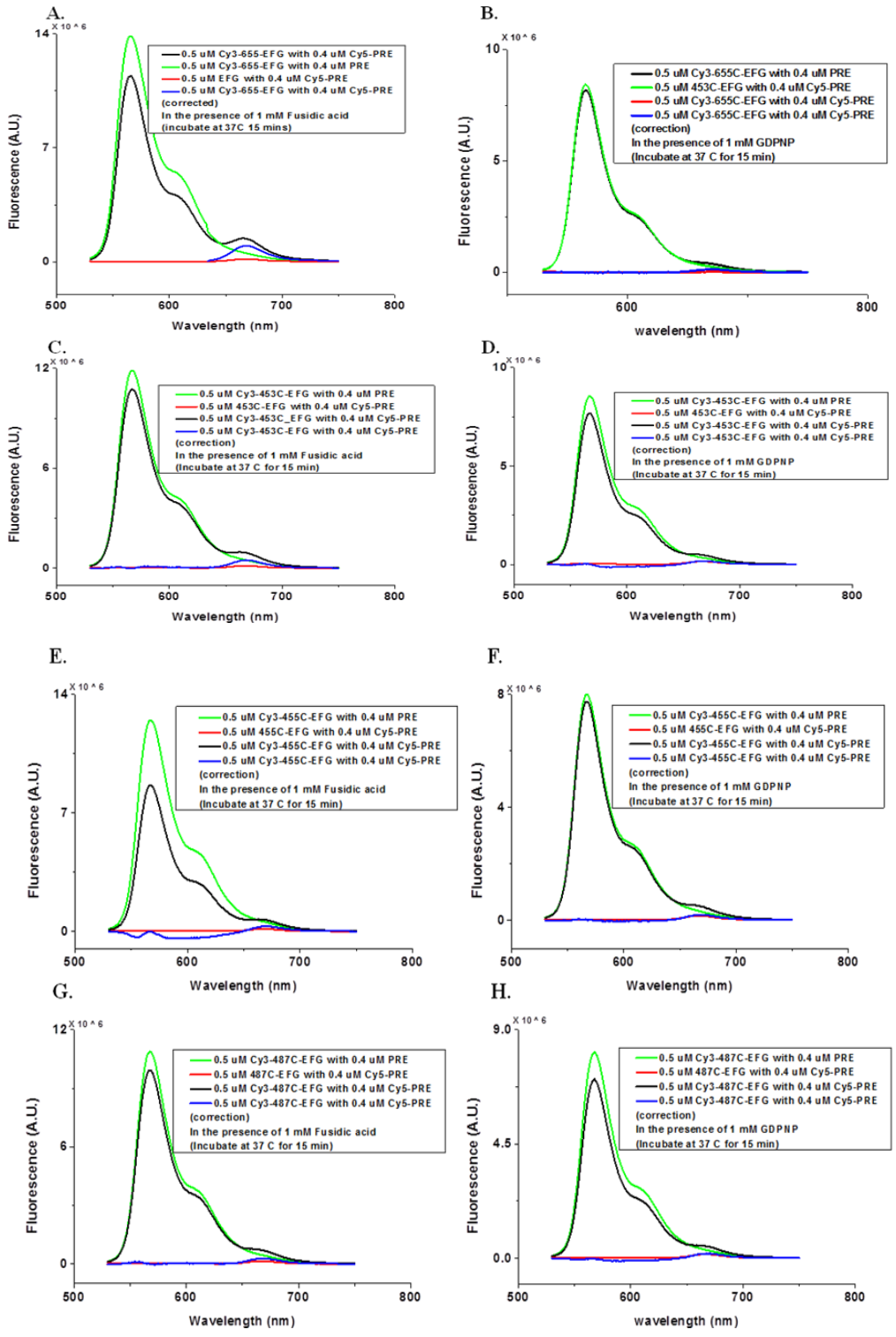
A.
X 10 ^ 6
14
7
0
Fluorescence (A.U.)
500
600
700
800
Wavelength (nm)
0.5 uM Cy3-655-EFG with 0.4 uM Cy5-PRE
0.5 uM Cy3-655-EFG with 0.4 uM PRE
0.5 uM EFG with 0.4 uM Cy5-PRE
0.5 uM Cy3-655-EFG with 0.4 uM Cy5-PRE
(corrected)
In the presence of 1 mM Fusidic acid
(incubate at 37C 15 mins)
B.
X 10 ^ 6
10
5
0
Fluorescence (A.U.)
600
800
wavelength (nm)
0.5 uM Cy3-655C-EFG with 0.4 uM PRE
0.5 uM 453C-EFG with 0.4 uM Cy5-PRE
0.5 uM Cy3-655C-EFG with 0.4 uM Cy5-PRE
0.5 uM Cy3-655C-EFG with 0.4 uM Cy5-PRE
(correction)
In the presence of 1 mM GDPNP
(Incubate at 37 C for 15 min)
C.
X 10 ^ 6
12
6
0
Fluorescence (A.U.)
500
600
700
800
Wavelength (nm)
0.5 uM Cy3-453C-EFG with 0.4 uM PRE
0.5 uM 453C-EFG with 0.4 uM Cy5-PRE
0.5 uM Cy3-453C_EFG with 0.4 uM Cy5-PRE
0.5 uM Cy3-453C-EFG with 0.4 uM Cy5-PRE
(correction)
In the presence of 1 mM Fusidic acid
(Incubate at 37 C for 15 min)
D.
X 10 ^ 6
10
5
0
Fluorescence (A.U.)
500
600
700
800
Wavelength (nm)
0.5 uM Cy3-453C-EFG with 0.4 uM PRE
0.5 uM 453C-EFG with 0.4 uM Cy5-PRE
0.5 uM Cy3-453C-EFG with 0.4 uM Cy5-PRE
0.5 uM Cy3-453C-EFG with 0.4 uM Cy5-PRE
(correction)
In the presence of 1 mM GDPNP
(Incubate at 37 C for 15 min)
E.
X 10 ^ 6
14
7
0
Fluorescence (A.U.)
500
600
700
800
Wavelength (nm)
0.5 uM Cy3-455C-EFG with 0.4 uM PRE
0.5 uM 455C-EFG with 0.4 uM Cy5-PRE
0.5 uM Cy3-455C-EFG with 0.4 uM Cy5-PRE
0.5 uM Cy3-455C-EFG with 0.4 uM Cy5-PRE
(correction)
In the presence of 1 mM Fusidic acid
(Incubate at 37 C for 15 min)
F.
X 10 ^ 6
8
4
0
Fluorescence (A.U.)
500
600
700
800
Wavelength (nm)
0.5 uM Cy3-455C-EFG with 0.4 uM PRE
0.5 uM 455C-EFG with 0.4 uM Cy5-PRE
0.5 uM Cy3-455C-EFG with 0.4 uM Cy5-PRE
0.5 uM Cy3-455C-EFG with 0.4 uM Cy5-PRE
(correction)
In the presence of 1 mM GDPNP
(Incubate at 37 C for 15 min)
G.
X 10 ^ 6
12
6
0
Fluorescence (A.U.)
500
600
700
800
Wavelength (nm)
0.5 uM Cy3-487C-EFG with 0.4 uM PRE
0.5 uM 487C-EFG with 0.4 uM Cy5-PRE
0.5 uM Cy3-487C-EFG with 0.4 uM Cy5-PRE
0.5 uM Cy3-487C-EFG with 0.4 uM Cy5-PRE
(correction)
In the presence of 1 mM Fusidic acid
(Incubate at 37 C for 15 min)
H.
X 10 ^ 6
9.0
4.5
0.0
Fluorescence (A.U.)
500
600
700
800
wavelength (nm)
0.5 uM Cy3-487C-EFG with 0.4 uM PRE
0.5 uM 487C-EFG with 0.4 uM Cy5-PRE
0.5 uM Cy3-487C-EFG with 0.4 uM Cy5-PRE
0.5 uM Cy3-487C-EFG with 0.4 uM Cy5-PRE
(correction)
In the presence of 1 mM GDPNP
(Incubate at 37 C for 15 min)

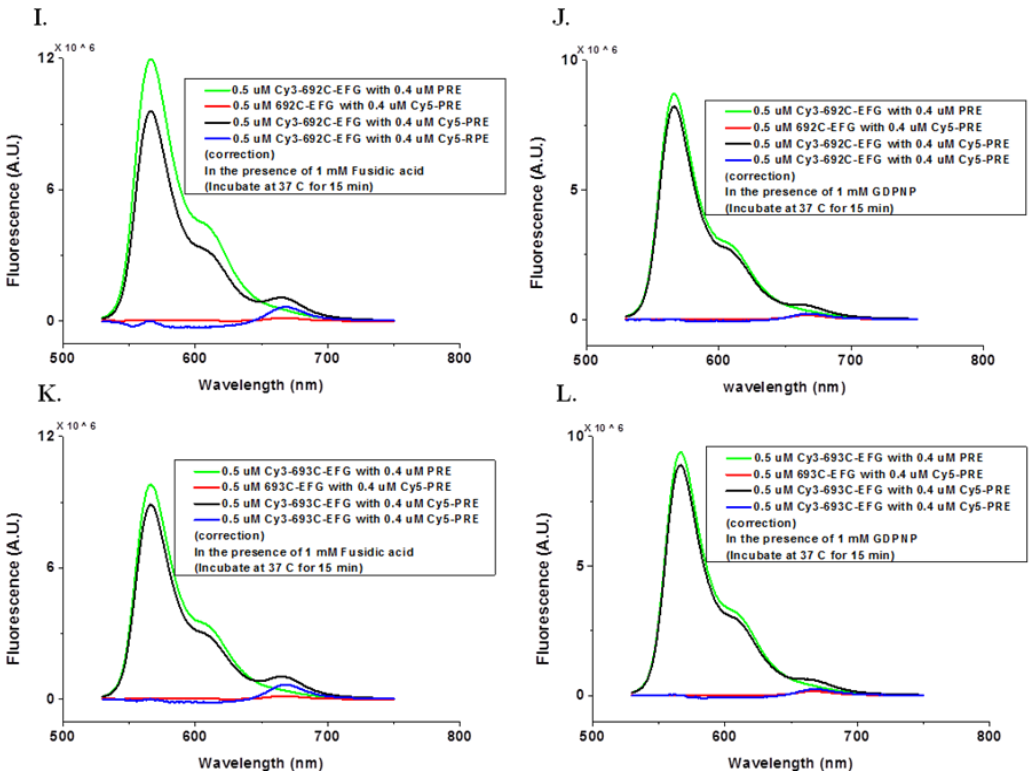

Figure 3.7 Static FRET of EF-G^{Cy3}:PRE$^{38\text{-}Cy5}$. Samples were prepared at 25 °C in WB buffer, containing PRE-II (0.4 µM), EF-G (0.5 µM) and either 1 mM FA/GTP (left) or 1mM of GDPNP (right) for all EF-G derivatives.

EF-G derivatives (Domain)	Experimental conditions	Labeling efficiency	EF-G:L11 FRET efficiency E_{corr}
H655C(V)	PRE, FA	0.60	0.29
	PRE, GDPNP	0.60	0.09
S453C(III)	PRE, FA	0.92	0.09
	PRE, GDPNP	0.92	0.11
Q455C(III)	PRE, FA	0.93	0.33
	PRE, GDPNP	0.93	0.03
Q487C (III)	PRE, FA	0.77	0.11
	PRE, GDPNP	0.77	0.17
S692C (CTD)	PRE, FA	0.82	0.25
	PRE, GDPNP	0.82	0.07
N693C (CTD)	PRE, FA	0.90	0.10
	PRE, GDPNP	0.90	0.06

Table 3.3 Summary of static FRET of EF-G^{Cy3}:PRE-II$^{38\text{-}Cy5}$. All Static FRET measurements were performed in WB at 25 °C. Samples were prepared containing PRE-II (0.4 µM) with EF-G (0.5 µM) and either 1mM FA/GTP or 1mM of GDPNP. FRET efficiencies are calculated as described in Seo *et al*., 2006.

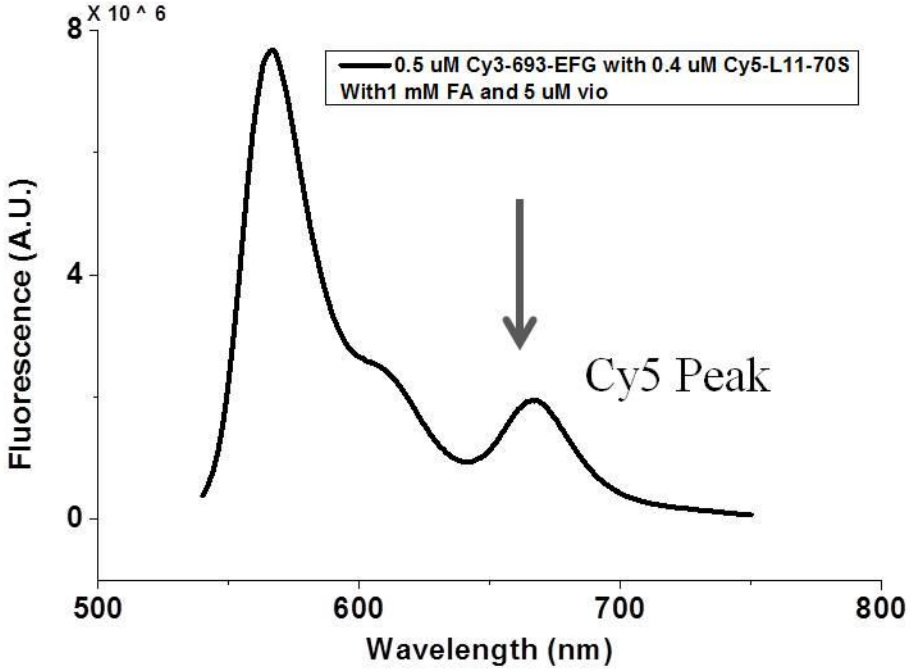

Figure 3.8 Test of EF-G binding to the ribosome with both FA and VIO. Samples were prepared at 25 °C in WB buffer, containing $70S^{38\text{-}Cy5}$ (0.4 µM), $EF\text{-}G^{693\text{-}Cy3}$ (0.5 µM), 1 mM FA, 1 mM GTP and 5 µM viomycin.

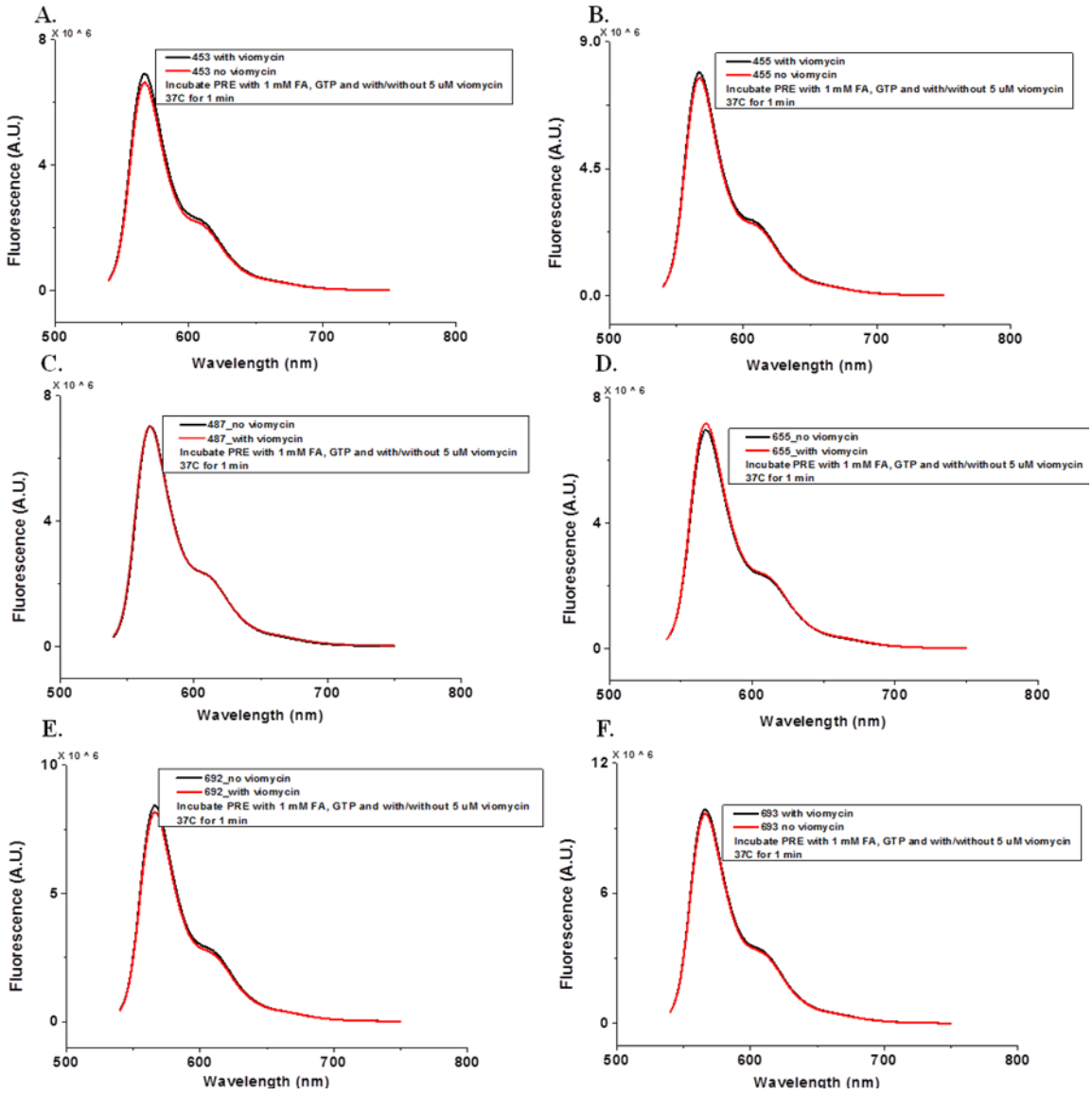

Figure 3.9 Static FRET of EF-G^{Cy3}:PRE-II$^{tRNA\text{-}Cy5}$. Samples were prepared at 25 °C in WB buffer, containing PRE-II$^{tRNA\text{-}Cy5}$ (0.4 μM), Cy3-EF-G (0.5 μM), 1 mM FA/GTP and with or without 5 μM viomycin.

Structure	Distances (Å)	
EF-G	L11	tRNA
H655C(V)	24.8	80.3
S453C(III)	53.9	66.6
Q455C(III)	53.9	71.4
Q487C (III)	51.5	67.3
S692C (V)	48.4	54.9
N693C (V)	51.0	55.7

Table 3.4 Summary of distances. Distances of EF-G mutants to L11 and tRNA were calculated based on the ribosome structure containing ap/ap pe/E site tRNAs, mRNA, GTP and FA. (Zhou *et al*., 2014)

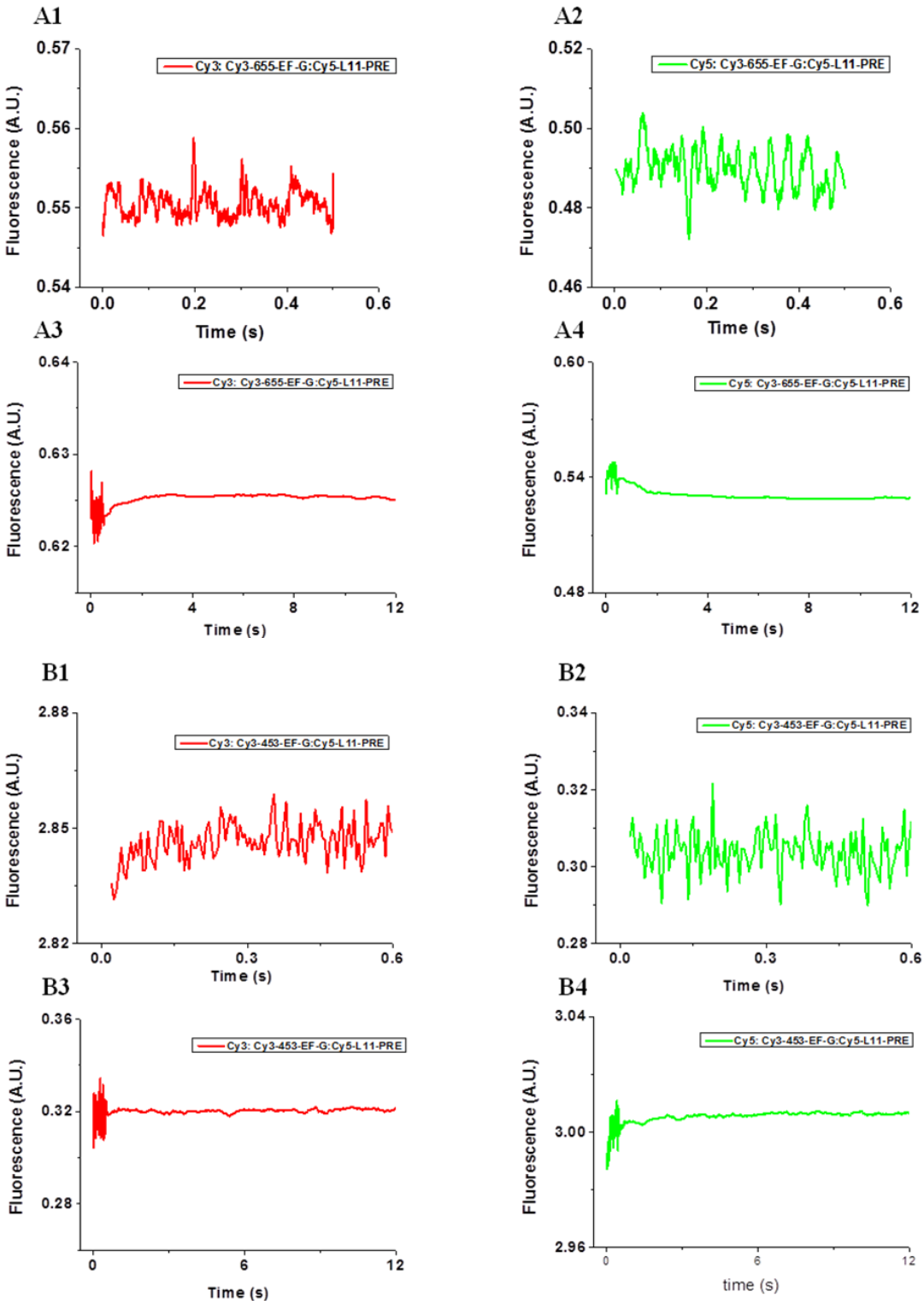
A1
Cy3: Cy3-655-EF-G:Cy5-L11-PRE
Fluorescence (A.U.)
Time (s)
A2
Cy5: Cy3-655-EF-G:Cy5-L11-PRE
Fluorescence (A.U.)
Time (s)
A3
Cy3: Cy3-655-EF-G:Cy5-L11-PRE
Fluorescence (A.U.)
Time (s)
A4
Cy5: Cy3-655-EF-G:Cy5-L11-PRE
Fluorescence (A.U.)
Time (s)
B1
Cy3: Cy3-453-EF-G:Cy5-L11-PRE
Fluorescence (A.U.)
Time (s)
B2
Cy5: Cy3-453-EF-G:Cy5-L11-PRE
Fluorescence (A.U.)
Time (s)
B3
Cy3: Cy3-453-EF-G:Cy5-L11-PRE
Fluorescence (A.U.)
Time (s)
B4
Cy5: Cy3-453-EF-G:Cy5-L11-PRE
Fluorescence (A.U.)
time (s)

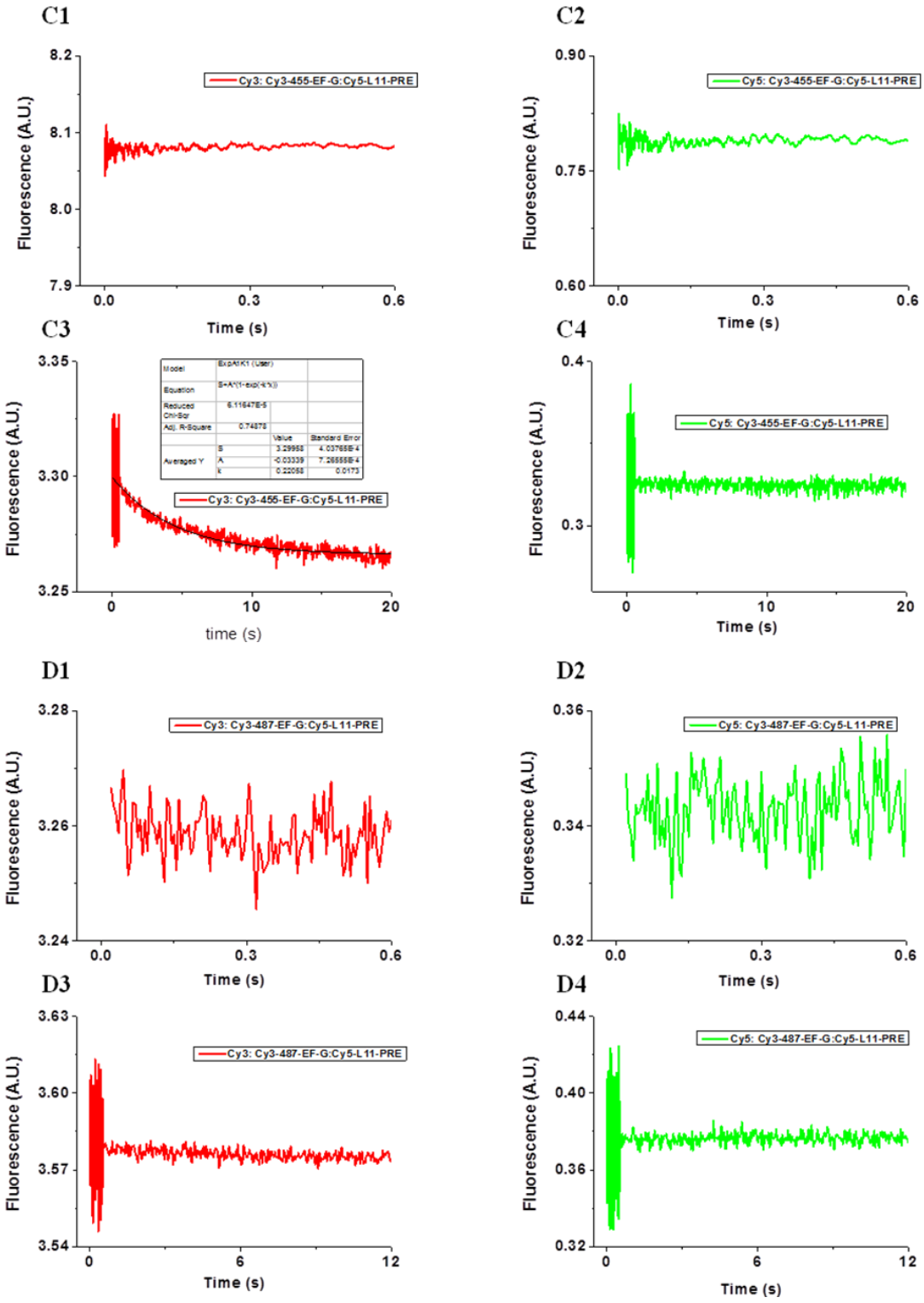
C1
Cy3: Cy3-455-EF-G:Cy5-L11-PRE
Fluorescence (A.U.)
Time (s)
C2
Cy5: Cy3-455-EF-G:Cy5-L11-PRE
Fluorescence (A.U.)
Time (s)
C3
Cy3: Cy3-455-EF-G:Cy5-L11-PRE
Fluorescence (A.U.)
time (s)
C4
Cy5: Cy3-455-EF-G:Cy5-L11-PRE
Fluorescence (A.U.)
Time (s)
D1
Cy3: Cy3-487-EF-G:Cy5-L11-PRE
Fluorescence (A.U.)
Time (s)
D2
Cy5: Cy3-487-EF-G:Cy5-L11-PRE
Fluorescence (A.U.)
Time (s)
D3
Cy3: Cy3-487-EF-G:Cy5-L11-PRE
Fluorescence (A.U.)
Time (s)
D4
Cy5: Cy3-487-EF-G:Cy5-L11-PRE
Fluorescence (A.U.)
Time (s)

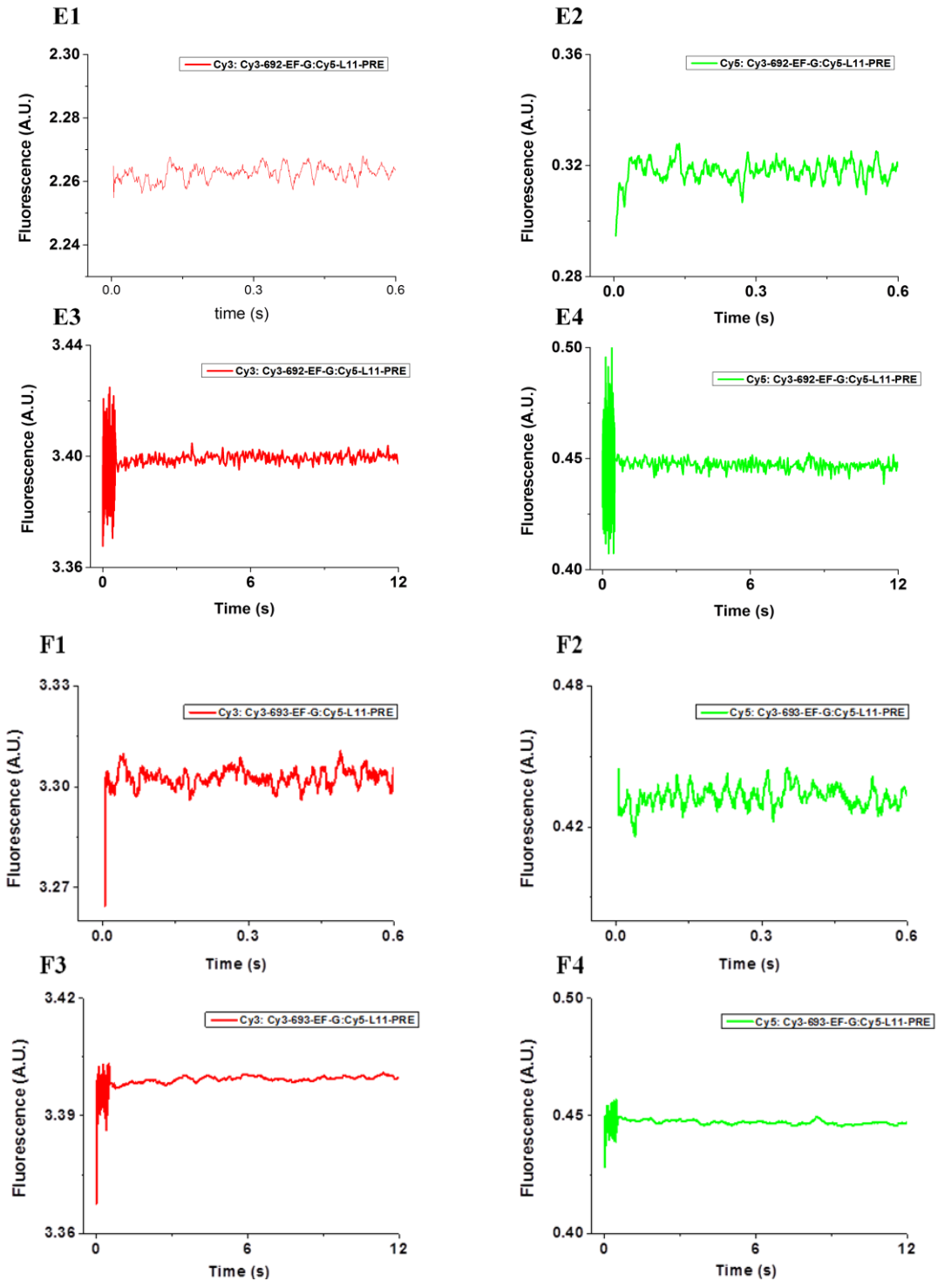

Figure 3.10 Fast kinetic of EF-G^{Cy3} and PRE-II$^{38\text{-}Cy5}$. Experiments were performed at 25 °C in WB buffer. All the results were obtained by mixing 400 µL of PRE-II$^{38\text{-}Cy5}$ (0.5 µM) with 400 µL of EF-G^{Cy3} (0.75 µM). Cy3 (left, red) and Cy5 (right, green) signal collected from both short time (0.5 s) and long time scales (12 s) are plotted and no anti-correlated Cy3/Cy5 signals with comparable rate constants are obtained.

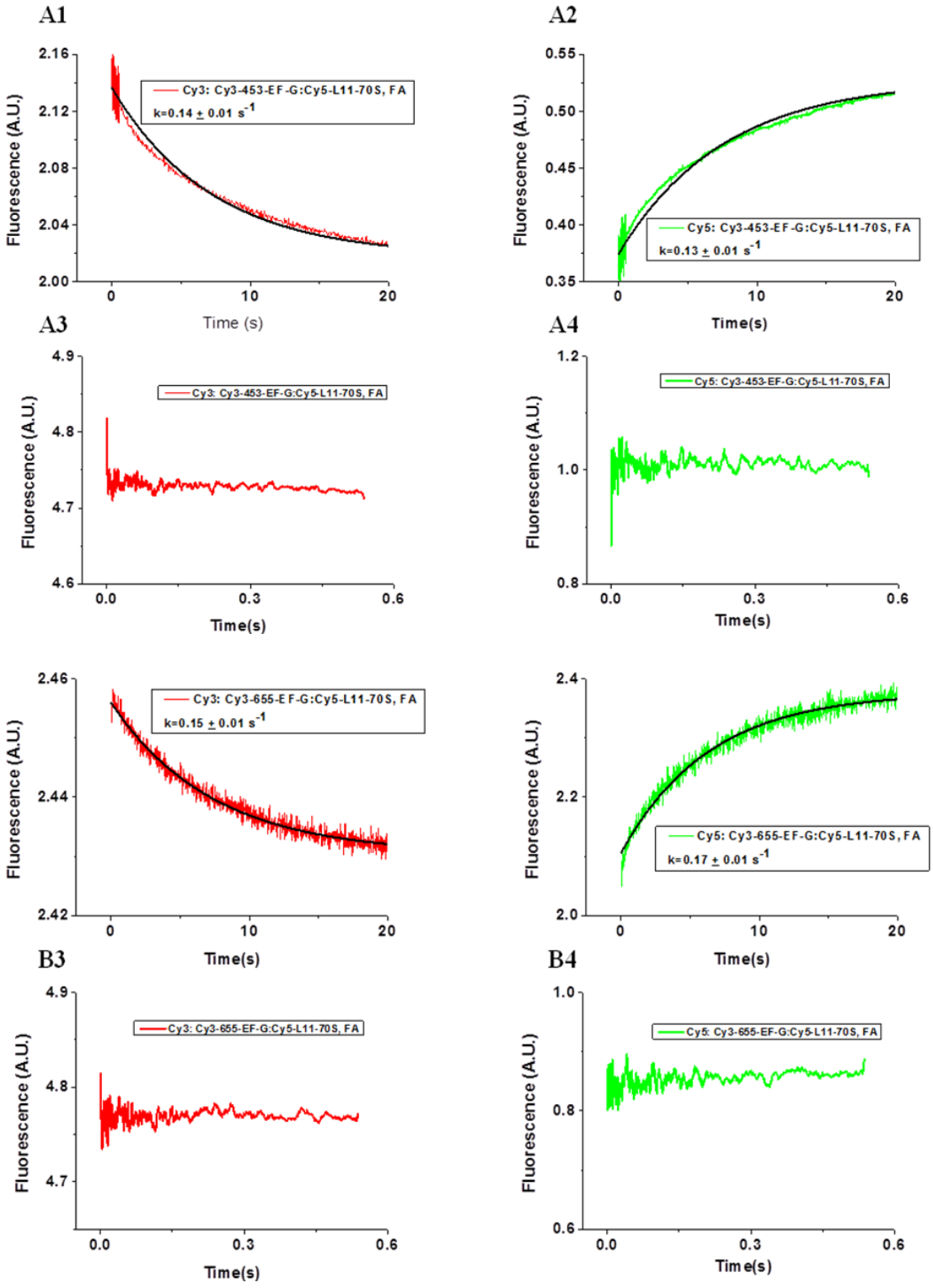
A1
Cy3: Cy3-453-EF-G:Cy5-L11-70S, FA
k=0.14 ± 0.01 s-1
Fluorescence (A.U.)
Time (s)
A2
Cy5: Cy3-453-EF-G:Cy5-L11-70S, FA
k=0.13 ± 0.01 s-1
Fluorescence (A.U.)
Time(s)
A3
Cy3: Cy3-453-EF-G:Cy5-L11-70S, FA
Fluorescence (A.U.)
Time(s)
A4
Cy5: Cy3-453-EF-G:Cy5-L11-70S, FA
Fluorescence (A.U.)
Time(s)
Cy3: Cy3-655-EF-G:Cy5-L11-70S, FA
k=0.15 ± 0.01 s-1
Fluorescence (A.U.)
Time(s)
Cy5: Cy3-655-EF-G:Cy5-L11-70S, FA
k=0.17 ± 0.01 s-1
Fluorescence (A.U.)
Time(s)
B3
Cy3: Cy3-655-EF-G:Cy5-L11-70S, FA
Fluorescence (A.U.)
Time(s)
B4
Cy5: Cy3-655-EF-G:Cy5-L11-70S, FA
Fluorescence (A.U.)
Time(s)

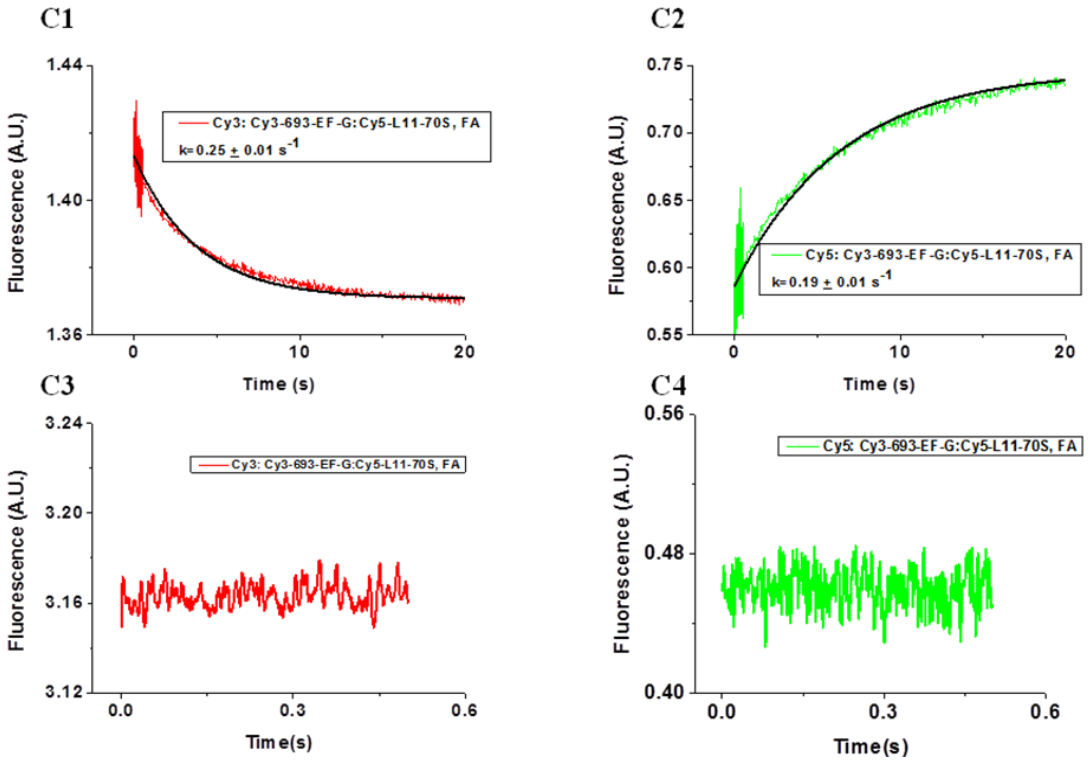

Figure 3.11 Fast kinetic measurements of EF-G^{Cy3} with 70S$^{38\text{-}Cy5}$. Experiments were performed at 25 °C in WB buffer. All the results were obtained by mixing 400 µL of 70S$^{38\text{-}Cy5}$ (0.5 µM) with 400 µL of 0.75 µM Cy3-EF-G (EF-G$^{453\text{-}Cy3}$, EF-G$^{655\text{-}Cy3}$ or EF-G$^{693\text{-}Cy3}$), FA (1 mM) and GTP (1 mM). Cy3 (left, red) and Cy5 (right, green) signal collected from both short time scale (0.5 s) and long time scale (20 s) are plotted and anti-correlated Cy3/Cy5 signals are obtained for results on 20 s time scale.

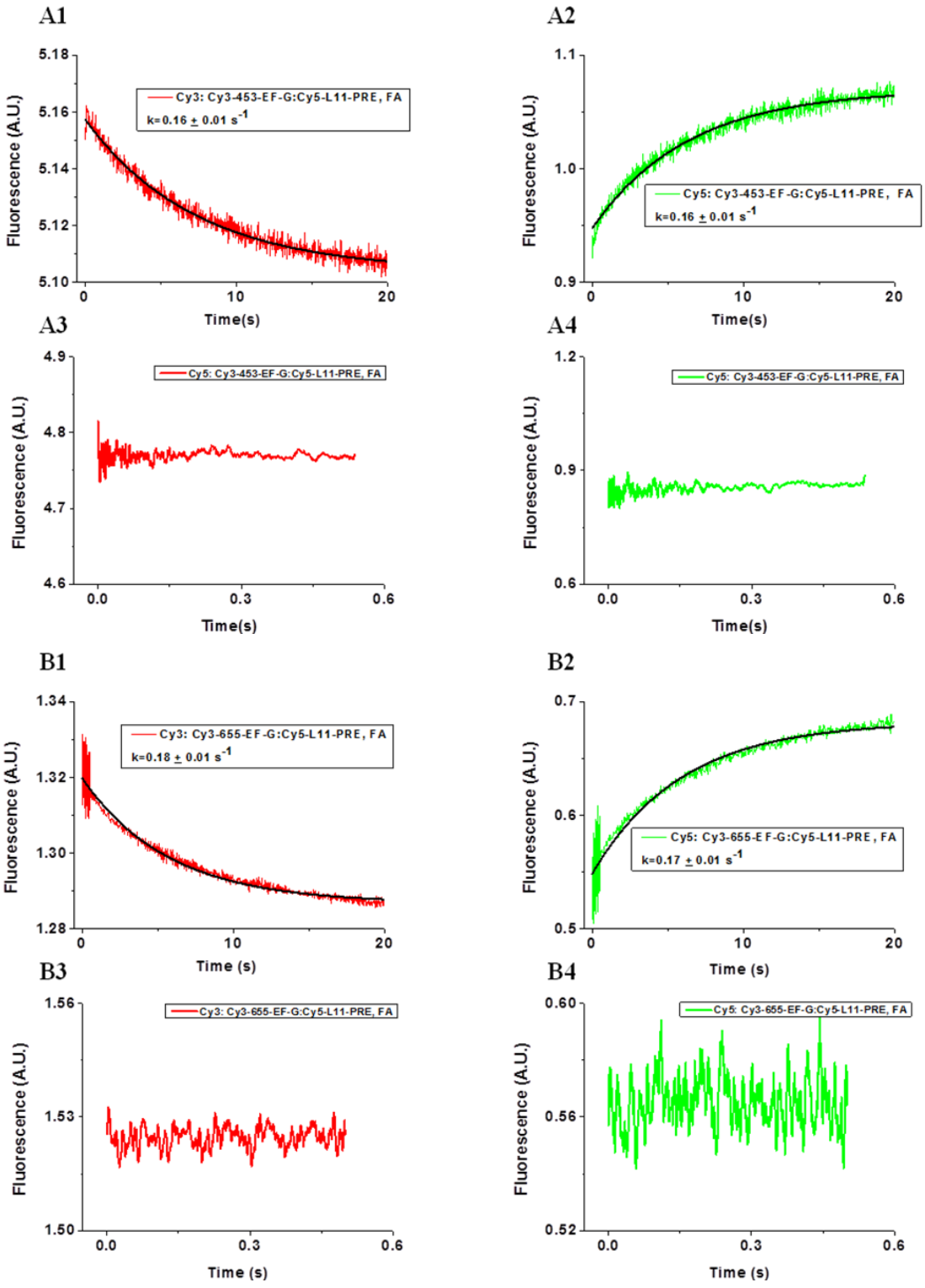
A1
Cy3: Cy3-453-EF-G:Cy5-L11-PRE, FA
k=0.16 ± 0.01 s-1
Fluorescence (A.U.)
Time(s)
A2
Cy5: Cy3-453-EF-G:Cy5-L11-PRE, FA
k=0.16 ± 0.01 s-1
Fluorescence (A.U.)
Time(s)
A3
Cy5: Cy3-453-EF-G:Cy5-L11-PRE, FA
Fluorescence (A.U.)
Time(s)
A4
Cy5: Cy3-453-EF-G:Cy5-L11-PRE, FA
Fluorescence (A.U.)
Time(s)
B1
Cy3: Cy3-655-EF-G:Cy5-L11-PRE, FA
k=0.18 ± 0.01 s-1
Fluorescence (A.U.)
Time (s)
B2
Cy5: Cy3-655-EF-G:Cy5-L11-PRE, FA
k=0.17 ± 0.01 s-1
Fluorescence (A.U.)
Time (s)
B3
Cy3: Cy3-655-EF-G:Cy5-L11-PRE, FA
Fluorescence (A.U.)
Time (s)
B4
Cy5: Cy3-655-EF-G:Cy5-L11-PRE, FA
Fluorescence (A.U.)
Time (s)

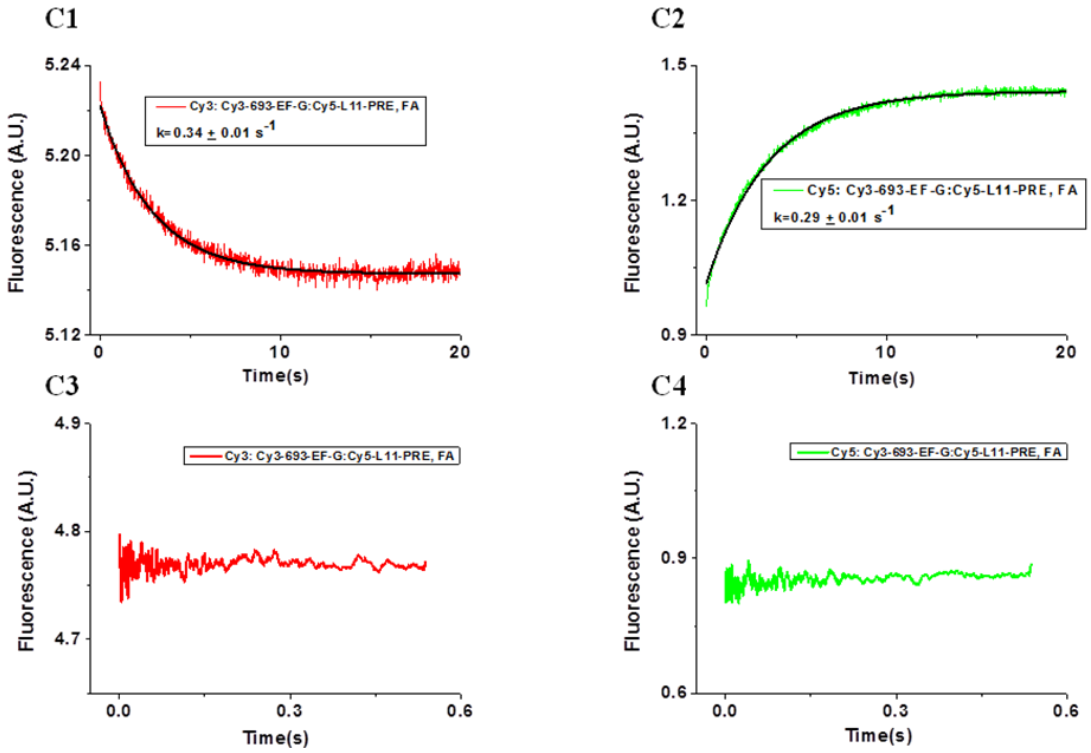

Figure 3.12 Fast kinetic measurements of EF-G^{Cy3} with PRE-II$^{38\text{-}Cy5}$. Experiments were performed at 25 °C in WB buffer. All the results were obtained by mixing 400 µL of PRE-II$^{38\text{-}Cy5}$ (0.5 µM) with 400 µL of 0.75 µM Cy3-EF-G (EF-G$^{453\text{-}Cy3}$, EF-G$^{655\text{-}Cy3}$ or EF-G$^{693\text{-}Cy3}$), FA (1 mM) and GTP (1mM). Cy3 (left, red) and Cy5 (right, green) signal collected from both short time (0.5 s) and long time scale (20 s) are plotted and anti-correlated Cy3/Cy5 signals are obtained for results of 20 s time scale.

Kinetic Exp	EF-G$^{655\text{-Cy3}}$	EF-G$^{453\text{-Cy3}}$	EF-G$^{455\text{-Cy3}}$	EF-G$^{487\text{-Cy3}}$	EF-G$^{692\text{-Cy3}}$	EF-G$^{693\text{-Cy3}}$
Cy3-EF-G : 70S$^{38\text{-Cy5}}$ (GTP) 0.5 s, 12s	NO	NO	NO	NO	NO	NO
Cy3-EF-G : 70S$^{38\text{-Cy5}}$ (FA, GTP) 0.5 s	NO	NO	NO	NO	NO	NO
Cy3-EF-G : 70S$^{38\text{-Cy5}}$ (FA, GTP) 20 s	YES	YES	NO	NO	NO	YES
Cy3-EF-G : PRE-II$^{38\text{-Cy5}}$ (GTP) 0.5 s	NO	NO	NO	NO	NO	NO
Cy3-EF-G : PRE-II$^{38\text{-Cy5}}$ (FA,GTP) 20 s	YES	YES	NO	NO	NO	YES
Cy3-EF-G : PREII$^{38\text{-Cy5}}$ (GDPNP) 5 s, 100 s	NO	NO	NO	NO	NO	NO
Cy3-EF-G : PREII$^{tRNA\text{-Cy5}}$ (GTP) 1 s	NO	NO	NO	NO	NO	NO

Table 3.5 Summary of ensemble rapid kinetic FRET experiments. Experiments were performed at 25 °C in WB buffer. All the results were obtained by mixing 400 µL of 70S$^{38\text{-Cy5}}$ (0.5 µM) or PRE-II$^{38\text{-Cy5}}$ (0.5 µM) with 400 µL of 0.75 µM Cy3-EF-Gs, or PRE-II$^{tRNA\text{-Cy5}}$ (0.1 µM) with 400 µL of 2 µM Cy3-EF-Gs, with GTP (1 mM) or GDPNP (1 mM) or GTP (1 mM) and FA (1 mM). Yes or No indicates whether FRET change was observed over the time ranges indicated.

CHAPTER IV SINGLE MOLECULE FRET STUDIES OF TRANSLOCATION

Abstract

Prokaryotic elongation factor G (EF-G) catalyzes the coupled translocations on the ribosome of mRNA and A- and P-site bound tRNAs during the polypeptide elongation cycle. However, the kinetic pathway of this important step has not been fully elucidated. Here, we describe the application of single molecule fluorescence resonance energy transfer (smFRET) to probe the mechanism of this key process in real time. Attaching a fluorescent probe within domain IV of EF-G permits monitoring of FRET efficiencies to sites in both ribosomal protein L11 and A-site tRNA. Two different sites on L11, position 38 or position 87, as well as two different A-site tRNAs, Phe-tRNA^{Phe} or Val-tRNA^{Val}, were labeled with Cy5. The EF-G:L11 FRET efficiency is constant during EF-G occupancy on the ribosome (300 - 400 ms), whereas EF-G:tRNA FRET proceeds from high to intermediate to low FRET values. This indicates that the EF-G:A-site tRNA distance increases progressively during translocation, with our results providing the first good estimates of the timing of such changes. For both tRNAs, the EF-G:tRNA pair spends most of its time in the intermediate FRET state, with shorter lifetimes in the high and low FRET states. Each transition in the FRET value corresponds to a relative distance change of about 5 to 7 Å, so in total, we capture a 12 Å relative movement of A-site tRNA away from EF-G during translocation. EF-G:A-site tRNA FRET is sensitive to buffer conditions, with high Mg^{2+} and polyamines stabilizing the high FRET state. In addition, the translocation inhibitors viomycin and spectinomycin block formation of the low FRET state, although spectinomycin allows more movement between EF-G and tRNA than viomycin.

4.1 Introduction

Bacterial translation can be dissected into three major stages, including initial, elongation and termination, which requires the correlated movements among the ribosome, tRNAs, as well as important ribosomal factors, e.g., elongation factor G (EF-G) and elongation factor Tu (EF-Tu) (Schmeing *et al*., 2009a). In the elongation cycle, EF-G, a GTPase works dynamically on the ribosome, promoting translocation of tRNAs and mRNA by precisely one codon. Continued progress has been achieved in understanding this key process, including results of structural (Agrawal *et al*., 2000; Cate *et al*., 2013; Tourigny *et al*., 2013; Zhou *et al*., 2013) ensemble (Dorner *et al*., 2006; Pan *et al*., 2007; Savelsbergh *et al*., 2003; Wilden *et al*., 2006) and single-molecule studies (Chen *et al*., 2011a; Chen *et al*., 2013a; Fei *et al*., 2009; Munro *et al*., 2010; Munro *et al*., 2007). However, most of the work has been focused on the pre-equilibrium states of this fast process, leaving the real time dynamics, especially how EF-G first interacts with the A-site tRNA in the pretranslocation complex not fully elucidated (Scheme 4.1). In this work, we studied how EF-G correlated its movement with tRNAs, ribosomal proteins to promote different sub-steps of translocation.

EF-G comprises five domains, the overall structure mimics the structure of the ternary complex, with Domains I-III resemble EF-Tu structure and Domain IV corresponds to the anti-codon region of the tRNA (AEvarsson *et al*., 1994; Czworkowski *et al*., 1994). After peptidyl transfer, a peptide chain is formed in the A-site, leaving a deacylated tRNA in the P site. The A- and P-site tRNAs were observed to fluctuate between the non-rotated (A/A, P/P) and rotated states (A/P, P/E), and adding EF-G promoted translocation of the A, P-site tRNA to the P, E-sites respectively. While some

previous studies showed that EF-G·GTP bound to the rotated state of the ribosome and promoted translocation of tRNAs only from the hybrid states (Fei *et al*., 2008), the most recent single molecule FRET experiments indicated that EF-G can bind to both rotated and non-rotated ribosomes to promote translocation (Chen *et al*., 2011a; Chen *et al*., 2013a). It was proposed that EF-G made its initial contact with the L7/L12 stalk and L10 protein which comprised EF-G binding sites on the large subunit (Savelsbergh *et al*., 2005). While the intrinsic hydrolysis rate of EF-G·GTP is very low (less than 10^{-5} s^{-1}), binding to the ribosome largely enhances the hydrolysis activity of EF-G (at least 5 fold faster than translocation) and the energy released from this process further drives tRNA movements (Rodnina *et al.*, 1997). Upon EF-G binding, it functions allosterically with ribosomal protein L1, located near the exit tunnel, to control the delivery of tRNAs. Domain IV of EF-G reaches out to the A-site decoding center (Gao *et al.*, 2009), preventing back movements of tRNAs, then EF-G finally dissociates from the ribosome in the GDP form after translocation (Fei *et al*., 2009).

4.2 Results

4.2.1 The Design of the experiment

Two FRET pairs, EF-G:L11 and EF-G:tRNA, were studied in the experiment. Ribosomal protein L11 or the A-site tRNA were labeled with Cy5 fluorescence dye. For EF-G:L11 pair, $L11^{Cy5}$-initiation complex (IC) was pre-incubated with WT-ternary complex (TC) to form pretranslocation complex (PRE). For EF-G:tRNA pair, WT-IC was incubated with $tRNA^{Cy5}$-TC. Cy5 labeled PRE was then attached to the slide surface via a single biotin labeled mRNA (Fig 4.1). As TAM^{15} buffer has been used extensively in single molecule studies of ribosomes, both in our laboratory (Chen *et al*., 2011a) and

others (Munro *et al*., 2010), we chose TAM^{15} as the standard buffer condition. Also, 100 nM next TC was added simultaneously with EF-G^{Cy3} for two reasons. First, both PRE and POST complexes (posttranslocation complex) were formed in our system and EF-G bound to both complexes without showing a difference in the binding affinity. As we are only interested in characterizing the EF-G interaction with PRE, we want to block EF-G binding to the POST which blurs the results of PRE. TC shares the same binding site with EF-G and competes with EF-G for binding to the POST. Therefore, 100 nM TC was added. As POST complex had a higher affinity to TC compared to EF-G, and the concentration of TC applied was 100 nM, which was about 10 to 20 fold of EF-G concentration (5nM to 10 nM) used in the experiments, the addition of 100 nM TC should effectively block EF-G binding to the POST. Second, in case EF-G binds, with 100 nM next TC, the second round of translocation would be promoted. The A-site labeled tRNA would move to the E-site, which was far from EF-G^{Cy3} after two cycles of translocation. In this way, we were able to mitigate the contribution of FRET from the P-site labeled tRNA and focus on studying FRET of tRNA translocation from the A-site to the P-site. Unless otherwise mentioned, all experiments were performed under the standard experimental condition, which is TAM^{15} in the presence of 100 nM next round TC. All single molecule experiments were performed at 21°C.

4.2.2 EF-G mutants

4.2.2.1 EF-G mutant selection

The relative movements between EF-G:tRNA and EF-G:L11 were studied to reveal how EF-G works cooperatively with different ribosomal components. The potential mutant sites on EF-G for introduction of a fluorescent label should meet the following

criteria: 1) The distances between the mutant site and either ribosomal protein L11 or the A site tRNA are within FRET (R_o) range of a Cy3/Cy5 pair (about 53 Å); 2) the site should be exposed to the solvent instead of buried inside the structure; 3) the amino acid should not be conserved, and less likely to have functional importance. As we have material stocks and developed matured labeling strategies for both C38 and S87C on large ribosomal protein L11 and labeled tRNAs at the elbow region, the site of EF-G labeling was selected based on its distance to these three sites (Seo *et al.*, 2006). As there was no accessible structure of EF-G bound to the ribosome in the presence of A site tRNA when we started the mutant selection, the EF4 (Lep A) bound ribosome structure was used to find proper mutant sites. Here, cryo-EM structure of EF4, with A/L (Connell *et al.*, 2008) and P/P site tRNAs on ribosomes was selected as the structural model of EF-G bound to PRE.

Three Cy3-labeled EF-G mutants, containing Cys at positions 453, 655, and 693, show L11:EF-G FRET changes in the presence of FA (Section **3.2.5**). Preliminary single molecule FRET experiments were performed by adding each of these labeled mutants to PRE-II$^{tRNA\text{-}Cy5}$ in the absence of antibiotics. Only EF-G$^{693\text{-}Cy3}$ showed an observable FRET with the A-site tRNA. Accordingly, EF-G$^{693\text{-}Cy3}$ was selected for detailed smFRET studies on two FRET pairs, EF-G:L11 and EF-G:tRNA.

4.2.2.2 Ensemble FRET events confirmed the activity of EF-G$^{693\text{-}Cy3}$

The kinetic activity of EF-G$^{693\text{-}Cy3}$ was measured by a translocation assay, proflavin (prf) labeled Phe-tRNA$^{prf\text{-}Phe}$ programmed at the ribosomal A site at 25 °C in WB buffer. Prf substitution of dihydrouridine group was attached within the elbow region of the A site tRNA and translocation of the A site tRNA to the P site leads to an increase of prf

fluorescence intensity (Pan *et al*., 2007). Upon rapid mixing of prf labeled PRE with the same concentration of WT-EF-G or EF-$G^{693\text{-}Cy3}$ in stopped-flow, a single exponential increase of prf fluorescence was observed in both experiments. In the presence of EF-$G^{693\text{-}Cy3}$, the fitted rate constant was 2.5 ± 0.6 s^{-1} at 25 °C, which was about 70% of rate constant in the presence of WT-EF-G (3.5 ± 0.8 s^{-1}), indicating the competency of Cy3 labeled EF-G^{693} in catalyzing fast translocation (see Section **3.2.3.2**).

4.2.3 Characterization of EF-G:L11 FRET interaction

$L11^{38\text{-}Cy5}$ or $L11^{87\text{-}Cy5}$ IC was pre-incubated with WT-TC to form PRE and denoted PRE-$L11^{38\text{-}Cy5}$ or PRE-$L11^{87\text{-}Cy5}$, followed by addition of EF-$G^{693\text{-}Cy3}$. The experiment was performed by using a total internal reflection fluorescence (TIRF) microscope as described in Chapter 2 and green laser (532 nm) was illuminated to excite Cy3 fluorophore directly. The results in both cases are similar to one another, showing FRET between PRE-$L11^{Cy5}$ and EF-$G^{693\text{-}Cy3}$ upon initial excitation. All the observed FRET events presented an increase of Cy3 and Cy5 signals simultaneously, indicating that EF-G binds to the ribosome with a conformation showing detectable FRET to the labeled sites on L11 (Fig 4.2). Dwell time of the FRET events was about 200 - 400 ms with only one fitted peak for both N-terminal (position C38) and C-terminal (position C87) labeled L11. The FRET efficiencies were equal to 0.41 ± 0.01 and 0.67 ± 0.01 for PRE-$L11^{38\text{-}Cy5}$ and PRE-$L11^{87\text{-}Cy5}$, respectively (Fig 4.3). All the FRET events lasted until EF-$G^{693\text{-}Cy3}$ dissociation from the ribosome, with a simultaneous decrease of Cy3 and Cy5 fluorescence.

4.2.3.1 FRET efficiency between Cy3-labeled EF-G and Cy5-labeled L11 (C38S/S87C variant) is constant during EF-G occupancy of the ribosome

FRET events between EF-$G^{693\text{-}Cy3}$ and C-terminal labeled $L11^{87\text{-}Cy5}$ were collected

and further analyzed. Dwell time was fitted by a single exponential function $\boldsymbol{y} = A\exp(-kt)$, with a fitted value equal to 250 ± 5 ms under standard experimental condition (Fig 4.3). FRET efficiency was fitted by Gaussian function $\boldsymbol{y}=y_0 + \left(\frac{A}{\sigma\sqrt{2\pi}} e^{-\frac{(x-xc)^2}{2\sigma^2}}\right)$, showing a single peak value of 0.67 ± 0.01. Averaged FRET values as a function of time were calculated by lining up all FRET events either to the same starting time point or end time point to generate one pre-synchronization trace and one post-synchronization trace (Chen *et al*., 2012; Chen *et al*., 2011a). Synchronized FRET efficiency was plotted as a function of time and showed a constant value for both pre-synchronization and post-synchronization (Fig 4.4, **A**), implying that there was only single FRET state over the entire dwell time of EF-G on the ribosome.

This result was further confirmed by FRET difference distribution and transition density map. FRET events which lasted longer than 6 frames with duration longer than 210 ms (35 ms per frame) were selected. The first and last three frames were averaged separately, defined as initial and final FRET. Difference between the final and initial FRET was calculated and the distribution was plotted, showing a symmetrical ΔFRET distribution relative to $\boldsymbol{x} = 0$ (Fig 4.4, **B**). Some FRET events showed an increased FRET efficiency after translocation (located in the regions $\boldsymbol{x} > 0$), while some showed decreased efficiency (located in the regions $\boldsymbol{x} < 0$), but the majority of events presented similar or unchanged FRET efficiency. As similar numbers of events with increased or decreased FRET were observed, it implied that those events showing changes were mostly due to the noise, instead of being attributable to the relative distance changes between EF-$G^{693\text{-}Cy3}$ and $L11^{87\text{-}Cy5}$ during EF-G residence on the ribosome. Additionally, the initial and final FRET values were plotted as a transition density map. Events located on the

diagonal line on the map presented exactly same initial and final FRET values. The transition density contour map showed a symmetrical pattern relative to the diagonal line with the majority of traces located in the region where ΔFRET was between -0.1 to 0.1(Fig 4.4 **C**), indicating that most events had similar initial and final FRET values.

4.2.3.2 FRET efficiency between Cy3-labeled EF-G and Cy5-labeled L11 (C38) behaves similarly as Cy5-labeled L11 (C38S/S87C variant)

The FRET results between EF-$G^{693\text{-}Cy3}$ and N-terminal domain labeled $L11^{38\text{-}Cy5}$ are similar to those of EF-$G^{693\text{-}Cy3}$:$L11^{87\text{-}Cy5}$ pair, with dwell time equal to 327 ± 5 ms and a lower FRET efficiency of 0.41 ± 0.01 (Fig 4.3, **C, D**). A single FRET state was observed during EF-G residence on the ribosome, as confirmed by postsynchronized analysis, FRET difference distribution and transition density map (Fig 4.4 **D, E, F**). Protein L11 is located at the base of the L7/L12 protein stalk and has significant structural flexibility on the ribosome (Agrawal *et al*., 2000; Agrawal *et al*., 2001). Previous study showed that C-terminal (CTD) and N-terminal domains (NTD) of L11 are connected by a linker which is composed of two proline amino acids. Two L11 structures were compared (Agrawal *et al*., 2001; Wimberly *et al*., 1999) and an inter-domain conformational change by an approximate 7Å shift and 40° rotation between CTD and NTD was observed, which is due to the movement in the linker region. Only a single FRET state was obtained in our work for both N-terminal and C-terminal labeled EF-G, implying that EF-G interacted with C-terminal and N-terminal domains of L11 in a similar manner and that such interaction occurred without L11 inter-domain conformational change.

The EF-G^{693}:$L11^{38}$ and EF-G^{693}:$L11^{87}$ FRET efficiencies of 0.41 and 0.67, respectively, correspond to approximate distances of 56 Å and 47 Å, respectively,

assuming a Förster R_o value of 53 Å (Seo *et al*., 2006). These distances are in qualitative accord with the coordinates from a recently published structure (Zhou *et al*., 2014) in which EF-G and A-site peptidyl-tRNA are bound simultaneously to the ribosome, albeit in the presence of fusidic acid and neomycin, in which the distances between Cβ of N693C and Cβ of C38L11 or S87L11 are 51Å and 37Å, respectively (Fig 4.5). That the FRET distances of EF-G with either L11 or tRNA measured in our work are somewhat larger could be explained by three reasons: 1) the fluorophore-fluorophore distance measured in our work could be considerably greater than α-C-α-C distances calculated from the reported structure; 2) the structure was obtained from *Thermus thermophilus* and our experiments were based on the ribosome from *E. coli*; 3) fusidic acid (FA) was applied in the structural work which could result in a relative conformational change between EF-G and the ribosome/tRNA (Sections **3.2.4.1** and **3.2.5.1**).

4.2.4 Characterization of EF-G:tRNA FRET interaction showing relative distances changes during translocation under standard conditions

4.2.4.1 Overview

To monitor the relative movements between EF-G and the A-site tRNA, the Cy3-labeled EF-G mutant used in the previous L11 experiment, EF-$G^{693\text{-}Cy3}$, was utilized. Two different A-site tRNAs, Val-$tRNA^{Val}$ at dihydrouridine position 17 and Phe-$tRNA^{Phe}$ at dihydrouridine positions 16/20 were labeled with Cy5 hydrazide dye (Kaur *et al*., 2011). PRE-I contains Val-$tRNA^{Val\text{-}Cy5}$ and PRE-II contains Phe-$tRNA^{Phe\text{-}Cy5}$. By immobilizing pretranslocation complexes onto the surface of the slide in a pre-incubation step, and then quickly injecting Cy3 labeled EF-G together with 100 nM wild type next ternary complex, the real-time kinetics of translocation can be monitored**.** The synchronization analysis of all FRET events showed a small FRET decrease as a result of translocation, indicating

that there were relative distance changes between EF-G$^{693\text{-}Cy3}$ and the A-site tRNA^{Cy5} (Detailed discussion in section **4.2.4.3**). In this section, both FRET and kinetic results are described as follows: Sections **4.2.4.2** - **4.2.4.6**, FRET results, including **4.2.4.2**, characterization of FRET; **4.2.4.3**, FRET segmentation; **4.2.4.4**, initial and final FRET distributions; **4.2.4.5**, FRET of POST complexes; **4.2.4.6**, proposed explanations for two different groups of traces. Section **4.2.4.7**, kinetics of translocation for Group I trace.

4.2.4.2 EF-G$^{693\text{-}Cy3}$: tRNA FRET characterization of all FRET results

Single molecule FRET experiments between Cy5 labeled PRE and EF-G$^{693\text{-}Cy3}$ were carried out under standard experimental conditions, as described above. Upon EF-G binding, a simultaneous increase of Cy3 and Cy5 fluorescence was observed, similarly to what was seen in the EF-G:L11 experiment, indicating that EF-G binding to the ribosome gives rise to a detectable FRET signal (Fig 4.6). The dwell time of FRET for PRE-I was 424 ± 9 ms and FRET efficiency distribution was fitted by two peaks with values of 0.18 ± 0.01 and 0.37 ± 0.02, respectively. Similarly, the dwell time for PRE-II was equal to 457 ± 8 ms and FRET distribution was fitted by two peaks, having values of 0.22 ± 0.01 and 0.36 ± 0.03 (Fig 4.7). Importantly, these average dwell times are consistent with the overall ensemble rate constant for translocation of 2.5 ± 0.6 s^{-1}, allowing for the somewhat lower temperature at which the single molecule experiments are performed (ensemble, 25 ^{o}C, smFRET, 21 ^{o}C).

4.2.4.3 Partial resolution of traces showing EF-G:tRNA FRET into two groups

More than one FRET state was observed over the entire FRET events, demonstrated by the results of postsynchronized analysis, FRET difference distribution and transition heat contour map. As discussed in Chapter 2, if there were no relative distance changes

between two labeled positions, pre- and post- synchronization traces should show a single constant FRET value, as what was observed in EF-G:L11 experiments. However, a decrease of final FRET efficiency of EF-G:tRNA FRET pair was obtained, implying there was more than one FRET state during translocation (Fig 4.8). The FRET difference distribution of PRE-I was plotted to study the details of the changes. Interestingly, although the majority of the events still presented no significant FRET changes during translocation, the distribution was not symmetrical, in contrast to what was seen in the EF-G:L11 interaction. A larger proportion of events was observed located in $x < 0$ region with a negative FRET change (Fig 4.9, **A**). The transition heat contour map further confirmed our observation by showing a large proportion of events under the line of identity (Fig 4.9 **B, C**). To determine if these results suggested that the tRNA:EF-G interaction was heterogeneous and could be further segmented by FRET efficiency changes during translocation, a manually selected ΔFRET cutoff value (- 0.1 for PRE-I and - 0.12 for PRE-II) was applied to further segment the traces into two groups, without confirming whether the two groups are really different from each other or not. For PRE-II, essentially similar results were obtained from postsynchronized analysis, FRET difference distributions and transition heat contour maps (Fig 4.8 **B**, Fig 4.9 **D, E, F**).

Traces with large decreased FRET changes (ΔFRET < - 0.1 for PRE-I and ΔFRET < - 0.12 for PRE-II) were placed in Group I, and all other traces (ΔFRET > - 0.1 for PRE-I and ΔFRET > - 0.12 for PRE-II) were placed in Group II. Group I traces constitute 15 - 40 % of the total population depending on different experimental conditions (Detailed discussion in section **4.2.5**). Dwell time analysis provided an indication that these two groups represented two different types of EF-G:tRNA interactions. The dwell times

averaged 555 ± 10 ms (PRE-I) and 543 ± 19 ms (PRE-II) for Group I, which were 1.25 - 1.5 fold longer than the dwell times of Group II (374 ± 13 ms, PRE-I; 435 ± 10 ms, PRE-II). Thus, these two Groups not only had different ΔFRET values during EF-G binding, but also showed a difference in FRET signal duration (Fig 4.10). This suggested that the two Groups were different and could be at least partially resolved.

4.2.4.4 Initial and Final FRET distributions for the EF-G:tRNA pair under standard conditions

In this section we focused on FRET efficiencies measured between EF-G$^{693\text{-}Cy3}$ and the A-site tRNA^{Cy5} upon the first binding of EF-G to the PRE complex or just before EF-G departing from the ribosome, as a prelude to the discussion of the kinetics of EF-G:tRNA FRET efficiency changes during translocation (Section **4.2.4.7**).

Initial and final FRET values were calculated as the average values of the first three and last three frames of the FRET events, respectively. For PRE-I, the initial FRET distribution showed two major peaks, with FRET efficiency values of 0.23 ± 0.01 and 0.42 ± 0.01, and relative areas of 0.45 and 0.55, respectively (Fig 4.11, **top, left**). The initial FRET distribution was broad, which indicated that tRNAs were in a variety of states when EF-G bound to the ribosome. The final FRET distribution also had two peaks with approximately the same values as the initial FRET distribution (0.22 ± 0.01 and 0.41 ± 0.01) but with very different relative areas (0.65 and 0.35, respectively) (Fig 4.11, **top, right**), indicating that 36% ((0.55-0.35)/0.55=0.36) of the PRE complexes with an initial high FRET efficiency successfully converted to the low FRET state.

The results for the PRE-II complex were qualitatively similar but, for the most part, quantitatively different. The initial FRET distribution showed two major peaks, with

FRET efficiencies of 0.27 ± 0.01 and 0.45 ± 0.05 and with relative areas of 0.70 and 0.30 (Fig 4.11, **bottom, left**). The corresponding final values were 0.25 ± 0.01 and 0.40 ± 0.04 for the FRET efficiencies and 0.80 and 0.20 for the relative areas (Fig 4.11, **bottom, right**). One quantitatively similar result was obtained in the percentage of traces in PRE-II having initial high FRET efficiency that was successfully converted to the low FRET state (33% vs. 36% in PRE-I).

As EF-G:L11 interaction indicated that the EF-G:L11 FRET pair only presented a single FRET value, the differences in EF-G:tRNA FRET efficiencies and distributions between PRE-I and PRE-II are likely due to differences in the binding of different peptidyl-tRNAs [$tRNA^{Val}$ (PRE-I) vs. $tRNA^{Phe}$ (PRE-II)] at the A-site. PRE-I with Val-$tRNA^{Val\text{-}Cy5}$ showing a higher preference for the high FRET efficiency state compared to PRE-II with A site Phe-$tRNA^{Phe\text{-}Cy5}$, which is consistent with the results from Chen *et al.* (2011).

It is reasonable to assume that the initial FRET distribution was determined by both the equilibrium states of the A-site tRNA before EF-G binding and the binding affinity of EF-G to the corresponding states. Chen *et al*. (2011) reported that at equilibrium in the same buffer condition, the classic and hybrid populations of tRNAs in the absence of EF-G were in 1:1 ratio for PRE-II complex. In our experiments, the relative populations of high and low FRET states on EF-G addition, which correspond to class and hybrid tRNA states (Detailed discussion in Section **4.2.6.1**) was 0.3:0.7, implying the binding affinity of EF-G to the hybrid FRET state was approximately two fold of that to the classic state. The initial FRET distribution plots were broad for PRE-I and PRE-II, suggesting the possibility that EF-G bound to different states of tRNAs which were located along the

translocation trajectories between classic and hybrid states. This result is consistent with Fischer *et al*. (2010) study which showed that while classic and hybrid tRNAs were the two most abundant populations, tRNA possessed a number of different conformations along the translocation trajectories that could be captured by EF-G (Fischer *et al*., 2010).

Initial FRET distributions of Group I and Group II were plotted separately for both PRE-I and PRE-II (Figure 4.12). For Group I, most of the initial FRET events displayed high FRET values for both PRE-I and II, but with a broad distribution (Fig 4.12 **A**, **C**). This further supported that multiple high FRET states existed at the beginning of translocation that could be captured by EF-G. For Group II, the initial FRET values were dominated by the lower FRET values in both PRE complexes, but still a certain proportion of high FRET state was observed. Since Group II is characterized by traces showing similar initial and final FRET values, this distribution of initial FRET states suggests that Group II includes both translocation events that start from low FRET states and non-productive binding events to the high FRET states (Fig 4.12 **B**, **D**).

4.2.4.5 Binding of EF-G $^{693\text{-}Cy3}$ to POST Complex

Characterizations of FRET between EF-G$^{693\text{-}Cy3}$ and PRE^{Cy5} were the focus of this study. However, after one cycle of translocation, Cy5 labeled peptidyl tRNA in the P-site gives rise to FRET signals with EF-G$^{693\text{-}Cy3}$ that could affect the interpretation of our results. Although 100 nM next TC was added to lessen such a FRET contribution, still there is certain possibility that FRET between EF-G$^{693\text{-}Cy3}$ with POST^{Cy5} were counted. Therefore, binding of EF-G$^{693\text{-}Cy3}$ to POST^{Cy5} complexes was studied as negative controls.

WT-EF-G was added to the pre-formed PRE to produce post translocation complex (POST) in TAM^{15} buffer. POST complexes formed by PRE-I and PRE-II were denoted

POST-I and POST-II, respectively. Each POST complex was formed after one cycle of translocation and active peptidyl-tRNA^{Cy5} was translocated to the P site. POST was attached to the slide surface by using the same single biotin labeled mRNA as previously described, followed by addition of EF-G$^{693\text{-}Cy3}$ in the absence of next TC. EF-G$^{693\text{-}Cy3}$ bound and dissociated from the ribosome, resulting in a FRET between EF-G$^{693\text{-}Cy3}$ and P site peptidyl-tRNA^{Cy5}. FRET efficiency distribution of POST-I had lower values compared to the results of EF-G binding to the PRE complex, giving values of 0.14 ± 0.01 and 0.22 ± 0.01 (Fig. 4.13, **A**), which correspond to distances of 72 Å and 65 Å, respectively. Zhou *et al*. (2014) reported tRNA in the pe/E site showing a distance of 88 Å to the position 693 on EF-G, which is larger but comparable to the calculated result of 72 Å. Therefore, 0.14 ± 0.01 may correspond to the FRET of Cy5-P-site tRNA: Cy3-EF-G pair and 0.22 ± 0.01 may be attributed to FRET between the inactive tRNA in the A/P site and EF-G. Also, the dwell time of the POST complex was 301 ± 6 ms, significantly shorter than for EF-G interaction with the PRE complex (Fig. 4.13, **B)**. A single FRET state over the entire duration was obtained, demonstrated by postsynchronized analysis which showed only one constant value for both pre- and post-synchronizations, indicating that, unlike in PRE, there were no relative distance changes between the P-site tRNA^{Cy5} in POST-I and EF-G$^{693\text{-}Cy3}$ (Fig 4.13, **C**). The ΔFRET distribution of POST-I further confirmed this conclusion (Fig 4.14). Unlike in PRE, the distribution of delta FRET for POST showed a symmetrical pattern relative to $\boldsymbol{x} = 0$. The Group I population was largely suppressed in POST-I complexes, suggesting that Group I can be attributed to translocation, which involves movements of tRNAs and mRNA by one codon. Similar results were obtained for POST-II complexes. FRET efficiencies were equal to 0.16 ±

0.01 and 0.29 ± 0.02, respectively with a dwell time of 275 ± 3 ms (Fig. 4.13, **D, E**). A constant FRET value was obtained in postsynchronized analysis and Group I traces were again not present (Fig. 4.13, **F** and Fig 4.14).

4.2.4.6 Proposed explanations of Group I and Group II traces

Previous studies showed that EF-G binding to the ribosome could be both productive, catalyzing active translocation, and non-productive, with EF-G dissociation occurring prior to translocation (Chen *et al*., 2013a; Munro *et al*., 2010). For the reasons cited above (longer residence time of EF-G, reflecting the longer time needed to complete the translocation process, and decreases in FRET during the residence time, expected as a result of peptidyl-tRNA movement from the A- to the P-site) we conclude that Group I traces reflect largely productive, translocation events. On the other hand, we believe that Group II traces comprised both translocation events starting from lower FRET states and non-productive binding events during which EF-G binds and dissociates from the same state without completing translocation. Here, it is noteworthy that high FRET events (E > 0.4) in Group II had much shorter dwell times (112 ± 2 ms for PRE-I and 169 ± 6 ms for PRE-II) than events started with high FRET in Group I (Fig 4.15)

4.2.4.7 Translocation kinetics of Group I

Synchronization analysis was applied to extract FRET efficiencies and durations of FRET events in Group I and characterize the kinetics of tRNA translocation (Chen *et al*., 2011a). The postsynchronized traces were calculated from the averaged FRET values as a function of time. All FRET events were lined up at an identifiable trigger transition and averaged. To get equal durations, all individual traces were extended at the prior and subsequent segment ends. FRET traces were aligned at the beginning (pre-

synchronization) or end (post-synchronization). The fitted results of synchronization analysis of Group I traces showed three FRET states, with the conversion of the intermediate FRET state to the low FRET state constituting the rate limiting step.

4.2.4.7.1 Group I traces show three FRET states

PRE and post synchronization traces were each fitted with a single exponential function. The apparent overall translocation rate is the reciprocal of the summed lifetimes of all the states. Both two- and three- state models were applied to the two PRE complexes. The three state model turn out to show better fitting results to the raw data for both PRE complexes (Fig 4.16, Fig 4.17). Therefore, the three-state model will be applied in our following kinetic analysis.

For PRE-I, FRET events started with a high FRET value of 0.47 ± 0.01, via an intermediate FRET 0.25 ± 0.01, and finally disappeared with a low FRET of 0.24 ± 0.01, corresponding to a distance change from about 54.1 Å to 63.6 Å and then to 64.2 Å. These values agree reasonably well with the average distance between Cβ of N693C in EF-G and C4 of positions 16/20 of the A-site bound N-acetyl-Val-tRNA^{Val} in the recent structure of Zhou *et al*. (2014). The transitions from 0.47 to 0.25 and 0.24 to zero proceeded with rate constants of 18.0 ± 0.4 s^{-1}, 18.4 ± 1.8 s^{-1} respectively, while the conversion from 0.25 to 0.24 was slower, with a rate constant of 1.8 ± 0.1 s^{-1} (Table 4.4 and Fig 4.17, **A**). For PRE-II, essentially similar results were obtained. FRET events started with a high FRET value of 0.49 ± 0.01, via an intermediate FRET of 0.31 ± 0.01, and finally disappeared with a low FRET of 0.26 ± 0.01, corresponding to a distance change from about 53.7 Å to 60.6 Å and then to 63.1 Å. The transitions from 0.49 to 0.31 and 0.26 to zero proceeded with rate constants of 24.4 ± 1.1 s^{-1}, 12.6 ± 1.1 s^{-1} and

the conversion from 0.31 to 0.26 proceeded more slowly, with a rate constant of 1.6 ± 0.1 s^{-1} (Table 4.4 and Fig 4.17, **B**).

4.2.4.7.2 Transition from INT to Low is the rate determining step

As described above, for both PRE complexes, transition from intermediate FRET (INT) to low FRET (Low) is the rate limiting step but with a small FRET change, and from high FRET (High) to intermediate FRET (INT) is not rate limiting but shows a large FRET change. As Group II also contains active translocation events which only give rise to a small FRET change, it is likely that transition from INT to Low FRET is included in Group II. Such transitions should have a longer duration as they correspond to the rate-limiting step in translocation. To further examine this point, the timing of translocation events with an initial FRET value of 0.35 to 0.27 and final FRET of 0.27 to 0.21 in Group II was analyzed. The average dwell time of this group for PRE-I complexes was determined to be 670 ± 43 ms (Fig 4.18, **A**), considerably longer than the dwell time of the total population 424 ± 9 ms (Fig 4.7), consistent with the notion that FRET conversion from INT to Low was the rate determining step. Similar results were found for PRE-II, with an average dwell time of the selected traces equal to be 630 ± 30 ms (Fig 4.18, **B)**, suggesting that different tRNAs have similar translocation trajectories.

4.2.4.7.3 Choosing different ΔFRET cutoffs does not substantially alter the kinetics of Group I traces

By definition, Group I and Group II are two types of events with different ΔFRET values. As the 0.1 cutoff value was selected somewhat arbitrarily, several different cutoff values were applied to test the robustness of our interpretation of the results (Table 4.2). We want to examine how many traces were placed in Group I when different cutoff

values applied, but the noise was counted in our measurement which complicated the results. To get rid of the noise, the number of traces in corresponding positive ΔFRET regions was used as the benchmark value of noise (for instance, number of traces with ΔFRET > + 0.10 was counted as noise for the traces with ΔFRET < - 0.10), for the noise should present a normal distribution as a function of ΔFRET. Therefore, a larger cutoff value (absolute value) would reduce noise counted in Group I (for instance, for PRE-I complexes, the numbers of traces with ΔFRET > + 0.10 and ΔFRET > + 0.20 were 522 and 67, respectively). Global fitting was applied to Group I with different cutoff values to test the robustness of our results. Transition rates were fitted with the cutoff values between - 0.12 and - 0.20. The fitted transition rates were little affected, confirming the robustness of the three-state model. Similar results were found for PRE-II (Table 4.2 **a, b**).

4.2.5 Characterization of EF-G:tRNA FRET interaction showing relative distances changes during translocation under non-standard conditions

4.2.5.1 Ternary complex concentration effect on translocation kinetics

Elongation factor Tu (Tu) is believed to bind to the ribosome at L7/L12, sharing the same binding site with EF-G. As there are two copies of L7/L12 dimer per *E. coli* ribosome, it is possible, even likely, that Tu and EF-G could bind to the ribosome simultaneously at some point. Therefore, ternary complex (TC) binding may have three possible effects on EF-G catalyzed translocation: 1) binding to the A-site - expected to be codon dependent; 2) binding to L7/L12 - expected to be codon independent 3) uncharged tRNA (present within TC preparations) binding to the E-site - expected to be codon independent (Lill *et al*., 1987). As explained above, we added 100 nM of the next cognate TC as part of the standard reaction mixture for studying EF-G:peptidyl-tRNA interaction during translocation. To further examine the effect of TC complex on

translocation, here we examine the effects of either eliminating the next cognate TC (0 nM TC) or of increasing the TC concentration to 500 nM. TC was added along with EF-$G^{693\text{-}Cy3}$ to both PRE-I and PRE-II. As compared with adding 100 nM TC, eliminating TC did not alter FRET efficiency distribution, while adding 500 nM TC shifted the high FRET peak to an even higher value for both PRE-I and PRE-II (Fig 4.19). The total dwell time of FRET events was unchanged for PRE-I and was shorter for PRE-II in the absence of TC. Interestingly, the total dwell time was reduced to half of its value with the addition of large concentration (500 nM) TCs (Table 4.4) for both PRE-I and PRE-II. Further analysis was applied to Groups I and II traces, respectively. For PRE-I, a similar trend of dwell time change at different TC concentrations was observed for Groups I and II, with unchanged dwell time at 0 nM TC and half reduced dwell time at 500 nM TCs. For PRE-II, under 0 nM TC, dwell time of both Groups I and II was reduced and similar reduction in dwell time was obtained for 500 nM TCs condition. To test whether this effect was codon dependent or not, 500 nM non-cognate Arg-$tRNA^{Arg}$ was applied and showed a similar dwell time reduction (Total dwell times are 202 ± 4 ms for PRE-I and 249 ± 5 ms for PRE-II), implying that this effect was not codon dependent and could be attributed to either the binding effect of EF-Tu to L7/L12 on the 50S subunit or of deacylated tRNA to the E-site. Either of these possibilities could decrease the affinity of EF-G on the ribosome and promote its release. While eliminating TC did not change the transition rates for PRE-I, 500 nM TC did reduce the transition rate from High to INT (k_1 from 18.1 ± 0.4 s^{-1} to 15.7 ± 1.2 s^{-1} for PRE-I and from 24.4 ± 1.1 s^{-1} to 12.8 ± 0.5 s^{-1} for PRE-II) and increased the dissociation of EF-G (k_3 from 18.4 ± 1.8 s^{-1} to 38.6 ± 18.7 s^{-1} for PRE-I and from 12.6 ± 1.1 s^{-1} to 20.9 ± 3.6 s^{-1} for PRE-II), leaving the transition rate constant

from INT to Low unchanged (Table 4.4). The possible explanation for the decreased transition rates from High to INT for PRE-I and PRE-II would be that with high concentration of TC complexes, uncharged tRNA within the TC preparation, bound to the E-site non-specifically, favoring the classic state position for A-site tRNA and extending the life-time of the high FRET state.

4.2.5.2 Buffer effect on translocation kinetics

Our standard conditions employed 15 mM Mg^{2+} in the absence of polyamines. We determined the effects of both reducing Mg^{2+} and adding polyamines on translocation kinetics, as reflected in the measurement of FRET values, dwell times and kinetics (Table 4.6, Fig 4.21 and Fig 4.22). For PRE-I, the high FRET proportion was increased in both polyamine buffer and by reducing Mg^{2+} to 7 mM, with the effect being more marked in the presence of polyamine. By contrast, for PRE-II the overall FRET efficiency distribution was essentially unchanged by reduced Mg^{2+} concentration or addition of polyamine (Table 4.5).

Decreasing Mg^{2+} from 15 mM to 7 mM resulted in shorter dwell times for both PRE-I and PRE-II, with reduced values for both Groups I and II. For PRE-I, the transition rate constant (k_1) from High to INT was slightly increased (from 18.1 ± 0.4 s^{-1} to 21.6 ± 1.1 s^{-1}), while the rate constants from INT to Low (k_2) was increased by a factor of two (from 1.8 ± 0.1 s^{-1} to 3.9 ± 0.1 s^{-1}). Similar fitting results were obtained for PRE-II, except that the transition rate constants from Low to dissociation was unchanged and from High to INT was slightly decreased (Table 4.6).

Addition of polyamines did not much change overall dwell times. For PRE-I, a decrease in the dwell time of Group II was offset by an increase on the dwell time of

Group I, while for PRE-II added polyamine had little effect on either overall dwell time or the dwell times for Groups I and II. For PRE-I, adding polyamine significantly decreased the transition rates (from 18.1 ± 1.8 s^{-1} to 10.2 ± 0.5 s^{-1} for k_1, from 1.8 ± 0.1 s^{-1} to 1.1 ± 0.3 s^{-1} for k_2, and from 18.4 ± 0.1 s^{-1} to 9.2 ± 1.2 $s^{-1}$for k_3). For PRE-II adding polyamine had only minor effects, slightly decreasing k_1 and k_3 and having little effect on k_2. Added polyamine also increased the percentage of Group I traces from 29.8 % to 37.7 % for PRE-I and from 19.0 % to 25.1 % for PRE-II (Table 4.6).

In summary, added polyamine stabilized high FRET states in PRE I and II by both reducing the transition rate from High to INT and increasing the portion of tRNA starting translocation from a high FRET state.

4.2.6 Antibiotics effect on EF-G:tRNA FRET interaction

Many biochemical and structural studies have revealed that a diverse array of antibiotics function during translocation to inhibit protein synthesis. Fusidic acid (FA) binds to Domains G, II and III of EF-G, prevents EF-G conformational changes following GTP hydrolysis, but does not inhibit translocation (Gao *et al*., 2009). Viomycin (VIO) decouples the movements between EF-G and the A-site tRNA, blocking the effective translocation of the A-site tRNA and stabilizing the ribosome in both ratcheted and unratched states (Ermolenko *et al*., 2007; Peske *et al*., 2004; Stanley *et al*., 2010; VAZQUEZ *et al*., 1977). Spectinomycin (Spc) binds to helix 34 of the small subunit head domain on the ribosome and inhibits translocation after GTP hydrolysis and Pi release (Munro *et al*., 2010; Peske *et al*., 2004).

4.2.6.1 Viomycin perturbs EF-G:tRNA FRET state transitions

PRE-I and II interactions with EF-G^{Cy3} were carried out in the presence of 100 μM

VIO under standard experimental conditions. The FRET distribution was shifted to higher values on VIO addition with peak values of 0.27 ± 0.01, 0.42 ± 0.01 for PRE-I [compare Fig 4.23, middle left (+VIO) with Fig. 4.21B (-VIO)] and 0.31 ± 0.01, 0.52 ± 0.02 for PRE-II [compare Fig 4.23, middle right (+VIO) with Fig. 4.21E (-VIO)]. Previous studies suggest that VIO blocks translocation of the A-site tRNA to the P site and stabilizes tRNAs in both A/A classic and A/P hybrid states. Therefore, the 0.27 and 0.42 FRET states are attributed to the EF-G:A/P tRNA and EF-G:A/A tRNA structures for PRE-I. Similarly, 0.31 and 0.52 FRET states are attributed to the EF-G:A/P tRNA and EF-G:A/A tRNA structures for PRE-II . In the absence of VIO, FRET conversions from High to INT and to Low efficiencies were observed. Added VIO suppressed these FRET conversions, demonstrated by both synchronization analysis and ΔFRET distribution. Postsynchronized analysis showed constant values for both pre and post synchronization traces, indicating that there were no FRET efficiency changes during the entire residence time of EF-G on the ribosome (Fig 4.24 **A, B**). Similarly, added VIO completely suppressed Group I traces as plotted in Fig 4.24 **C, D**.

The same experiments were repeated under different buffer conditions described above (Section **4.2.5.2**). Adding polyamine at 15 mM Mg^{2+} led to an increases in the fraction of PRE complex in the high FRET state (E ≈ 0.5) which was more pronounced for PRE-II than for PRE-I, suggesting that high Mg^{2+} and polyamine concentrations stabilize a classic-like state (Fig 4.23). To sum up, these findings together revealed that EF-G:A/A site tRNA revealed a high FRET value ~ 0.5, and EF-G:A/P hybrid tRNA showed an intermediate FRET value ~ 0.3, while the low FRET state (0.23 for PRE-I and 0.26 for PRE-II) was not observed in the presence of VIO. This indicates that low the

FRET state observed in the absence of antibiotics is attributable, at least in part, be contributed by tRNAs in the late steps of translocation, which were not populated in the presence of VIO.

4.2.6.2 Spectinomycin (Spc) inhibits complete translocation

PRE-I and II interactions with EF-G^{Cy3} were repeated in the presence of 5 mM Spc. Added Spc suppressed the population of traces showing a complete FRET change as what was observed with no antibiotics, but still allowed some FRET changes. In the presence of Spc, the FRET distribution was shifted to lower values compared to that seen with added VIO and shifted to higher values compared to the experiments lacking antibiotic, with peak values of 0.19 ± 0.01 and 0.38 ± 0.02 for PRE-I, and 0.23 ± 0.01 and 0.45 ± 0.01 for PRE-II (Fig 4.25). This indicated that Spc hindered translocation in a later step compared to VIO, in accord with published results (Pan *et al*., 2007, Munro *et al*., 2010). Interestingly, with Spc, we captured a smaller FRET change, demonstrated by synchronization analysis, and the transition was a one step process with no intermediate FRET state observed. Also, Group I traces were observed in ΔFRET distribution but the population was smaller compared to that in the absence of antibiotics (Fig 4.26 **B, D** and Fig 4.14 **A, C**). Taken together, these data suggested that Spc allowed the initial EF-G to engage in the GTPase activation center and A-site tRNA conformational change, but inhibited a later step of translocation. Similar global fitting analysis was applied here to the traces with large FRET change. Two FRET states were obtained for both PRE-I and PRE-II complexes. For the PRE-I complex, transition rate constants from the High (0.53 ± 0.01) to the Low FRET state (0.26 ± 0.01) and from Low FRET state to dissociation are 5.7 ± 0.2 s^{-1} and 3.3 ± 0.1 s^{-1}, respectively. Similar results were calculated for PRE-II,

with efficiencies for both FRET states equal to 0.53 ± 0.01 and 0.27 ±0.01 and transition rates of 5.7 ± 0.1s^{-1} and 4.5 ± 0.1 s^{-1} (Fig 4.27). The results suggest that in the presence of Spc, the lowest FRET state, which was observed in the absence of antibiotic, was not populated, and that EF-G dissociated from an intermediate state, with a FRET value similar to that of a hybrid state, without catalyzing the complete translocation.

4.3 Discussion

Comparing our results with previous smFRET studies using labeled EF-G

smFRET studies have the potential to elucidate reaction mechanism by identifying the important intermediates that may be too short-lived or weakly populated to be detected in the ensemble FRET measurements. Since 2007, several smFRET studies have been published focusing on different aspects of the role of EF-G in translocation. Wang in our group first reported smFRET studies measuring FRET between position 231 in the G' domain of EF-G, which is far from residue 693, the labeling position most utilized in our work, and the NTD of L11 (C38) on a ribosome engaged in poly Phe synthesis, showing that two FRET states can be identified, with efficiencies of 0.3 and 0.6 respectively (Wang *et at*., 2007). However, due to the low time resolution of the experiment, no dwell time or transition rates were reported in this work. In 2010, Munro *et al*. reported another smFRET work of translocation. Cy3 labeled $tRNA^{fMet}$ (U8) and Cy5 labeled L1 (S55C) construct were used to study the formation of the unlocked state. Cy3-fMet-Phe-$tRNA^{Phe}$ (U47) and Cy5-EF-G were used to study the EF-G interaction with the A site tRNA. But in this work, EF-G was enzymatically labeled via the Sfp phosphoantetheinyl transferase reaction to a peptide (12 aa in length) fused at the C terminus. As a result, the dye could be far away from EF-G protein, making questionable utilizing the FRET signal to

monitor the relative movements between EF-G and A-site tRNA. This work focused on the ribosome spontaneous movement which results in an unlocked state, suggesting that this intrinsic conformational change of the ribosome determines the rate of translocation. They observed FRET between EF-G and the A-site tRNA with a dwell time of 385 ms, which matches the dwell time of total FRET events in our work (424 ± 9 ms, PRE-I; 457 ± 8 ms, PRE-II). However, at the time resolution used in Munro's work, transition rates between FRET states could not be accurately determined (Munro *e al.*, 2010). Chen *et al*. (2013) correlated the composition and conformation of the ribosome during translocation and focused on elucidating the ratcheting and back ratcheting motions of the ribosome by using Cy3 labeled 30S and quencher labeled 50S. They reported dwell times for translocation of 122 ms at 5 mM Mg^{2+} increasing to 270 ms at 15 mM Mg^{2+}, somewhat shorter than our results for translocation. However, in their measurement, dwell time is based on measuring multiple cycles of translocation. In contrast, our result is obtained from the first round of translocation, which is believed to be longer than translocation occurring in the later cycles (Chen *et al*., 2011b). The most recently published EF-G translocation work (Salsi *et al*., 2014) followed the movement of Domain IV on EF-G (either position 538 or 541) by measuring FRET between labeling sites on Domain IV of EF-G and small ribosomal protein S12, which is the only protein located at the subunit interface near the A-site. By comparing FRET measured in the presence of different antibiotics which are believed to stabilize either PRE or POST complexes, this work describes a nice picture of EF-G Domain IV moving toward the A-site to facilitate the movement of peptidyl-tRNA from the A site to the P site. However, due to weak EF-G binding, all the results are obtained with antibiotics FA and/or VIO, no real-time

translocation with dwell times and transition rates characterized.

Here, we monitor FRET between fluorophores attached to EF-G^{693} and ribosome protein L11 or the A site tRNA to directly observe the relative distance changes between EF-G:L11 and EF-G:tRNA. Our work provides the first good estimation of translocation kinetics with rate constants of each transition accurately determined and coupled movements between EF-G:tRNA and EF-G:L11.

EF-G:L11 shows constant FRET during translocation

For the EF-G:L11 pair, constant FRET was obtained for both a N-terminal domain (NTD) labeled residue (C38) and a C-terminal domain (CTD) labeled residue (C87). L11 has a flexible structure with a linker region that is composed of two proline amino acids. A comparison between EF-G bound ribosome with EF-G free ribosome structures reveals that the NTD of L11 undergoes a large conformational change and large rearrangements upon EF-G binding, with the EF-G binding regions on the NTD and the CTD moving toward each other (Wimberly *et al*., 1999; Agrawal *et al.*, 2001). In addition, during translocation, Domains III-V of EF-G are believed to undergo large distance displacements (Agirrezabala *et al*., 2009; Tourigny *et al*., 2013; Zhou *et al*., 2013), Despite these results from structural studies, we observe no FRET efficiency changes between EF-G and either NTD or CTD labeled L11 during the entire occupancy of EF-G on the ribosome, as demonstrated by synchronization analysis. This implies that L11 internal conformational changes that are induced by EF-G binding occur prior to translocation, and that, during translocation, either L11 moves together with EF-G or that the labeled positions of EF-G (CTD) and L11 do not move, which seems less likely.

Group I traces measure the translocation trajectory

A significant fraction of traces for the EF-G:tRNA FRET pair, denoted Group I traces, showed decreased FRET efficiency during translocation and had a longer EF-G residence time on the ribosome than traces showing little FRET change (Fig 4.9, Fig 4.10). We propose that the FRET efficiency changes in Group I traces reflect changes in EF-G:tRNA distance during translocation, based on the following considerations. EF-$G^{693\text{-}Cy3}$ is active in translocation confirmed by fluorescence increase of prf labeled tRNA programmed at the ribosomal A-site (Fig 3.5). The residence time of EF-$G^{693\text{-}Cy3}$ for Group I traces is similar to the overall rate of translocation measured in rapid kinetic ensemble experiments, considering a) the measured ensemble rate constant in this work at 2 μM EF-G concentration is 2.5 ± 0.6 s^{-1} for EF-$G^{693\text{-}Cy3}$ mutant and the measured EF-G residence time of Group I in smFRET is ~0.5 s, corresponding to a rate constant of 2 s^{-1}; b) the Km for EF-G in Pan *et al.* (2007) is ~ 1.14 - 1.6 μM, so the saturated ensemble rate would be about 4.5 s^{-1}; c) the smFRET experiments are performed at 21 ^{o}C and the ensemble experiments are performed at 25 ^{o}C. Increasing the temperature by 4 ° C, it is likely to raise the smFRET rate by 1.5 - 2 fold which is about 3 - 4 s^{-1}, and matches the results of ensemble measurements both in our work and Pan's work in 2007.

EF-G interactions with POST were also studied. PRE complex (about 10 ~ 30 nM) was pre-incubated with fully active wild type EF-G (~ 3 μM) to form the POST complex. The direct comparison of ΔFRET distributions between EF-G:POST and EF-G:PRE suggests that, unlike in PRE complex, Group I traces are not present in POST complex (Fig 4.14). The result is further supported by the postsynchronization analysis as a constant FRET efficiency is obtained (Fig 4.13 **C, F**), suggesting that there are no relative distance changes between EF-G and POST complex bearing Cy5 labeled tRNA in the P

site. This result suggests that Group I traces report on those A-site tRNAs which undergo translocation to the P site.

This suggestion is further supported by results that measure PRE complex interactions with EF-G in the presence of viomycin (VIO) or spectinomycin (Spc). VIO is a cyclic peptide antibiotic that binds at the 16S and 23S ribosomal RNA interface and inhibits translocation by stabilizing tRNAs in the A and P sites (Modolell *et al.*, 1977), while allowing both EF-G binding and fast GTP hydrolysis (Ermolenko *et al.*, 2007, Stanley *et al.*, 2010). Translocation is completely inhibited by 100 μM VIO, the concentration used in our experiment. The ΔFRET distribution of PRE bearing Cy5 labeled A-site tRNA in the presence of VIO shows that Group I traces are fully suppressed (Fig 4.24), indicating that Group I traces are attributable to translocation of the A-site tRNA to the P-site. Spc binds to h34 of 30S neck region and disturbs translocation by inhibiting swivelling of the head of the 30S subunit, but does not block the movements of tRNAs in 50S subunit (Pan *et al.*, 2007). In our experiments, Spc suppresses the population of traces showing a complete FRET change. Moreover, global fitting of the results with PRE-II clearly show that, in the presence of Spc, good fits can be obtained by using a two-state model (Fig 4.27), while without Spc, a three-state model is required for a good fit (4.17). This result suggests that, with Spc, EF-G dissociates in an intermediate state without finishing catalyzing the complete translocation process. This conclusion is in agreement with Pan *et al*. (2007) who reported that Spc stabilizes a kinetically competent intermediate state of EF-G induced translocation, with puromycin activity falling between that of PRE and POST complexes. Combining all the aforementioned evidence leads to the conclusion that Group I traces arise from A-site

tRNA translocation.

Translocation kinetics of EF-G:tRNA

Unlike EF-G:L11 which shows a constant FRET value during the whole EF-G duration on the ribosome, EF-G:tRNA interaction possesses heterogeneous properties. The previous view raised by Gonzalez and coworkers in 2008 suggested that EF-G only binds to the hybrid state of tRNAs and shifts the equilibrium of the ribosome to the ratcheted state. In 2011, Chen *et al.* demonstrated that EF-G binds to both rotated and non-rotated states of the ribosome, by studying the tRNA: tRNA FRET and tRNA:L11 FRET. This idea was later confirmed by Chen *et al.* (2013) as EF-G binding to both rotated and nonrated states was observed with Cy3 labeled 30S and quencher labeled 50S.

In our work, by measuring the dynamics of FRET interaction between the EF-G:tRNA pair, we are able to directly characterize how EF-G samples tRNAs states. The initial FRET distribution is broad and implies that EF-G samples tRNAs in various states located along the translocation trajectory. To further understand what these FRET states structurally correspond to, the EF-G:tRNA FRET pair is studied under 100 μM VIO which traps tRNAs in both classic and hybrid states with a higher portion staying in the hybrid state in the TAM[15] buffer used in this work (unpublished results from Chunlai Chen). It reveals that FRET between EF-G and classic or hybrid tRNAs are 0.42 ± 0.01 and 0.27 ± 0.01 for PRE-I and 0.52 ± 0.02 and 0.31 ± 0.01 for PRE-II, respective (Fig 4.23, **middle**). The initial FRET distributions (Fig 4.11, **left**) suggest that EF-G could sample tRNAs in both classic and hybrid states with Val-tRNA preferring the classic state and Phe-tRNA preferring to stay in the hybrid state.

EF-G can catalyze translocation of both classic and hybrid state tRNAs. Group II

traces, which our results suggest include hybrid state tRNAs, show a FRET efficiency which is close to that seen for EF-G:P-site tRNA FRET (Fig 4.13 **A, D**). This explains why a significant portion of EF-G:tRNA FRET pairs corresponding to tRNAs translocating from hybrid states, show no large FRET changes during translocation. On the other hand, Group I traces, which we assign to translocation events starting from the classic state, show large FRET changes during translocation. Specifically, the PRE-II complex has an initial FRET efficiency of 0.49 ± 0.01, proceeds to 0.31 ± 0.01 to 0.26 ± 0.01. For PRE-I, the intermediate and final states have similar FRET efficiencies. However, based on the PRE-II results, we used a three-state model to give a good fit to our results, showing FRET values proceeding from 0.47 ± 0.01 to 0.25 ± 0.01 to 0.24 ± 0.01. These results suggest that EF-G:tRNA FRET proceeds from classic to hybrid to POST-like FRET. The transition from hybrid state to POST-like state is the rate limiting step, but proceeds with only a small FRET change, whereas the transition from classic state to hybrid state is not rate limiting but shows a large FRET change. While Group I traces are made up mostly of translocation events that start with A-site tRNAs in a classic state, Group II traces reflect a more complex mixture of states, containing unproductive bindings as well as translocation events starting from hybrid states. If the transition from hybrid state to POST-like state is the rate-limiting step as observed in Group I, translocation events in Group II should present a longer dwell time than non-productive binding events. The dwell time of translocation events with an initial FRET value of 0.35 to 0.27 and final FRET of 0.27 to 0.21 in Group II was analyzed. The average dwell time of this group for PRE-I and PRE-II are 670 ± 43 ms and 630 ± 30 ms (Fig 4.18, **A**), respectively, which are considerably longer than the dwell times of the total Group II

populations (374 ± 13 ms and 434 ± 10 ms, respectively, Fig 4.10 **B, D**), confirming the notion that FRET conversion from hybrid state to POST-like state is the rate determining step.

Combining all the aforementioned results, we propose a kinetic model of EF-G catalyzed translocation. EF-G samples both classic and hybrid state tRNAs. EF-G binding to the classic state shows a high FRET efficiency, and then tRNAs quickly move to the hybrid states revealing an intermediate FRET with EF-G. The transition from hybrid state constitutes the rate-limiting step for translocation with a rate constant about 10 fold slower than the transition rate from classic state to hybrid state. After hybrid state tRNA translocating to the P-site, EF-G quickly dissociates from the ribosome (Fig 4.28). On the other hand, the inter-domain movements of L11 occur before translocation, and during translocation L11, if it moves at all**,** moves together with the C-terminal domain of EF-G, showing no relative distance changes.

4.4 Conclusion

A simultaneous increase of Cy3 and Cy5 fluorescence intensities was observed for two FRET pairs, indicating that EF-G binds to the ribosome in a conformation revealing detectable FRET with both L11 and tRNA. For the EF-G:L11 FRET pair, a constant FRET value was obtained over the entire EF-G residence time for both N-terminal and C-terminal labeled L11. In contrast, a decreasing FRET efficiency was observed for EF-G:tRNA interaction. Our data provides evidence that tRNAs behave heterogeneously during translocation. We are able to formulate a detailed kinetic scheme for translocating complexes that show large negative FRET efficiency changes, suggesting that EF-G:tRNA FRET proceeds from High to INT to Low FRET values. The transition from INT

to Low is the rate-limiting step with a small FRET change, whereas the transition from High to INT is rapid and displays a large FRET change. Both high concentration of the next ternary complex (500 μM) and high Mg^{2+} with polyamine favor the High FRET state. By comparing the FRET efficiencies obtained with VIO, we propose that High, INT and Low FRET states correspond to peptidyl-tRNAs in A/A, A/P and near P-site like states as translocation proceeds.

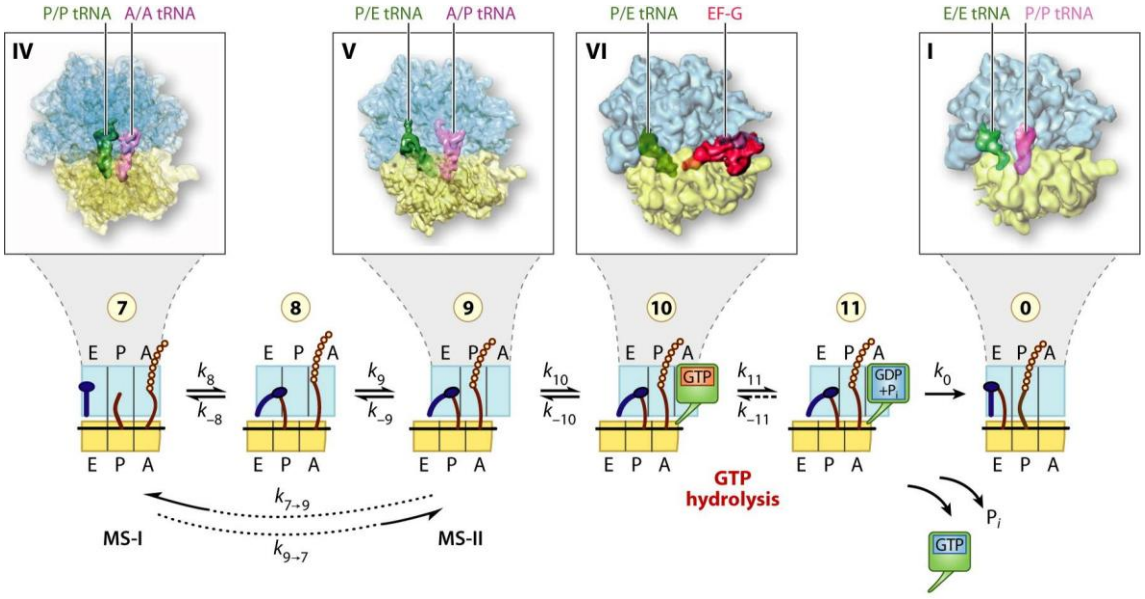

Scheme 4.1 EF-G catalyzed translocation of A, P site tRNAs to P, E sites. Distinct tRNAs and ribosome states are labeled: State 7, PRE complex with tRNAs in their classic states (A/A, P/P); State 8, PRE complex in an intermediate state of ratcheting, with tRNAs in A/A, P/E sites; State 9: PRE complex with a larger relative rotation between 50S and 30S and tRNAs in A/P, P/E sites; State 10: PRE complex with EF-G bound in GTP form; State 11: PRE complex with EF-G bound in GDP·Pi form; 0 state, POST complex with P/P, E/E site tRNAs (Frank and Gonzalez, 2010).

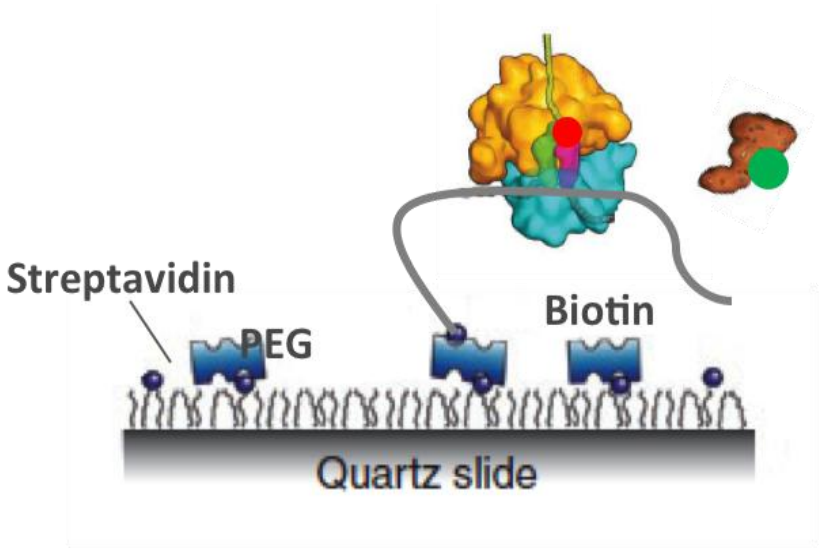

Figure 4.1 Cartoon of single molecule experimental setup. PRE complex containing $tRNA^{Cy5}$ or $L11^{Cy5}$ was attached to the slide surface via a single biotin labeled mRNA. Then Cy3 labeled EF-G was injected into the system. A 532 nm laser was illuminated to excite Cy3 fluorophore.

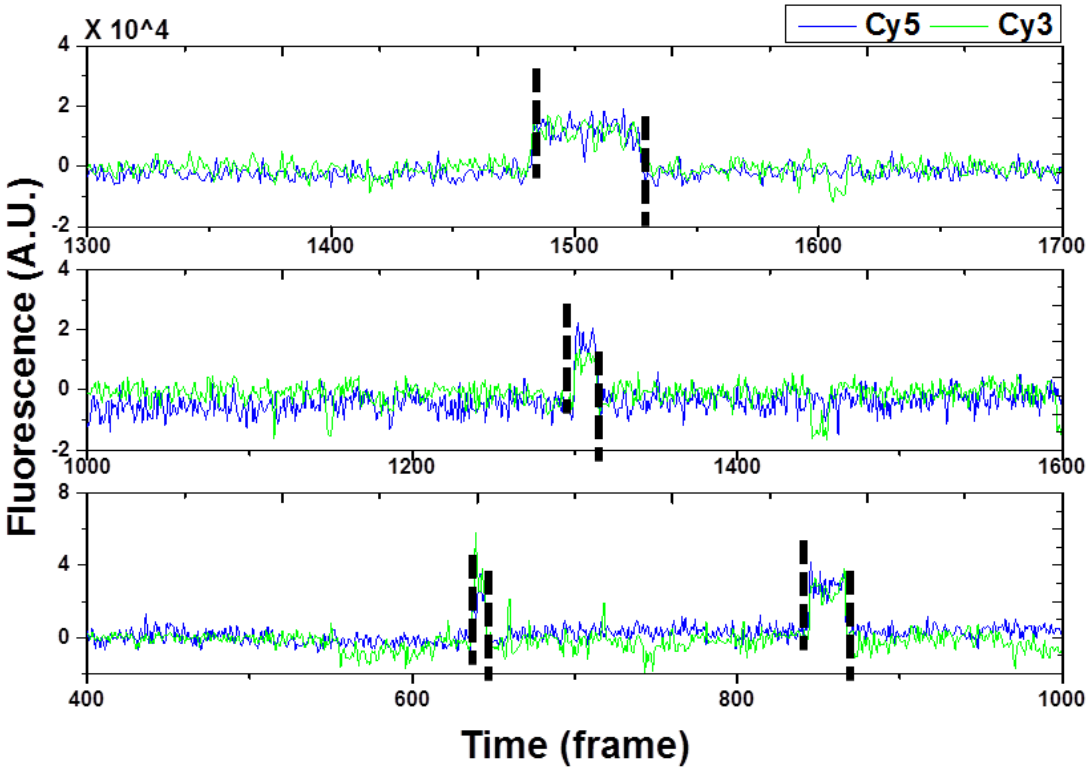

Figure 4.2 Representative FRET traces of PRE-L11^{Cy5}:EF-G$^{693\text{-}Cy3}$ pair. Experiment was performed in TAM[15] buffer with 100 nM next TC. Cy3 fluorescence (Green) and Cy5 fluorescence (blue) showed a simultaneous increase for all FRET events. The initial appearance and final disappearance of FRET are indicated by black dashed lines.

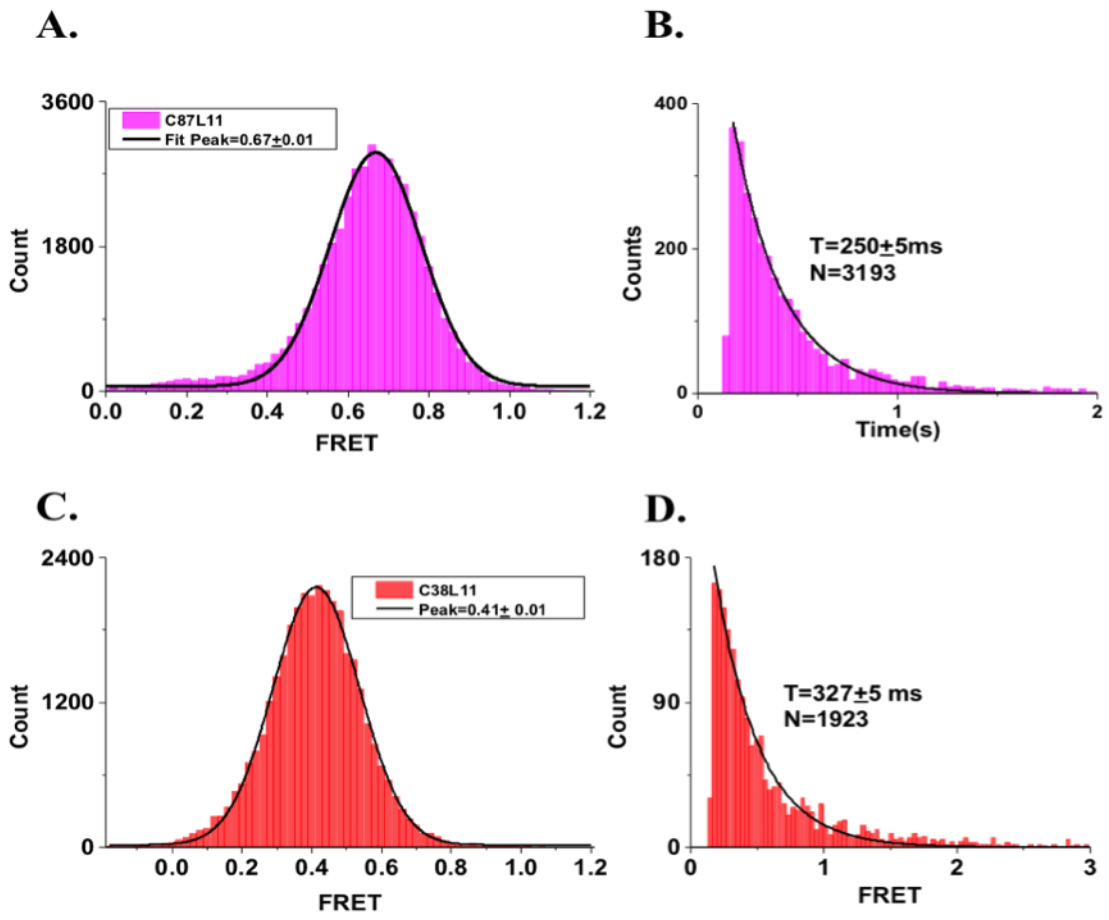

Figure 4.3 FRET analysis of EF-G$^{693\text{-Cy3}}$:L11^{Cy5}. EF-G$^{693\text{-Cy3}}$ interactions with L11$^{87\text{-Cy5}}$ (top) or L11$^{38\text{-Cy5}}$ (bottom) were studied in TAM^{15} buffer with 100 nM next TC. **A, C.** FRET efficiency distributions are fitted by Gaussian function $y=y_0 + (\frac{A}{\sigma\sqrt{2\pi}} e^{-\frac{(x-xc)^2}{2\sigma^2}})$. **B, D.** Dwell time distribution is fit by single exponential decay $y = A\exp(-kt)$.

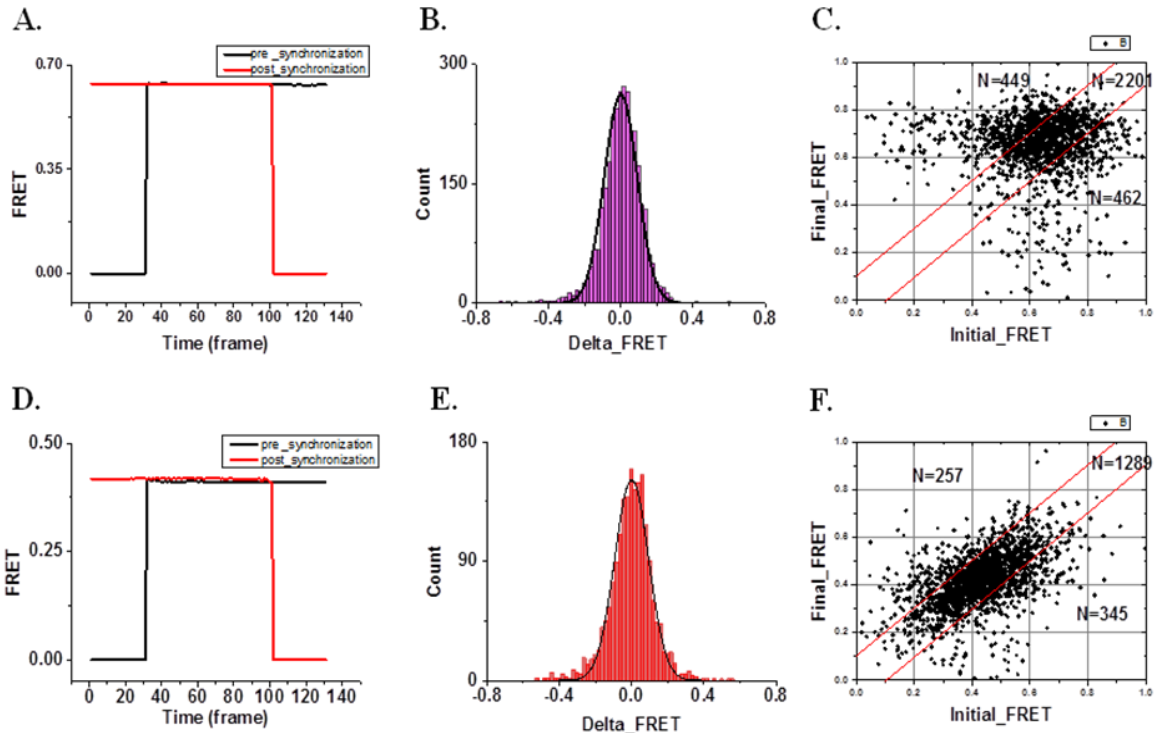

Figure 4.4 FRET state analysis of EF-G$^{693\text{-}Cy3}$:L11^{Cy5}. EF-G$^{693\text{-}Cy3}$ interaction with L11$^{87\text{-}Cy5}$ (top) or L11$^{38\text{-}Cy5}$ (bottom) was studied in TAM^{15} buffer with 100 nM next TC. **A, D.** Postsynchronized traces are obtained by aligning all FRET events at the beginning (black) or at the end (red) and plotted as a function of time. **B, E.** FRET events which last longer than 6 frames (210 ms, 35 ms per frame) are selected. The first and last three frames are averaged separately, defined as initial and final FRET. The differences between final and initial FRET are calculated and delta FRET distributions are plotted. **C, F.** Initial and final FRET are plotted as a transition density map with the number of events in each region indicated.

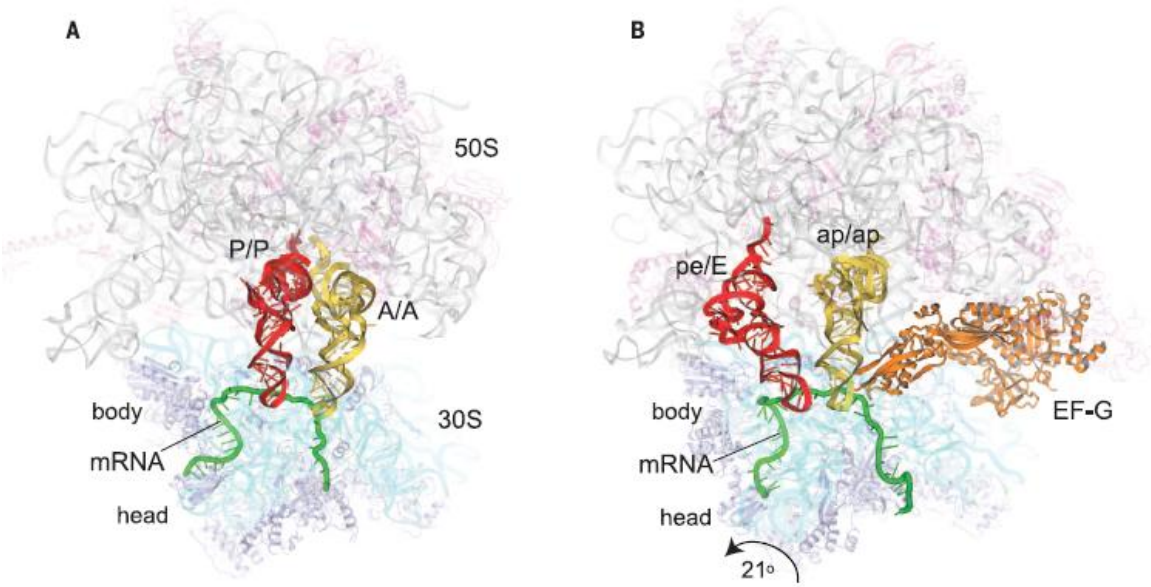

Figure 4.5 Structure of pretranslocation complex. A. 70S ribosome with tRNAs bound in classical A/A and P/P states with FA and mRNA. **B.** Translocation intermediate complex, containing ap/ap and pe/E site tRNAs, EF-G mRNA and FA (Zhou *et al.*, 2014).

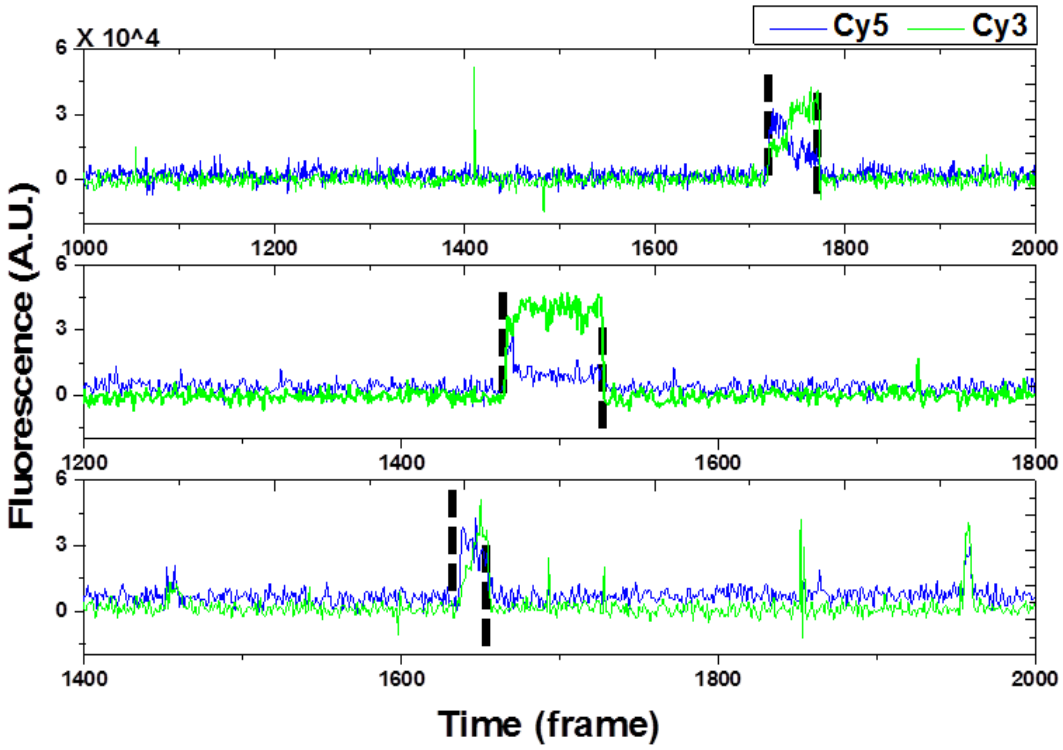

Figure 4.6 Representative FRET traces of PRE$^{tRNA\text{-}Cy5}$:EF-G$^{693\text{-}Cy3}$ pair. Experiment was performed in TAM[15] buffer with 100 nM next TC. Cy3 fluorescence (green) and Cy5 fluorescence (blue) showed a simultaneous increase for all FRET events. The initial appearance and final disappearance of FRET are indicated by black dashed lines.

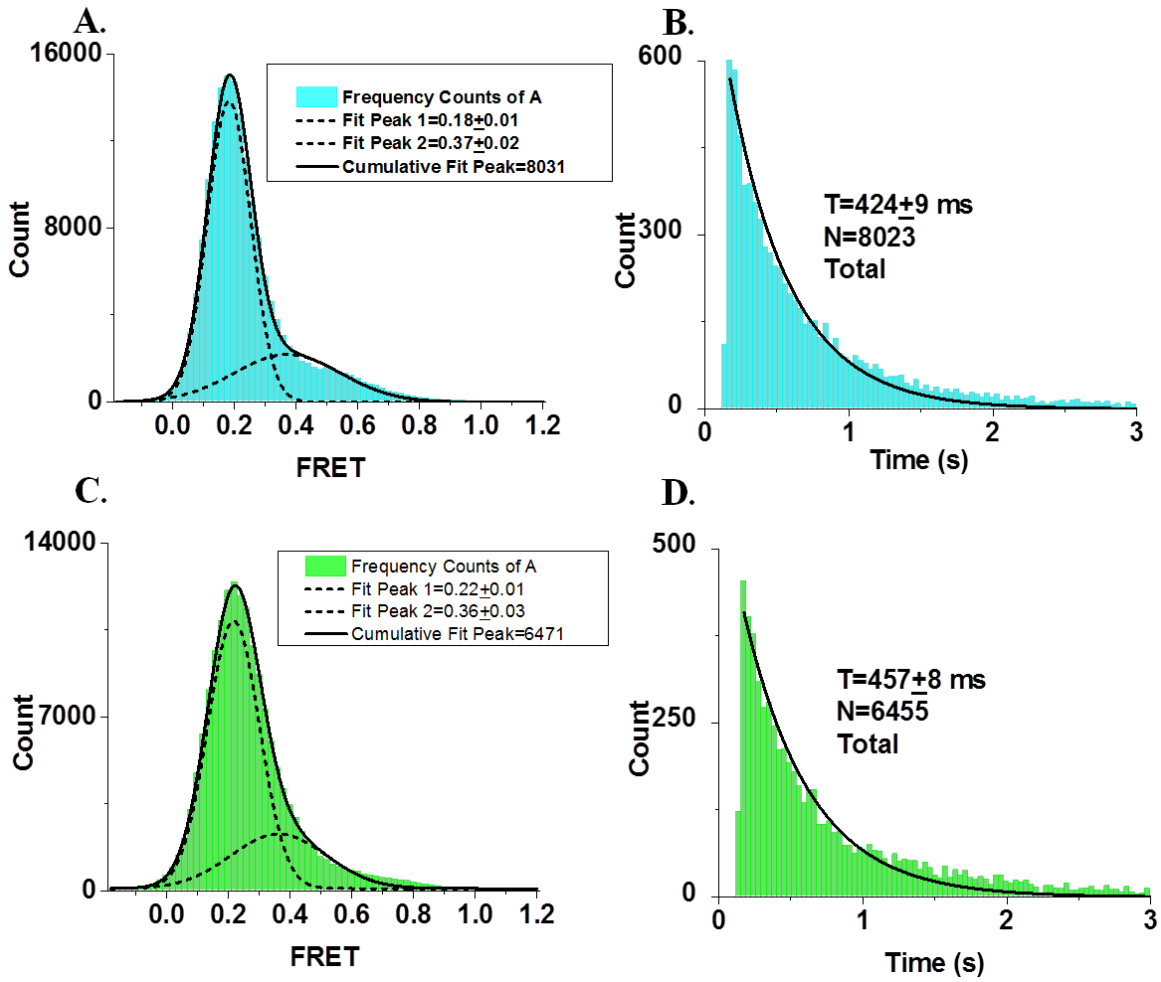

Figure 4.7 FRET analysis of EF-G$^{693\text{-Cy3}}$:PRE$^{tRNA\text{-Cy5}}$. EF-G$^{693\text{-Cy3}}$ interactions with PRE-I$^{tRNA\text{-Cy5}}$ (top) or PRE-II$^{tRNA\text{-Cy5}}$ (bottom) were studied in TAM^{15} buffer with 100 nM next round TC. **A, C.** FRET distribution plot and two peak values are fitted to a Gaussian function. **B, D.** Dwell times are each fit by a single exponential decay.

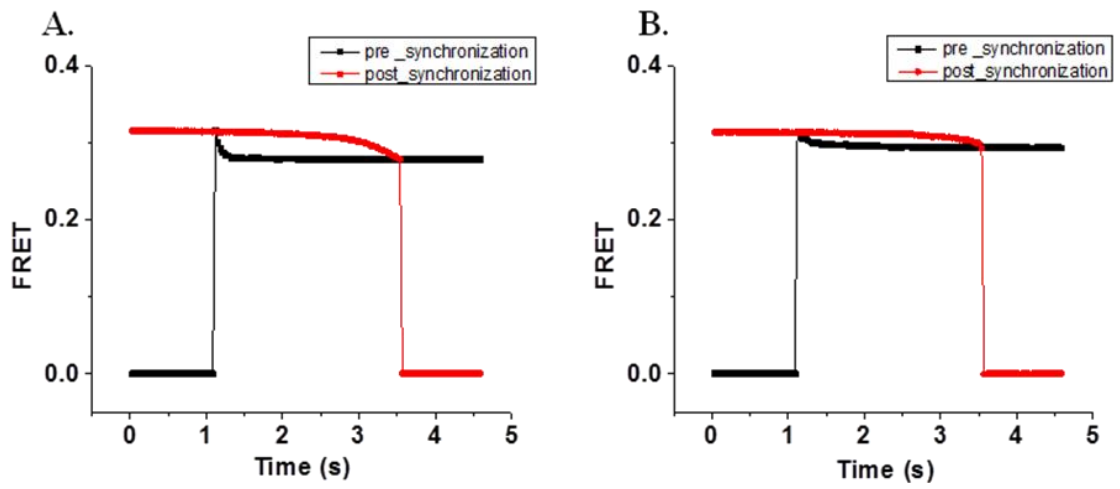

Figure 4.8 Synchronization analysis of EF-G$^{693\text{-}Cy3}$:PRE$^{tRNA\text{-}Cy5}$. EF-G$^{693\text{-}Cy3}$ interaction with PRE-I$^{tRNA\text{-}Cy5}$ (left) or PRE-II$^{tRNA\text{-}Cy5}$ (right) for total events was studied in TAM[15] buffer with 100 nM next round TC. Postsynchronized traces are obtained by aligning all FRET events at the beginning (black) or at the end (red) and plotted as a function of time.

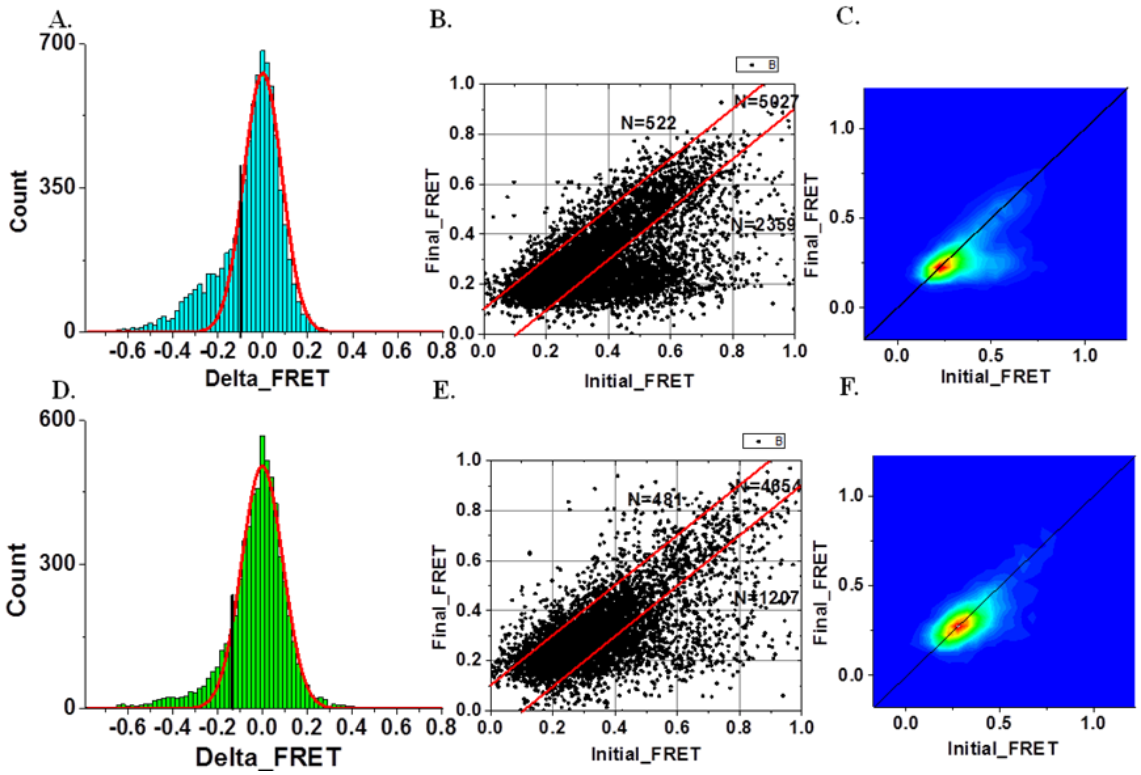

Figure 4.9 FRET state analysis of EF-G$^{693\text{-}Cy3}$:PRE^{Cy5}. EF-G$^{693\text{-}Cy3}$ interaction with PRE-I$^{tRNA\text{-}Cy5}$ (top) or PRE-II$^{tRNA\text{-}Cy5}$ (bottom) was studied in TAM^{15} buffer with 100 nM next round TC. FRET events which last longer than 6 frames (210 ms) are selected. The first and last three frames are averaged separately, defined as initial and final FRET. **A, D.** Delta FRET distribution of EF-G:tRNA. The differences between final and initial FRET are calculated and delta FRET distributions are plotted. **B, E.** Initial and final FRET are plotted relative to each other. **C, F.** Initial and final FRET values are plotted as two-dimensional transition density contour maps.

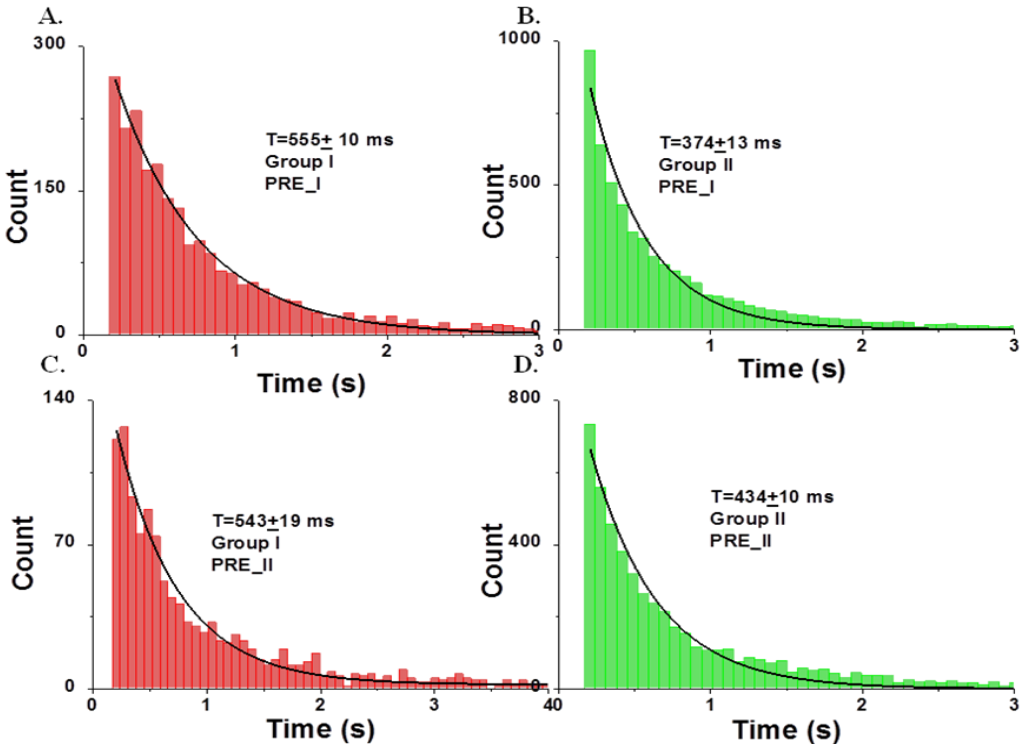

Figure 4.10 FRET distribution and dwell time distribution of EF-G$^{693\text{-}Cy3}$:PRE$^{tRNA\text{-}Cy5}$. EF-G$^{693\text{-}Cy3}$:PRE-I$^{tRNA\text{-}Cy5}$ (top) or EF-G$^{693\text{-}Cy3}$:PRE-II$^{tRNA\text{-}Cy5}$ (bottom) was studied in TAM[15] buffer with 100 nM next round TC. Dwell time distributions of traces of Group I (red), II (green) are fitted by a single exponential decay. **A, B.** FRET distribution of Group I (red) and Group II (Green) of PRE-I. **C, D.** FRET distribution of Group I (red) and Group II (Green) of PRE-II.

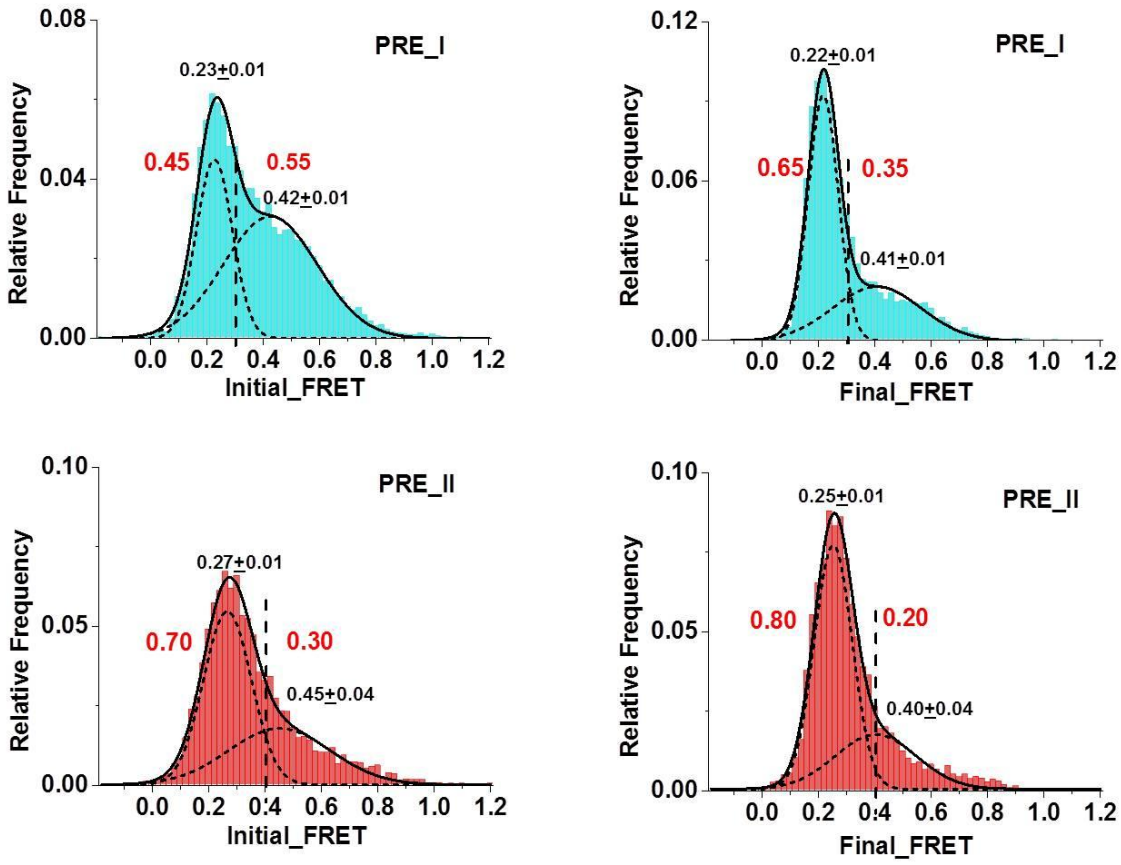

Figure 4.11 Initial and Final FRET distributions of EF-G$^{693\text{-}Cy3}$:PRE$^{tRNA\text{-}Cy5}$ pair. EF-G$^{693\text{-}Cy3}$:PRE-I$^{tRNA\text{-}Cy5}$ (top) and EF-G$^{693\text{-}Cy3}$:PRE-II$^{tRNA\text{-}Cy5}$ (bottom) were studied under TAM[15] buffer with 100 nM next round TC. Percentages of two FRET states are labeled separately in red (cutoff FRET value: E=0.3 for PRE-I and E=0.4 for PRE-II). Fitted FRET peak values are labeled in black.

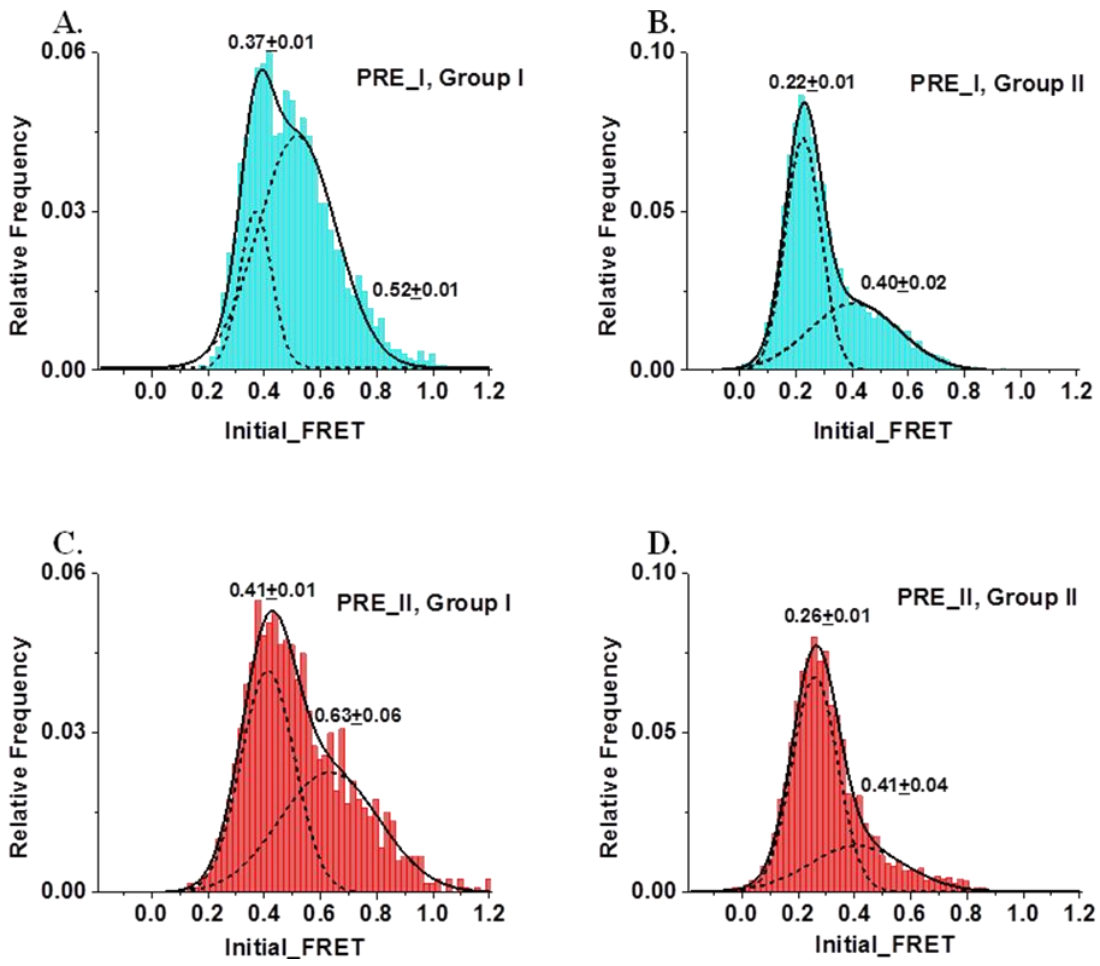

Figure 4.12 Initial FRET distributions of EF-G$^{693\text{-}Cy3}$:PRE$^{tRNA\text{-}Cy5}$ for Groups I and II. EF-G$^{693\text{-}Cy3}$:PRE-I$^{tRNA\text{-}Cy5}$ (top) and EF-G$^{693\text{-}Cy3}$: PRE-II$^{tRNA\text{-}Cy5}$ (bottom) were studied in TAM^{15} buffer with 100 nM next round TC. Distribution of initial FRET values for Groups I and II traces are plotted with peak values labeled separately. The detailed fitting results, including standard deviations of the peak values and percentages of high FRET state are listed in **Table 4.1**.

Complex		Fitted Peak of Initial FRET distribution	[a] σ (SD)	[b] High FRET
PRE-I MVF	Total	Peak1=0.23±0.01[c] Peak2=0.42±0.01	σ_1= 0.06 σ_2= 0.17	55%
	Group I	Peak1=0.37±0.01 Peak2=0.52±0.01	σ_1= 0.06 σ_2= 0.14	73%
	Group II	Peak1=0.22±0.01 Peak2=0.40±0.02	σ_1= 0.06 σ_2= 0.16	32%
PRE-II MFK	Total	Peak1=0.27±0.01 Peak2=0.45±0.04	σ_1= 0.08 σ_2= 0.18	30%
	Group I	Peak1=0.41±0.01 Peak2=0.63±0.06	σ_1= 0.10 σ_2= 0.18	41%
	Group II	Peak1=0.26±0.01 Peak2=0.41±0.04	σ_1= 0.08 σ_2= 0.17	20%

Table 4.1 FRET result summary of EF-G$^{693\text{-}Cy3}$:PRE$^{tRNA\text{-}Cy5}$. Results of initial FRET distributions of EF-G$^{693\text{-}Cy3}$:PRE-I^{Cy5} and EF-G$^{693\text{-}Cy3}$:PRE-II^{Cy5} are summarized. The experiments were performed under TAM[15] buffer with 100 nM next round TC. The initial FRET information of total events, Group I and Group II are summarized separately.

[a] SD of FRET distribution

[b] The intersect FRET value of the two Gaussian fitted curve (E = IS) is obtained. High FRET percentage is calculated by using the number of events (E > IS) divided by the number of total events.

[c] Standard error of the fitted peak value

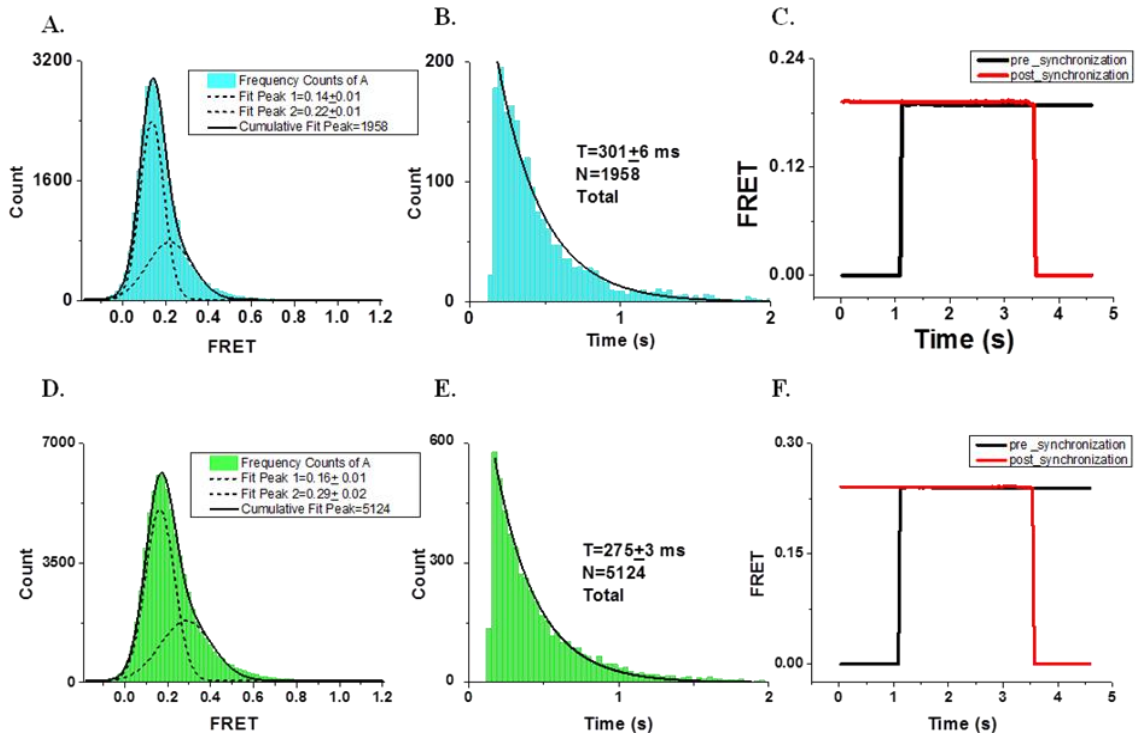

Figure 4.13 FRET analysis of EF-G$^{693\text{-}Cy3}$:POST$^{tRNA\text{-}Cy5}$. EF-G$^{693\text{-}Cy3}$ interaction with P site fMet-Val-tRNA$^{Val\text{-}Cy5}$ (top) or fMet-Phe-tRNA$^{Phe\text{-}Cy5}$ (bottom) in TAM^{15} buffer was studied in the absence of next TC. **A, D.** FRET distributions are fitted by Gaussian function. **B, E.** Dwell times are fitted by a single exponential decay. **C, F.** Postsynchronized traces are obtained by aligning all FRET events at the beginning (black) or at the end (red) and plotted as a function of time.

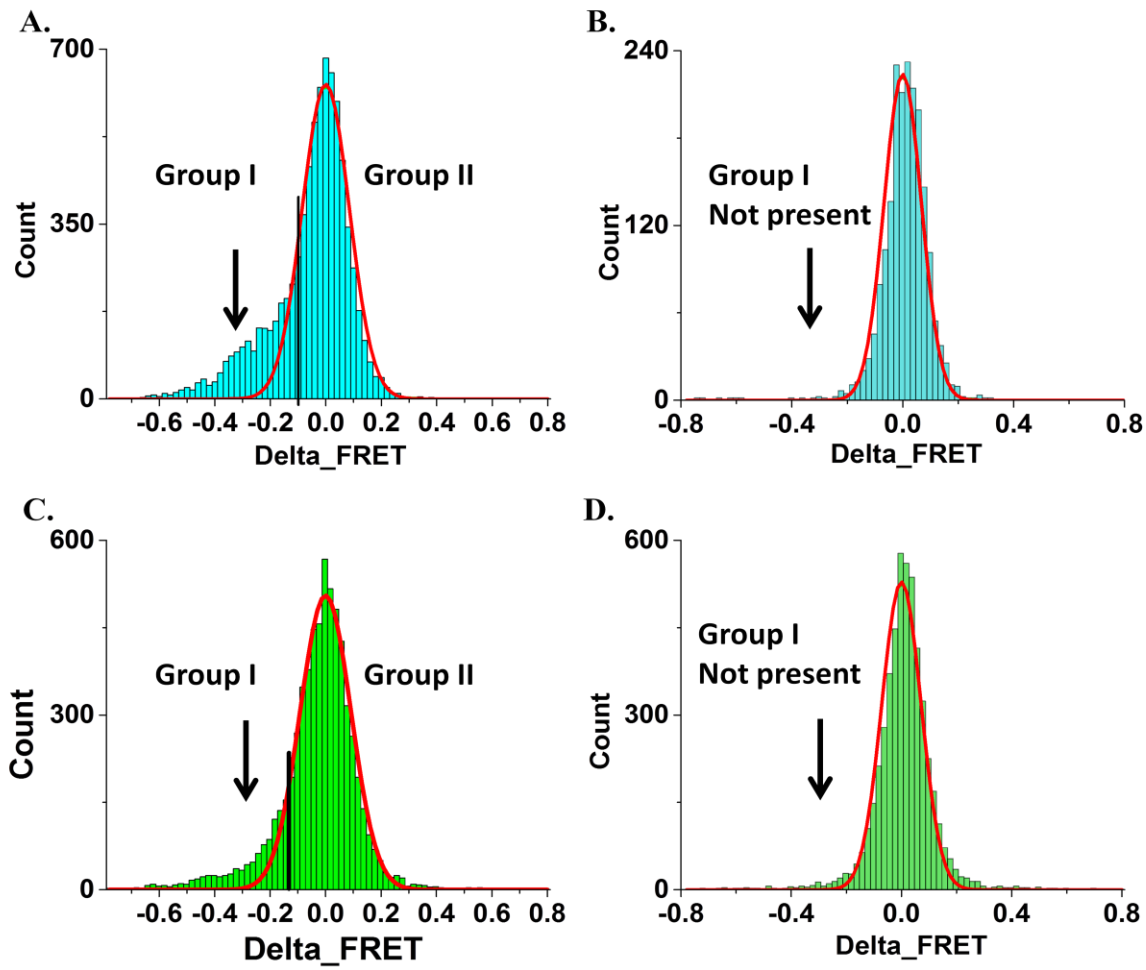

Figure 4.14 Comparison of ΔFRET distribution between PRE and POST. FRET events which lasted longer than 6 frames are selected. The first and last three frames are averaged separately, defined as initial and final FRET, respectively. The differences between final and initial FRET are calculated and ΔFRET distributions are plotted. **A.** ΔFRET distribution of EF-G: PRE-I$^{tRNA\text{-}Cy5}$. **B.** ΔFRET distribution of EF-G: POST-I$^{tRNA\text{-}Cy5}$. **C.** ΔFRET distribution of EF-G: PRE-II$^{tRNA\text{-}Cy5}$. **D.** ΔFRET distribution of EF-G: POST-II$^{tRNA\text{-}Cy5}$.

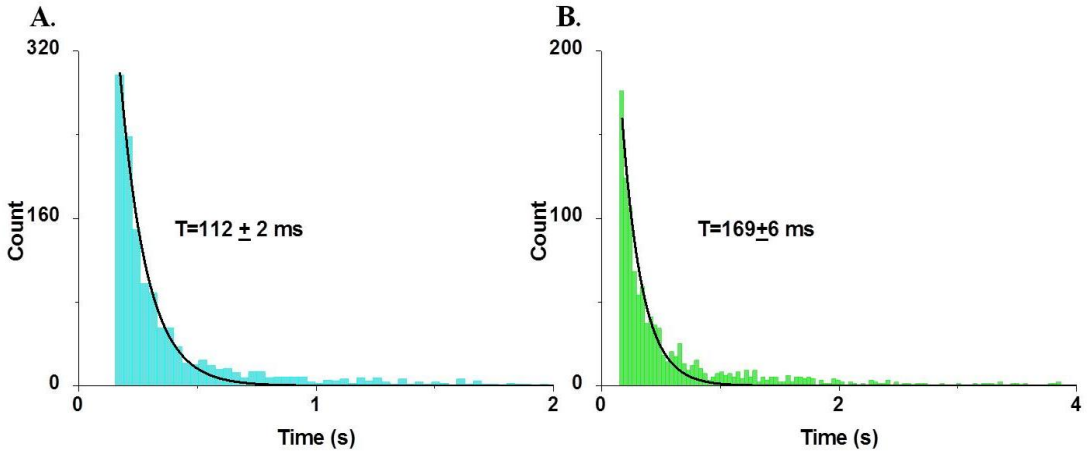

Figure 4.15 Dwell time distributions of high FRET traces (E > 0.4) in Group II. EF-G$^{693\text{-}Cy3}$:PRE-I^{Cy5} (left) and PRE-II^{Cy5} (right) were studied in TAM^{15} buffer with 100 nM next round TC. Dwell time distributions are each fitted by a single exponential $\boldsymbol{y} = A\exp(-kt)$.

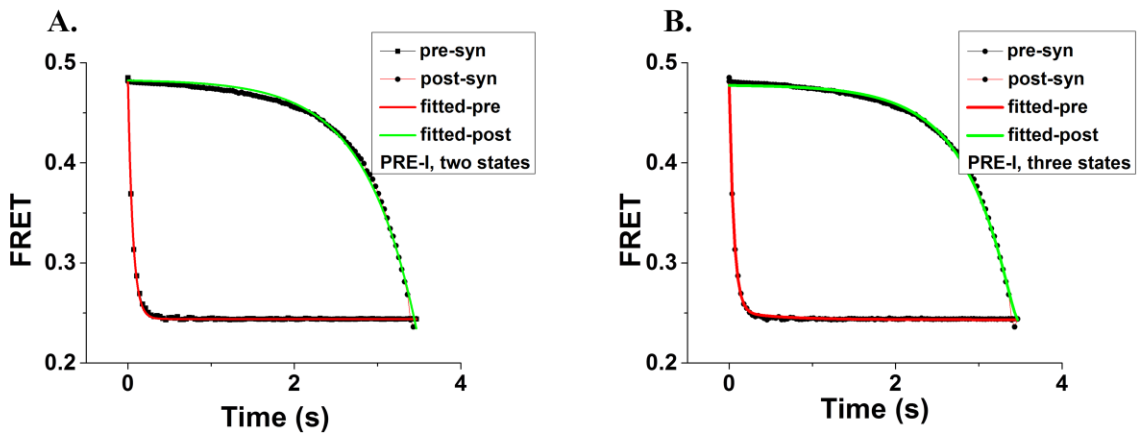

Figure 4.16 Synchronization analysis of EF-G$^{693\text{-}Cy3}$:PRE-I$^{tRNA\text{-}Cy5}$. EF-G$^{693\text{-}Cy3}$ interaction with PRE-I$^{tRNA\text{-}Cy5}$ was performed in TAM^{15} buffer with 100 nM next round TC. Post-synchronization traces are fitted by a two-state model (left) or a three-state model (right).

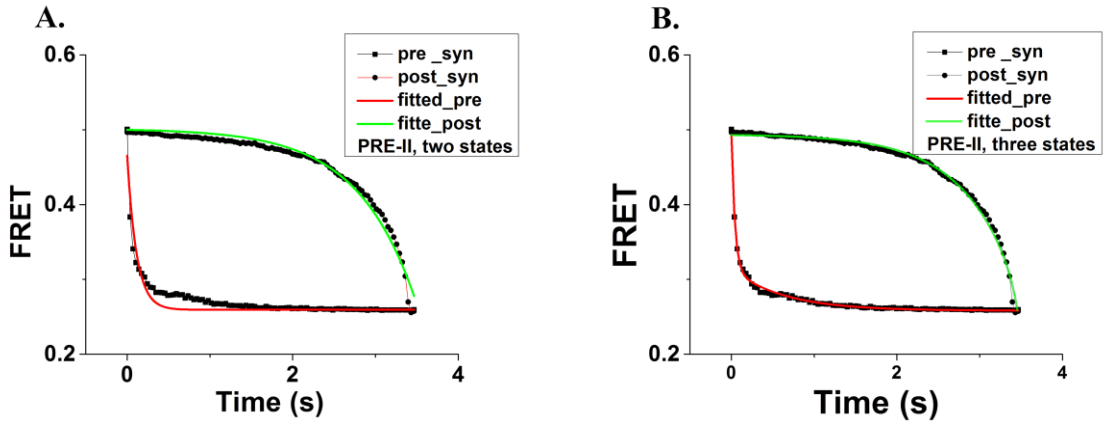

Figure 4.17 Synchronization analysis of EF-G$^{693\text{-}Cy3}$:PRE-II$^{tRNA\text{-}Cy5}$. EF-G$^{693\text{-}Cy3}$ interaction with PRE-II$^{tRNA\text{-}Cy5}$ was performed in TAM^{15} buffer with 100 nM next round TC. Post-synchronization traces are fitted by a two-state model (left) or a three-state model (right).

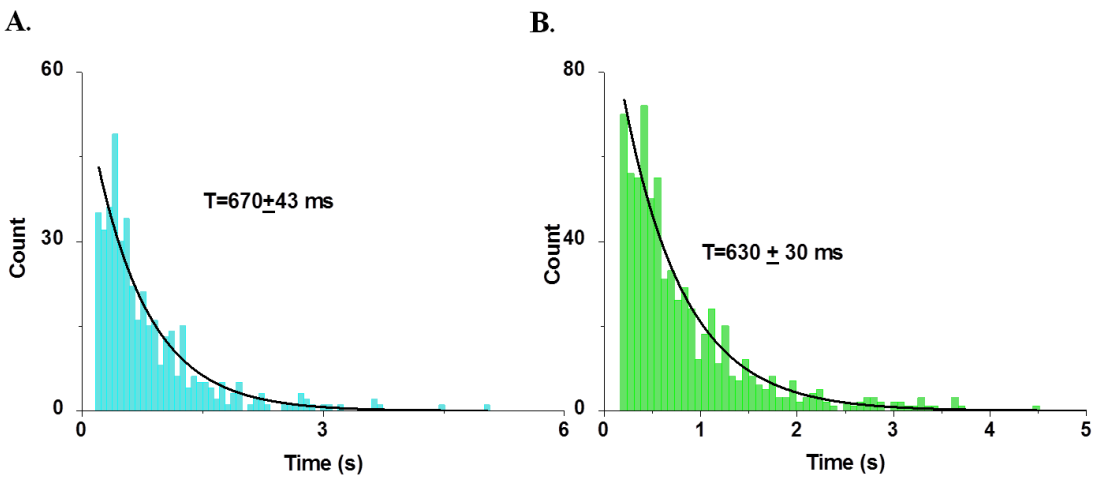

Figure 4.18 Dwell time distribution of certain traces in Group II. EF-G$^{693\text{-Cy3}}$:PRE-I$^{tRNA\text{-Cy5}}$ (left) and PRE-II$^{tRNA\text{-Cy5}}$ (right) were obtained in TAM^{15} buffer with 100 nM next round TC. Traces with initial FRET (0.35 to 0.27) and final FRET (0.27 to 0.21) in Group II are selected. Dwell time distributions of these traces are fitted by a single exponential $y = A\exp(-kt)$.

Delta FRET cutoff values PRE-I	**<-0.10**	**<-0.12**	**<-0.14**	**<-0.16**	**<-0.18**	**<-0.2**
Number of events	2359	2075	1845	1638	1452	1296
Percentage	100%	88%	78%	69%	62%	55%
[1]Rate constant (Global fitting)	k1=18.1±0.4 k2=1.8±0.1 k3=18.4±1.8	k1=22.1±0.9 k2=1.8±0.1 k3=8.9±0.8	-----	-----	-----	k1=22.4±1.2 k2=1.8±0.1 k3=6.4±0.6
FRET Efficiency	F1=0.47±0.01 F2=0.25±0.01 F3=0.24±0.01	F1=0.49±0.01 F2=0.27±0.01 F3=0.24±0.01	-----	-----	-----	F1=0.54±0.01 F2=0.27±0.01 F3=0.22±0.01
Delta FRET values	**>0.1**	**>0.12**	**>0.14**	**>0.16**	**>0.18**	**>0.20**
Number of events	522	346	229	155	110	67
Ratio	100%	66%	44%	30%	21%	13%

Table 4.2a Global fitting results summary using different ΔFRET cutoff values of PRE-I. EF-$G^{693\text{-}Cy3}$ interaction with PRE-$I^{tRNA\text{-}Cy5}$ and 100 nM next TC was studied in TAM^{15} buffer.
[1]Global fitting results are based on traces with decreased FRET changes

Delta FRET cutoff values PRE-II	**<-0.12**	**<-0.14**	**<-0.16**	**<-0.18**	**<-0.2**
Number of events	1207	1017	865	730	610
Percentage	100%	84%	72%	60%	50%
[1]Rate constant (Global fitting)	k1=24.4±1.1 k2=1.6±0.1 k3=12.6±1.1				k1=23.1±1.2 k2=1.6±0.2 k3=10.4±0.5
FRET Efficiency	F1=0.49±0.1 F2=0.31±0.1 F3=0.26±0.1				F1=0.53±0.01 F2=0.33±0.01 F3=0.28±0.01
Delta FRET values	**>0.12**	**>0.14**	**>0.16**	**>0.18**	**>0.20**
Number of events	481	345	252	184	134
Ratio	100%	72%	52%	38%	28%

Table 4.2b Global fitting results summary using different ΔFRET cutoff values of PRE-II. EF-$G^{693\text{-}Cy3}$ interaction with PRE-$II^{tRNA\text{-}Cy5}$ and 100 nM next TC was studied in TAM[15] buffer.
[1]Global fitting results are based on traces with decreased FRET changes

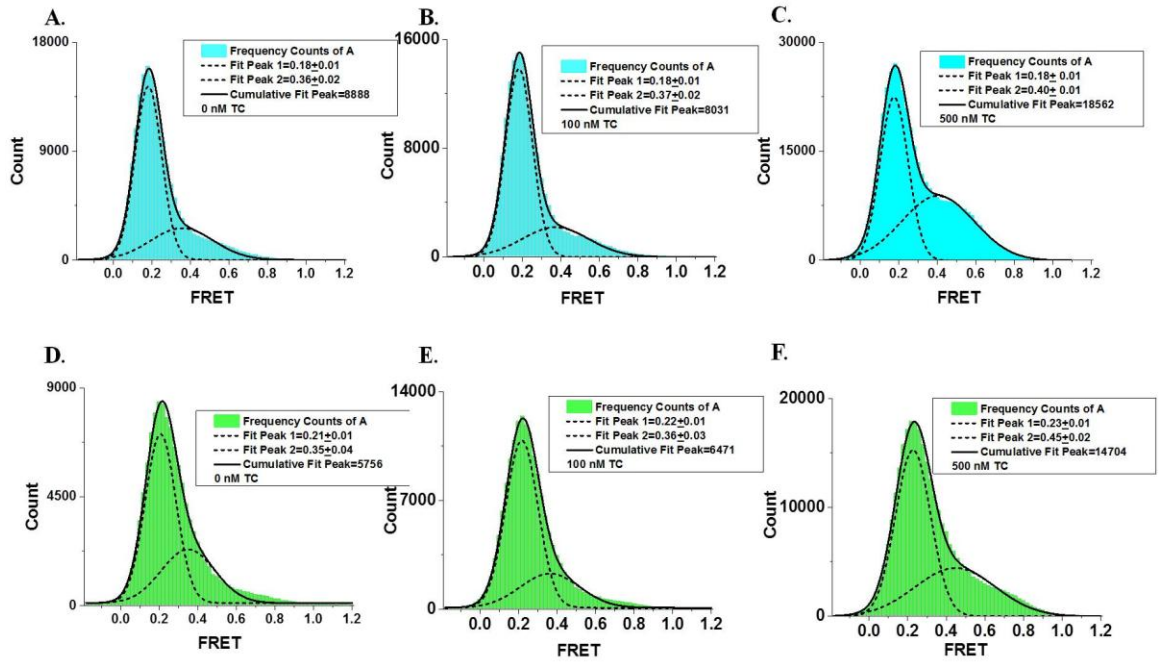

Figure 4.19 FRET distribution of EF-G$^{693\text{-Cy3}}$:PRE$^{tRNA\text{-Cy5}}$ under different next TC concentrations. EF-G$^{693\text{-Cy3}}$ interaction with PRE-I$^{tRNA\text{-Cy5}}$ (top) and PRE-II$^{tRNA\text{-Cy5}}$ (bottom) was studied in TAM[15] buffer with 0, 100, 500 nM next TC. FRET distribution is plotted and two peak values are fitted by Gaussian function. The detailed fitting results, including standard deviations of the peak values and the percentage of high FRET state are listed in Table 4.3.

Complex		Fitted Peak of Total FRET distribution	[a] σ (SD)	[b]High FRET percentage
PRE-I MVF	0	Peak1=0.18±0.01[c] Peak2=0.36±0.02	σ_1= 0.07 σ_2= 0.16	22%
	100	Peak1=0.18±0.01 Peak2=0.37±0.02	σ_1= 0.07 σ_2= 0.17	20%
	500	Peak1=0.18±0.01 Peak2=0.40±0.01	σ_1= 0.07 σ_2= 0.19	41%
PRE-II MFK	0	Peak1=0.21±0.01 Peak2=0.35±0.04	σ_1= 0.08 σ_2= 0.14	27%
	100	Peak1=0.22±0.01 Peak2=0.36±0.03	σ_1= 0.08 σ_2= 0.15	19%
	500	Peak1=0.23±0.01 Peak2=0.45±0.02	σ_1= 0.09 σ_2= 0.20	30%

Table 4.3 Summary of FRET distributions of EF-G$^{693\text{-}Cy3}$:PRE$^{tRNA\text{-}Cy5}$ at different next TC concentrations. The experiments were performed under TAM[15] buffer with 0, 100, 500 nM next round TC.

[a] SD of FRET distribution

[b] The intersect FRET value of the two Gaussian fitted curve (E = IS) is obtained. High FRET percentage is calculated by using the number of events (E > IS) divided by the number of total events.

[c] Standard error of the fitted peak value

Complex	TC Concentration	Dwell time (ms)			[d]Transition rate (s^{-1})		
					k_1	k_2	k_3
PRE-I MVF	0 [1]	[a]Dw=386±8	[b]Dw1=557±8	[c]Dw2=336±9	18.7±0.5	1.8±0.1	18.6±2.0
	100 nM [1]	Dw=424±9	Dw1=555±10	Dw2=374±13	18.1±0.4	1.8±0.1	18.4±1.8
	500 nM [1]	Dw=199±3	Dw1=288±8	Dw2=185±3	15.7±1.2	1.8±0.1	38.6±18.7
PRE-II MFK	0 [3]	Dw=291±6	Dw1=394±14	Dw2=278±7	22.9±1.5	2.1±0.1	13.8±1.4
	100 nM [2]	Dw=457±8	Dw1=573±21	Dw2=434±10	24.4±1.1	1.6±0.1	12.6±1.1
	500 nM [2]	Dw=250±4	Dw1=417±12	Dw2=229±4	12.8±0.5	1.5±0.1	20.9±3.6

Table 4.4 Summary of kinetics of EF-G promoted translocation at different next TC complex concentrations.

[a]Dwell time of total events
[b]Dwell time of Group I traces
[c]Dwell time of Group II traces
[d]Transition rates are fitted by using the three FRET states model
[1] Cognate Phe-tRNA^{Phe}
[2] Cognate Lys-tRNA^{Lys}

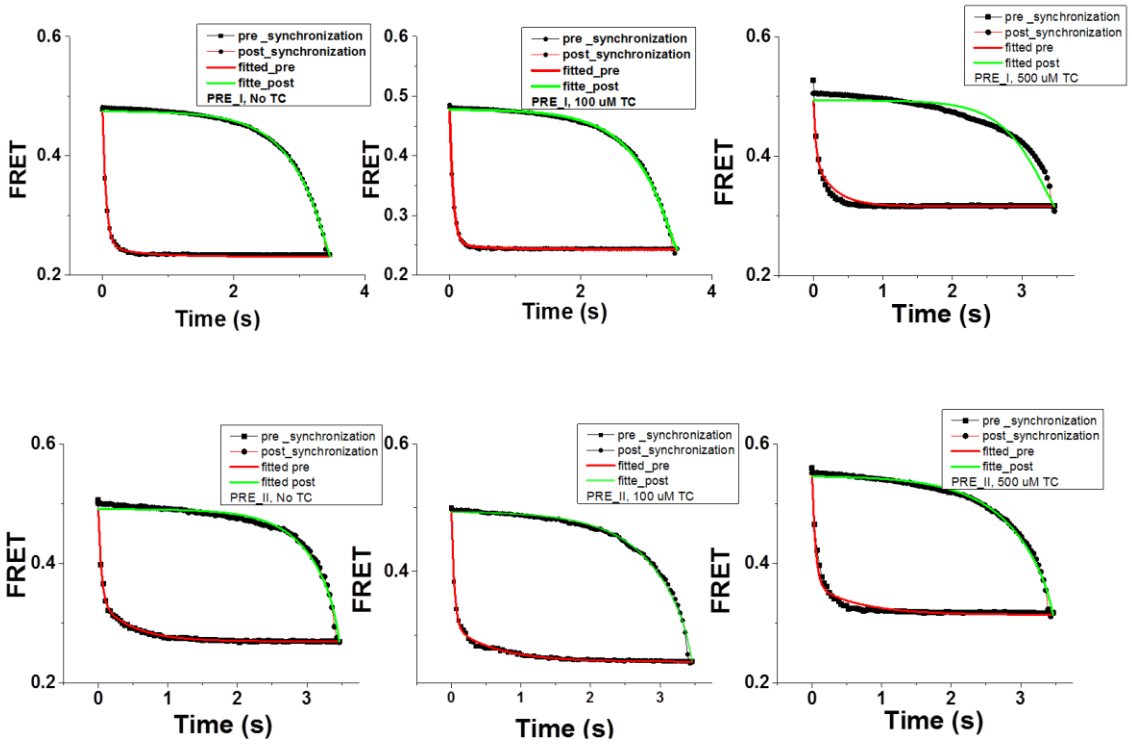

Figure 4.20 Global fitting of synchronization traces at different next TC complex concentrations. FRET between EF-G693-Cy3 and PRE-I$^{tRNA\text{-}Cy5}$ (top) or PRE-II$^{tRNA\text{-}Cy5}$ (bottom) in TAM15 buffer with 0, 100 or 500 nM next round TC. Fitting results are listed in Table 4.4.

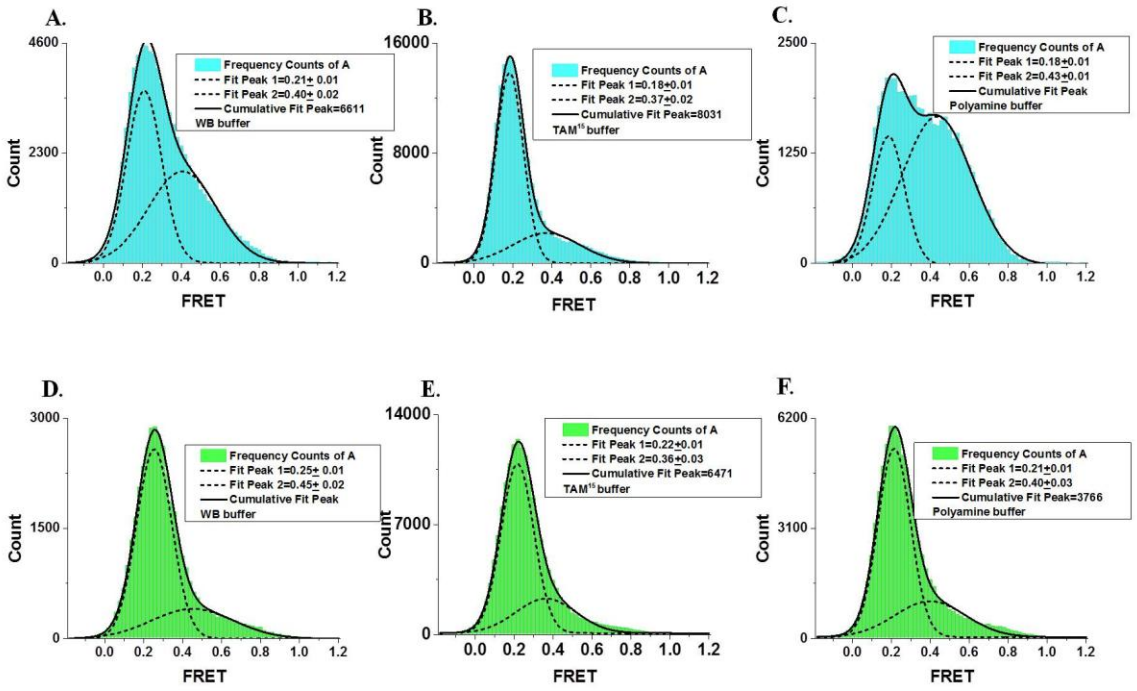

Figure 4.21 FRET distribution of EF-G$^{693\text{-}Cy3}$:PRE$^{tRNA\text{-}Cy5}$ under different buffer conditions. FRET results between EF-G$^{693\text{-}Cy3}$ and PRE-I$^{tRNA\text{-}Cy5}$ (top) or PRE-II$^{tRNA\text{-}Cy5}$ (bottom) in WB buffer, TAM^{15} buffer and Polyamine buffer with 100 nM next round TC are studied. FRET distribution is plotted and two peak values are fitted by Gaussian function. The detailed fitting results, including standard deviation of the peak values and percentages of high FRET state are listed in Table 4.5.

Complex		Fitted Peak of Total FRET distribution	[a] σ (SD)	[b] High FRET percentage
PRE-I MVF	WB	Peak1=0.21±0.01[c] Peak2=0.40±0.02	σ_1= 0.09 σ_2= 0.17	41%
	TAM[15]	Peak1=0.18±0.01 Peak2=0.37±0.02	σ_1= 0.07 σ_2= 0.17	20%
	Polyamine	Peak1=0.18±0.01 Peak2=0.43±0.01	σ_1= 0.08 σ_2= 0.18	67%
PRE-II MFK	WB	Peak1=0.25±0.01 Peak2=0.45±0.02	σ_1= 0.09 σ_2= 0.21	18%
	TAM[15]	Peak1=0.22±0.01 Peak2=0.36±0.03	σ_1= 0.08 σ_2= 0.15	19%
	Polyamine	Peak1=0.21±0.01 Peak2=0.40±0.03	σ_1= 0.08 σ_2= 0.18	22%

Table 4.5 Summary of FRET distributions of EF-G$^{693\text{-}Cy3}$:PRE$^{tRNA\text{-}Cy5}$ at different buffer conditions. The experiments were performed in WB buffer, TAM[15] buffer and Polyamine buffer with 100 nM next round TC.

[a] SD of FRET distribution

[b] The intersect FRET value of the two Gaussian fitted curve (E = IS) is obtained. High FRET percentage is calculated by using the number of events (E > IS) divided by the number of total events.

[c] Standard error of the fitted peak value

Complex	Buffer	Dwell time (ms)			[d]Group I ratio	[e]Transition rate (s^{-1})		
						k_1	k_2	k_3
PRE-I MVF	WB	[a]Dw=204±3	[b]Dw1=275±3	[c]Dw2=186±4	26.1%	21.6±1.1	3.9±0.1	12.6±1.3
	TAM[15]	Dw=424±9	Dw1=555±10	Dw2=374±13	29.8%	18.1±0.4	1.8±0.1	18.4±1.8
	Polyamine	Dw=359±8	Dw1=679±26	Dw2=286±7	37.7%	10.2±0.5	1.1±0.3	9.2±1.2
PRE-II MFK	WB	Dw=266±3	Dw1=322±7	Dw2=255±3	18.9%	21.5±0.8	4.0±0.1	11.2±0.8
	TAM[15]	Dw=457±8	Dw1=573±21	Dw2=434±10	19.0%	24.4±1.1	1.6±0.1	12.6±1.1
	Polyamine	Dw=509±8	Dw1=596±20	Dw2=479±6	25.1%	16.6±0.5	1.9±0.1	8.5±0.4

Table 4.6 Summary of kinetics of EF-G promoted translocation at different buffer conditions.

[a]Dwell time of total events

[b]Dwell time of Group I traces

[c]Dwell time of Group II traces

[d]Percentage of Group I is calculated by using the number of traces from Group I divided by the number of total events

[e]Transition rate constants are fitted by the three-state model.

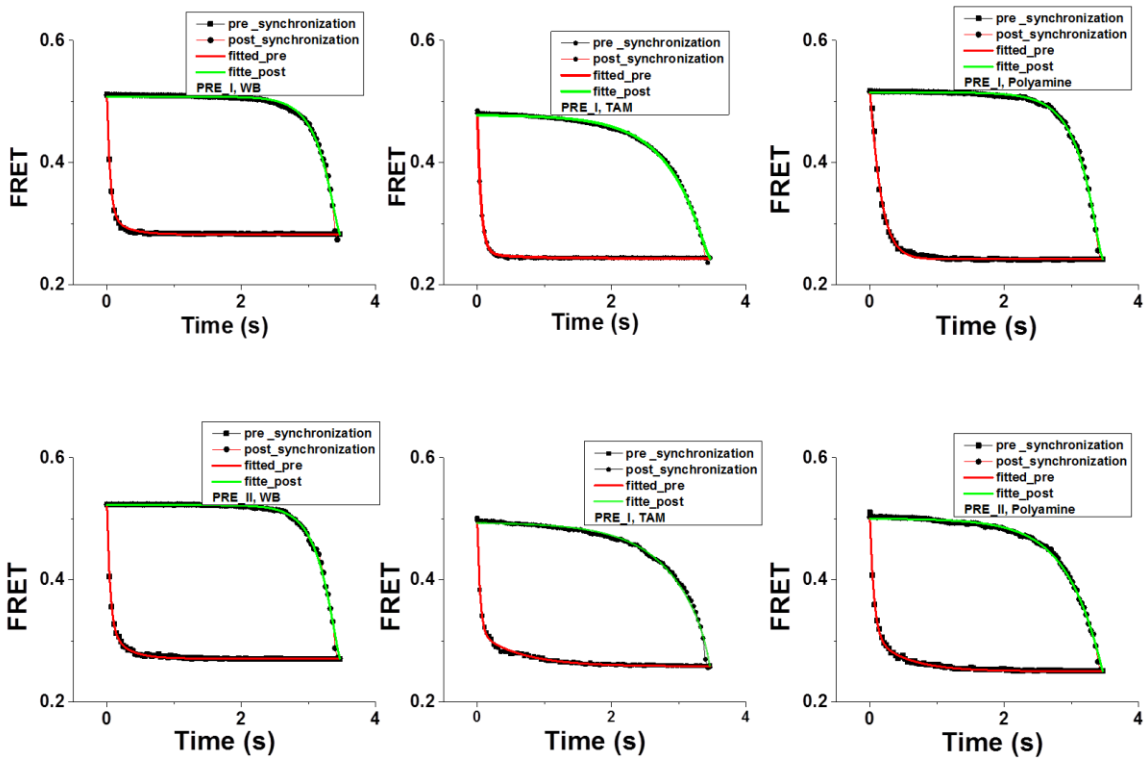

Figure 4.22 Global fitting results of postsynchronized traces at different buffer conditions. FRET results between EF-G$^{693\text{-Cy3}}$ and PRE-I$^{\text{tRNA-Cy5}}$ (top) or PRE-II$^{\text{tRNA-Cy5}}$ (bottom) in WB buffer, TAM[15] buffer or polyamine buffer with 100 nM next round TC are fitted separately. Detailed fitting results are listed in Table 4.6.

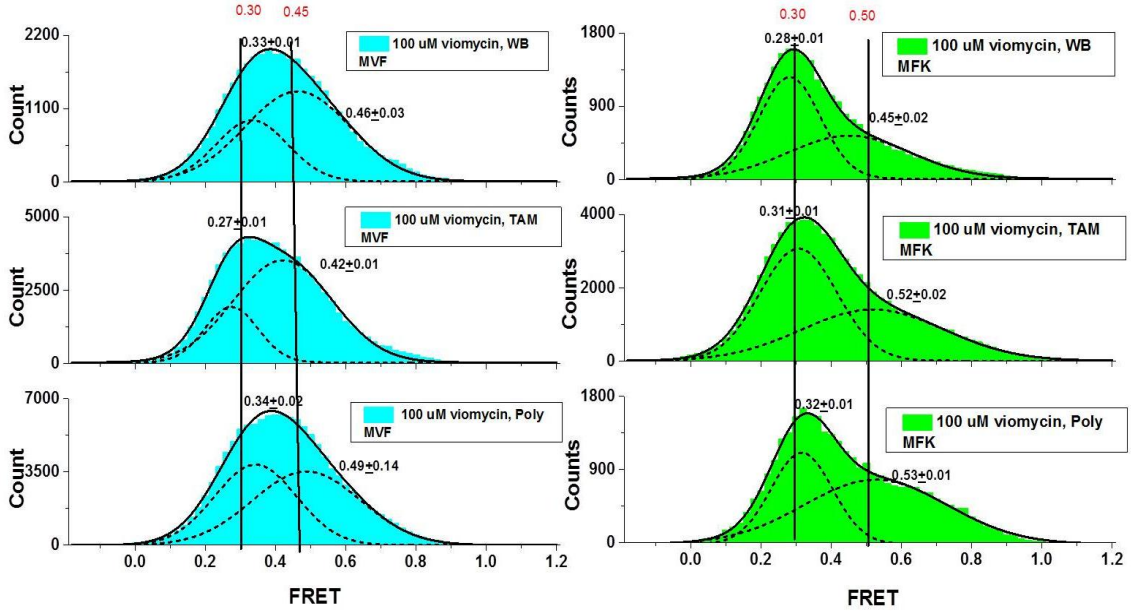

Figure 4.23 FRET distribution of EF-G$^{693\text{-}Cy3}$:PRE$^{tRNA\text{-}Cy5}$ with VIO. EF-G$^{693\text{-}Cy3}$ interaction with PRE-I$^{tRNA\text{-}Cy5}$ (left) or PRE-II$^{tRNA\text{-}Cy5}$ (right) in different buffer conditions with 100 nM next round TC and 100 μM VIO. FRET distributions are plotted, with two major peaks indicated in the Figures. The detailed fitting results, including standard deviation of the peak values and the percentages of high FRET states are listed in Table 4.7.

Complex	Buffer	FRET Peaks	[a] Dwell time	[b] σ (SD)	[c] High FRET percentage
PRE-I MVF	WB	Peak1=0.33±0.01[d] Peak2=0.45±0.03	Dw=275±3	σ_1= 0.10 σ_2= 0.15	54%
	TAM[15]	Peak1=0.27±0.01 Peak2=0.42±0.01	Dw=550±10	σ_1= 0.08 σ_2= 0.14	46%
	Polyamine	Peak1=0.34±0.02 Peak2=0.49±0.14	Dw=359±4	σ_1= 0.12 σ_2= 0.15	54%
PRE-II MFK	WB	Peak1=0.28±0.01 Peak2=0.45±0.02	Dw=266±3	σ_1= 0.09 σ_2= 0.17	37%
	TAM[15]	Peak1=0.31±0.01 Peak2=0.52±0.02	Dw=235±3	σ_1= 0.11 σ_2= 0.20	44%
	Polyamine	Peak1=0.32±0.01 Peak2=0.53±0.01	Dw=298±4	σ_1= 0.09 σ_2= 0.20	52%

Table 4.7 Summary of FRET distributions of EF-G$^{693\text{-}Cy3}$:PRE$^{tRNA\text{-}Cy5}$ with VIO. FRET between EF-G$^{693\text{-}Cy3}$ and PRE-I$^{tRNA\text{-}Cy5}$ or PRE-II$^{tRNA\text{-}Cy5}$ are studied under different buffer conditions with 100 nM next round TC and 100 μM VIO.

[a] Dwell time of total events

[b] SD of FRET distribution

[c] High FRET percentage is calculated by using the number of events (E > 0.4) divided by the number of total events

[d] Standard error of the fitted peak value

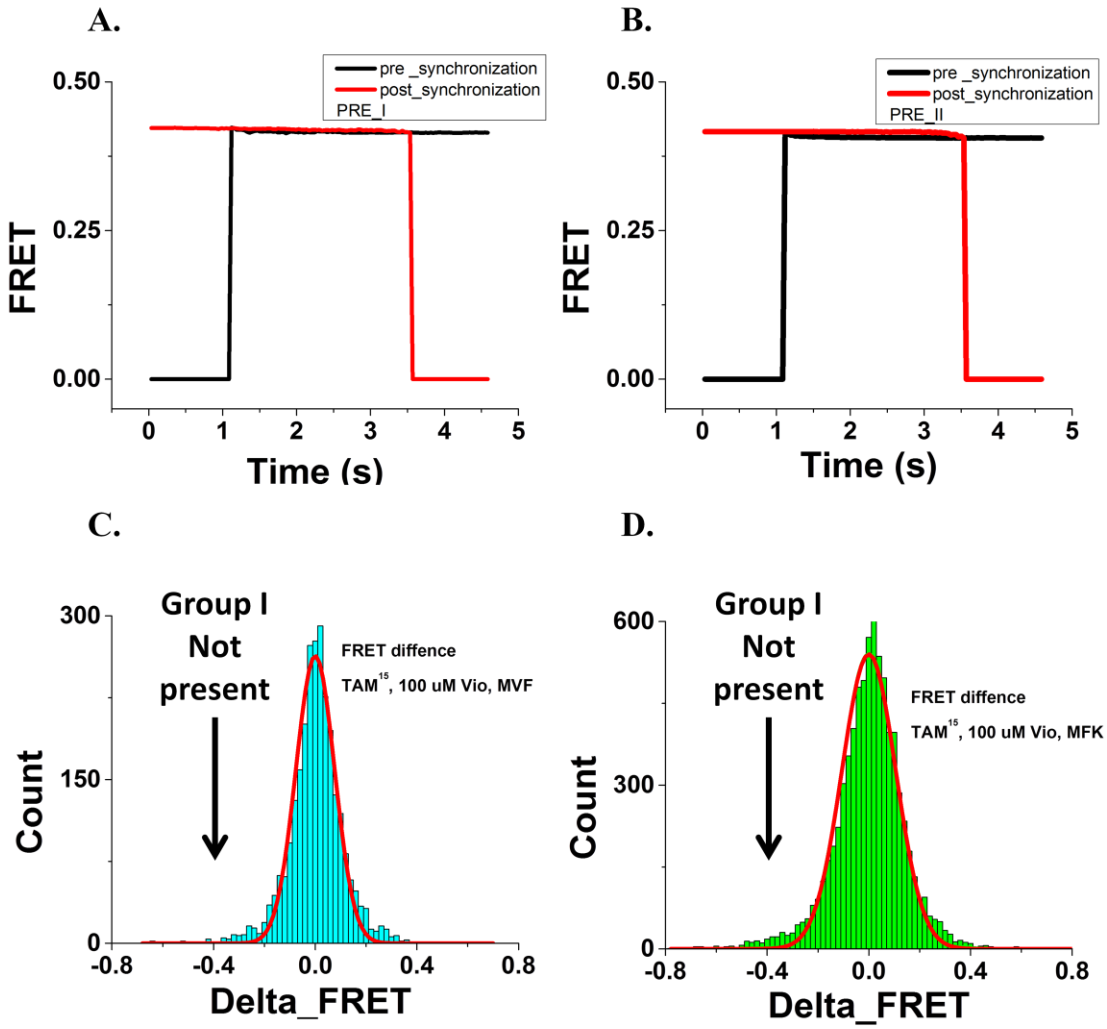

Figure 4.24 VIO suppresses FRET conversions. A, B. Postsynchronized traces under standard conditions in the presence of 100 μM VIO are obtained by aligning all FRET traces at the beginning (black) or at the end (red) and plotted as a function of time. **C, D.** ΔFRET distribution of EF-G$^{693\text{-}Cy3}$:PRE-I$^{tRNA\text{-}Cy5}$ (left) and EF-G$^{693\text{-}Cy3}$:PRE-II$^{tRNA\text{-}Cy5}$ (right) in TAM^{15} buffer with 100 μM VIO. FRET events which last longer than 6 frames are selected. The first and last three frames are averaged separately, defined as initial and final FRET, respectively. The differences between final and initial FRET are calculated and delta FRET distributions are plotted.

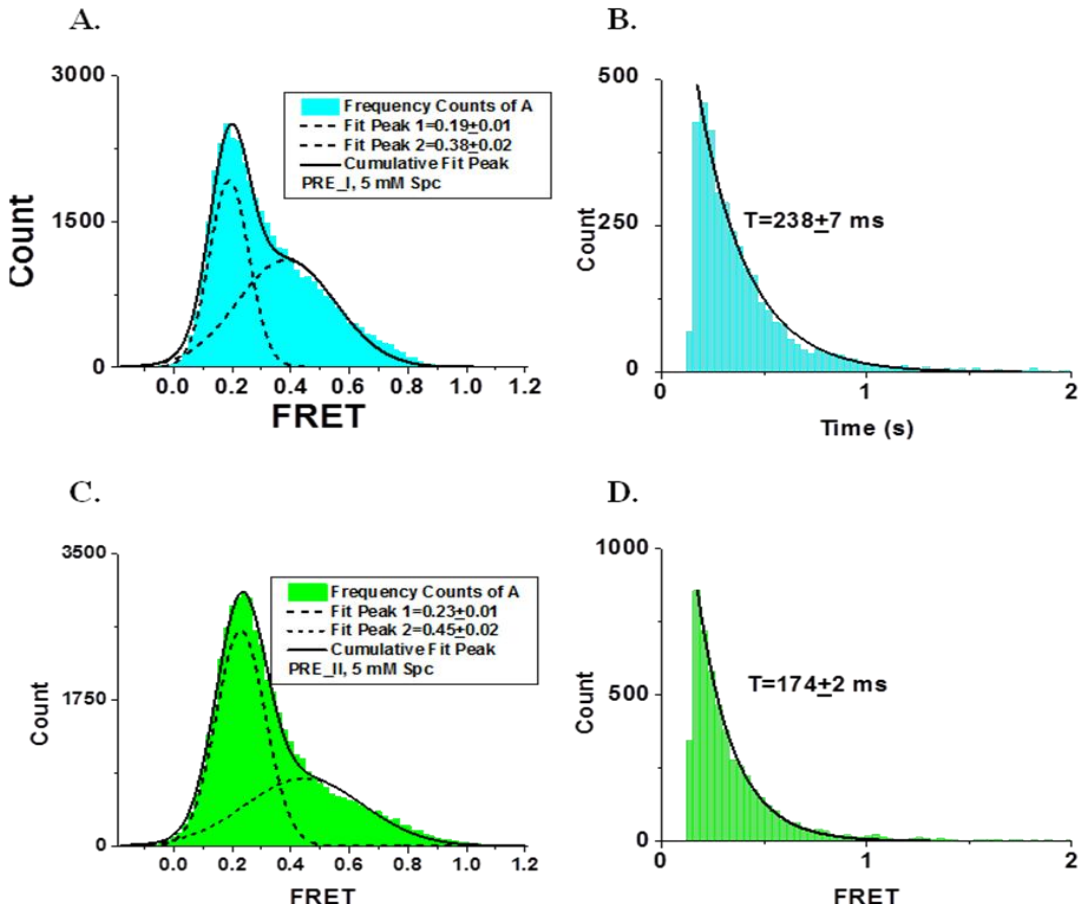

Figure 4.25 FRET distribution of EF-G$^{693\text{-Cy3}}$:PRE$^{tRNA\text{-Cy5}}$ with Spc. EF-G$^{693\text{-Cy3}}$ interaction with PRE-I$^{tRNA\text{-Cy5}}$ (top) and PRE-II$^{tRNA\text{-Cy5}}$ (bottom) under TAM^{15} buffer with 100 nM next round TC and 5mM Spc. **A, C**. FRET distributions are plotted with two major peaks. **B, D**. Dwell time distributions are each fitted by a single exponential $y = A\exp(-kt)$. The detailed fitting results, including standard deviations of peak values and the percentages of high FRET state are listed in Table 4.8.

Complex	Buffer	Fitted Peak of Total FRET distribution	[a] σ (SD)	[b]High FRET ratio
PRE-I MVF	TAM^{15}	Peak1=0.19±0.01[c] Peak2=0.38±0.02	σ_1= 0.07 σ_2= 0.17	51%
PRE-II MFK	TAM^{15}	Peak1=0.23±0.01 Peak2=0.45±0.02	σ_1= 0.08 σ_2= 0.20	32%

Table 4.8 Summary of FRET distributions of EF-$G^{693\text{-}Cy3}$:$PRE^{tRNA\text{-}Cy5}$ with Spc. FRET between EF-$G^{693\text{-}Cy3}$ and PRE-I^{Cy5} or PRE-II^{Cy5} is obtained under TAM^{15} with 100 nM next round TC and 5 mM Spc.

[a] SD of FRET distribution

[b] The intersect FRET value of the two fitted Gaussian curves (IS) is obtained. High FRET percentage is calculated by using the number of events (E > IS) divided by the number of total events.

[c] Standard error of the fitted peak value

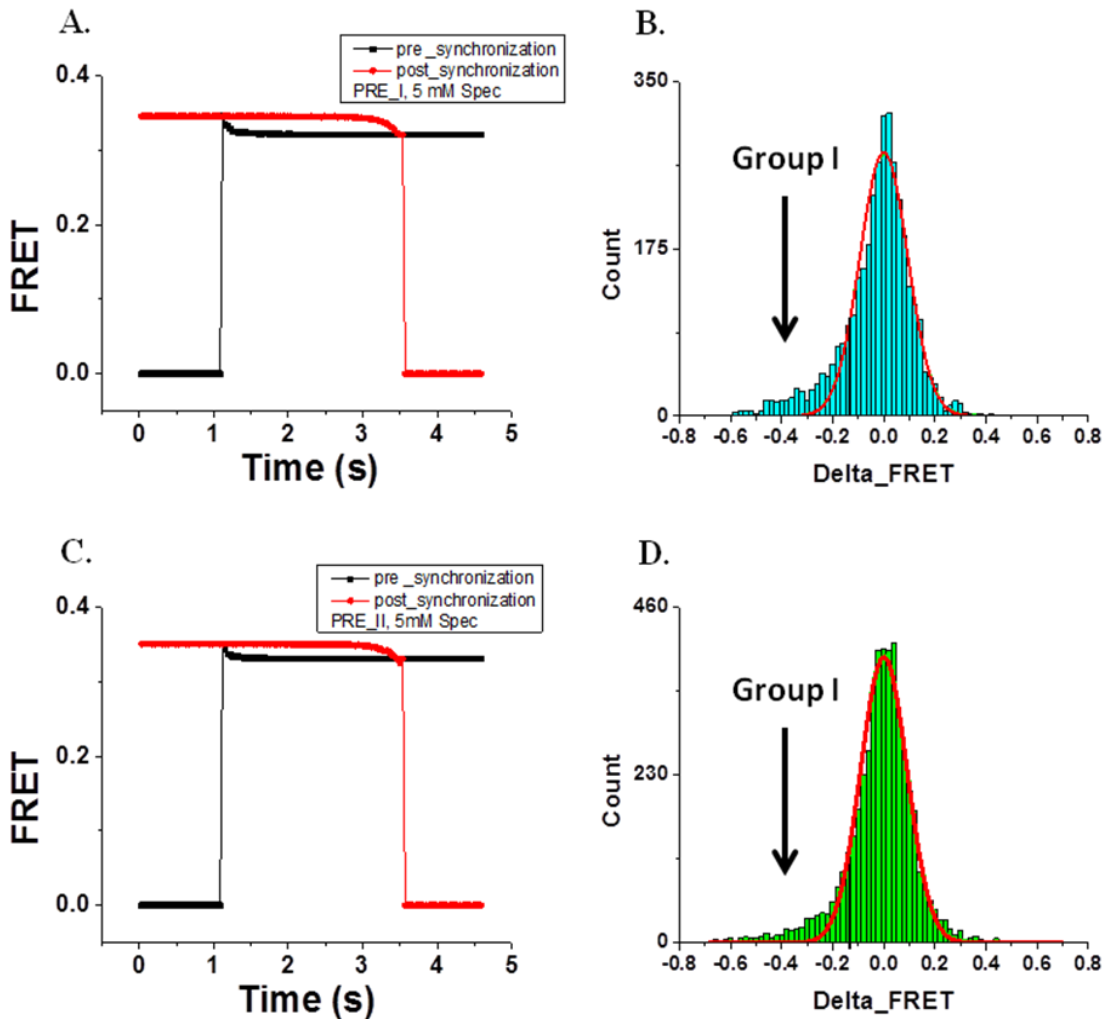

Figure 4.26 FRET state analysis of EF-G$^{693\text{-}Cy3}$:PRE$^{tRNA\text{-}Cy5}$ with Spc. FRET between EF-G$^{693\text{-}Cy3}$ and PRE-I$^{tRNA\text{-}Cy5}$ (top) or PRE-II$^{tRNA\text{-}Cy5}$ (bottom) is obtained under TAM^{15} buffer with 100 nM next round TC and 5mM Spc. **A**, **C** Postsynchronized traces are calculated by synchronizing all FRET events at the beginning (black) or at the end (red) and plotted as a function of time. **B, D** FRET events which last longer than 6 frames are selected. The first and last three frames are averaged separately, defined as initial and final FRET, respectively. The differences between final and initial FRET values are calculated and delta FRET distributions are plotted.

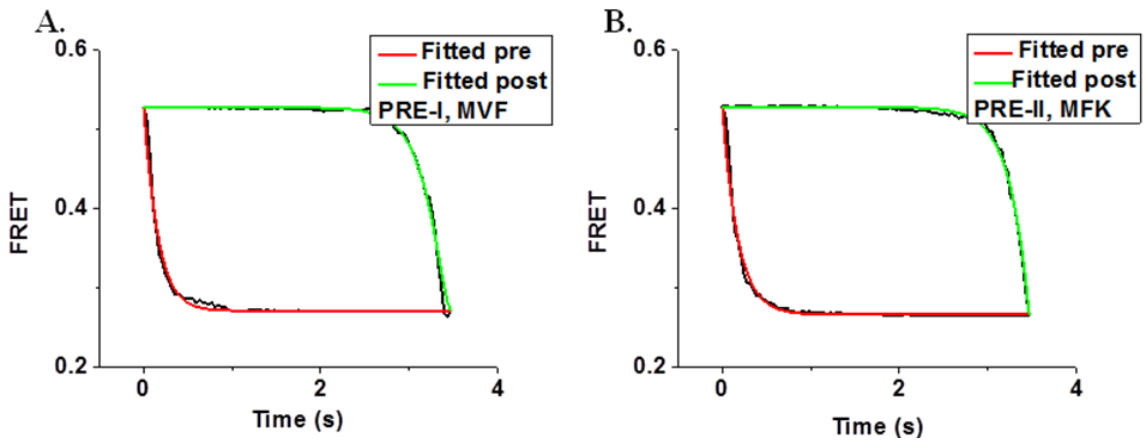

Figure 4.27 Global fitting results of postsynchronized traces of EF-G$^{693\text{-}Cy3}$:PRE$^{tRNA\text{-}Cy5}$ with Spc. EF-G$^{693\text{-}Cy3}$ interactions with PRE-I$^{tRNA\text{-}Cy5}$ (left) and PRE-II$^{tRNA\text{-}Cy5}$ (right) were studied in TAM^{15} buffer, 100 nM next round TC and 5 mM Spc.

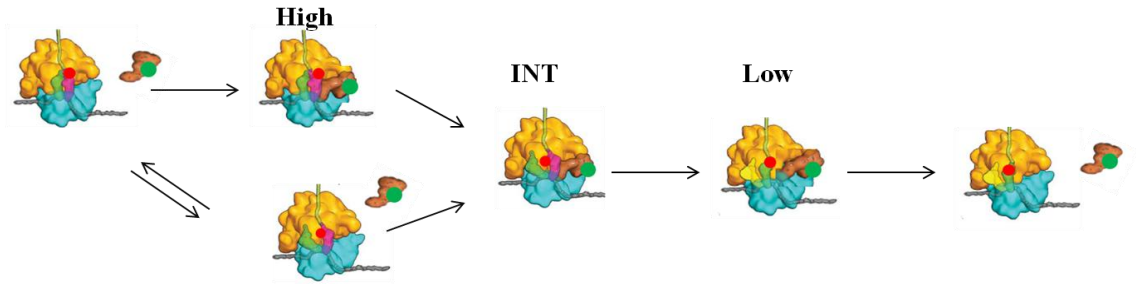

Figure 4.28 Kinetic models of EF-G catalyzed translocation.

CHAPTER V SMFRET STUDY OF BIFUNCTIONAL RHODAMINE LABELED EF-G

Abstract

Elongation factor G (EF-G) catalyzes translocation of mRNA, A- and P-site bound tRNAs on the ribosome during the polypeptide elongation cycle. Previous studies show that EF-G has significant conformational flexibility with different conformations observed for EF-G·GTP and EF-G·GDP forms (Agirrezabala *et al*., 2009). Upon binding to the ribosome, EF-G undergoes large conformational changes as it transitions from bound EF-G·GTP to bound EF-G·GDP·Pi and to bound EF-G·GDP that include both distance displacement and orientation changes. To understand how these two different movements occur on the ribosome, bifunctional rhodamine labeled EF-G derivatives (BR-EF-G) were utilized to compare the timing of changes in EF-G orientation on the ribosome, as measured by single molecule polarized total internal reflection fluorescence (polTIRF) microscopy (Chen *et al*., manuscript in preparation) with changes in EF-G:tRNA FRET efficiency measurement, presented below. In our work, Phe-tRNA^{Phe} was labeled with Cy5 and six EF-G derivatives were labeled with a bifunctional tetramethylrhodamine (BR). Four of the six mutants showed measurable BR:Cy5 FRET, with dwell times of 150 - 350 ms, depending on which mutant was used. A major FRET change during EF-G occupancy of the ribosome was observed for only one BR-EF-G, as determined from synchronization analysis, ΔFRET distributions, and transition heat contour maps. Interestingly, for the four BR-EF-Gs showing FRET, FRET changes during EF-G occupancy were larger if the BR group was located closer to the EF-G hinge region, suggesting that parts of Domain IV of EF-G, which penetrate to the decoding region of the ribosome, move together with the A-site tRNA during translocation.

5.1 Introduction

EF-G·GTP first binds to the GTPase activation center (GAC) of a pretranslocation (PRE) complex, followed by a fast GTP hydrolysis (k = 170 s^{-1}). The tip of Domain IV on EF-G is believed to penetrate to the A-site during translocation. At the same time, the interactions of EF-G with tRNAs and mRNA are retained to help to maintain the reading frame (Pulk *et al*., 2013; Tourigny *et al*., 2013; Zhou *et al*., 2013). The translocation movements of tRNA and mRNA occur at the same rate and according to the most recent research, this movement is also coupled with the back ratcheting of the ribosome (Chen *et al*., 2013a). As the EF-G·GDP form has a much lower affinity to the ribosome, after Pi release, EF-G·GDP dissociates from the ribosome spontaneously (Rodnina *et al*., 1997). The conformational changes during EF-G residence on the ribosome can be described as a hinge-like motion of Domains III, IV and V relative to Domains I and II, directly confirmed by the structural results (Fig 5.1).

In Chapter 4, we identified time-dependent FRET changes between EF-G^{693} and the A-site tRNA or L11 during translocation, which revealed important insights regarding the dynamics of distance changes between one position on C-terminal domain (CTD) of EF-G (N693C-EF-G) and the D-loop of tRNA (position 16/20) during translocation. Here, we extended such measurements to six different BR-labeled EF-G derivatives. The results obtained provide a more comprehensive view of relative EF-G:tRNA motion during translocation, and ultimately will be useful in comparing the timing of changes in EF-G:tRNA distance to changes in EF-G orientation on the ribosome during translocation. The latter, which is carried out using single molecule polarized total internal reflection fluorescence (polTIRF) microscopy, employs the same six BR-labeled EF-G derivatives

(Chen *et al*., manuscript in preparation). These derivatives are designed to diminish the free rotation of the dye relative to EF-G. For this purpose, two engineered cysteines (Cys) located within the same α-helix seven residues apart are cross-linked with BR (Fig 5.2).

5.2 Results

5.2.1 The design of the experiment

PRE-II complex containing Cy5 labeled Phe-tRNA^{Phe}, hereinafter denoted PRE-II^{Cy5}, was prepared as described (Section **2.2.4.4**) and attached to the slide surface via a 5' and 3' double biotin labeled mRNA (MFV) to restrict ribosome free rotation (Fig 5.3, Fig 5.4). To keep the results of polTIRF and smFRET-TIRF comparable to one another, the standard buffer condition in our lab (TAM^{15} buffer) was used. Also, 20 nM next TC (WT-Val-TC) and 10 nM Cy5-Phe-TC were added to reduce the likelihood of EF-G binding to the POST complex and carry out multiple rounds of translocation. All experiments were performed at 21 °C with a frame rate of 10 ms/frame.

5.2.2 EF-G mutant selections

Six BR-EF-G derivatives which showed full translocation activity (Chen *et al*., unpublished results) were screened for FRET with the A-site Cy5 labeled tRNA, including BR-EF-G$^{429\text{-}436}$ (Domain III), BR-EF-G$^{630\text{-}637}$ (Domain V), BR-EF-G$^{467\text{-}474}$ (Domain III), BR-EF-G$^{555\text{-}562}$ (Domain IV), BR-EF-G$^{599\text{-}606}$ (Domain IV) and BR-EF-G$^{692\text{-}699}$(CTD). The latter four all gave FRET with the A-site bound fMet-Phe-tRNA^{Phe} (Cy5) and were selected for further studies. Each of the labeled sites fell within α-helices that were solvent-exposed and contained amino acids that were not strongly conserved.

5.2.3 Characterization of the EF-G:tRNA FRET interactions

5.2.3.1 FRET efficiency distributions and BR-EF-G dwell times

For each of the four BR-EF-Gs giving FRET with the A-site bound fMet-Phe-tRNA^{Phe} (Cy5), binding to PRE-II$^{tRNA\text{-}Cy5}$ led to a simultaneous increase of BR and Cy5 fluorescence. FRET efficiency distributions (Fig. 5.5) were fitted with Gaussian function and all BR-EF-G dwell times (Fig 5.6) were fitted with a double exponential decay. FRET efficiencies were fitted by two major peaks except for BR-EF-G$^{599\text{-}606}$ as only one peak was obtained. Among these four EF-G derivatives, FRET efficiencies were largest for BR-EF-G$^{599\text{-}606}$ and lowest for BR-EF-G$^{555\text{-}562}$. FRET efficiencies of BR-EF-G$^{467\text{-}474}$ and BR-EF-G$^{692\text{-}699}$ were similar but a high FRET proportion was more prominent in BR-EF-G$^{692\text{-}699}$ mutant. BR-EF-G$^{467\text{-}474}$ and BR-EF-G$^{555\text{-}562}$ showed comparable FRET dwell time with values of $\tau1$= 33 ± 9 ms, $\tau2$= 123 ± 8 ms and $\tau1$= 16 ± 2 ms, $\tau2$= 182 ± 3 ms, respectively, whereas $\tau2$ for EF-G$^{692\text{-}699}$ was much longer with a value of 335 ± 9 ms. The differences in dwell times among different EF-G derivatives are likely due to the position where the dye is attached and all of the dwell time obtained in this work is similar to previous characterized dwell time of translocation (Chen *et al*., 2013a; Munro *et al*., 2010).

5.2.3.2 Characterization of BR-EF-G:tRNA FRET efficiency change

Following the logic employed in analyzing the interaction of EF-G$^{693\text{-}Cy3}$ with PRE-I and PRE-II (Section **4.2.4.3**), we utilized synchronization analysis (Fig 5.7), ΔFRET distribution (Fig 5.8) and transition heat contour maps (Figure 5.9) to determine whether BR-EF-G:tRNA FRET efficiency showed changes during translocation. Postsynchronized traces of both BR-EF-G$^{467\text{-}474}$ and BR-EF-G$^{692\text{-}699}$ presented a small

FRET change, while the other two mutants only had one constant FRET value over the entire FRET duration. ΔFRET distributions were plotted, and although the majority of the events still showed no significant FRET changes, for BR-EF-$G^{692-699}$, a certain proportion of events was observed located in $\boldsymbol{x} < 0$ region with a negative FRET change (left side of the dashed line in Fig 5.8 **D**). In contrast, this population was not prominent in BR-EF-$G^{467-474}$ mutant, likely due to only a low proportion of traces with large FRET changes. As discussed in Chapter 4, the FRET events of BR-EF-$G^{692-699}$ mutant were further segmented into two groups to study the heterogeneity of EF-G:tRNA interactions. We denoted the group of traces with large decreased FRET (ΔFRET < - 0.2) for the BR-EF-$G^{692-699}$:PRE-$II^{tRNA-Cy5}$ FRET pair as Group I. All the other traces were placed in Group II (ΔFRET > - 0.2). The dwell time averaged 408 ± 19 ms for Group I and 372 ± 10 ms for Group II (Fig 5.10). This small difference is not as large as what was obtained for EF-$G^{Cy3-693}$ (543 ± 19 ms for Group I and 434 ± 10 ms for Group II, Section **4.2.4.3**).

5.2.3.3 Initial and Final FRET distributions for the BR-EF-$G^{692-699}$:tRNA pair

We next examined the distributions of initial and final FRET values for the BR-EF-$G^{692-699}$:tRNA pair, which were calculated as the average values of the first three and last three frames of the FRET events, respectively (Fig 5.11). A clear decrease was observed for the final FRET as compared to the initial FRET efficiencies, with FRET values of 0.27 ± 0.01 and 0.47 ± 0.01 for initial FRET shifting to 0.23 ± 0.01 and 0.37 ± 0.04 for final FRET. Also, the initial FRET distribution was broader compared to the final FRET distribution. Detailed analysis was applied to postsynchronized traces to characterize the kinetics of tRNA translocation

5.2.3.4 Translocation kinetics of Group I for the BR-EF-G$^{692-699}$:tRNA pair

Following the procedure described in Section **4.2.4.7**, we fit the postsynchronized traces in Group I to characterize the kinetics of BR-EF-G$^{692-699}$ catalyzed translocation. Global fitting was applied to postsynchronized traces using two-state or three-state models (Fig 5.12). A better fit to the raw data was obtained using the three-state model. Accordingly, the results obtained from the three-state model will be used for the later discussion.

The fitted results showed that in Group I, FRET events started with a high FRET value of 0.53 ± 0.01, proceeded via an intermediate FRET of 0.28 ± 0.01, and finally disappeared with a low FRET of 0.24 ± 0.01, corresponding to a distance change from about 52Å to 62 Å and then to 64 Å. The transitions from 0.53 to 0.28, 0.28 to 0.24, and 0.24 to zero proceeded with rate constants of 45.5 ± 1.7 s^{-1}, 2.5 ± 0.1 s^{-1}, and 24.8 ± 2.2 s^{-1} (Table 5.3). These results are similar to what we found for EF-G$^{Cy3-693}$ catalyzed translocation (Section **4.2.4.7** - FRET states: 0.49, 0.31, 0.26; rate constants 24.4 ± 1.1 s^{-1}, 1.6 ± 0.1 s^{-1}, 12.6 ± 1.1 s^{-1}), although the rate constants for BR-EF-G$^{692-699}$ are 1.5 - 2 times larger. The slower rate constants for EF-G$^{Cy3-693}$ might be due to interaction of the singly tethered Cy3 dye with the ribosome. The double tethered BR dye would be expected to interact much less with the ribosome. The smallest rate difference between the two labeled EF-Gs is in the rate limiting step, which is accompanied by only a small FRET change. This step, which presumably involves large movements of tRNA and/or mRNA but only shows a small relative FRET change between labeled positions on EF-G and the A-site tRNA, might be less influenced by differences in dye-ribosome interaction.

5.2.3.5 ΔFRET and BR placement within EF-G

The results presented in Fig 5.13 could be used to address the question of how the extent of negative FRET change correlated with the position of BR cross-linking to the EF-G molecule. For each BR-EF-G, the measured variable D, defined as the number of traces showing a ≥ 0.2 decrease in FRET efficiency minus the number of traces showing a ≥ 0.2 increase in FRET efficiency, was divided by the total number of FRET recordings (T) (Table 5.4). This results in the following ordering of the percentage of net negative FRET changes: EF-$G^{692\text{-}699}$ (CTD) > BR-EF-$G^{467\text{-}474}$ (Domain III) > EF-$G^{599\text{-}606}$ (Domain IV) or BR-EF-$G^{555\text{-}562}$ (Domain IV), supporting the conclusion that negative FRET changes were larger if the BR group was located closer to the EF-G hinge region.

5.3 Discussion

In Chapter 4, we proposed a kinetic model of EF-G:tRNA interaction during translocation with the FRET efficiencies and rate constants of each state characterized for the first time. This model suggests that EF-G:tRNA FRET proceeds from High to INT to Low FRET, which correspond to FRET values of EF-G:tRNA pair when tRNAs are in classic, hybrid or POST-like states. This kinetic model is further confirmed by analyzing post-synchronized FRET between the A-site tRNA and bifunctional rhodamine labeled EF-Gs(BR-EF-Gs) located at the IV:V interface. The global fitting results of post-synchronized FRET of BR-EF-Gs:tRNA suggest that the FRET efficiency starts with a high FRET value, and proceeds to an intermediate value, to a low FRET value. Similar as what was obtained in Chapter 4, the transition rate from INT to Low is the rate limiting step, while only a small FRET change occurs during this process. However, the transition rates of BR-EF-Gs:tRNA pair are comparably faster (~ 2 fold) than those of Cy3-EF-

G:tRNA (Table 5.1, Table 4,4). This difference could be due to the difference in the labeling strategies. The BR dye on EF-G is more restricted and has less freedom of rotational movements. In contrast, Cy3 dye is only singly attached to EF-G. When it is tethered onto the ribosome, more contacts could be formed between the dye and ribosomal proteins or rRNAs, which are likely to extend EF-G lifetime on the ribosome.

Both postsynchronization analysis and delta FRET distributions (Fig 5.7, Fig 5.8) show that larger changes in FRET efficiency are found when the BR group is located closer to the EF-G hinge region (Agirrezabala *et al*., 2009; Agrawal *et al*., 1998; Frank *et al*., 2007; Valle *et al*., 2003) about which Domains III-V move relative to Domains I and II, than when the BR group is in a part of Domain IV that extends into the A-site decoding center. During translocation, both A-site tRNAs and Domain IV of EF-G are believed to undergo large distance displacements in the decoding center (Agirrezabala *et al*., 2009). Our present results of FRET changes detected by BR-EF-Gs and previous structural information about the large distance displacements of tRNA and EF-G together suggest that Domain IV, which extends into the decoding center, moves together with the A-site tRNA during translocation. Thus, we detect no relative movement between Domain IV of EF-G and the A-site tRNA during translocation. In contrast, other parts of EF-G which are located closer to the hinge region, do not undergo such large movement. The resulting large distance changes between those domains and peptidyl-tRNA during translocation result in the significant FRET efficiency changes we observe during translocation.

5.4 Conclusion

By using bifunctional tetramethylrhodamine labeled EF-G derivatives, restricting the free rotation of dye attached to EF-G, we were able to study the relative movements between EF-G and the A-site peptidyl-tRNA. Our data suggest that during EF-G catalyzed translocation, some parts of Domain IV of EF-G move together with the peptidyl-tRNA, so that the EF-G:tRNA FRET efficiency doesn't change (Fig 5.2). In contrast, when the BR group is located closer to the EF-G hinge region, at which position, Domains III, IV and V undergo a large movement relative to Domains I and II during translocation (Agirrezabala *et al*., 2009), FRET efficiency decreases, consistent with a growing distance between those parts of EF-G and peptidyl-tRNA.

Fitting results by using two-state or three-state models suggest that an intermediate state existed in our BR-EF-G:Cy5-tRNA FRET interaction. The fitted rate constants of BR-EF-$G^{692\text{-}699}$ are larger than those for EF-$G^{Cy3\text{-}693}$. This is likely due to the free rotation of the fluorophore in EF-$G^{Cy3\text{-}693}$, which could, by forming contacts with parts of the ribosome, extend EF-G lifetime on the ribosome. The smallest rate difference between the two labeled EF-Gs is in the rate limiting step which only shows a small EF-G:tRNA FRET change, suggesting that tRNA and mRNA movement at the decoding center may occur at this stage.

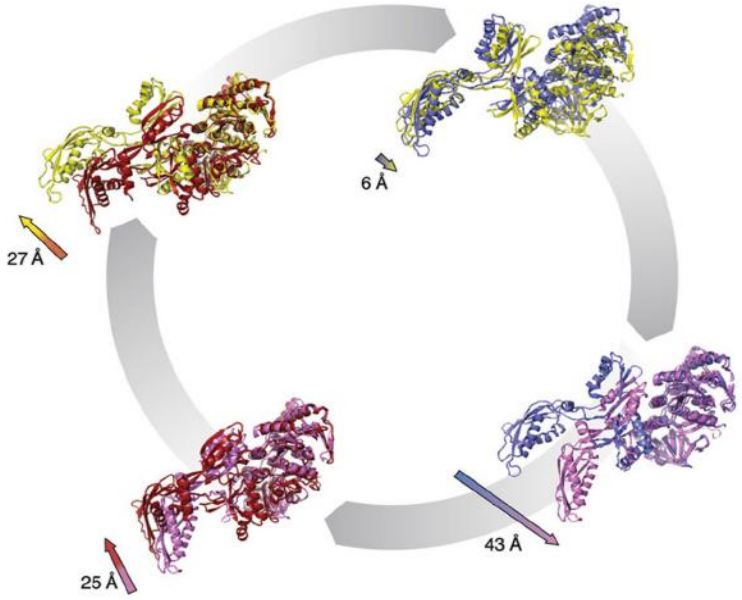

Figure 5.1 Comparison of structural changes observed in EF-G [from (Agirrezabala, *et al.*, 2009)]. The conformations observed in EF-G/eEF2 by means of cryo-EM (ribosome-bound forms) and X-ray crystallography (in solution) can be summarized as follows: EF-G in complex with GTP in solution (red), before interacting with the ribosome, as seen in the crystal structure of the EF-G analog EF-G-2 (PDB code: 1WDT). EF-G•GTP•ribosome conformation was determined by cryo-EM using the non-hydrolyzable GTP analog GDPNP (PDB code: 1PN6). The conformational changes in ribosome-bound EF-G, upon GTP hydrolysis, are likely similar to those described for eEF2•80S complexes in Taylor *et al.* (2007). A comparison of the complexes before (yellow) and after GTP hydrolysis (blue, PDB code: 2P8Y). Conformational changes of EF-G•GDP from the ribosome-bound conformation (blue), determined by cryo-EM (PDB code: 2P8Y), to the solution structure (pink), determined by X-ray crystallography (PDB code: 1EFG), include a movement at the tip of domain IV by ~43 Å. A comparison of the GDP-bound conformation (pink) of EF-G with the GTP-bound conformation (red) reveals a shift at the tip of domain IV of the factor by ~25 Å. The presence of GTP also reveals an ordered Switch I loop and a different conformation of the Switch II loop. Altogether, these rearrangements likely are the basis of a much higher affinity of the pretranslocational ribosome for the GTP-bound conformation of EF-G.

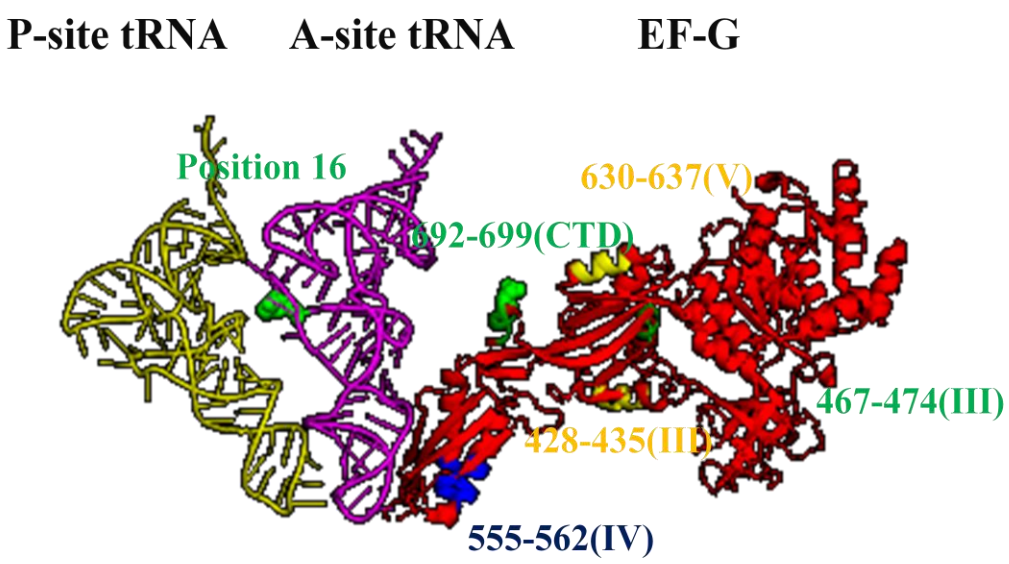

Figure 5.2 Carton figures of EF-G and cross-linked bifunctional rhodamine. EF-G (red), A-site tRNA (purple) and P-site tRNA (yellow). Mutated sites on EF-G are identified by amino acid number and domain labeled.

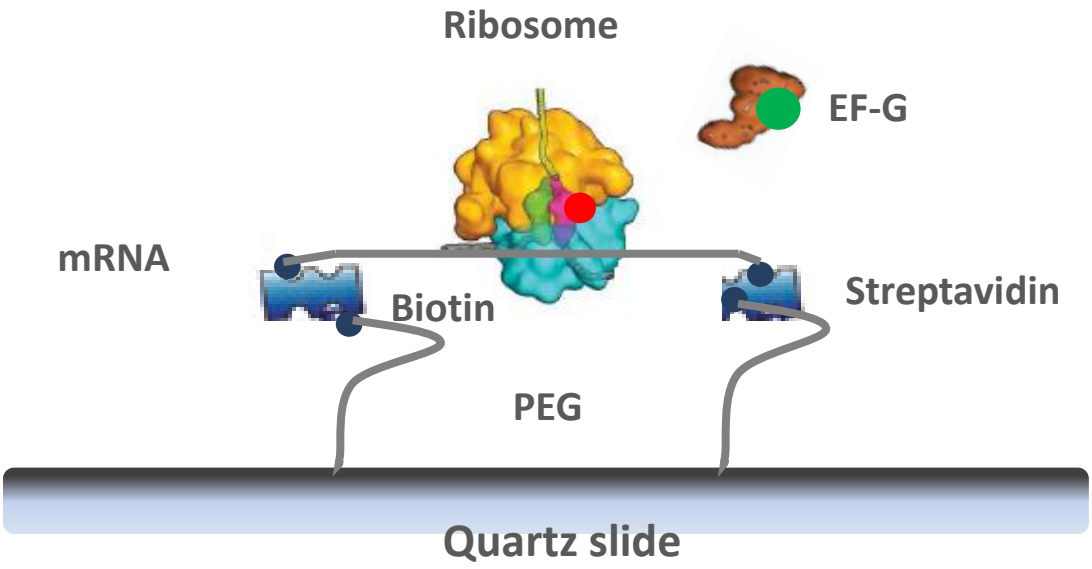

Figure 5.3 Cartoon of the single molecule experiment setup of BR-EF-G. Cy5 labeled PRE complex with $tRNA^{Cy5}$ was attached to the slide surface via a double biotin labeled mRNA. Then bifunctional rhodamine labeled EF-G was injected into the system. A green laser (532 nm) was illuminated to excite rhodamine fluorophore directly.

Nucleotide spacer *StrongSD* *Spacer* *Start* *F* *V* *F* *V* *F* *V*

5' biotin- G UUA AUA AGG AUA CAU ACU AUGUUC GUG UUC GUG UUC GUG -biotin 3'

Figure 5.4 The 5' and 3' double biotin labeled mRNA used in this work.

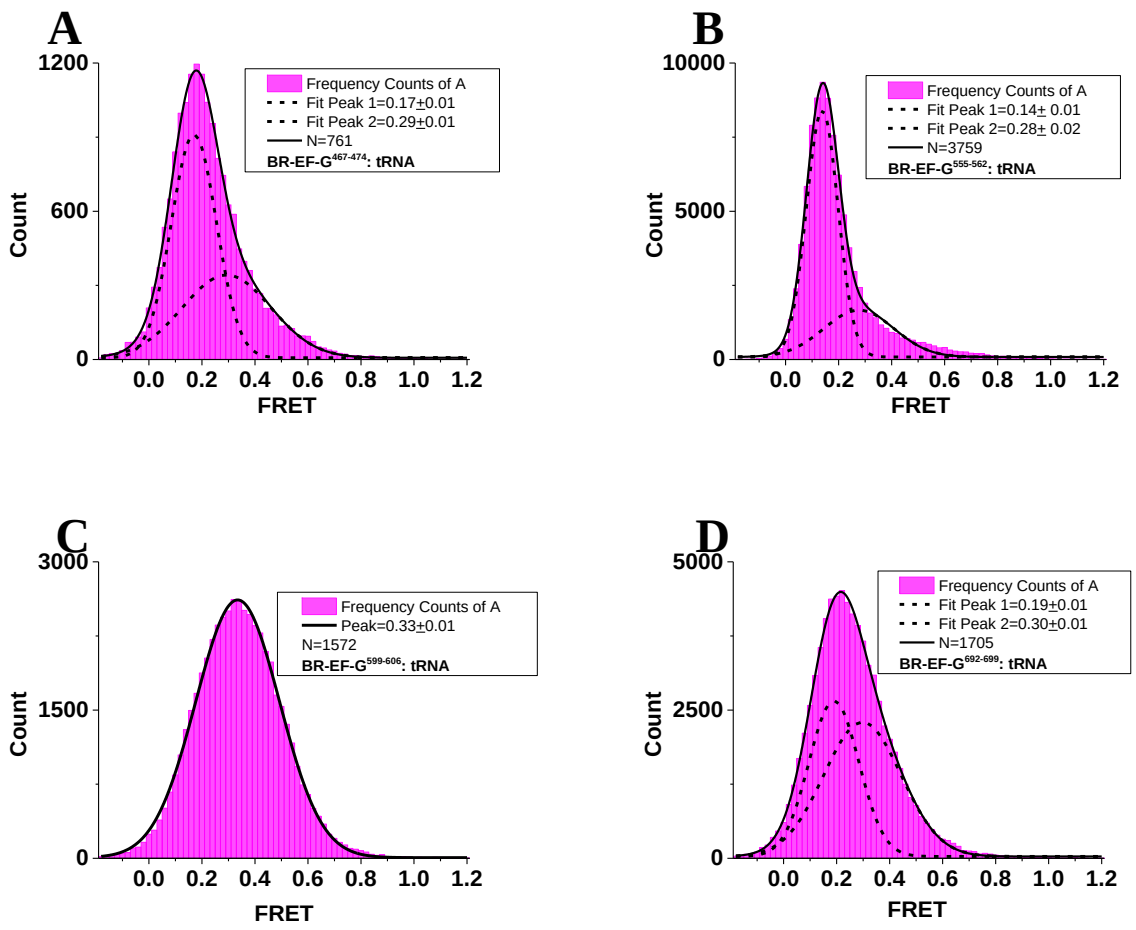

Figure 5.5 FRET distribution of BR-EF-G:PRE-II$^{tRNA\text{-}Cy5}$. Sample was prepared in TAM[15] buffer and contained BR-EF-Gs, 20 nM WT-Val-TC, 10 nM Cy5-Phe-TC and 1mM GTP. FRET efficiency distributions are fitted by Gaussian function:

$$y = y_0 + \left(\frac{A1}{\sigma\sqrt{2\pi}} e^{-\frac{(x-xc1)^2}{2\sigma_1^2}}\right) + \left(\frac{A2}{\sigma\sqrt{2\pi}} e^{-\frac{(x-xc2)^2}{2\sigma_2^2}}\right).$$

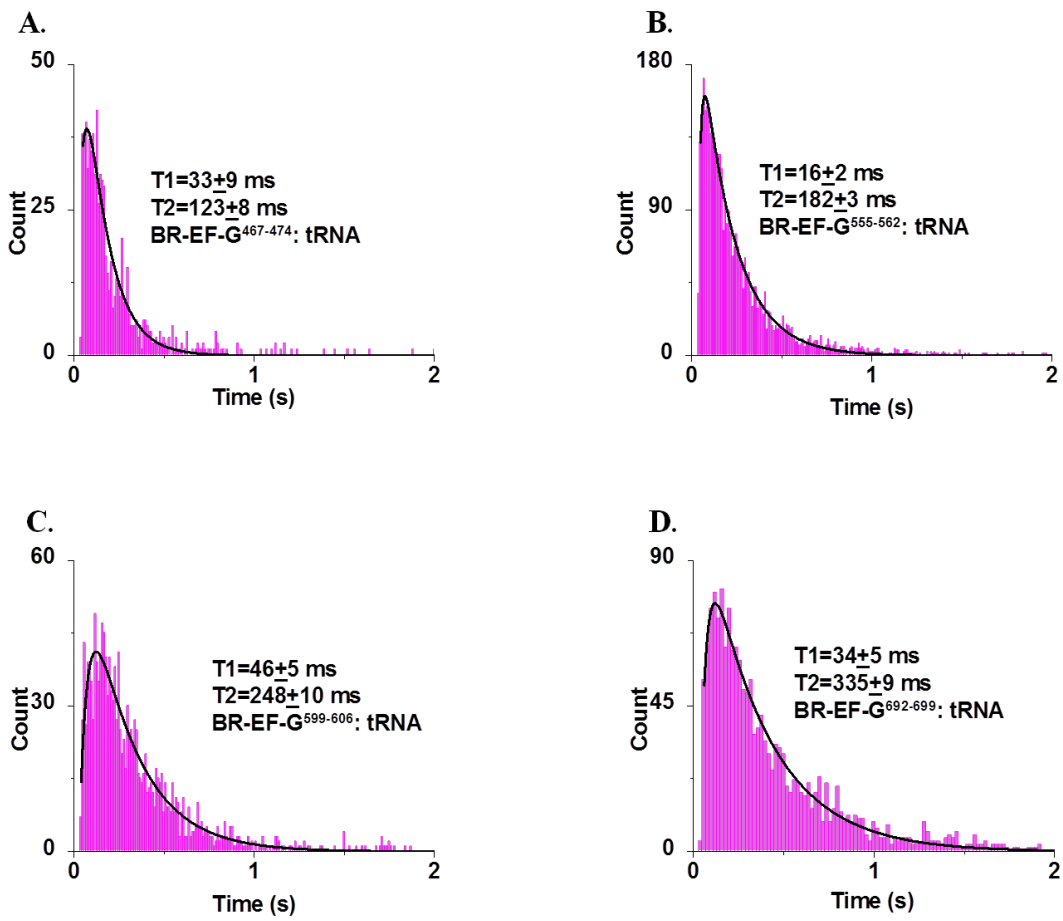

Figure 5.6 FRET dwell time distribution of BR-EF-G:PRE-II$^{tRNA\text{-}Cy5}$. Sample was prepared in TAM[15] buffer and contained BR-EF-Gs, 20 nM WT-Val-TC, 10 nM Cy5-Phe-TC and 1mM GTP. Dwell time distribution is fitted by double exponential decay:

$$y = y_0 + A_1 \times e^{-\frac{x-x_0}{t1}} + A_2 \times e^{-\frac{x-x_0}{t2}}$$

EF-G derivative (Domain)	Mutant sites	FRET efficiency		High FRET percentage	FRET dwell time (ms)	
		Peak 1	Peak 2		t_1	t_2
BR-EF-G$^{467-474}$ (III)	D467C,K474C, C114D, C266A, C397S	0.17 ± [2]0.01 ([1]0.08)	0.29 ± 0.01 (0.17)	0.26	33 ± 9	123 ± 8
BR-EF-G$^{555-562}$ (IV)	K555C, K562C, C114D, C266A, C397S	0.14 ± 0.01 (0.06)	0.28 ± 0.02 (0.13)	0.24	17 ± 2	162 ± 3
BR-EF-G$^{599-606}$ (IV)	I599C, K606C, C114D, C266A, C397S	0.33 ± 0.01 (0.16)	----	----	46 ± 5	248 ± 10
BR-EF-G$^{692-699}$ (CTD)	S692C, I699C, C114D, C266A, C397S	0.20 ± 0.01 (0.09)	0.31 ± 0.01 (0.15)	0.48	52 ± 9	334 ± 15

Table 5.1 FRET distributions and dwell time of BR-EF-Gs:PRE-II$^{tRNA-Cy5}$ FRET pair. Sample was prepared in TAM[15] buffer and contained BR-EF-Gs, 20 nM WT-Val-TC, 10 nM Cy5-Phe-TC and 1 mM GTP at 21 ^{o} C.

[1] SD of FRET distribution

[2] Standard error of the fitted peak

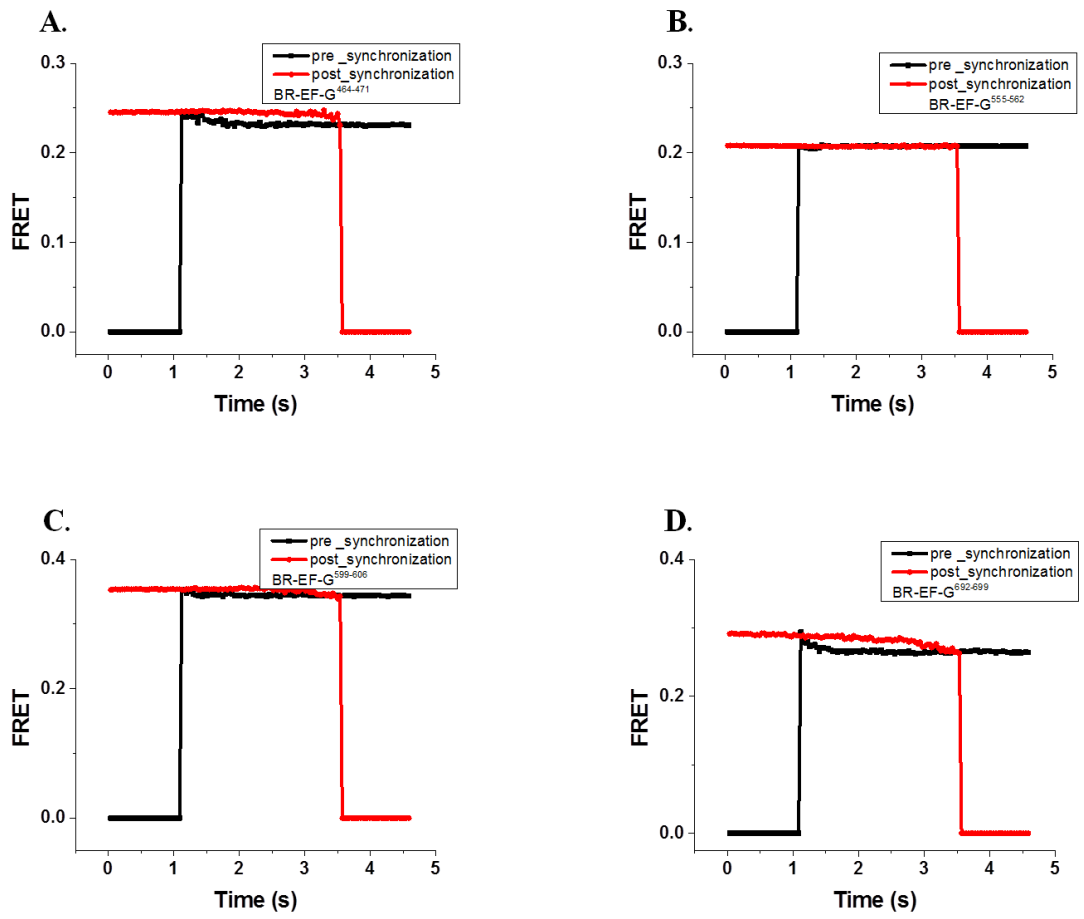

Figure 5.7 Postsynchronized analysis of BR-EF-G:PRE-II$^{tRNA\text{-}Cy5}$. Sample was prepared in TAM[15] buffer and contained BR-EF-Gs, 20 nM WT-Val-TC, 10 nM Cy5-Phe-TC and 1mM GTP. Postsynchronized traces are obtained by aligning all FRET events at the beginning (black) or at the end (red) and plotted as a function of time.

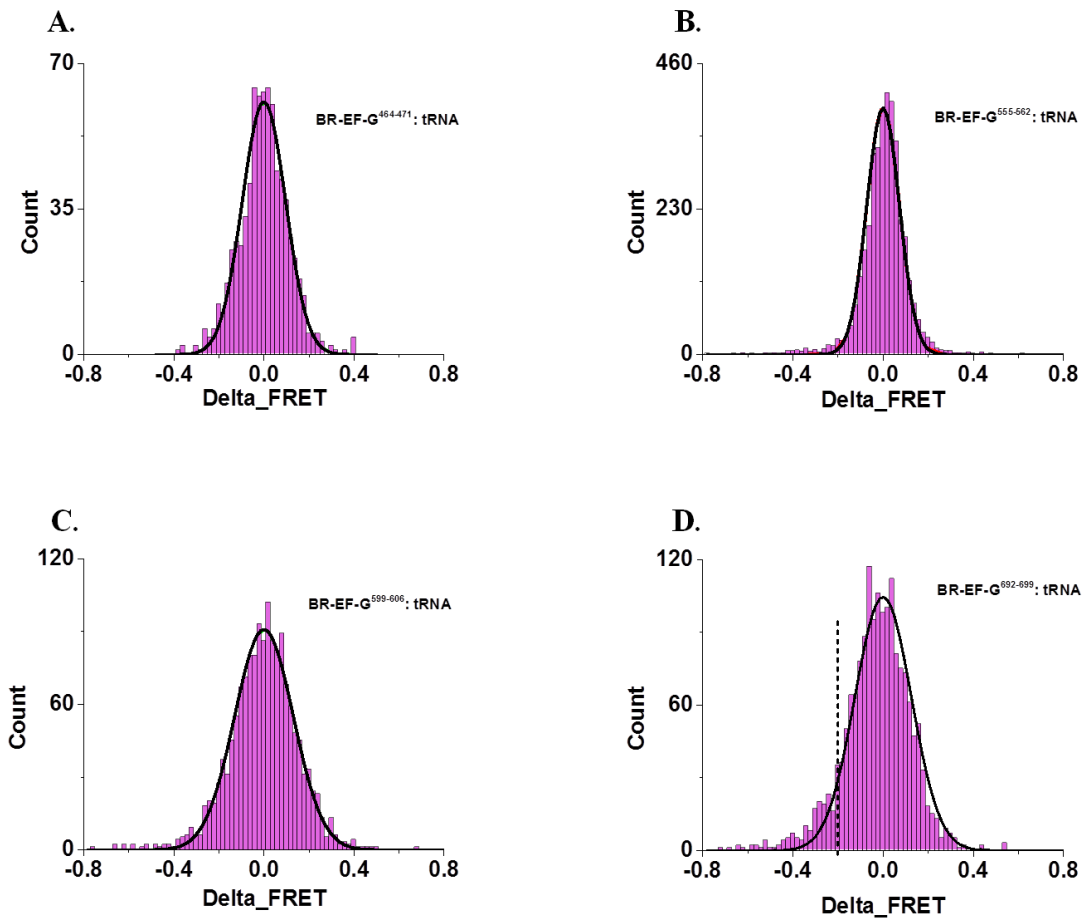

Figure 5.8 ΔFRET distributions of BR-EF-G:PRE-II$^{tRNA\text{-}Cy5}$. Sample was prepared in TAM[15] buffer and contained BR-EF-Gs, 20 nM WT-Val-TC, 10 nM Cy5-Phe-TC and 1 mM GTP. The initial and final FRET are calculated as the averaged results of the first three frames and last three frames, respectively. ΔFRET distribution is plotted with a bin size of 0.02.

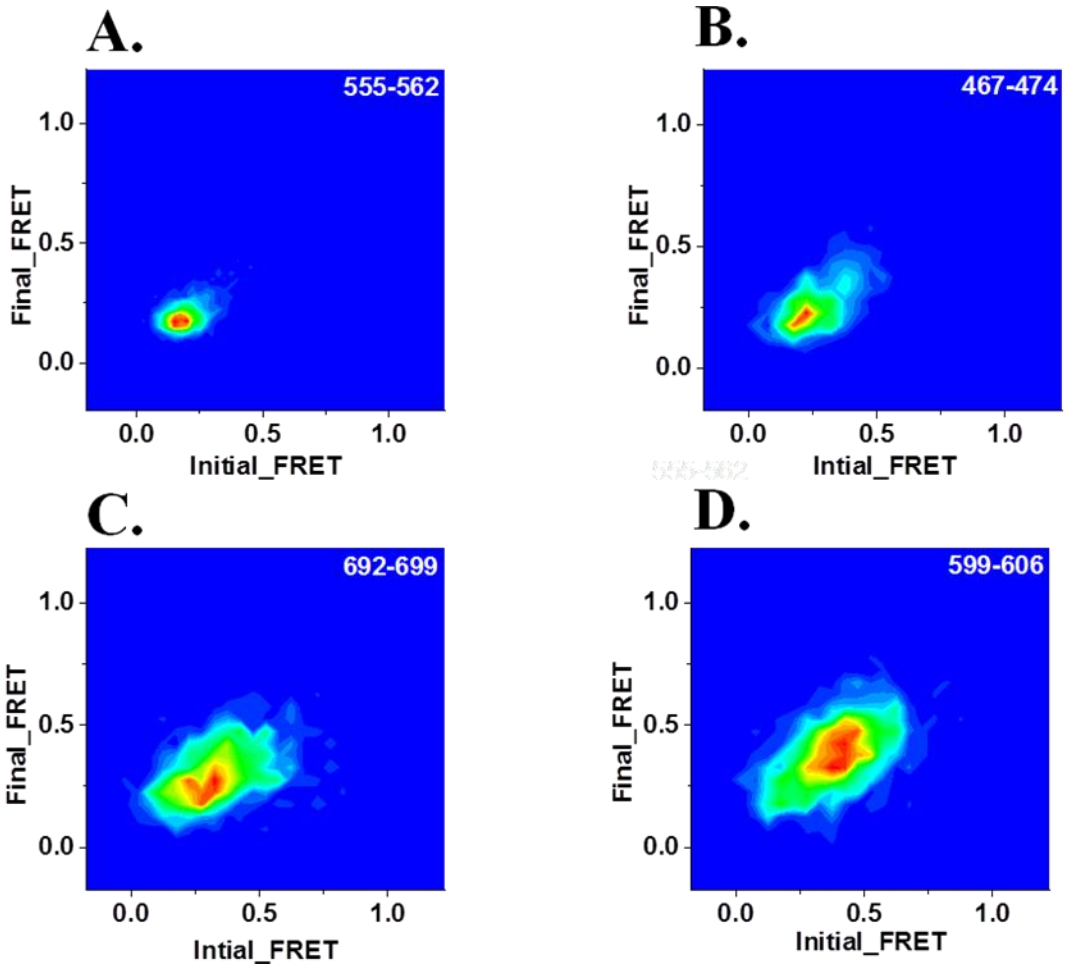

Figure 5.9 Transition density contour map of BR-EF-G:PRE-II$^{tRNA\text{-}Cy5}$. Sample was prepared in TAM[15] buffer and contained BR-EF-Gs, 20 nM WT-Val-TC, 10 nM Cy5-Phe-TC and 1mM GTP. The initial and final FRET are calculated as the averaged results of the first three frames and last three frames, respectively. Initial and final FRET values are plotted as two-dimensional transition density contour maps.

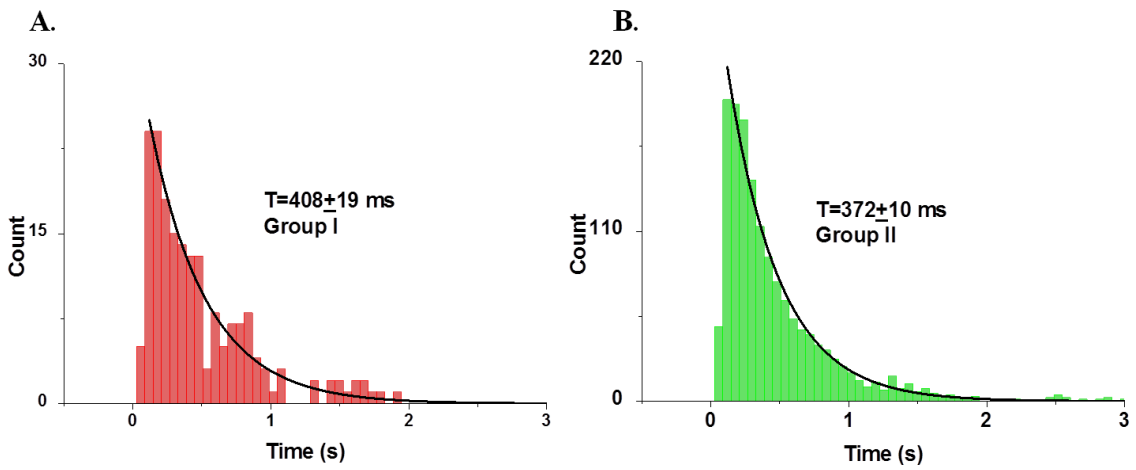

Figure 5.10 Dwell time distributions of Groups I and II traces. Sample was prepared in TAM^{15} buffer and contained BR-EF-G$^{692\text{-}699}$, 10 nM Cy5-Phe-TC, 20 nM WT-Val-TC and 1mM GTP. Dwell time distributions of Group I and Group II were each fitted by a single exponential decay.

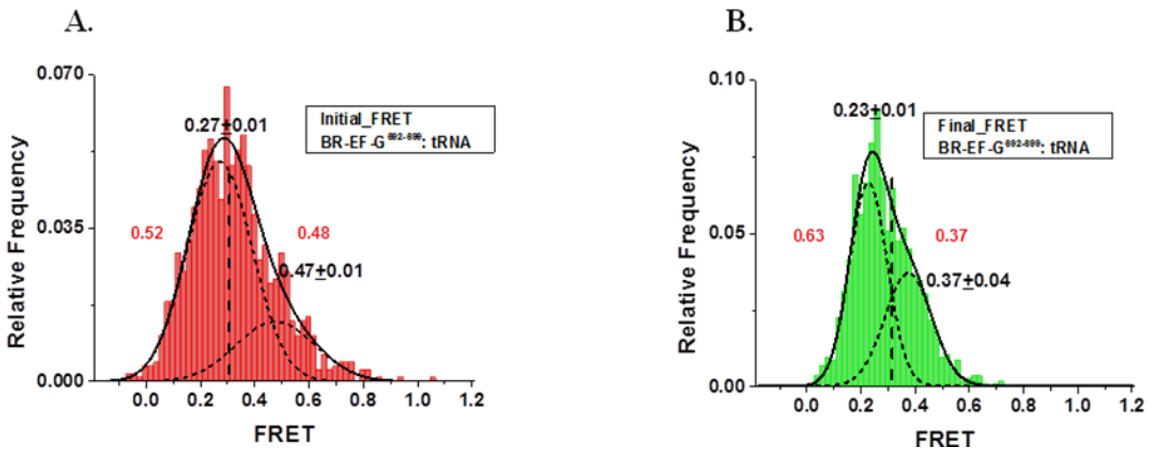

Figure 5.11 Initial and final FRET distributions. Sample was prepared in TAM[15] buffer and contained BR-EF-G[692-699], 10 nM Cy5-Phe-TC, 20 nM WT-Val-TC and 1mM GTP. The initial and final FRET are calculated as the averaged results of the first three frames and last three frames, respectively. Initial and final FRET distributions are plotted with a bin size of 0.02. The proportion of FRET events on each sides of the dashed line are indicated in red. The detailed fitting results, including standard deviation of the peak value and percentage of high FRET state are listed in Table 5.2.

Complex	Buffer	Fitted Peak of Total FRET distribution	[a] σ (SD)	[b]High FRET percentage
PRE-II MFK Initial FRET	TAM[15]	Peak1=0.27±0.01 Peak2=0.47±0.02	σ_1= 0.12 σ_2= 0.14	19%
PRE-II MFK Final FRET	TAM[15]	Peak1=0.23±0.01 Peak2=0.37±0.04	σ_1= 0.07 σ_2= 0.09	38%

Table 5.2 Statistics of fitted FRET peaks of BR-EF-G:PRE-II[tRNA-Cy5]. Sample was prepared in TAM[15] buffer and contained BR-EF-G[692-699], 10 nM Cy5-Phe-TC and 20 nM WT-Val-TC.
[a]SD of FRET distribution
[b]The intersect FRET value of the two fitted Gaussian curves (IS) is obtained. High FRET percentage is calculated by using the number of events (E > IS) divided by the number of total events
[c]Standard error of the fitted peak

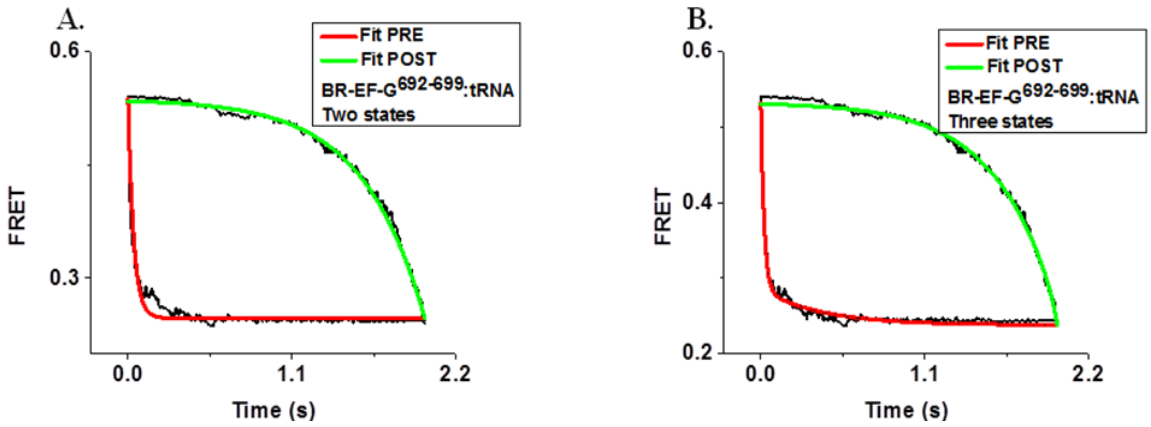

Figure 5.12 Global fitting results of Group I traces of BR-EF-G:PRE-II$^{tRNA\text{-}Cy5}$ pair. Sample was prepared in TAM[15] buffer and contained BR-EF-G$^{692\text{-}699}$, 10 nM Cy5-Phe-TC, 20 nM WT-Val-TC and 1mM GTP. Postsynchronized traces are obtained by aligning all FRET traces at the beginning (black) or at the end (red) and plotted as a function of time. Both two-state (A) and three-state (B) models are applied. Detailed fitting results are listed in Table 5.3.

Complex	**Buffer**	**Fitting model**	**Transition rate (s^{-1})**			**FRET state**		
			k_1	k_2	k_3	E_1	E_2	E_3
BR-EF-G$^{692\text{-}699}$ PRE-II$^{tRNA\text{-}Cy5}$	TAM[15]	Two state	26.2±0.7	1.6±0.1	-----	0.54±0.01	0.25±0.01	-----
	TAM[15]	Three state	45.5±1.7	2.5±0.1	24.8±2.2	0.53±0.01	0.28±0.01	0.24±0.01

Table 5.3 Global fitting results of Group I traces of BR-EF-G:PRE-II$^{tRNA\text{-}Cy5}$ pair. Sample was prepared in TAM[15] buffer and contained BR-EF-G$^{692\text{-}699}$, 10 nM Cy5-Phe-TC, 20 nM WT-Val-TC and 1mM GTP. Fitting results of two-state and three-state models are listed.

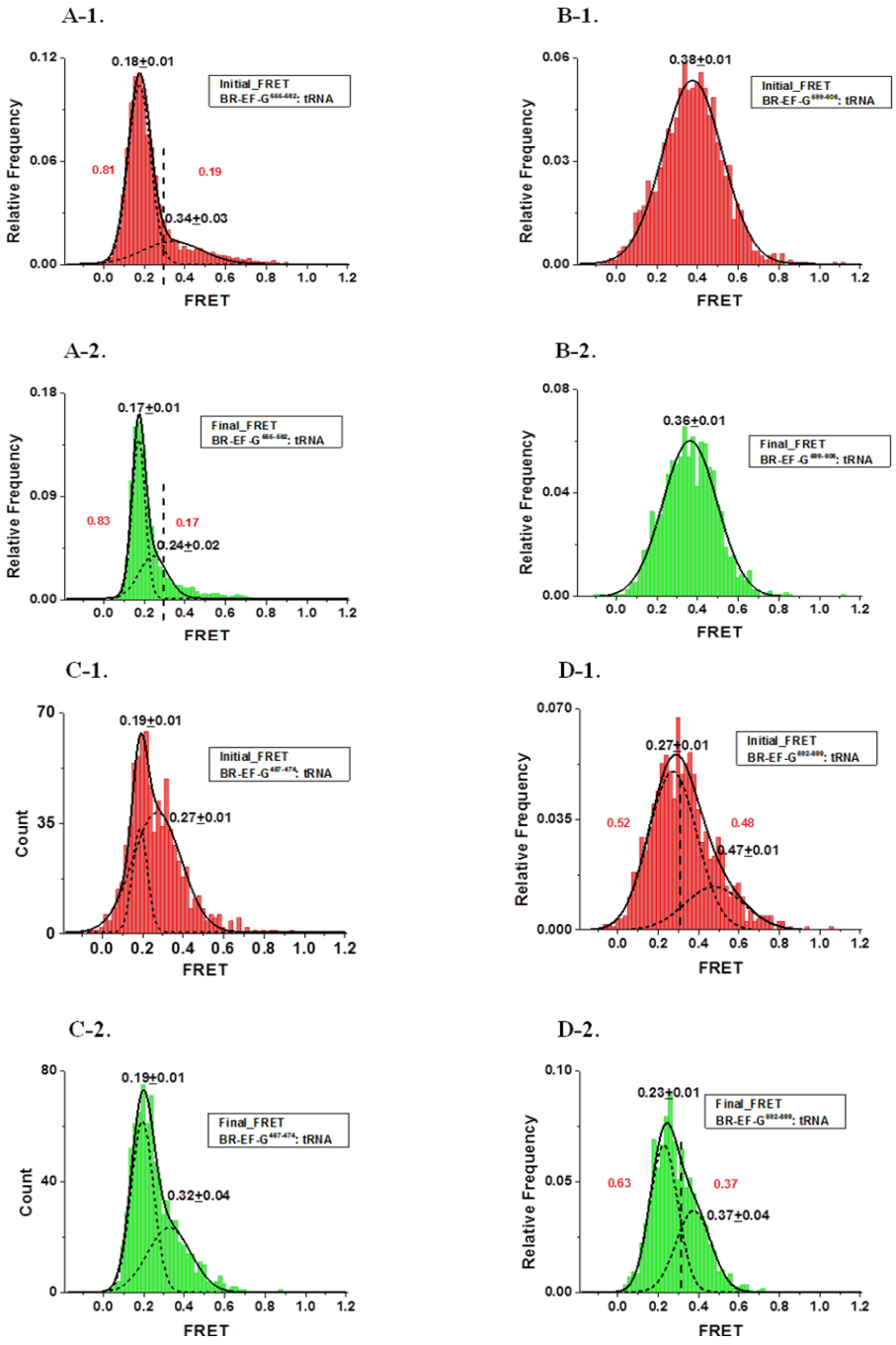

Figure 5.13 Initial and final FRET distributions of BR-EF-G:PRE-II$^{tRNA\text{-}Cy5}$ pair. Sample was prepared in TAM[15] buffer and contained BR-EF-Gs, 10 nM Cy5-Phe-TC, 20 nM WT-Val-TC and 1mM GTP. The initial and final FRET was calculated as the averaged results of the first three frames and last three frames respectively. Initial and final FRET distributions are plotted with a bin size of 0.02.

PRE-II	**BR-EF-G$^{467-474}$ (III)**	**BR-EF-G$^{555-562}$ (IV)**	**BR-EF-G$^{599-606}$ (IV)**	**BR-EF-G$^{692-699}$ (CTD)**
Total events (T)	759	3716	1527	1702
Number of events ΔFRET < - 0.20	55	**115**	138	191
Number of events ΔFRET > + 0.20	20	57	100	62
Difference in number of events (D)	35	58	38	129
Percentage (D/T)	4.6%	1.5%	2.4%	7.6%

Table 5.4 Statistical studies of ΔFRET of BR-EF-G:PRE-II$^{tRNA-Cy5}$ pair. Sample was prepared in TAM[15] buffer and contained BR-EF-Gs, 10 nM Cy5-Phe-TC, 20 nM WT-Val-TC and 1mM GTP. The first three frames and last three frames are averaged separately, defined as initial and final FRET. The difference between final and initial FRET is denoted ΔFRET.

BIBLIOGRAPHY

AEvarsson, A., Brazhnikov, E., Garber, M., Zheltonosova, J., Chirgadze, Y., al-Karadaghi, S., Svensson, L.A., Liljas, A. (1994). Three-dimensional structure of the ribosomal translocase: elongation factor G from Thermus thermophilus. EMBO J. *13*, 3669-3677.

Agirrezabala, X., Frank, J. (2009). Elongation in translation as a dynamic interaction among the ribosome, tRNA, and elongation factors EF-G and EF-Tu. Q Rev Biophys. *42*, 159-200.

Agirrezabala, X., Lei, J., Brunelle, J. L., Ortiz-Meoz, R.R., Green, R., and Frank, J. (2008). Visualization of the Hybrid Stateof tRNA Binding Promoted by Spontaneous Ratcheting of the Ribosome. *32*, 190-197.

Agrawal, J.F.a.R.K. (2000). A ratchet-like inter-subunit reorganization of the ribosome during translocation. Nature *406*, 3109-3322.

Agrawal, R.K., Linde, J., Sengupta, J., Nierhaus, K.H., Frank, J. (2001). Localization of L11 Protein on the Ribosome and Elucidation of its Involvement in EF-G-dependent Translocation. J Mol Biol. *311*, 777-787.

Agrawal, R.K., Penczek, P., Grassucci, R.A., Frank, J. (1998). Visualization of elongation factor G on the Escherichia coli 70S ribosome: the mechanism of translocation. Proc Natl Acad Sci U S A *95*, 6134–6138.

al-Karadaghi, S., Aevarsson, A., Garber, M., Zheltonosova, J., Liljas. A. (1996). The structure of elongation factor G in complex with GDP:conformational flexibility and nucleotide exchange. Structure. *4*, 555-565.

Ban, N., Nissen, P., Hansen, J., Moore, P.B., and Steitz, T.A. (2000). The complete atomic structure of the large ribosomal subunit at 2.4 Å resolution. Science *289*.

Black., D.L. (2003). Mechanisms of alternative pre-messenger RNA splicing. Annu Rev Biochem *72*, 291-336.

Blanchard, S.C., Gonzalez, R.L., Kim, H.D., Chu, S., and Puglisi, J.D. (2004a). tRNA selection and kinetic proofreading in translation. Nat. Struct. Mol. Biol. *11*, 1008–1014.

Blanchard, S.C., Kim, H.D., Gonzalez, R.L., Jr., Puglisi, J.D., and Chu, S (2004b). tRNA dynamics on the ribosome during translation. Proc. Natl. Acad. Sci. *101*, 12893–12898.

Bodley, J.W., Zieve, F.J., and Lin, L. (1970). Studies on translocation. IV. The hydrolysis of a single round of guanosine triphosphate in the presence of fusidic acid. J Biol Chem. *245*, 5662-5667.

Boelens, R., and Gualerzi, C.O. (2002). Structure and function of bacterial initiation factors. Curr Protein Pept Sci *3*, 107–119.

Bradford, M.M. (1976). Rapid and sensitive method for the quantitation of microgram quantities of protein utilizing the principle of protein-dye binding. Anal Biochem *72*, 248–254.

Brilot, A.F., Korostelev, A.A., Ermolenko, D.N., Grigorieff, N. (2013). Structure of the ribosome with elongation factor G trapped in the pretranslocation state. Proc Natl Acad Sci U S A. *110*, 20994-20999.

Carter, A.P., Clemons, W.M., Brodersen, D.E., Morgan-Warren, R.J., Wimberly, B.T., Ramakrishnan, V. (2000). Functional insights from the structure of the 30S ribosomal

subunit and its interactions with antibiotics. Nature *407*, 340-348.

Caruthers, J.M., and David B McKay (2002). Helicase structure and mechanism. Current Opinion in Structural Biology *12*, 123–133.

Cate, A.P.a.J.H.D. (2013). Control of Ribosomal Subunit Rotation by Elongation Factor G. Science *340*, DOI: 10.1126.

Chen, C., Greenberg, M.J., Laakso, J.M., Ostap, E.M., Goldman, Y.E., Shuman, H. (2012). Kinetic Schemes for Post-Synchronized Single Molecule Dynamics. Biophys J. *102*, 23-25.

Chen, C., Stevens, B,, Kaur, J,, Cabral, D., Liu, H., Wang, Y,, Zhang, H., Rosenblum, G., Smilansky, Z., Goldman, Y.E., Cooperman, B.S. (2011a). Single-molecule fluorescence measurements of ribosomal translocation dynamics. Mol Cell. *42*, 367-377.

Chen, C., Stevens, B., Kaur, J., Smilansky, Z., Cooperman, B.S., Goldman, Y.E. (2011b). Allosteric vs. spontaneous exit-site (E-site) tRNA dissociation early in protein synthesis. Proc Natl Acad Sci U S A *108*, 16980-16985.

Chen, J., Petrov, A., Tsai, A., O'Leary, S.E., Puglisi, J.D. (2013a). Coordinated conformational and compositional dynamics drive ribosome translocation Nat Struct Mol Biol. *20*, 718-727.

Chen, Y., Feng, S., Kumar, V., Ero, R., Gao, Y.G. (2013b). Structure of EF-G–ribosome complex in a pretranslocation state. Nat Struct Mol Biol. *20*, 1077-1084.

Congdon, R.W., Muth, G.W., Splittgerber, A.G. (1993). The binding interaction of Coomassie blue with proteins. Anal Biochem *213*, 407-413.

Connell, S.R., Topf, M., Qin, Y., Wilson, D.N., Mielke, T., Fucini, P., Nierhaus, K.H., Spahn, C.M. (2008). A new tRNA intermediate revealed on the ribosome during EF4-mediated back-translocation. Nat Struct Mol Biol *15*, 910-915.

Cramer, P. (2002). Multisubunit RNA polymerases. Curr Opin Struct Biol *12*, 89-97.

Crick, F. (1970). Central dogma of molecular biology. Nature *227*, 561–563.

Czworkowski, J., Wang, J., Steitz, T.A., Moore, P.B. (1994). The crystal structure of elongation factor G complexed with GDP, at 2.7 A resolution. EMBO J. *13*, 3661-3668.

Demeshkina, N., Jenner, L., Westhof, E., Yusupov, M., and Yusupova, G. (2012). A new understanding of the decoding principle on the ribosome. Nature *484*.

Dorner, S., Brunelle, J.L., Sharma, D., and Green, R. (2006). The hybrid state of tRNA binding is an authentic translation elongation intermediate. Nat. Struct. Mol. Biol. *13*, 234–241.

Dubnoff, J.S., and Marita, U. (1971). Isolation and properties of protein factors involved in polypeptide chain initiation in Escherichia coli. Methods Enzymol *20*, 248–261.

Ermolenko, D.N., Spiegel, P.C., Majumdar, Z.K., Hickerson, R.P., Clegg, R.M., Noller, H.F. (2007). The antibiotic viomycin traps the ribosome in an intermediate state of translocation Nat Struct Mol Biol. *14*, 493-497.

Evans, R.N., Blaha, G., Bailey, S., Steitz, T.A. (2008). The structure of LepA, the ribosomal back translocase. Proc Natl Acad Sci U S A. *105*, 4673-4678.

Fei, J., Bronson, J.E., Hofman, J.M., Srinivas, R.L., Wiggins, C.H., Gonzalez, R.L.Jr.

(2009). Allosteric collaboration between elongation factor G and the ribosomal L1 stalk directs tRNA movements during translation. Proc Natl Acad Sci U S A. *106*, 15702-15707.

Fei, J., Kosuri, P., MacDougall, D.D., and Gonzalez, R.L., Jr. (2008). Coupling of ribosomal L1 stalk and tRNA dynamics during translation elongation. Mol. Cell *30*, 348–359.

Fischer, N., Konevega, A.L., Wintermeyer, W., Rodnina, M.V., Stark, H. (2010). Ribosome dynamics and tRNA movement by time-resolved electron cryomicroscopy. nature *466*, 329-333.

Franckenberg, S., Becker, T., and Beckmann, R. (2012). Structural view on recycling of archaeal and eukaryotic ribosomes after canonical termination and ribosome rescue. Curr Opin Struct Biol *22*, 786–796.

Frank, J., Agrawal, R.K. (2000). A ratchet-like inter-subunit reorganization of the ribosome during translocation. Nature *406*, 318-322.

Frank, J., Gao, H., Sengupta, J., Gao, N., Taylor, D. (2007). The process of mRNA–tRNA translocation. Proc Natl Acad Sci U S A *104*, 19671-19678.

Frank, J., Verschoor, A., Wagenknecht, T., Radermacher, M. , Rosenthal, M., and Boublik, M. (1986). New Strategies for Determining Ribosomal Subunit Structure from Electron Micrographs by Single Particle Averaging Methods. Biophys J. *49*, 9-11.

Fu, J., Munro, J.B., Blanchard, S.C., Frank, J. (2011). Cryoelectron microscopy structures of the ribosome complex in intermediate states during tRNA translocation. Proc Natl

Acad Sci *108*, 4817-4821.

Gao, Y.G., Selmer. M., Dunham, C.M., Weixlbaumer, A., Kelley, A.C., Ramakrishnan, V. (2009). The structure of the ribosome with elongation factor G trapped in the posttranslocational state. Science *326*, 694-699.

Hall, C.E., Slayter, H.S. (1959). Electron microscopy of ribonucleoprotein particles from E. Coli J. mol. Biol. *1*, 329–332.

Hansson, S., Singh, R., Gudkov, A.T., Liljas, A., Logan, D.T. (2005). Crystal structure of a mutant elongation factor G trapped with a GTP analogue. FEBS Lett. *579*, 4492-4497.

Harms, J., Schluenzen, F., Zarivach, R., Bashan, A., Gat, S., Agmon, I., Bartels, H., Franceschi, F., Yonath, A. (2001). High resolution structure of the large ribosomal subunit from a mesophilic eubacterium. Cell *107*, 679-688.

Hirashima, A.a.K., A. (1973). Role of elongation factor G and a protein factor on the release of ribosome from messenger ribonucleic acid. J Bio Chem *248*, 7580–7587.

Hirokawa, G., Iwakura, N., Kaji, A., and Kaji, H. (2008). The role of GTP in transient splitting of 70S ribosomes by RRF (ribosome recycling factor) and EF-G (elongation factor G). Nucleic Acids Res *36*, 6676–6687.

Illingworth, J., and Kittler, J. (1988). A Survey of the Hough Transform. Comput Vision Graph *44*, 87-116.

Jenner, L., Demeshkina, N., Yusupova, G., and Yusupov, M. (2010). Structural rearrangements of the ribosome at the tRNA proofreading step. Nat Struct Mol Bio *7*, 1072–1078.

Julián, P., Konevega, A.L., Scheres, S.H., Lázaro, M., Gil, D., Wintermeyer, W., Rodnina, M.V., Valle, M. (2008). Structure of ratcheted ribosomes with tRNAs in hybrid states. Proc Natl Acad Sci U S A *105*, 16924-16927.

Kaltschmidt, E., and Wittmann, H.G. (1970). Ribosomal proteins. XII. Number of proteins in small and large ribosomal subunits of Escherichia coli as determined by two-dimensional gel electrophoresis. Proc Natl Acad Sci *67*, 1276–1282.

Karimi, R., Pavlov, M.Y., Buckingham, R.H., and Ehrenberg, M. (1999). Novel roles for classical factors at the interface between translation termination and initiation. Mol. Cell *3*, 601–609.

Kaur, J., Raj, M. and Cooperman, B.S. (2011). Fluorescent labeling of tRNA dihydrouridine residues: mechanism and distribution. RNA *17*, 1393–1400.

Kim, H.D., Puglisi, J.D., Chu, S. (2007). Fluctuations of Transfer RNAs between Classical and Hybrid States. Biophys J. *93*, 3575-3582.

Kirillov, S.V., Katunin, V.I., Semenkov, Y.P. (1981). Mechanism of codon-anticodon interaction in ribosomes: comparative study of interaction of Phe-tRNAPhe and N-acetyl-Phe-tRNAPhe with the donor site of Escherichia coli ribosomes. FEBS Lett. *125*, 15-19.

Korostelev, A., Asahara, H., Lancaster, L., Laurberg, M., Hirschi, A., Zhu, J., Trakhanov, S., Scott, W.G., Noller, H.F. (2008). Crystal structure of a translation termination complex formed with release factor RF2. Proc Natl Acad Sci USA *105*, 19684–19689.

Laurberg, M., Asahara, H., Korostelev, A., Zhu, J., Trakhanov, S., and Noller, H.F. (2008). Structural basis for translation termination on the 70S ribosome. Nature *454*, 852–857.

Laurberg, M., Kristensen, O., Martemyanov, K., Gudkov, A.T., Nagaev, I., Hughes, D., Liljas, A. (2000). Structure of a mutant EF-G reveals domain III and possibly the fusidic acid binding site. J Mol Biol. *303*, 593-603.

Lill, R., Wintermeyer, W. (1987). Destabilization of Codon-Anticodon Interaction in the Ribosomal Exit Site. J Mol Biol. *196*, 137-148.

Liu, H., Chen, C., Zhang, H., Kaur, J., Goldman, Y.E., and Cooperman, B.S. (2011). The conserved protein EF4 (LepA) modulates the elongation cycle of protein synthesis. Proc Natl Acad Sci USA *108*, 16223–16228.

Liu, H., Pan, D., Pech, M., and Cooperman, B. S. (2010). Interrupted catalysis: the EF4 (LepA) effect on bach-translocation. J Mol Bio *396*, 1043–1052.

Liu, W., Kavaliauskas, D., Schrader, J.M., Poruri, K., Birkedal, V., Goldman, E., Jakubowski, H., Mandecki, W., Uhlenbeck, O.C., Knudsen, C.R., Goldman, Y.E., Cooperman, B.S. (2014). Labeled EF-Tus for Rapid Kinetic Studies of Pretranslocation Complex Formation. ACS Chem Biol. *9*, 2421-2431.

Marshall, R.A., Aitken, C.E., Dorywalska, M., and Puglisi, J.D. (2008a). Translation at the single-molecule level. Annu Rev Biochem *77*, 177–203.

Marshall, R.A., Dorywalska, M., Puglisi, J.D. (2008b). Irreversible chemical steps control intersubunit dynamics during translation. Proc Natl Acad Sci U S A. *105*, 15364-15369.

Moazed, D., Samaha, R.R., Gualerzi, C., and Noller, H.F. (1995). Specific protection of 16 S rRNA by translational initiation factors. J Mol Bio *248*, 207–210.

Modolell, J., Vázquez. (1977). The inhibition of ribosomal translocation by viomycin. Eur J Biochem. *3*, 491-497.

Munro, J.B., Altman, R.B., O'Connor, N., and Blanchard, S.C. (2007). Identification of two distinct hybrid state intermediates on the ribosome. Mol. Cell. *35*, 505–517.

Munro, J.B., Wasserman, M.R., Altman, R.B., Wang, L., Blanchard, S.C. (2010). Correlated conformational events in EF-G and the ribosome regulate translocation. Nat Struct Mol Biol. *17*, 1470-1477.

Nishikura, K. (2006). Editor meets silencer: crosstalk between RNA editing and RNA interference. Nat Rev Mol Cell Biol *7*, 919–931.

Nissen, P., Kjeldgaard, M., Thriup, S., Polekhina, G., Reshetnikova, L., Clark, B., and Nyborg, J. (1995). Crystal structure of the ternary complex of Phe-tRNAPhe, EF-Tu and a GTP analog. Science *270*, 1464–1472.

Nureki, O., Vassylyev, D. G., Tateno, M., Shimada, A., Nakama, T., Fukai, S., Konno, M., Hendrickson, M., Schimmel, P., Yokoyama S. (1998). Enzyme Structure with Two Catalytic Sites for Double-Sieve Selection of Substrate. Science *280* 578-582

Pan, D., Qin, H., and Cooperman, B.S. (2009). Synthesis and functional activity of tRNAs labeled with fluorescent hydrazides in the D-loop. RNA *15*, 346–354.

Pan, D., Zhang, C., Kirillov, S., Hou, Y., and Cooperman, B.S. (2008). Perturbation of the tRNA tertiary core differentially affects specific steps of the elongation cycle. J Biol Chem *283*, 18431–18440.

Pan, D.L., Kirillov, S.V., and Cooperman, B.S. (2007). Kinetically competent

intermediates in the translocation step of protein synthesis. Mol. Cell *25*, 519–529.

Pape, T., Wintermeyer, W., and Rodnina, M.V. (1998). Complete kinetic mechanism of elongation factor Tu-dependent binding of aminoacyl-tRNA to the A site of the E. coli ribosome. EMBO J *17*, 7490–7497.

Peske, F., Matassova, N.B., Savelsbergh, A., Rodnina, M.V., Wintermeyer, W. (2000). Conformationally restricted elongation factor G retains GTPase activity but is inactive in translocation on the ribosome. Mol Cell. *6*, 501-505.

Peske, F., Savelsbergh, A., Katunin, V., Rodnina, M.V., Wintermeyer, W. (2004). Conformational changes of the small ribosomal subunit during elongation factor G-dependent tRNA-mRNA translocation. J Mol Biol. *343*, 1183-1194.

Pulk, A., Cate, J.H. (2013). Control of Ribosomal Subunit Rotation by Elongation Factor G. Science *340*.

Qin, Y., Polacek, N., Vesper, O., Staub, E., Einfeldt, E., Wilson, D.N., Nierhaus, K.H. (2006). The highly conserved LepA is a ribosomal elongation factor that back-translocates the ribosome. Cell *127*, 721-733.

Ramrath, D.J., Lancaster, L., Sprink, T., Mielke, T., Loerke. J., Noller, H.F., Spahn, C.M. (2013). Visualization of two transfer RNAs trapped in transit during elongation factor G-mediated translocation. Proc Natl Acad Sci U S A. *110*, 20964-20969.

Ratje, A.H., Loerke, J., Mikolajka, A., Brünner, M., Hildebrand, P.W., Starosta, A.L., Dönhöfer, A., Connell, S.R., Fucini, P., Mielke, T., Whitford, P.C., Onuchic, J.N., Yu, Y., Sanbonmatsu, K.Y., Hartmann, R.K., Penczek, P.A., Wilson, D.N., Spahn, C.M. (2010).

Head swivel on the ribosome facilitates translocation by means of intra-subunit tRNA hybrid sites. Nature, 713-716.

Rodnina, M.V., Fricke, R., and Wintermeyer, W. (1994). Transient conformational states of aminoacyl-tRNA during ribosome binding catalyzed by elongation factor Tu. Biochemistry *33*, 12267–12275.

Rodnina, M.V., Savelsbergh, A., Katunin, V., Wintermeyer, W. (1997). Hydrolysis of GTP by elongation factor G drives tRNA movement on the ribosom. nature *385*, 37-41.

Rothwell, P.J., Waksman, G. (2005). Structure and mechanism of DNA polymerases. Advances in Protein Chemistry *04*.

Roy, R., Hohng, S., and Ha, T. (2008). A practical guide to single-molecule FRET. Nat Methods *5*, 507-516.

Salsi, E., Farah, E., Dann, J., Ermolenko, D.N. (2014). Following movement of domain IV of elongation factor G during ribosomal translocation. Proc Natl Acad Sci U S A. *111*, 15060-15065.

Savelsbergh, A., Katunin, V.I., Mohr, D., Peske, F., Rodnina, M.V., and Wintermeyer, W. (2003). An elongation factor G-induced ribosome rearrangement precedes tRNA-mRNA translocation. Mol. Cell *11*, 1517–1523.

Savelsbergh, A., Matassova, N.B., Rodnina, M.V., Wintermeyer, W. (2000). Role of Domains 4 and 5 in Elongation Factor G Functions on the Ribosome. J Mol Biol. *300*, 951-961.

Savelsbergh, A., Mohr, D., Kothe, U., Wintermeyer, W., Rodnina, M.V. (2005). Control

of phosphate release from elongation factor G by ribosomal protein L7/12. EMBO J. *24*, 4316-4323.

Schluenzen, F., Tocilj, A., Zarivach, R., Harms, J., Gluehmann, M., Janell, D., Bashan, A., Bartels, H., Agmon, I., Franceschi, F., Yonath, A. (2000). Structure of Functionally Activated Small Ribosomal Subunit at 3.3 A Resolution. Cell *192*, 615-623.

Schmeing, T.M., and Ramakrishnan, V. (2009a). What recent ribosomal structures have revealed about the mechanism of translation. Nature *461*, 1234-1242.

Schmeing, T.M., Voorhees, R.M., Kelley, A.C., Gao, Y, Murphy, F.V., Weir, J. R., and Ramakrishnan, V. (2009b). The crystal structure of the ribosome bound to EF-Tu and aminoacyl-tRNA. Science *326*, 688–694.

Schuwirth, B.S., Borovinskaya, M.A., Hau, C.W., Zhang, W., Vila-Sanjurjo, A., Holton, J.M., Cate, J.H. (2005). Structures of the bacterial ribosome at 3.5 A resolution. Science *310*, 827-834.

Selmer, M., Dunham, C.M., Murphy. F.V., Weixlbaumer, A., Petry. S., Kelley, A.C., Weir, J.R., Ramakrishnan, V. (2006). Structure of the 70S Ribosome Complexed with mRNA and tRNA. Science *313*, 1935-1942.

Semenkov, Y.P., Shapkina, T.G., and Kirillov, S.V. (1992). Puromycin reaction of the A-site bound peptidyl-tRNA. Biochimie. Biochimie *74*, 411–417.

Seo, H.S., Abedin, S., Kamp, D., Wilson, D.N., Nierhaus, K.H., Cooperman, B.S. (2006). EF-G-Dependent GTPase on the Ribosome. Conformational Change and Fusidic Acid Inhibition. Biochemistry *45*, 2504-2514.

Sharma, D., Southworth, D.R., and Green, R. (2004). EF-G-independent reactivity of a pre-translocation-state ribosome complex with the aminoacyl tRNA substrate puromycin supports an intermediate (hybrid) state of tRNA binding. RNA *10*, 102–113.

Stanley, R.E., Blaha, G., Grodzicki, R.L., Strickler, M.D., Steitz, T.A. (2010). The structures of the anti-tuberculosis antibiotics viomycin and capreomycin bound to the 70S ribosome. Nat Struct Mol Biol. *17*, 289-293.

Tourigny, D.S., Fernández, I.S., Kelley, A.C., Ramakrishnan, V. (2013). Elongation Factor G Bound to the Ribosome in an Intermediate State of Translocation. Science *340*.

Tsai, A., Petrov, A., Marshall, R.A., Korlach, J., Uemura, S., and Puglisi, J.D. (2012). Heterogeneous pathways and timing of factor departure during translation initiation. Nature *487*, 390–393.

Valle, M., Zavialov. A., Sengupta, J., Rawat, U., Ehrenberg. M., Frank, J. (2003). Locking and Unlocking of Ribosomal Motions. Cell *114*, 123-134.

Voorhees, R.M., Schmeing, T.M., Kelley, A.C. and Ramakrishnan, V. (2010). The mechanism for activation of GTP hydrolysis on the ribosome. Science *350*, 835–838.

Wahl, M.C., Will, C.L., and Lührmann, R (2009). The spliceosome: design principles of a dynamic RNA machine. Cell *136*, 701–718.

Watson, J.D., and Crick, F. H. (1953a). Genetical implications of the structure of deoxyribonucleic acid. Nature *171*, 964–967.

Watson, J.D., and Crick, F. H. (1953b). Molecular structure of nucleic acids; a structure for deoxyribose nucleic acid. Nature *171*, 737–738.

Weixlbaumer, A., Jin, H., Neubauer, C., Voorhees, R.M., Petry, S., Kelley, A.C., and Ramakrishnan, V. (2008). Insights into translational termination from the structure of RF2 bound the ribosome. Science *322*, 953–956.

Wilden, B., Savelsbergh, A., Rodnina, M.V., Wintermeyer, W. (2006). Role and timing of GTP binding and hydrolysis during EF-G-dependent tRNA translocation on the ribosome. Proc Natl Acad Sci U S A. *103*, 13670-13675.

Wimberly, B.T., Brodersen, D.E., Clemons, W.M.Jr., Morgan-Warren, R.J., Carter, A.P., Vonrhein, C., Hartsch, T., Ramakrishnan, V. (2000). Structure of the 30S ribosomal subunit. Nature *407*, 327-339.

Wimberly, B.T., Guymon, R., McCutcheon, J.P., White, S.W., and Ramakrishnan,V. (1999). A detailed view of a ribosomal active site: the structure of the L11- RNA complex. Cell *97*, 491–502.

Yonath, A. (2010). Polar bears, antibiotics, and the evolving ribosome. Angew Chem Int Ed *49*, 4340–4354.

Yusupov, M.M., Yusupova, G.Z., Baucom, A., Lieberman, K., Earnest, T.N., Cate, J.H., Noller, H.F. (2001). Crystal Structure of the Ribosome at 5.5 Å Resolution. Science *292*, 883-896.

Zavialov, A.V., Ehrenberg. M. (2003). Peptidyl-tRNA regulates the GTPase activity of translation factors. Cell *114*, 113-122.

Zavialov, A.V., Mora, L., Buckingham, R.H., Ehrenberg, M. (2002). Release of peptide promoted by the GGQ motif of class 1 release factors regulates the GTPase activity of

RF3. Mol Cell. *10*, 789-798.

Zhang, W., Dunkle, J.A., and Cate, J.H.D. (2009). Structures of the ribosome in intermediate states of ratcheting. Science *325*, 1014–1017.

Zhou, J., Lancaster, L,, Donohue, J.P., Noller, H.F. (2014). How the ribosome hands the A-site tRNA to the P site during EF-G–catalyzed translocation. Science *345*, 1188-1191.

Zhou, J., Lancaster, L., Donohue, J.P., Noller, H.F. (2013). Crystal Structures of EF-G–Ribosome Complexes Trapped in Intermediate States of Translocation. Science *340*.